KU LEUVEN

ARENBERG DOCTORAL SCHOOL
Faculty of Science

Supported ionic liquid phases for extraction and separation of medical radiolanthanides

Towards purification of medical samarium-153

Michiel Van de Voorde

Supervisors:
Prof. dr. Koen Binnemans
Prof. dr. Thomas Cardinaels

Dissertation presented in partial fulfillment of the requirements for the degree of Doctor of Science (PhD): Chemistry

August 2019

Supported ionic liquid phases for extraction and separation of medical radiolanthanides

Towards purification of medical samarium-153

Michiel VAN DE VOORDE

Examination committee:
Prof. dr. Wim De Borggraeve, chair
Prof. dr. Koen Binnemans, supervisor
Prof. dr. Thomas Cardinaels, supervisor
Prof. dr. ir. Jan Fransaer
Prof. dr. Tatjana Parac-Vogt
Dr. Sofía Riaño Torres
Prof. dr. Giuseppe Modolo
(Fz Jülich)

Dissertation presented in partial fulfillment of the requirements for the degree of Doctor of Science (PhD): Chemistry

August 2019

Uitgegeven in eigen beheer, Michiel Van de Voorde, Celestijnenlaan 200F box 2404, B-3001 Leuven (Belgium)

Acknowledgements

The presented PhD dissertation is the result of the research that was performed over the last four years in a collaborative project between KU Leuven and SCK•CEN. The project was generously funded by the SCK•CEN Academy. Although the project was a very individual one, this project could not have been successful without the help and support many people, both directly and indirectly involved. In this section, I would like to express my gratitude to these people.

First of all, I would like to sincerely thank my supervisor prof. dr. Koen Binnemans and co-supervisor prof. dr. Thomas Cardinaels who made this PhD project possible in first place. I am grateful to both of you for giving me the opportunity to perform this research project and for your support and advice. Along the project, both of you made me a better scientist than I could have ever imagined. I have pushed multiple boundaries, and have experienced things that I could only dream of. Koen, I truly have the deepest respect for your devotion, inexhaustible knowledge and infinite memory. Also the way you manage and keep improving the – quite extensive and internationally high-level – SOLVOMET research group serves as an example. Notwithstanding your super busy schedule, you are still able to give the required attention to every single team member to discuss their individual research project or any other problem. I am really proud that I could be a team member ever since my master thesis. Thomas, I admire your scientific curiosity and determination to continuously keep on improving. The latter initiated the development of the RCY expertise group at SCK•CEN, which has evolved into a bunch of young and motivated researchers tackling highly interesting research projects. You were always eager to be able to understand every single detail in the project, and made me question and rethink the things I did.

I am also very grateful to the members of the Examination Committee, prof. dr. Tatjana Parac-Vogt (assessor), prof. dr. ir. Jan Fransaer (assessor), prof. dr. Wim De Borggraeve (chair), prof. dr. Giuseppe Modolo (external, Fz Jülich)

and dr. Sofía Riaño Torres. First of all for agreeing to be a member of the EC, but also for proof-reading the thesis text. Your critical remarks, valuable advice and other helpful contributions during the preliminary defense further improved the quality of this PhD dissertation.

I would like to thank my RCY/RCA colleagues and my 'dear fellow PhD student colleagues' at SCK•CEN. In special, I deeply appreciate the help I received from dr. Karen Van Hecke and dr. Bart Geboes, who guided me through the project. Karen, thank you for sharing your expertise in solvent extraction, extraction chromatography and radiochemistry from the very beginning of the project. Bart, thank you for joining in the project later on whenever I had to deal with electrochemistry and for the countless times you passionately explained the electrochemical phenomena in an attempt to properly describe my observations. Also a big thank you to Peter, Christian, Meryem and Liliane for the great moments, endless discussions, useful (or less useful) advice and coffee breaks in the office. Maarten, thank you very much for helping me out with the radiopharmaceutical aspects in my project. Anja, thank you for helping me out with all my administration at SCK•CEN.

Many thanks also go to the extraordinary people with whom I had the great opportunity to work with in the SOLVOMET (former LIC) research group at KU Leuven. I really enjoyed to be part of the team ever since my master thesis, and to get to know all these truly great people. Thank you for the many nice memories! The Christmas parties, social activities, Friday evening's pintjes time and all other fun moments in the lab and offices are definitely unforgettable. Special words of gratitude go to the (mental) Cavemen, *i.e.* Arne, Stijn R., Jonas, Pieter and Stijn V.R., for their camaraderie, to Tom and Bieke for their help with XAFS and to Dženita for sharing her experiences with column experiments. Bart, Dirk, Paul, Gerrit and Dominik are highly acknowledged for their technical support in the lab, whereas Rita is highly acknowledged for her administrative support.

To relief the pressure during the weekends and free moments, I could count on my amazing Chiro friends over and over again. All of them are different. Some of them are present more frequently than others. But whenever we meet, we always have a great time. So, a really big thank you to you guys! Also the weekly games of the football enthusiasts club Halder United ensured a great pressure relief. But more importantly, I got to know a bunch of new people over the last few years with whom I can also have good times. Combating together and being accepted in the team truly is a great feeling. Maybe one day we might even win our league.

All things come to an end. This also applies to my time as a student. The path I walked was certainly not the shortest, nor the easiest. I came across

failure, I came across success. But in the end, I achieved something far beyond expectations. This was definitely not possible without the unconditional support of my family, who always kept believing in my ability to succeed. Special thanks to my parents, who gave – and still give – me and my brother the freedom and the opportunity to become successful in life. Mom, unfortunately you were suddenly and unexpectedly taken from us about a year ago. I know for sure you would have been very proud...and that you would have spoiled the guests after the public defense with a kick-ass and over-the-top reception. This achievement is definitely also yours.

Last but not least, I would like to thank my lovely girlfriend Lyske for her immense patience, but even greater support and understanding. Although I always (try to) hide my difficult moments, you are always there to back me up. Of course, also thank you for making sure dinner was ready whenever I arrived home after spending another too (in your opinion at least) long day at work. I promise, I will try my best to work on it.

Abstract

Radiolanthanides are gaining more importance in nuclear medicine because of their favorable decay characteristics. The emission of β^- particles with energies suitable to destroy malicous tumor cells is very useful in cancer therapy, whereas the emission of γ photons can be used for diagnostic purposes. Some radiolantanides are even able to serve both purposes concurrently (theranostics) making it possible to follow the effectiveness of the therapy *in situ*. Radiolanthanides have the potential to be deployed in a wide variety of applications in nuclear medicine.

Because of the very similar chemical properties across the lanthanide series, different radiolanthanides can be linked to the same chelator. This makes them easily interchangeable, by which radiopharmaceuticals can be tailored to serve a specific purpose. Selecting the most proper particle emission energy for therapy is important to keep radiation damage to healthy tissue and vital organs as low as possible. This way, a high tumor-to-normal tissue absorbed dose can be assured. However, the very similar chemical properties also imply that separation of two neighboring lanthanides is very challenging, and is one of the main challenges in the production of radiolanthanides for medical applications.

Radiolanthanides are most efficiently produced in a nuclear research reactor *via* (n, γ) irradiation, which involves the bombardment of an enriched target with neutrons. Depending on the production strategy followed, the obtained radiolanthanide is carrier-added or non-carrier-added. The product resulting from each production pathway might require a purification step for different reasons before being used in a radiopharmaceutical. Isolation of non-carrier-added radiolanthanides from their target material results in a product with high specific activity, which is highly suitable for targeted radiotherapy. Carrier-added-produced radiolanthanides cannot be separated from their target material, and thus will have limited specific activities only. Therefore, they are not applied in targeted radiotherapy, but are found to be very suitable for bone pain palliation, radiation synovectomy and imaging. During neutron irradiation,

long-lived radionuclidic impurities might be produced concurrently, impeding the medicinal use of the carrier-added radiolanthanide and limiting its shelf-life. After all, background radiation levels of the patient have to be limited, and are strictly regulated. A purification step for these radiolanthanides might thus be required to achieve adequate radionuclidic purity.

The use of a certain radiopharmaceutical in nuclear medicine is highly dependent on the availability of the radiolanthanide of interest, its decay characteristics and its achievable specific activity. Therefore, a lot of research has been conducted to find suitable purification and isolation methods for medical radiolanthanides produced in nuclear research reactors. A comprehensive overview for nuclear-reactor-produced medical radiolathanides is given within the framework of this research project.

In this PhD dissertation, a new and innovative approach for the separation of samarium and europium towards the purification of medical ^{153}Sm is presented. ^{153}Sm serves well in nuclear medicine because of its favorable decay characteristics, *i.e.* a very manageable physical half-life of 46.284 h and the emission of β^- particles with a mean energy of 233 keV, which is suitable for radiotherapy. The simultaneous emission of γ photons of 103.2 keV can be used for imaging, making ^{153}Sm suitable for diagnosis and theranostics. ^{153}Sm is produced carrier-added in a nuclear research reactor. Long-lived ^{154}Eu impurities are produced concurrently, limiting the use of ^{153}Sm radiopharmaceuticals.

Separation of Sm^{3+} and Eu^{3+} is challenging because of their very similar chemical properties. A change in valence state induces a significant change in chemical properties, leading to possibilities for a more efficient separation. Reduction of Eu^{3+} to its divalent state is the most easy to achieve in the lanthanide series because of its electron configuration. Reduction of Eu^{3+} was already well-studied before in media stable to reduction, like aqueous chloride solutions. However, in this dissertation it is shown that reduction of Eu^{3+} is also possible in aqueous nitrate media, and that Eu^{2+} remains relatively stable in these media. Nevertheless, high nitrate salt concentrations are needed to achieve this reduction and stability. These high nitrate salt concentrations also proved to be very advantageous in the separation step, making use of the salting-out principle. A solvent extraction method making use of Aliquat 336 nitrate ([A336][NO_3]) as the organic phase was developed to selectively extract Sm^{3+}, leaving Eu^{2+} in the aqueous phase.

This promising and highly efficient separation method for samarium and europium was further developed towards an extraction chromatography method. In this approach, [A336][NO_3] was immobilized on a solid support, *i.e.* a *supported ionic liquid phase* (SILP). Extraction chromatography already proved to be very useful in radiochemical processing of medical radionuclides because of

its easiness of operation, its ability to achieve high separation efficiencies and its automation possibilities. Moreover, any processing problems caused by the high viscosity of neat [A336][NO_3] could be avoided. Based on the solvent extraction step, Sm^{3+} was extracted to the ionic liquid layer of the SILP when using a concentrated nitrate salt solution as mobile phase. In these conditions, Eu^{2+} was not retained by the SILP when passing through the column material. Sm^{3+} could be easily removed from the SILP material by the use of water, reducing the salt concentration in the system. This way, the samarium-rich fraction contains less nitrate salts, which is beneficial for further radiopharmaceutical processing.

Beknopte samenvatting

Radiolanthaniden worden steeds belangrijker in nucleaire geneeskunde vanwege hun aantrekkelijke vervaleigenschappen. Het uitzenden van β^- deeltjes met een energie die geschikt is om kwaadaardige tumorcellen te vernietigen is erg waardevol in kankertherapie. Het uitzenden van γ fotonen kan gebruikt worden voor diagnostische doeleinden. Sommige radiolanthaniden kunnen zelfs gebruikt worden voor beide doeleinden tegelijkertijd (theranostiek), waardoor het mogelijk wordt om de doeltreffendheid van de therapie *in situ* op te volgen. Daarom hebben radiolanthaniden een hoog potentiëel om ingezet te worden in een brede waaier aan medische toepassingen.

Door de zeer gelijkaardige chemische eigenschappen doorheen de lanthanidenreeks kunnen verschillende radiolanthaniden gelinkt worden aan eenzelfde dragermolecule. Dit maakt hen gemakkelijk uitwisselbaar, waardoor radiofarmaceutica op maat gemaakt kunnen worden voor een specifiek doel. Selectie van de meest geschikte energie uit deeljesemissie voor therapie is belangrijk om stralingsschade aan gezond weefsel en vitale organen zo laag als mogelijk te houden. Op deze manier kan een hoge geabsorbeerde dosis voor de tumor ten opzichte van het normaal weefsel verzekerd worden. Echter, de zeer gelijkaardige chemische eigenschappen betekenen ook dat scheiding van twee lanthaniden een erg grote uitdaging is. Dit is zeker het geval voor twee naburige lanthaniden, en is een van de grootste uitdagingen in de productie van radiolanthaniden voor medische toepassingen.

Radiolanthaniden worden het meest efficiënt geproduceerd in een nucleaire onderzoeksreactor *via* (n, γ) bestraling, hetgeen inhoudt dat verrijkt doelwitmateriaal gebombardeerd wordt met neutronen. Afhankelijk van de gevolgde productiestrategie, is het bekomen radiolanthanide drager-toegevoegd of niet-drager-toegevoegd. Het product resulterend uit beide productiestrategieën kan een opzuiveringsstap vereisen alvorens gebruikt te kunnen worden in een radiofarmaceutisch product. Afzondering van niet-drager-toegevoegde radiolanthaniden van hun dragermateriaal resulteert in een product met

hoge specifieke activiteit, hetgeen erg geschikt is voor gerichte radiotherapie. Radiolanthaniden die drager-toegevoegd geproduceerd zijn kunnen daarentegen niet van hun dragermateriaal afgescheiden worden. Ze zullen dus slechts een beperkte specifieke activiteit bevatten. Daarom komen ze niet in aanmerking voor gerichte radiotherapie, maar worden ze erg bruikbaar bevonden in palliatieve behandeling van botkanker en in bestrijding van beenderpijn en gewrichtsontstekingen. Bovendien kunnen ze ook toegepast worden in medische beeldvorming. Tijdens neutronenbestralingen kunnen echter langlevende radionuclidische onzuiverheden gevormd worden, waardoor het medisch gebruik van drager-toegevoegde radiolanthaniden verhinderd wordt. Dit heeft een beperkte houdbaarheidstermijn tot gevolg. Het niveau van achtergrondstraling voor de patiënt moet immers beperkt blijven, en wordt strikt gereguleerd. Bijgevolg is een zuiveringsstap voor deze radiolanthaniden vereist om een geschikte radionuclidische zuiverheid te bekomen.

Het gebruik van een bepaald radiofarmaceutisch product in nucleaire geneeskunde is erg afhankelijk van de beschikbaarheid van het radiolanthanide, de vervaleigenschappen en de bereikbare specifieke activiteit ervan. Om die reden wordt veel onderzoek gedaan naar het vinden van geschikte scheidings- en zuiveringsmethoden voor radiolanthaniden die geproduceerd worden in een nucleaire onderzoeksreactor. Een uitgebreid overzicht voor medische radiolanthaniden geproduceerd in een nucleaire onderzoeksreactor wordt hier weergegeven als onderdeel van dit onderzoeksproject.

In dit doctoraatsproefschrift wordt een haalbaarheidsstudie voorgesteld voor de scheiding van samarium en europium richting de zuivering van medisch ^{153}Sm. In de nucleaire geneeskunde kan ^{153}Sm goed gebruikt worden vanwege de gunstige vervaleigenschappen, *i.e.* een erg handelbare fysische halfwaardetijd van 46.284 h en het uitzenden van β^- deeltjes met een gemiddelde energie van 233 keV, dewelke bruikbaar is voor radiotherapie. Het gelijktijdige uitzenden van γ fotonen van 103.2 keV kan gebruikt worden voor medische beeldvorming, waardoor ^{153}Sm geschikt is voor diagnose en theranostiek. ^{153}Sm wordt drager-toegevoegd geproduceerd in een nucleaire onderzoeksreactor. Langlevende ^{154}Eu onzuiverheden worden echter gelijktijdig geproduceerd, waardoor het gebruik van ^{153}Sm radiofarmaceutica beperkt is.

De scheiding van Sm^{3+} en Eu^{3+} is erg uitdagend vanwege hun erg gelijkaardige chemische eigenschappen. Een verandering in valentietoestand brengt echter een significante wijziging in chemische eigenschappen teweeg, hetgeen leidt tot mogelijkheden voor efficiëntere scheidingsmethoden. Reductie van Eu^{3+} naar de tweewaardige toestand is het gemakkelijkste te bereiken in de lanthanidenreeks vanwege de gunstige elektronenconfiguratie. Reductie van Eu^{3+} was reeds goed bestudeerd in reductie-stabiele milieu, zoals waterige chloride-oplossingen. In dit proefschrift wordt echter aangetoond dat de reductie van Eu^{3+} ook mogelijk is in

waterig nitraatmilieu, en dat Eu^{2+} relatief stabiel blijft in dit milieu. Niettemin zijn hoge nitraatzoutconcentraties nodig om deze reductie en stabiliteit te bekomen. Deze hoge nitraatzoutconcentraties bleken ook een groot voordeel in de scheidingsstap, waar gebruik gemaakt kan worden van het uitzoutingsprincipe. Zo werd een solventextractiemethode gebaseerd op het gebruik van Aliquat 336 nitraat ([A336][NO_3]) als organische fase ontwikkeld, waarbij Sm^{3+} selectief geëxtraheerd werd. Eu^{2+} werd achtergelaten in de waterige fase.

Deze veelbelovende en uiterst efficiënte scheidingsmethode voor samarium en europium werd verder ontwikkeld richting een extractiechromatografische methode. In deze aanpak werd [A336][NO_3] geïmmobiliseerd op een vaste drager, *i.e.* een *gedragen ionische vloeistoffase* (SILP). Extractiechromatografie bewees reeds erg nuttig te zijn in radiochemische verwerking van medische radionuclide vanwege het gebruiksgemak, het vermogen om hoge scheidingsefficiënties te bekomen en de mogelijkheid tot automatisatie. Bovendien werden mogelijke procesmoeilijkheden veroorzaakt door de hoge viscositeit van onverdund [A336][NO_3] vermeden. Gebaseerd op de solventextractiestap, werd Sm^{3+} geëxtraheerd naar de ionische vloeistoflaag van de SILP wanneer een geconcentreerde nitraatzoutoplossing gebruikt werd als mobiele fase. In deze omstandigheden werd Eu^{2+} niet weerhouden door de SILP wanneer deze door het kolommateriaal passeerde. Sm^{3+} kon nadien gemakkelijk verwijderd worden van het SILP materiaal door gebruik te maken van water, waardoor de zoutconcentratie in het systeem werd verminderd. Door deze aanpak bevat de fractie rijk aan samarium minder nitraatzouten, hetgeen voordelig is voor verdere radiofarmaceutische verwerking.

Outline

This PhD dissertation is a summary of four years of research on the development of a purification method for medical radionuclides, in particular radiolanthanides produced in a nuclear research reactor. The research in this dissertation comprises the gradual development of a novel separation method for the two adjacent lathanides samarium and europium in scope of the removal of long-lived ^{154}Eu from the medical ^{153}Sm radionuclide. The ability to purify the medical ^{153}Sm radionuclide is beneficial from both a medical and economical perspective. Different stages in the purification approach were investigated in detail to arrive at a method that makes use of supported ionic liquid phases in an extraction chromatography setup.

The four major chapters that are included in this dissertation are based on manuscripts that have been published or are currently being peer-reviewed for publication in a scientific journal.

Chapter 1 includes a comprehensive literature study regarding radiochemical processing of nuclear-reactor-produced radiolanthanides for medical applications. This chapter provides essential background information needed to understand the basic principles of medical radiolanthanide production, clarifies the challenges in (radio-)lanthanide separation, and outlines the context in which the research project was performed. Different pathways to produce radiolanthanides are explained, with a strong focus on the production by neutron irradiation in medium to high flux nuclear reactors. Additionally, the different emission possibilities involved in the decay of radiolanthanides and how these emissions can be used in nuclear medicine are explained. Several radiolanthanides find their application in nuclear medicine because of their favorable decay characteristics, the most important ones being ^{143}Pr, ^{149}Pm, ^{153}Sm, ^{165}Dy, ^{161}Tb, ^{166}Ho, ^{169}Er, ^{170}Tm and ^{177}Lu. Production pathways, specific decay characteristics, examples of their (possible) application in medicine and a variety of current-state purification approaches for these medical radiolanthanides are discussed. For completeness, ^{47}Sc and ^{90}Y are described briefly as well, because the chemical

properties of scandium and yttrium are very similar to those of the lanthanides.

The objectives set with regard of development of a novel purification method for the purification of medical radiolanthanides are comprised in Chapter 2. The research strategy followed is based on these objectives. The experiments conducted and results obtained within the different research steps are discussed in the following three chapters.

Chapter 3 is dedicated to the reduction of Eu^{3+} to Eu^{2+} using chemical and electrochemical reduction techniques. Reduction of Eu^{3+} in reduction-stable media is already well-described in the literature. However, it was found that Eu^{3+} can also be efficiently reduced in aqueous media containing high nitrate salt concentrations throughout this research project. An in-depth study was performed using different analysis methods in an attempt to characterize the reduction process, and to achieve more insights in the stability of Eu^{2+} in these media.

Chapter 4 comprises a study that was dedicated to finding an efficient separation process for Sm^{3+} and Eu^{2+} based on a *solvent extraction* (SX) method. The organic phase in these SX studies consisted of a bulk *ionic liquid* (IL), more specifically Aliquat 336 nitrate. Two different approaches were investigated. In a first approach, it was attempted to selectively extract Eu^{2+} to the organic phase by making use of a *crown ether* (CE), a size-selective extractant. This way, a common separation strategy for Sr^{2+}, an alkaline earth ion that shows similarities to Eu^{2+}, was assessed. A second approach made use of the basic extractant properties of the quaternary ammonium ionic liquid itself, selectively extracting Sm^{3+} at high salt concentrations. Different extraction parameters were investigated to be able to select the most efficient separation system. Both chloride and nitrate aqueous feed solutions are considered.

Extraction chromatography poses several important advantages in comparison with solvent extraction, including its easiness of operation, its automation possibilities and its possibility to treat low amounts of material. For these reasons, different extraction chromatography methods are already well-established in radiochemistry, especially in the field of medical radionuclide purification. For this reason, the most promising SX method was converted into an extraction chromatography method, and is presented in Chapter 5. The bulk ionic liquid of the SX method was impregnated onto an inert polymeric support, forming a *supported ionic liquid phase* (SILP). The self-made SILP was fully characterized using various analysis techniques. Its extraction performances for Sm^{3+} were explored in batch extraction experiments, and were compared to the extraction performance of TEVA particles, a commercially available equivalent. The best performing SILP particles were tested for the separation of Sm^{3+} and Eu^{2+} by extraction chromatography.

Conclusions and an outlook to future research possibilities are listed in Chapter 6 and Chapter 7, respectively.

Abbreviations

α-HIBA	α-Hydroxyisobutyric acid
A336-XAD	[A336][NO_3] impregnated onto Amberlite XAD-16N solid support
[A336][NO_3]	Aliquat 336 nitrate, tricaprylmethylammonium nitrate
BET	Brunauer-Emmet-Teller method
BFCA	Bifunctional chelating agent
BJT	Barret-Joyner-Halenda method
BR2	Belgian Reactor 2
CE	Counter electrode (in electrochemistry)
CE	Crown ether (in extraction chemistry)
CHN	Carbon-hydrogen-nitrogen
CHON	Carbon-hydrogen-oxygen-nitrogen
CN	Coordination number
DCH18C6	Dicyclohexano-18-crown-6
DGA	Diglycolamide
DNA	Deoxyribonucleic acid
DO3A	1,4,7,10-Tetraazacyclododecane-1,4,7-triacetic acid
DOTA	1,4,7,10-Tetraazacyclododecane-1,4,7,10-tetraacetic acid
DOTMP	1,4,7,10-Tetraazacyclododecane-1,4,7,10-tetramethyl phosphonic acid (also DOTP)
DTPA	Diethylenetriamine-pentaacetic acid
DUBBLE	Dutch-Belgian Beamline
EDTMP	Ethylene diamine tetra(methylene phosphonate)
EMA	European Medicine Agency
ESRF	European Synchrotron Radiation Facility
EXAFS	Extended X-ray absorption fine structure
FDA	Food and Drug Administration
FTIR	Fourier-transform infra red
HA	Acidic extractant
HDEHP	Di-(2-ethylhexyl) phosphoric acid (also DEHPA or D2EHPA)
HEH[EHP]	2-Ethylhexyl phosphonic acid mono-2-ethylhexyl ester

HLLW	High-level liquid waste
HPIC	High-performance ion chromatography
HPLC	High-performance liquid chromatography
HSAB	Hard Soft Acid Base
IAEA	International Atomic Energy Agency
ICP-OES	Inductively coupled plasma - optical emission spectrometry
IL	Ionic liquid
LET	Linear energy transfer
LMCT	Ligand-to-metal charge transfer
NMR	Nuclear magnetic resonance
MRI	Magnetic resonance imaging
MSB	Magnetic susceptibility balance
NOTA	1,4,7-Triazacyclononane-1,4,7-triacetic acid
NSF	Nephrogenic systemic fibrosis
PET	Positron emission tomography
RBE	Relative biological effect
RE	Reference electrode
REE	Rare earth element
SCK•CEN	Studiecentrum voor Kernenergie•Centre d'Etude de l'Energy Nucléaire (Belgian Nuclear Research Center)
SEM	Scanning electron microscopy
SHE	Standard hydrogen electrode
SILP	Supported ionic liquid phase
SIRT	Selective internal radiotherapy
SPECT	Single-photon emission computed tomography
SS	Solid support
SX	Solvent extraction
TEVA	Tetravalent actinide
TBP	Tri-*n*-butylphosphate
TXRF	Total reflection X-ray fluorescence
UV	Ultraviolet
VIS	Visible
WE	Working electrode
WHO	World Health Organization
XANES	X-ray absorption near edge structure

Nomenclature

α	Separation factor (in extraction chemistry)
α	Alpha particle: $^{4}_{2}\mathrm{He}$ (in radiochemistry)
A	Atomic mass number
A	Activity (in radiochemistry)
β^-	Beta particle: electron, e^-
β	Complex formation constant
BV	Bed volume
C_0^*	Bulk concentration of the redox sensitive species
D	Distribution ratio (in extraction chemistry)
D	Diffusion coefficient (in electrochemistry)
D_w	Weight distribution ratio
$\%E$	Fraction extracted
e^-	Electron
E^0	Standard reduction potential
$\Delta E^0_{\mathrm{cell}}$	Cell potential
$E_{P,a}$	Anodic peak potential
$E_{P,c}$	Cathodic peak potential
ΔE_P	Peak separation potential
E_n	Neutron energy
η	Viscosity (dynamic)
H	Induced magnetic field
h	Fraction of isotopes relevant for neutron capture
ΔH_{hydr}	Hydration energy
I	Intensity of magnetism induced in a substance
IL:SS	Ionic liquid-to-solid support mass ratio
i_P	Peak current
j_P	Peak current density
$\mathrm{k_B}$	Boltzmann's constant
λ	Decay constant of a radionuclide, $\lambda = ln2/t_{1/2}$
Ln^{3+}	Trivalent lanthanide (or lanthanoid) ion

μ	Effective magnetic moment
m	Mass
M^{n+}	Any metal ion with charge $n+$
N	Number of neutrons
N	Number of lanthanide target atoms in the target material before irradiation (in radiochemistry)
n	Neutron
n	Number of electrons (in electrochemistry)
(n, γ)	Neutron capture reaction, followed by γ emission
(n, p)	Neutron capture reaction, followed by proton emission
$(n, fission)$	Neutron capture reaction, followed by a fission reaction
$\overline{\nu}_e$	Anti-neutrino
$\varnothing$	Diameter
O:A	Organic-to-aqueous volume ratio
ρ	Density
q	Amount of metal ion M^{n+} extracted to the SILP per gram of dry SILP
R	Resolution
r	Radius
σ_{th}	Neutron cross section for thermal neutrons
υ	Linear scan rate
ϕ_{th}	Thermal neutron flux
T	Temperature
t	Time
$t_{1/2}$	Half-life
χ	Magnetic susceptibility
χ_V	Volume magnetic susceptibility
Z	Atomic number

Contents

List of Figures

List of Tables

Chapter 1

Introduction

This chapter is based on the published review article:

Michiel Van de Voorde, Karen Van Hecke, Thomas Cardinaels and Koen Binnemans, Coordination Chemistry Reviews, 2019, 382, 103–125

The text might contain minor adjustments to the original publication.

The literature search and compilation of the manuscript were performed by the author of this thesis.

1.1 Abstract

Several radiolanthanides find their application in nuclear medicine because of their favorable decay properties, the most important ones being ^{143}Pr, ^{149}Pm, ^{153}Sm, ^{165}Dy, ^{161}Tb, ^{166}Ho, ^{169}Er, ^{170}Tm and ^{177}Lu. These radiolanthanides can be efficiently produced *via* neutron irradiation in a high-flux nuclear research reactor. Radiochemical processing of the irradiated target is required to obtain the required purity or to remove redundant target material. Long-lived impurities can be removed to extend the expiration time of carrier-added radiolanthanides, whereas non-carrier-added radiolanthanides with high radionuclidic purity and high specific activities can be obtained for targeted radiotherapy. Transport and distribution criteria might become more flexible, helping to safeguard the supply of radiolanthanides for medical purposes. Valuable and expensive target material can be regenerated after separation of the medical radiolanthanide. Different radiochemical separation processes are discussed which are able to separate two adjacent lanthanides, with a focus on those techniques making use of the underlying coordination chemistry.

1.2 Introduction

The use of radionuclides in medicine for diagnosis and treatment of various diseases, like cancers, cardiovascular and brain disorders, is already well established [1]. According to the World Nuclear Association and the European Commission, over 10,000 hospitals worldwide use radionuclides, diagnosing and treating about 30–50 million patients every year [2, 3].

Technetium-99m (^{99m}Tc) is by far the most widely used and best known (diagnostic) isotope, but many other radionuclides are being applied in nuclear medicine for very specific diagnostic studies and treatment of different diseases [4, 5]. Amongst them the radiolanthanides, which are already being applied routinely in nuclear medicine nowadays [6, 7]. Their use will increase further as new targeted therapies are being developed, resulting in an increased demand for therapeutic radionuclides. If assumed that only about 1 % of the patients diagnosed by nuclear medicine procedures require targeted radiotherapy, it can be estimated that 300,000–500,000 patients can benefit annually from radionuclide therapy worldwide [8]. Radioactivity levels required for targeted radiotherapy vary widely depending on the application and the radionuclide being used, but overall it is anticipated that thousands of terabecquerels (*i.e.* a few millions of Curies) of radionuclides are needed to treat the estimated number of patients. It is highly probable that this number will increase sharply considering the increasing number of patients suffering from various types of cancer, and new and efficacious products are being developed. Therefore, different approaches are needed to meet the demand for medical radionuclides at a reasonable cost [8, 9].

In this chapter, the different pathways are discussed to produce and purify radiolanthanides for medical applications. Emphasis is put on those radiolanthanides that are of highest medical relevance and are produced in a nuclear research reactor, *i.e.* ^{143}Pr, ^{149}Pm, ^{153}Sm, ^{165}Dy, ^{161}Tb, ^{166}Ho, ^{169}Er, ^{170}Tm and ^{177}Lu. In addition, production methods for ^{47}Sc and ^{90}Y using a nuclear reactor are described briefly as well, because the chemical properties of scandium and yttrium are very similar to those of the lanthanides.

Nuclear research reactors are commonly used to produce medical radiolanthanides using a high thermal neutron flux to ensure high yield and high specific activity. In some production pathways, direct use of the irradiated target material is not possible. For example, large quantities of the remaining target material in the non-carrier-added production method lead to a lower specific activity and result in a non-selective coordination of the radionuclide of interest (*e.g.* ^{160}Gd in ^{161}Tb), hampering its use. Another example is the presence of harmful side products, like long-lived isotopes (*e.g.* ^{154}Eu in ^{153}Sm), which have

to be removed prior to use, even when present in low quantities. National and international organizations (*e.g.* FDA, EMA, IAEA, WHO) that are responsible for well-being of the treated patients and application of radionuclides have put strict limits for different kinds of impurities.

Appropriate radiochemical purification processes are implemented to yield a radionuclide of suitable purity and specific activity. Removal of long-lived radionuclidic impurities or redundant target material leads to an increased application time of the radionuclide for medical use, implying an increased availability of medical radionuclides to meet clinical demands. Removal of long-lived impurities will reduce the background radioactivity of the treated patient significantly and disposal of residuals at hospitals will be facilitated. Waste containing short-lived isotopes can be treated conveniently *via* decay storage only. Valuable and expensive highly enriched target material can be used more efficiently by increasing irradiation times. Target material of non-carrier-added produced isotopes can be recycled after removal of the radionuclides for medical use. Expired radiopharmaceutical products that were produced *via* the carrier-added production method can be looked at as new resources for production of highly enriched target materials. This way, the linear production method can be converted into a (semi-)circular one, and the cost of radionuclide production can be reduced significantly.

The critical challenge of producing medical radionuclides using nuclear reactors is reliability of supply. Because of their relatively short half-life ($t_{1/2}$), transportation and distribution of medical radionuclides is not straightforward. Regions that are not in close proximity of a production facility might be in danger of not having access to radionuclides for medical purposes. Additionally, increased maintenance requirements of aging reactors, phasing out of old reactors and unexpected outages might lead to a supply risk. Transport criteria might become more flexible by purifying the medical radionuclides, by which research reactors producing medical radionuclides can back up each other more easily. This way, global radionuclide supply can be assured. Thus, purification of radionuclides for medical use can be considered to be beneficial for both medical and economic reasons.

The main focus in this chapter is on those purification techniques that make use of underlying coordination chemistry, *i.e.* the ones based on liquid-liquid extraction, ion-exchange and extraction chromatography. Synthesis and application of chelating agents to coordinate the radionuclides for radiopharmaceutical use is beyond the scope of this review as this is already described comprehensively elsewhere [9–17].

1.3 Production pathways of radiolanthanides

In general, radiolanthanides can be produced efficiently *via* two major methods of production. In the first production method, target material consisting of stable lanthanides is irradiated by a thermal or epithermal neutron flux. These neutron fluxes are associated with the nuclear fission reaction in the nuclear reactor. Only a few countries in the world are able to produce medical radiolanthanides *via* this highly efficient process because of the need of a nuclear research reactor. A total of 97 research reactors (planned, under construction, operational and temporary shutdown) distributed over 44 member states are able to perform isotope production according to the IAEA Research Reactor Database [18]. Not all of them are able to produce medical radiolanthanides as medium to high thermal neutron fluxes are required. A non-limiting list of the most important medium- and high-flux isotope-producing research reactors is presented in Table 1.1.

Despite the small number of suitable operational nuclear reactors, reactor-produced radionuclides represent a large percentage of the total consumption of radionuclides [19, 20]. Key advantages include the ability to irradiate a high volume, the possibility to irradiate several samples simultaneously and the

Table 1.1: Non-limiting list of major medium-flux ($10^{14} - 10^{15}\,\mathrm{n\,cm^{-2}\,s^{-1}}$) and high-flux ($> 10^{15}\,\mathrm{n\,cm^{-2}\,s^{-1}}$) research reactors that are being used, or were recently being used for the production of medical radionuclides. The French OSIRIS reactor and the Canadian NRU reactor were taken permanently out of operation since 2015 and 2016 (back up until March 2018), respectively. (Source: IAEA Research Reactor Database).

Reactor	Country	Max. thermal neutron flux ($\times 10^{14}\,\mathrm{n\,cm^{-2}\,s^{-1}}$)	Power (MW)	First criticality
SM-3	Russia	50	100	1961
HFIR	United States	25	85	1965
BR2	Belgium	10	100	1961
FRM-II	Germany	8	20	2004
MURR	United States	6	10	1966
HANARO	Republic of Korea	4.5	30	1995
NRU[(1)]	Canada	4	135	1957
MARIA	Poland	3.5	30	1974
HFR	The Netherlands	2.7	45	1961
SAFARI-1	South Africa	2.4	20	1965
OSIRIS[(1)]	France	2	70	1966
OPAL	Australia	2	20	2006
LVR-15	Czech Republic	1.5	10	1957

[(1)] Reactor is permanently out of operation.

possibility to produce a wide variety of radionuclides, leading to a favorable production economy. The production of radiolanthanides in a nuclear reactor will be discussed in more detail in Section 1.4.

In the second production method, radiolanthanides are generated by a particle accelerator (cyclotron) *via* direct and spallation reactions. Different types of particles, like protons, deuterons and α-particles, can be accelerated in cyclotrons to bombard targets of interest. Radionuclides produced *via* cyclotrons are usually rather unstable because of the addition of heavier particles, resulting in radionuclides with short half-lives. Therefore, on site production of these medical radionuclides in hospitals is often required. Worldwide, more than 1200 cyclotrons are in use to produce medical radionuclides, making use of more accessible equipment. More details about cyclotron-produced radiolanthanides can be found elsewhere in literature [1].

Nuclide generators are often mentioned as a third production method. The longer-lived parent nuclide is produced in a nuclear research reactor *via* neutron irradiation, as described in the first production method. The shorter-lived medical radionuclide accumulates in the generator after decay of the parent nuclide, and can be chemically separated afterwards. In fact, the nuclide generator system can be considered as an extension of the production method using high thermal neutron fluxes, producing non-carrier-added radiolanthanides. Therefore, the working principle of the nuclide generator will be discussed in greater detail elsewhere in this chapter (Section 1.6).

1.4 Reactor-produced radiolanthanides

Several radiolanthanides can be produced very efficiently by irradiating a target material containing isotopically enriched stable lanthanide isotopes with a high thermal neutron flux (Table 2) [5, 8, 9, 19–29]. Commonly, the availability of a high thermal neutron flux of *ca.* $10^{15}\,\mathrm{n\,cm^{-2}\,s^{-1}}$ in a nuclear research reactor allows routine production of medical radionuclides with high activities. Thermal neutrons have an energy (E_n) of about 0.025 eV. Also epithermal neutrons, *i.e.* neutrons with an energy higher than thermal neutrons (0.025 eV) to a few hundred eV, are present upon neutron irradiation. The absorption of an epithermal neutron might contribute to the (n,γ) reaction for the production of the targeted radionuclide. Because of their higher energy, absorption of epithermal neutrons might sometimes result in the emission of a proton (*i.e.* (n,p) reaction). In general, neutron cross-sections for epithermal neutrons are low, and therefore result in low production yields only.

The neutrons are captured by the stable lanthanide isotopes, resulting in the nuclear reaction ${}^{A}_{Z}Ln(n,\gamma){}^{A+1}_{Z}Ln$ (in short: (n,γ)), whereby a different isotope of the same lanthanide is formed. The obtained radiolanthanide remains carrier-added (ca) because the radiolanthanide cannot be separated from the target material. Only separation of other, long-lived impurities that were formed during the irradiation process can be performed. Sometimes a double neutron capture is required to arrive at the desired or intermediate radiolanthanide, like ^{164}Dy for the production of ^{166}Dy as a parent nuclide for ^{166}Ho (see Section 1.6.6), resulting in the ${}^{A}_{Z}Ln(n,\gamma){}^{A+1}_{Z}Ln(n,\gamma){}^{A+2}_{Z}Ln$ nuclear reaction (in short: $(2n,\gamma)$). In several cases, the neutron capture reaction results in a very short-lived radiolanthanide, which decays *via* β^- to obtain the radiolanthanide of interest, *i.e.* ${}^{A}_{Z}Ln(n,\gamma){}^{A+1}_{Z}Ln(\beta^-){}^{A+1}_{Z+1}Ln$ (in short: $(n,\gamma) \rightarrow \beta^-$)). A radionuclide that is isotonic to the targeted nucleus is formed. This way, non-carrier-added (nca) radiolanthanides can be obtained, as it is possible to separate these radiolanthanides from the target material. In some irradiation strategies a longer lived parent radionuclide (*e.g.* ^{166}Dy) is produced, which subsequently decays into the shorter-lived medical radionuclide (*e.g.* ^{166}Ho). This latter one accumulates over time after irradiation, and can be chemically separated from the parent radionuclide. A so-called radionuclide generator system is established this way (see Section 1.6).

Important for both techniques is to start with highly enriched target material of high purity, usually the oxide or an inorganic salt, consisting of stable lanthanide isotopes. Highly enriched target materials can be produced *via* electromagnetic isotope separation [30]. The lanthanide isotopes used as target material should possess sufficiently large neutron capture cross-sections to achieve a product with high yield, high specific activity and high isotopic purity. Additionally, the production of radionuclides is highly dependent on the irradiation time, the physical half-lives of the isotopes and the applied thermal neutron flux. The activity yield of the (n,γ) isotope production process can be determined according to Eq. 1.1.

$$A = [h \cdot N] \cdot \sigma_{th} \cdot \phi_{th} \cdot (1 - e^{-\lambda t}) \tag{1.1}$$

In this equation, N represents the number of lanthanide target atoms in the target material before irradiation, h represents the fraction of the isotope relevant for neutron capture, A represents the activity of the produced radiolanthanide atoms (in Bq = s^{-1}), σ_{th} represents the neutron capture cross-section (in cm^2, with 1 barn = 10^{-28} m^2) for thermal neutrons (*i.e.* the probability to absorb neutrons of *ca.* 0.025 eV), ϕ_{th} represents the thermal neutron flux (in n cm^{-2} s^{-1}) and $(1 - e^{-\lambda t})$ represents the combined influence of the irradiation time and

decay. In the latter term, λ denotes the decay constant of the radionuclide ($\lambda = ln2/t_{1/2}$) and t denotes the irradiation time.

Eq. 1.1 clearly shows the exponential nature of the radiolanthanide production yield and specific activity while the target is being irradiated. The production reaches saturation in case the irradiation time becomes much longer compared to the half-life ($t_{1/2}$) of the radiolanthanide. A plateau region is established upon saturation. This saturation is governed by the neutron flux in the reactor. Irradiating the target material beyond the saturation level will not lead to the production of more radiolanthanides of interest. On the contrary, the production of undesired, long-lived side-products will only be favored with longer irradiation times, as will be shown in an example later in this review. It must be noted that the yield and activity generated by irradiation of the target can be different in reality from the ones calculated [28]. Several other factors influence the production, including self-shielding in the target, flux variation in the reactor, destruction of the product isotope due to subsequent neutron capture, flux depression due to adjacent samples with high neutron absorption *etc.*

Neutron irradiation of a heavy nucleus, such as ^{235}U, is another possibly to produce radiolanthanides in a nuclear reactor [9, 23]. The bombardment of neutrons induces a fission reaction ($n, fission$), leading to a spectrum of radiolanthanides, with a maximum yield in the distribution of nuclide mass at about 140. Chemical separation of these radiolanthanides from the target material and other fission products is possible, but they are not isotopically pure, because several isotopes of each lanthanide are produced during the fission process. Therefore, this production route is not the most favorable one, and will not be further discussed in this chapter.

The ability of reaching high specific activities of the resulting radionuclides remains a key advantage of the production method using a nuclear reactor. The specific activity represents the ratio of the radiolanthanide radioactivity to the total mass of all isotopes of that lanthanide present in the irradiated target, and is expressed in $\mathrm{Bq\,g^{-1}}$ (the old unit $\mathrm{Ci\,g^{-1}}$ is still frequently used in medicine).

Besides the production of radiolanthanides with high specific activity and high efficiency, isotope production using a nuclear reactor allows to produce relatively large amounts of different radiolanthanides simultaneously during the same irradiation campaign. Target materials for routine isotope production are loaded into suitable irradiation capsules. Most often, standardized cold-welded aluminium capsules with an inner graphite or aluminium cylinder or quartz ampoule are being used. The irradiation capsules are placed in designated positions within the reactor core *via* a pneumatic or hydraulic mechanism. Depending on the reactor core configuration, some irradiation devices allow the loading and unloading of irradiated targets during the operation of the reactor,

Table 1.2: Characteristics of most important reactor-produced β^- emitting radiolanthanides with accompanying γ emission studied for radionuclide therapy. Thermal neutron cross-sections are given for the target materials, except for the ^{164}Dy$(2n,\gamma)$ reaction where the thermal neutron cross-section of ^{165}Dy intermediate is given. In addition, data for ^{47}Sc and ^{90}Y are given as well. Data obtained from JEF-3.1 and ENDF/B-VII databases (at Nucleonica).

Radionuclide	Half-life	Major production route[(1)]	σ_{th} (barn)	$E_{\beta,max}$ (keV)	$E_{\gamma,main}$ (keV)(%*ab)
^{143}Pr	13.6 d	^{142}Ce$(n,\gamma)^{143}$Ce $\rightarrow \beta^-$	0.95	933	742 (38.5)
^{149}Pm	2.21 d	^{148}Nd$(n,\gamma)^{149}$Nd$\rightarrow \beta^-$	2.503	1071	285 (2.8)
^{153}Sm	1.95 d	^{152}Sm(n,γ)	206.2	808	103.2 (28.3)
^{161}Tb	6.91 d	^{160}Gd$(n,\gamma)^{161}$Gd$\rightarrow \beta^-$	1.5	593	74.6 (5.8)
^{165}Dy	2.33 h	^{164}Dy(n,γ)	2720	1286	94.7 (3.6)
^{166}Ho	1.12 d	^{165}Ho(n,γ)	61.2	1854	80.6 (6.2)
		^{164}Dy$(2n,\gamma)^{166}$Dy$\rightarrow \beta^-$	3900		
^{169}Er	9.40 d	^{168}Er(n,γ)	1.28	350	84 (0.16)
^{170}Tm	128.4 d	^{169}Tm(n,γ)	109	968	84 (3.26)
^{177}Lu	6.65 d	^{176}Yb$(n,\gamma)^{177}$Yb$\rightarrow \beta^-$	2.85	498	208.4 (11.1)
		^{176}Lu(n,γ)	2090		
^{47}Sc	3.35 d	^{46}Ca$(n,\gamma)^{47}$Ca$\rightarrow \beta^-$	0.7405	600	159.4 (68)
		^{47}Ti$(n,p)^{47}$Sc			
^{90}Y	2.67 d	^{89}Y$(n,\gamma)^{90}$Y	1.287	2280	1760.7 (0.017)
		^{90}Zr$(n,p)^{90}$Y			

[(1)] For simplicity, the simultaneous emission of gamma particles and neutrinos during β^- decay were omitted in the reaction equations.

leading to a high flexibility and ability to establish a tailor-made production process for each radionuclide. Optimum irradiation parameters can be applied this way to ensure the highest quality and most efficient production process. After irradiation, the target materials are temporary stored for cooling, after which they pass through a hot cell for de-canning and loading into suitable shipping containers. An example of routine medical radionuclide production can be found in the publication by Ponsard, which highlights the use of the BR2 reactor, one of the major production facilities for medical radionuclides [20, 31].

1.5 Medical radiolanthanides

Over the last decades, the number of radiolanthanides being studied for targeted radionuclide therapy (endoradiotherapy)increased significantly [6, 7, 9, 32–34].

Endoradiotherapy can be described as a systemic approach where a radiolabeled compound can deliver a cytotoxic level of ionizing radiation to the targeted disease site on molecular or cellular level. Thus, the radionuclide is carried by a molecule to cancer cells exactly where it is needed. Once the molecule has reached the right location (*e.g.* specific receptor, core) in the tumor cell, the radionuclide destroys its DNA *via* the emission of high linear energy transfer (LET) particles (*e.g.* α particles, Auger electrons) and lower LET particles (*e.g.* β^- particles). The carrier molecule ensures that the radionuclide accumulates fast at the site of the diseased cells after being administered to the patient. This way, identification and localization of abnormalities is relatively easy and damage to healthy cells remains limited.

Radiolanthanides are well suitable to be used in nuclear medicine because of their diverse decay characteristics, *i.e.* the use of a different radiolanthanide results in the emission of different particles, with different energies and half-lives. Chemically, lanthanides have the ability to replace Ca^{2+} in biological systems such as enzymes, proteins, cells and cytoplasm. Additionally, trivalent lanthanides possess very similar chemical properties, leading to very similar coordination chemistry. This provides a high flexibility to select the most suitable radiolanthanide to coordinate to a carrier molecule. If needed, the radiolanthanides are interchangeable in the molecular carrier to meet the required decay characteristics in accordance with their application. However, the very similar chemical properties also lead to a more difficult separation of two lanthanides, especially of adjacent lanthanides in the Periodic Table. Looking at the production routes (see Section 1.3), the irradiated target material mainly exists of a mixture of adjacent lanthanides of which the chemical properties are extremely similar.

Isolation or purification of the radiolanthanide might be needed before being applied as radiopharmaceutical since unwanted impurities should not be administered to a patient. After irradiation, high amounts of redundant target material remain in the end product. This leads to inefficient coordination and reduced specific activity of the radiolanthanide of interest. Moreover, highly pure radiolanthanides are needed for radiolabeling, for example with antibodies or nanobodies, because of the limited available receptors in the cell. Long-lived sideproducts can be formed upon neutron capture in the carrier-added production process, causing the radiopharmaceutical to expire early as the level of these long-lived side-products that can be administered to a patient is strictly regulated.

A radiopharmaceutical product consists of two major components, *i.e.* a radionuclide (the radiolanthanide in this case) and a carrier system or targeting vector (*e.g.* peptides, antibodies, chelators and nanobodies). The latter one directs the radionuclide to the targeted disease site (receptor), where its radiation

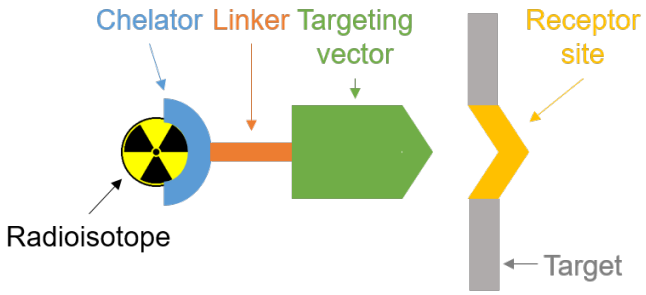

Figure 1.1: Schematic representation of a radiopharmaceutical product.

energy while decaying has a high probability to destroy the malicious cells. Most often, the radionuclide is attached to the targeting vector *via* a chelator and linker (Fig. 1.1). Development and selection of a chelator and linker has to be well considered, and is somewhat similar to ligand development for luminescence and molecular bio-imaging purposes [35–37]. Highly stable lanthanide complexes are being looked for to ensure that the radiolanthanide reaches the targeted malicious cancer cells without being detached on its way to the targeted cancer cells. Early release of the radiolanthanide might cause severe damage to healthy tissues.

The coordination number in lanthanide complexes is determined by a combination of crowding in the coordination sphere, the charge density of the positively charged lanthanide ion and the electron-rich ligand [38]. In lanthanide complexes, both first-order and second-order steric effects can influence the coordination. First-order crowding includes mutual hindrance among donor atoms bound directly to the lanthanide ion. Inter-donor atom repulsion causes a limited amount of atoms that can be packed in close proximity of the lanthanide ion. Second-order crowding refers to possible interactions between functional groups that are attached to the donor atoms. Therefore, chelators to coordinate lanthanide ions for pharmaceutical purposes are usually based on ligands in which the electrondonating atoms are located in an ideal position within a molecular structure. This way, the ligand is able to coordinate the radiolanthanide multidentately, forming thermodynamically and kinetically highly stable complexes.

Additional functional groups providing additional electron-donating atoms to coordinate to the lanthanide ion can be attached to the molecular structure to increase the complex stability. Octadentate complexes (*e.g.* DOTA, *vide infra*), with the highest stability known for lanthanide coordination can be achieved. Linkage of the chelator to a targeting vector is a second task of

the functional group. Thus, selection of the functional group is important for both complex stability and linking of the targeting vector. Because of their well-considered position in the molecular structure of the chelator, interactions between functional groups are limited, reducing the influence of the second order crowding.

Additionally, it is important to consider biocompatibility of the chelator and targeting vector. Toxic and harmful substances have to be avoided in pharmaceuticals, and are strictly monitored by regulating agencies. The majority of complexes for radiopharmaceutical use are derivatives of acyclic and macrocyclic (poly)aminophosphonic acids, (poly)aminocarboxylic acids and porphyrins. Important ligands include 1,4,7,10-tetraazacyclododecane-1,4,7,10-tetraacetic acid (DOTA), 1,4,7-triazacyclononane-1,4,7-triacetic acid (NOTA), 1,4,7,10-tetraazacyclododecane-1,4,7-triacetic acid (DO3A), diethylenetriamine-pentaacetic acid (DTPA), ethylene diamine tetra(methylene phosphonate) (EDTMP) and 1,4,7,10-tetraazacyclododecane-1,4,7,10-tetramethyl phosphonic acid (DOTMP or DOTP), of which the structures are shown in Fig. 1.2. The molecular structure of DOTATATE (also known as DOTATOC, DOTA-octreotate or DOTA-Tyr^3-octreotate) is shown in Fig. 1.3, serving as an example of a chelator (*i.e.* DOTA) linked to a targeting vector (*i.e.* the amino acid peptide Tyrosine3-octreotate) as part of a radiopharmaceutical that is frequently used in combination with radiolanthanides for treatment and diagnosis of cancer. Although these chelators and targeting vectors will be mentioned briefly in this chapter, they are not the main focus as they were already extensively described in a review by Amoroso *et al.* and references therein [10]. Production and purification possibilities of the radionuclide, more specifically the radiolanthanide, are emphasized in this chapter.

Not all radiolanthanides can be used in nuclear medicine. To be considered as appropriate radiopharmaceutical, several criteria have to be met [4, 9, 39, 40]. First of all, the decay characteristics of the radiolanthanide are important, including the type of radiation (*e.g.* α, β^-, γ, *etc.*) and energy of the emitted particles, the half-life and decay products. The energy and correlated penetration depth of the emitted particle have to be selected in such a way that the harmful cells are destroyed efficiently, leaving the surrounding healthy ones unaffected as much as possible. Each type of particle emission has different *linear energy transfer* (LET) values and different ranges in soft tissue (Fig. 1.4). LET is the measure of the energy transferred to the medium as an ionizing radiation passes through it, and is used to quantify the effect of ionizing radiation on the medium such as a biological specimen [41]. Particulate emissions such as α and β^- particles have high LET, whereas γ and X-rays have low LET. High LET results in higher radiation damage to the biological systems, *i.e.* a high *relative biological effect* (RBE).

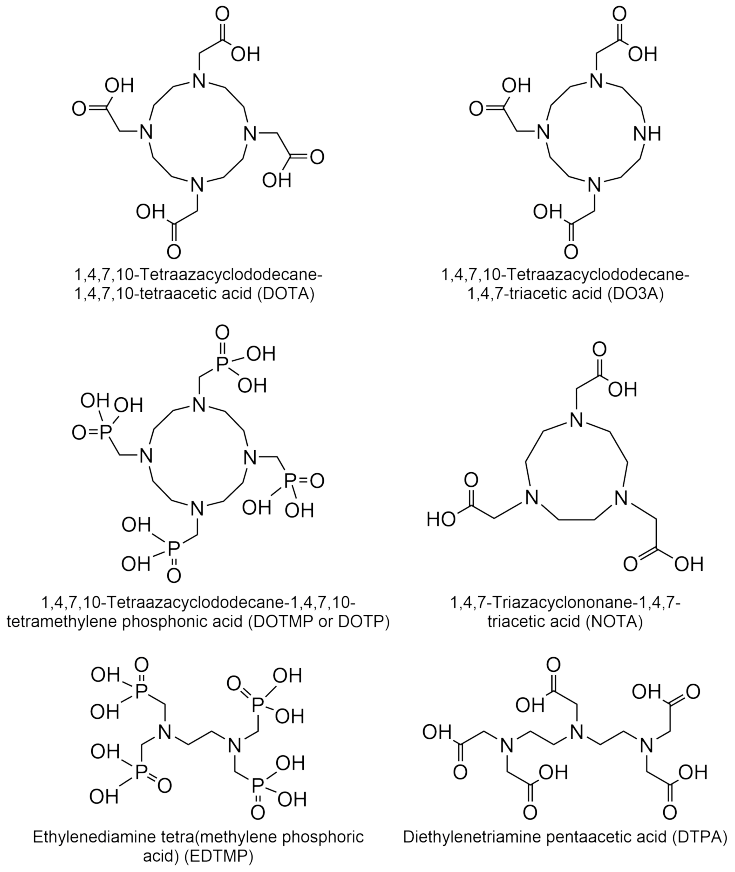

Figure 1.2: Structures of the coordinating ligands DOTA (top left), DOTMP (middle left), EDTMP (bottom left), DO3A (top right), NOTA (middle right) and DTPA (bottom right), on which chelators for the production of radiopharmaceuticals are frequently based.

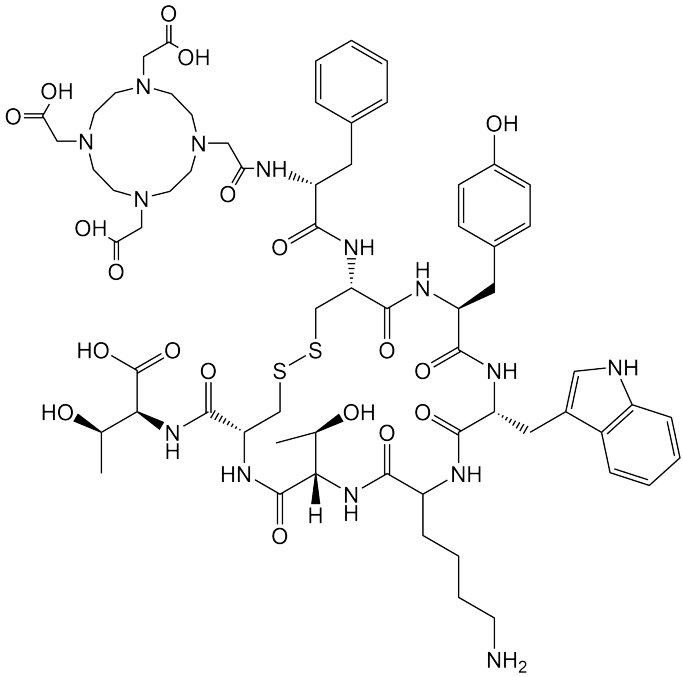

Figure 1.3: Molecular structure of DOTATATE as an example of a chelator coupled to a targeting vector as part of a frequently used radiopharmaceutical product containing radiolanthanide nuclides.

The γ emission energy has to be sufficiently high in case the radiolanthanide is used for imaging. However, too high γ energies might result in collimator problems, and should therefore be carefully selected. Several radiolanthanides emit β^- and γ simultaneously, by which their therapeutic and diagnostic features can be combined. This way, evolution of the treatment can be easily monitored *in situ*. Additional dosimetry measurements are helpful to plan and optimize the treatment.

The half-life of the selected radiolanthanide has to be sufficiently long to enable manipulation (purification and/or coordination) and transportation. A short half-life is only useful for therapy if the radiolabeling procedure and the radiopharmaceutical delivery to the target tissue can proceed fast. On the other hand, the half-life has to be limited for patient background radioactivity reasons. Moreover, a longer half-life is associated with a lower dose rate, which might lead to a lower therapeutic effect to the target tissue. Thus, the radiolanthanide half-life should be well-balanced and should correspond to the biological half-

life (*i.e.* the residence time of the compound in the human body) of the radiopharmaceutical, *i.e.* majority of the radioactive decay should occur after accumulation of the radiopharmaceutical in the targeted disease site [42]. Most favorably, the decay product, *i.e.* the daughter isotope of the radiolanthanide, is a stable isotope to avoid any additional radiotoxic side effects and should be removed from the body *via* natural excretion mechanisms. Secondly, the radiopharmaceutical has to be highly selective towards the targeted tissue to destroy the harmful cells with a low uptake by critical organs and healthy tissue, *i.e.* a high tumor to normal tissue absorbed dose.

A third important criterion is a straightforward production process, ensuring a high availability and reasonable cost. Moreover, too complicated production processes might influence the yield, purity and specific activity of the final product.

After diagnosis or therapy using radiolanthanides, the lanthanides are excreted from the body of the patient *via* natural outflow through the urinary system. Lately, it was reported that accumulation of lanthanides in the kidneys might lead to severe injuries. Diseases, like nephrogenic systemic fibrosis (NSF), were already linked to the use of gadolinium in magnetic resonance imaging (MRI) [43]. Free gadolinium was observed to be toxic and has been shown to induce tissue necrosis and fibrosis in animal studies, making prolonged exposure not desirable. Silberzweig *et al.* listed different strategies and techniques for the removal of gadolinium by dialysis, which can also be applied on the other lanthanides because of their very similar chemical properties throughout the lanthanide series [44]. However, much lower concentrations of radiolanthanides are being used in nuclear medicine, and do not possess any pharmacological properties. Therefore, monitoring is not strictly necessary for pharmacological reasons, but remains important for radiological dosimetry purposes.

1.5.1 α Emitting radiolanthanides

The use of α emitters for radionuclide therapy offers some important advantages, especially from a radiobiological point of view. The large mass difference between the α emitting nucleus and the α particle (*i.e.* a helium atom) causes the α particle to carry away almost all energy of the instable nucleus [45]. α particles possess higher decay energies compared to other emitted particles, like β^- particles, γ rays and Auger electrons, typically in the range of $4.0 - 8.8\,\mathrm{MeV}$. α particles are rather heavy, causing their penetration depth to be limited to a few cell diameters. The use of α particles results in a high local deposition of energy. Therefore, radiotoxicity to healthy tissue remains limited if the radionuclide can be deposited at the tumor site. However, the emission of α particles originates

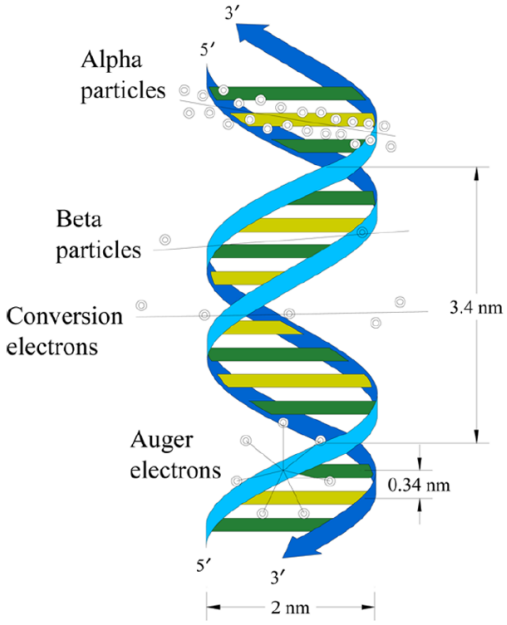

Figure 1.4: Illustration showing the interaction of different types of particulate radiation with DNA (path ranges not drawn according to scale). Each emitted particle has a different LET value and different ranges in soft tissue. The magnitude of the LET for each type of particle emission is represented by the white spheres. Reprinted with permission from Banerjee *et al.* Copyright © 2015 American Chemical Society.

from heavy nuclei. Therefore, the use of α emitting radiolanthanides is in general less abundant as only a few isotopes of the lanthanide series qualify to be applied in α particle therapy. In particular, only ^{149}Tb is being used in pre-clinical tests nowadays. This medical radiolanthanide will not be discussed in more detail in this chapter since ^{149}Tb cannot be produced *via* neutron irradiation in a nuclear reactor.

1.5.2 β^- Emitting radiolanthanides

β^- particle emitting isotopes for medical use are more widespread throughout the lanthanide series, including ^{143}Pr, ^{149}Pm, ^{153}Sm, ^{161}Tb, ^{165}Dy, ^{166}Ho, ^{169}Er, ^{170}Tm and ^{177}Lu. Each of them emits β^- particles with different energies, resulting in different tissue penetration depths, *i.e.* the β^- particle deposits its energy over about 5 to more than 150 cell diameters. Therefore, the

radiolanthanide series offers a broad range of isotopes available for radionuclide therapy to be used for a variety of target tissues. Longer-range electrons can effectively destroy malicious tumor cells at relatively long distance, whereas electrons with lower energies can be used to treat smaller tumors and small-disseminated metastases. After all, long-range electrons might also give high radiation dose to healthy tissue. A maximum absorbed dose fraction to the targeted tumor with a minimum effect to the surrounding normal tissue structures has to be strived for. Nevertheless, the success of the treatment with radionuclides is highly dependent on a homogeneous irradiation with complete destruction of the harmful tumor cells to avoid regrowth from an untreated subpopulation.

In general, the energy of a single β^- particle is insufficient to cause double strand breakage of the DNA molecule. Despite the highly heterogeneous distribution of the labeled molecules in solid tumors, studies already showed the advantage of β^- particles to cover a sufficiently large volume and destroy tumor cells *via* the so-called crossfire effect [8, 46–48]. For this reason, β^- particle emitting radiolanthanides will remain uttermost important in nuclear medicine. The advantage of some of these β^- particle emitting radiolanthanides is the ability to be efficiently produced in large quantities in a nuclear reactor. Neutron-rich nuclides are formed upon irradiation by a high thermal neutron flux, which primarily decay *via* β^- emission. Therefore, most of these β^- emitting radiolanthanides are commercially available to prepare radiopharmaceutical compounds.

1.5.3 Accompanying γ emission

With the emission of β^- particles, some radiolanthanides simultaneously emit useful γ photons. This γ radiation contributes only little to the therapeutic effectiveness, but can be helpful for diagnostics if emitted with sufficiently high energy. This accompanying γ radiation is desirable for following the pharmacokinetics by *in vivo* localization of the radiopharmaceuticals. Moreover, *in vivo* dosimetry studies in the patients can be performed simultaneously.

The γ emission can be imaged with commonly available γ detectors. The accompanying emission of γ photons will only lead to a minimal increase of the patient's dose burden. Thus, the simultaneous emission of β^- particles for therapy and γ photons for diagnosis is considered as a major advantage. The dual use, where therapy and diagnosis are combined, is also known as *theranostics*.

1.5.4 Accompanying neutrino emission

β^- decay also involves the emission of neutrinos (correctly speaking electron anti-neutrino, $\overline{\nu}_e$). These particles have no mass and no electrical charge, but carry away the missing energy between the maximum and actual energy of the β^- particle and have a spin value of $\frac{1}{2}$ to account for the emission of the electron, which is an elementary particle of spin $\frac{1}{2}$. This way, both the energy and the nuclear angular momentum are conserved. It is very unlikely for neutrinos to interact with mass, and they therefore have a high probability to travel a very large distance without reacting with matter. Neutrinos do not contribute to any radiopharmaceutical effect, and will therefore not be discussed in more detail in this chapter. More details can be found in a textbook on radiochemistry and nuclear chemistry [45].

1.5.5 Emission of Auger and conversion electrons

Auger and conversion electrons are usually emitted by radionuclides that decay by electron capture or internal conversion. In the latter one, an excited nucleus interacts electromagnetically (internal photoelectric effect) with one of the orbital electrons of the atom, which causes an electron to be emitted from the atom (conversion electron). The decay creates a vacancy in an inner electron shell, which is filled by electrons originating from higher shells. The electrons cascading down from higher shells involve electron transitions, which lead to the emission of characteristic X-ray photons. These X-ray photons may interact with electrons in the same electron shell *via* an internal photoelectric or Compton effect. As a result, these electrons will leave the atom as Auger electrons. At their turn, the resulting vacancies are filled with electrons originating from outer orbitals, which is accompanied by additional X-ray photon emission. These X-rays may again give rise to Auger electrons, and so forth. The energy of these Auger and conversion electrons depends on the shells that are involved in the electron transition. This energy is usually very low (20 – 500 eV).

Auger and conversion electrons have only very short ranges in soft tissue (nm to mm range), in which they deposit all their energy. Therefore, Auger and conversion electrons have a high linear energy transfer (LET), suitable for treatment of single tumor cells or tumor cell clusters. Because of their very short ranges in soft tissue, Auger and conversion electron emitters have to be targeted into the cell nucleus, *i.e.* in close proximity to the DNA, to obtain highest impact. During transit in blood or bone marrow, Auger and conversion electron emitters exhibit only low cellular toxicity.

The simultaneous emission of conversion and Auger electrons with β^- particles is an important feature of the ^{161}Tb radionuclide to achieve higher impact (Section 1.6.4). More localized radiation damage to the harmful tumor cells can be delivered due to the very high cytotoxicity levels.

1.6 Purification processes for reactor-produced medical radiolanthanides

Despite the ability of nuclear research reactors to produce medical radiolanthanides with high efficiency and high specific activities using highly enriched target materials, some impurities can impede the production of the radiopharmaceutical or can limit the time a radiopharmaceutical can be safely used (*i.e.* the shelf life). For example, non-carrier-added produced radiolanthanides have to be separated from the carrier material (*e.g.* ^{177}Lu from ^{176}Yb) before being used as precursor for radiopharmaceuticals.

Other applications, like bone pain palliation, can make use of carrier-added-produced radiolanthanides. Nevertheless, they might require purification as well since other impurities might be formed during irradiation (*e.g.* ^{154}Eu ingrowth in ^{153}Sm production, see later). Medical radionuclides, which have a relatively short half-life, will decay while being irradiated as the irradiation can take several days. Daughter nuclides that are produced by this radioactive decay can in turn be activated by neutrons, producing another isotope. If the half-life of this secondary radionuclide is much longer relative to the targeted medical radionuclide, the amount of this secondary isotope will increase exponentially with the irradiation time. The ingrowth of a long-lived radionuclide limits the use of a medical radionuclide severely as the background radiation for the patient becomes too high. Threshold limits to determine the radiopharmaceutical expiration based on the activity ratio between the medical radionuclide of interest and the longer-lived ingrowth isotope are strictly regulated by national and international regulating agencies. Therefore, the irradiation parameters have to be well balanced to find an optimum isotopic content.

A theoretical example of the ingrowth of a longer-lived radionuclide is given for the production of ^{153}Sm ($t_{1/2}$ = 46.284 h), where the longer-lived ^{154}Eu ($t_{1/2}$ = 8.593 y) radionuclide is produced in small quantities. If the enriched target material (98.70 % ^{152}Sm) is irradiated by a thermal neutron flux of $3.5 \times 10^{14}\,\mathrm{n\,cm^{-2}\,s^{-1}}$, 15.6 mg of ^{153}Sm per gram of target material ($\approx 250\,\mathrm{TBq\,g^{-1}}$ or $6900\,\mathrm{Ci\,g^{-1}}$ target material) can be obtained after irradiating for nine days (after nine days the plateau region is reached, Fig. 1.5). At this point, 1.117 mg of ^{154}Eu per gram of target material ($\approx 11\,\mathrm{GBq\,g^{-1}}$ or

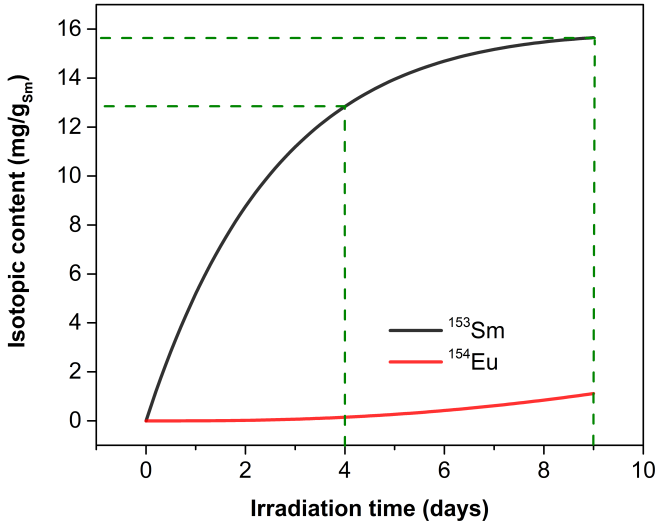

Figure 1.5: Production of ^{153}Sm and ingrowth of ^{154}Eu by irradiation of a highly enriched ^{152}Sm (98.70 %) target using a thermal neutron flux of $3.5 \times 10^{14}\,\mathrm{n\,cm^{-2}\,s^{-1}}$.

$0.3\,\mathrm{Ci\,g^{-1}}$ target material) is produced simultaneously. Regulating agencies have put the upper threshold limit for radiopharmaceutical use at 0.093 kBq ^{154}Eu per MBq ^{153}Sm(*i.e.* 0.093 mCi ^{154}Eu per mCi of ^{153}Sm). Without any purification, this limit would already be reached after almost two days (Fig. 1.6). Completing the radiopharmaceutical production chain is impossible in such a small time window, taking into account cooling down of the target material, transportation and linkage to a carrier vector. No patients will have the chance to be treated by the radionuclide without being exposed to too high amounts of the long-lived ^{154}Eu isotope this way. Therefore, shorter irradiation times are frequently used at the cost of a less efficient use of the target material, *i.e.* 12.8 mg of ^{153}Sm per gram of target material ($\approx 200\,\mathrm{TBq\,g^{-1}}$ or $5600\,\mathrm{Ci\,g^{-1}}$ target material) is reached after four days of irradiation. However, the amount of ^{154}Eu after irradiation is significantly lower, *i.e.* 0.151 mg of ^{154}Eu per gram of target material ($\approx 1.5\,\mathrm{GBq\,g^{-1}}$ or $0.4\,\mathrm{Ci\,g^{-1}}$ target material). Without any purification, the isotopes can be used up to 6.2 d after leaving the reactor, which is a significantly broader time window to finish the radiopharmaceutical production process and to treat patients in hospitals.

Rapid, reliable and efficient purification procedures are required to obtain high radiochemical purity of the final products. Some separation techniques are still

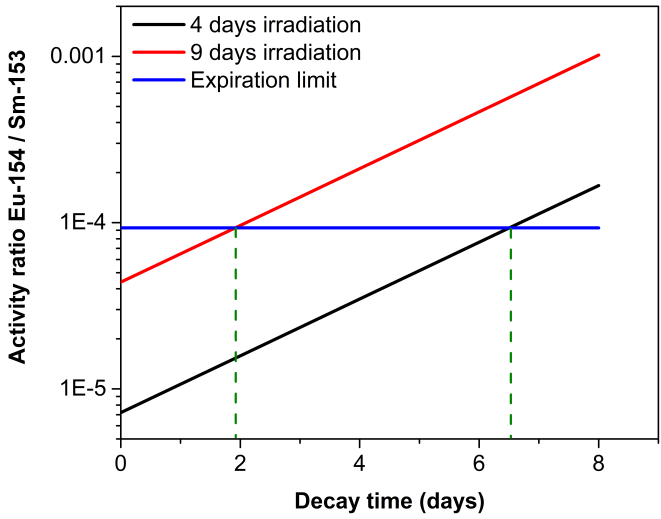

Figure 1.6: Evolution of the ^{154}Eu/^{153}Sm activity ratio after four days (black) and nine days (red) of irradiation. The blue horizontal line indicates the upper threshold limit of 0.093 kBq ^{154}Eu per MBq ^{153}Sm (or 0.093 µCi per mCi ^{153}Sm) for radiopharmaceutical use.

being developed, while several other techniques are already well established, such as the separation by means of a radionuclide generator system (*e.g.* the ^{166}Ho generator). After irradiation in a nuclear reactor, the parent radionuclide is loaded onto the nuclide generator system. Most often, this is a simple column separation setup. The medical radionuclide is formed in this nuclide generator system by decay of the parent radionuclide. The medical radionuclide accumulates in the system over time and can be selectively eluted from the generator system, leaving the parent radionuclides behind. This separation process is often denoted as 'milking' of the medical radionuclides, with the parent radionuclide denoted as the 'cow' and the daughter radionuclide denoted as the 'milk'. Availability of the daughter nuclide in non-carrier-added (nca) form is a key feature of this production method. No direct access to a nuclear reactor is needed because fresh medical radionuclides will be generated as long as the reactor-produced parent radionuclides are present in sufficient amount in the system. Thus, the desired medical radionuclides can be obtained on demand.

Radionuclide generator systems are, however, not the only way to separate and purify radiolanthanides. Besides, the production of some radiolanthanides,

in both carrier-added and non-carrier-added form, might require the removal of some long-lived impurities that are produced simultaneously by neutron irradiation of the target material. Radiolanthanides of high radionuclidic purity have to be obtained for radiopharmaceutical use. However, the removal of these impurities is challenging because it requires the separation of two lanthanides, and often the separation of two adjacent lanthanide elements [49, 50]. An additional difficulty for the production of radiolanthanides in the nca form, is the separation of a microscopic amount of one lanthanide (the desired radiolanthanide) from a macroscopic amount of another lanthanide (the redundant target material).

The $4f$ subshell is filled with electrons throughout the lanthanide series, which are tightly bound due to the high effective nuclear charge. Moreover, they are shielded by the filled $5s$ and $5p$ subshells. Therefore, the $4f$ electrons do not participate in bond formations and are not influenced by ligands surrounding lanthanide ion, *i.e.* the $4f$ electrons show a core-like behavior. Lanthanide chemistry is governed by the removal of the $5d$ and $6s$ valence electrons, leading to the +III oxidation state, which is by far the most stable one for all lanthanides. All trivalent lanthanides show very similar chemical properties because of their filled $5s$ and $5p$ subshells.

Cerium(+IV), europium(+II), terbium(+IV) and ytterbium(+II) are found to be relatively stable in other oxidation states as well, changing their chemical properties drastically. In some separation methods advantage is taken on the change in oxidation state of these lanthanides. Increase of the nuclear charge and poor shielding of the $5s$ and $5p$ electrons by the $4f$ subshell lead to a smaller atomic radius throughout the lanthanide series when moving from lanthanum (1.16 Å with CN = 8) to lutetium (0.977 Å with CN = 8). This phenomenon is often denoted as the '*lanthanide contraction*'. Therefore, the charge density and the hydration energy ($-\Delta H_{hydr}$) increase with increasing atomic number for the trivalent lanthanides (Ln^{3+}), also affecting the *coordination number* (CN). The tendency of forming the cationic aqua complexes, *i.e.* $[Ln(H_2O)_x]^{3+}$, gradually increases with a decrease in atomic number [51, 52].

The coordination number of $[Ln(H_2O)_x]^{3+}$ is assumed to be 9 for early lanthanides (La–Eu) and 8 for the later lanthanides (Dy–Lu), with the intermediate lanthanides exhibiting a mixture of 8-coordinate and 9-coordinate species. A change in coordination number leads to separation possibilities and might potentially lead to variations in biological behavior when bio-conjugates with the same chelator are labeled with a different lanthanide. The Ln^{3+} are categorized as hard Lewis acids according to the *Hard Soft Acid Base* (HSAB) theory because of their high charge density and are likely to be coordinated by oxygen- and nitrogen-bearing donor ligands. Maximum kinetic stability can be obtained by using macrocyclic ligands, like 1,4,7,10-

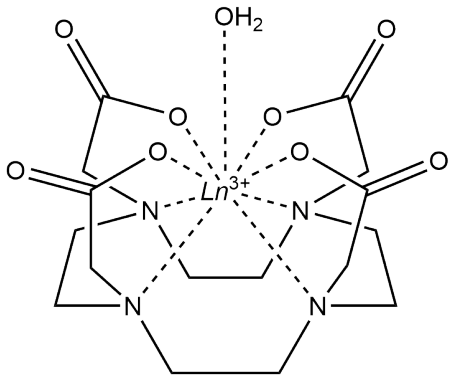

Figure 1.7: Representation of a trivalent lanthanide being captured in the DOTA cavity in formation of the Ln^{3+}-DOTA complex.

tetraazacyclododecane-1,4,7,10-tetraacetic acid (DOTA). Because of its spatial flexibility, DOTA is able to capture the lanthanide in its cavity, coordinating the trivalent lanthanide in an octadentate fashion (Fig. 1.7). A variety of lanthanide-containing radiopharmaceuticals and contrasting agents are DOTA derivatives because of their high thermodynamic, kinetic and *in vivo* stability [10, 41, 53]. Modifications to the DOTA structure or linking to a targeting vector ensures bio-distribution to the targeted region in the human body. However, the use of these highly stable complexes is not recommended for separation and purification processes as they will not show any selectivity. Moreover, these ligands are difficult to remove if further processing after separation and purification is required. Therefore, other ligands are being used.

Most separation methods for radiolanthanide purification are based on an extraction or ion-exchange chromatography technique because of their straightforward and reliable use. Solvent extraction proved to be efficient in separation of lanthanides as well. However, the requirement of a multistage process, which is essential to achieve the necessary decontamination due to the low separation factor, limits its wide-scale use. The resulting product is highly diluted as high volumes are being used. In these techniques, separation is based on the small differences in stability constant between two adjacent lanthanides and the ligand that is being used to coordinate the lanthanides. In a column separation setup, this ligand can be situated in the mobile phase or the stationary phase, influencing the elution order of the lanthanides. The difference in stability constant between two trivalent lanthanides originates from the different ionic radius, *i.e.* a different charge density, due to the lanthanide contraction. An increasing charge density generally leads to an increasing

stability constant.

Different complexing agents are being investigated in radiolanthanide purification technologies. The majority of them make use of α-hydroxyisobutyric acid (α-HIBA), which is, until present, the aqueous complexing agent with highest sensitivity to lanthanide cation radii [54–57]. The complexing agent being present in the aqueous phase is an advantage for separation of micro amounts of a non-carrier-added produced radiolanthanide (*e.g.* ^{177}Lu) from redundant target material (*e.g.* ^{176}Yb). Separation of lanthanides using α-HIBA is based on three equilibria, the first one being the acid–base equilibrium because α-HIBA is a weak acid (pK_a = 4.01). pH of the aqueous phase has to be carefully chosen. The addition of protons leads to blockage of the coordinating oxygen atoms. The second equilibrium is the complex formation between α-HIBA and the lanthanide, which varies with the ionic radius and charge density of the lanthanide. More stable complexes are being formed with the lanthanides having a higher charge density. Thus, the heavier lanthanide will elute from the column first because of the lanthanide contraction. The third equilibrium comprises the interaction of the lanthanide with the functional groups of the stationary phase that is being used as column material (*e.g.* sulfonic acid based cation-exchanger). The more interaction with the stationary phase, the slower the elution. Thus, protons can also establish the cation-exchange mechanism to the stationary phase as more protons can lead to lower distribution ratios. Frequently, other cations (*e.g.* NH_4^+) are being used to lower the extraction to the stationary phase in more neutral conditions when using α-HIBA. In general, the α-HIBA concentration, pH, cation concentration and selection of the stationary phase can be varied to optimize the separation protocol. Most often, a gradient of concentrations of the first three parameters in the mobile phase is being applied to shorten the retention times and minimize peak broadening. After the separation, an additional purification step is needed to remove the complexing agent from the radiolanthanide prior to radiolabeling. Acidification of the solution breaks the *Ln*-α-HIBA complex, after which both can be separated using a second cation-exchange column.

In other approaches, the acidic organophosphorous extractants di-(2-ethylhexyl) phosphoric acid (HDEHP, DEHPA or D2EHPA) and 2-ethylhexyl phosphonic acid mono-2-ethylhexyl ester (HEH[EHP]) (Fig. 1.8) are being used frequently in ion-exchange and extraction resins [58–63]. This way, the lanthanide complexes are being formed in the organic phase of the resin (stationary phase), causing the heavier lanthanide to elute last from the column. The stability constant of the complex increases with the atomic number. Reactions 1.1 and 1.2 represent the equilibria involved in the extraction process using these acidic extractants (represented by HA), *i.e.* the formation of extractable species in the aqueous phase and its partitioning between the two phases, respectively. Reaction 1.3

shows the example of the overall extraction mechanism of Ln^{3+} by HDEHP. Fig. 1.9 shows the coordination of Ln^{3+} by HDEHP and HEH[EHP].

$$Ln^{3+}{}_{(\mathrm{aq})} + 3\,(\mathrm{H}A)_{2(\mathrm{aq})} \rightleftharpoons Ln(\mathrm{H}A_2)_{3(\mathrm{aq})} + 3\,\mathrm{H}^{+}{}_{(\mathrm{aq})} \quad [1.1]$$

$$Ln(\mathrm{H}A_2)_{3(\mathrm{aq})} \rightleftharpoons Ln(\mathrm{H}A_2)_{3(\mathrm{org})} \quad [1.2]$$

$$Ln^{3+}{}_{(\mathrm{aq})} + 3\,(\mathrm{HDEHP})_{2(\mathrm{org})} \rightleftharpoons Ln[\mathrm{H(DEHP)}_2]_{3(\mathrm{org})} + 3\,\mathrm{H}^{+}{}_{(\mathrm{aq})} \quad [1.3]$$

This extraction mechanism is, however, only valid if the concentrations of both the mineral acid and the lanthanide salt are low [60]. In case of moderate or high acid concentrations, the distribution ratio tends to increase with the concentration of the acid, and is different for each lanthanide ion. The composition of the extracted species changes towards $Ln(X)_3 \cdot 3\,\mathrm{HDEHP}$, with X the inorganic anion of the mineral acid (*e.g.* NO_3^- , Cl^-, SCN^- or ClO_4^-). This way, the inorganic anions of the mineral acid neutralize the charge of the lanthanide cation and the organophosphorous extractant serves as a neutral extractant (represented by B). The formation of the extractable species in the aqueous phase and the partitioning over the two phases are represented by Reactions 1.4 and 1.5, respectively. Also the partitioning of the organophosphorous extractant between the two phases is important ($B_{(\mathrm{org})} \rightleftharpoons B_{(\mathrm{aq})}$).

$$Ln^{3+}{}_{(\mathrm{aq})} + 3\,X^{-}{}_{(\mathrm{aq})} + n\,B_{(\mathrm{aq})} \rightleftharpoons LnX_3 \cdot B_{\mathrm{n(aq)}} \quad [1.4]$$

$$LnX_3 \cdot B_{\mathrm{n(aq)}} \rightleftharpoons LnX_3 \cdot B_{\mathrm{n(org)}} \quad [1.5]$$

Polymeric species in the organic phase can be formed at high lanthanide salt concentrations, of which the composition was found to be $Ln(\mathrm{DEHP})_3$. The formation of these polymeric species, however, results in difficult separation of macro amounts of lanthanides by extraction chromatography when these organophosphorous extractants are being used as stationary phase. It is clear that the use of organophosphorous extractants serves three functions, *i.e.* neutralization of the charge of the lanthanide cation, removal of the water molecules from the coordination shells of the lanthanide cation and the increase of the molar volume of the metal-containing species. In the following paragraphs, the production and radiochemical processing of the most important reactor-produced medical radiolanthanides will be highlighted. Several examples on the use of the aforementioned organophosphorous extractants and α-HIBA

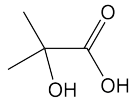

α-hydroxy isobutyric acid (α-HIBA)

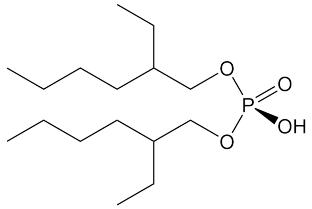

Di-2-(ethylhexyl)phosphoric acid (HDEHP, DEHPA, D2EHPA)

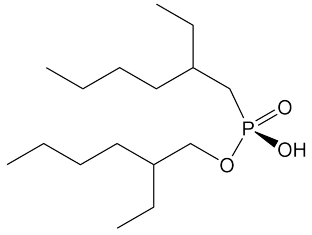

2-ethylhexyl 2-ethylhexylphosphonic acid (HEH[EHP])

Figure 1.8: Molecular structures of frequently used complexing agents in radiolanthanide purification methods.

for radiolanthanide purification will be mentioned. In addition, production methods for ^{47}Sc and ^{90}Y using a nuclear reactor are described briefly because both scandium and yttrium possess very similar chemical properties as the lanthanides. Together with the lanthanides, scandium and yttrium are denoted as the rare earth elements. Like the lanthanides, scandium and yttrium are primarily found in their trivalent state in solution. Their ionic radii are 0.87 Å (with CN = 8) and 1.01 Å (with CN = 8), respectively. Because of the large similarities with the lanthanides, the majority of the coordination strategies for the production of radiopharmaceuticals can be applied for these radioisotopes as well. Radiochemical processing to isolate ^{47}Sc and ^{90}Y are different because both isotopes have to be separated from alkaline earth or transition metals. No (adjacent) rare earths with very similar properties have to be separated from each other. Therefore, other approaches for efficient separation can be used, which will not be further discussed in this chapter.

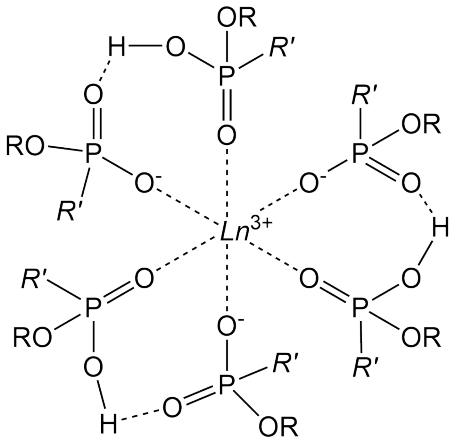

Figure 1.9: Coordination of Ln^{3+} by HDEHP and HEH[EHP], with R = 2-ethylhexyl and R' = OR (HDEHP) or R (HEH[EHP]).

1.6.1 Praseodymium-143

Despite its relatively long half-life, ^{143}Pr ($t_{1/2}$ = 13.6 d) is sometimes used in therapy because of its medium-energy β^- emission (933 keV) [1, 64]. The production route for ^{143}Pr by the irradiation of ^{141}Pr (σ_{th} = 11.49 barn) *via* a double neutron caption process $(2n, \gamma)$ is not preferable (Fig. 1.10). This production route results in a mixture of both ^{142}Pr ($t_{1/2}$ = 19.12 h, σ_{th} = 20.03 barn) and ^{143}Pr, of which the ratio depends on irradiation time and the post-irradiation decay period. Additionally, the production yield is very low given the low cross-sections of ^{141}Pr and ^{142}Pr with respect to the double neutron capture process. Large amounts of the ^{141}Pr carrier remain in the irradiated target.

Instead, the non-carrier-added $(n, \gamma) \rightarrow \beta^-$ production route by neutron irradiation of enriched ^{142}Ce is used [65, 66]. After irradiation, the target requires a cooling period of a few days to allow the shorter-lived ^{143}Ce ($t_{1/2}$ = 33.04 h) to decay to ^{143}Pr. Besides, long irradiation periods and high neutron fluxes are needed to produce sufficiently high activity levels of ^{143}Pr because of the rather low neutron cross-section of ^{142}Ce (σ_{th} = 0.95 barn). Nevertheless, the production route results in a ^{143}Pr product with high radionuclidic purity. No further purification steps are purely necessary for radiopharmaceutical use.

^{143}Pr can be separated from cerium rather efficiently if cerium is in its tetravalent state. Removal of the single 4f electron is favorable because of the stabilizing effect of an empty $4f$ subshell. For this reason, a target material consisting

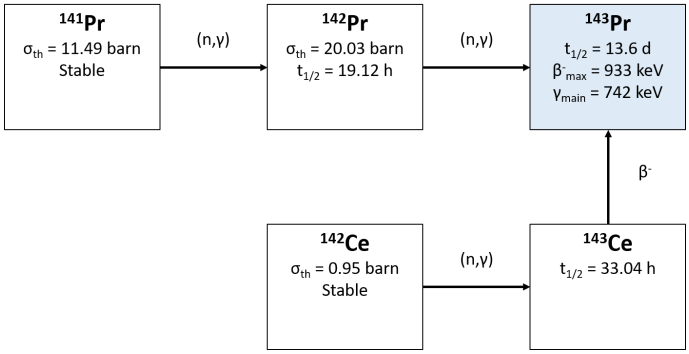

Figure 1.10: Production pathways of the medical ^{143}Pr radionuclide (highlighted). Only the non-carrier-added production pathway *via* neutron capture of ^{142}Ce and subsequent β^- decay leads to ^{143}Pr with sufficiently high radionuclidic purity for medical use.

of $^{142}CeO_2$ is frequently used for irradiation. However, dissolution of CeO_2 in concentrated HCl or HNO_3 solutions is difficult. Therefore, the irradiated target material is frequently dissolved in a mixture of concentrated HNO_3 and H_2O_2 (30 %), after which it is evaporated to near dryness.

In a first separation method, the mixture is reconstituted in $1\,mol\,L^{-1}$ $NaBrO_3$ [1]. After heating for 10 min at 80 °C in a water bath and subsequent cooling at 0 °C, cerium can be precipitated as ceric iodate by the addition of HIO_3. Filtration of the mixture ensures removal of the precipitate. The resulting filtrate can be evaporated to near dryness and reconstituted in a $0.1\,mol\,L^{-1}$ HCl solution for further radiopharmaceutical processing.

The use of extraction methods to remove Ce^{4+} is another possibility [67]. Ce^{4+} ions have a smaller ionic radius and higher charge density in comparison with trivalent lanthanide ions. Therefore, different interactions with ligands and extractants occur. In an ion-exchange chromatographic method described by Kubota, the residue after dissolution of target material in concentrated HNO_3 and H_2O_2 and evaporation to dryness was re-dissolved in $0.2\,mol\,L^{-1}$ HCl [65]. A cation-exchange column (Diaion SK-1) was loaded with the sample, after which the column was washed with water. Cerium and ^{143}Pr were eluted with a $0.25\,mol\,L^{-1}$ citrate solution, with praseodymium eluting first. A chemical yield of ^{143}Pr of > 99 % and a radiochemical purity of > 99.99 % were reached.

1.6.2 Promethium-149

^{149}Pm ($t_{1/2}$ = 2.21 d) is a high specific activity radiolanthanide that is suitable for targeting of limited numbers of specific receptors found on many tumor cells [68–72]. ^{149}Pm emits β^- particles of moderate energy (1.071 MeV) and γ photons with an energy of 285 keV (2.8 %), making *in vivo* imaging possible [73]. Stable isotopes of promethium do not exist, precluding the direct neutron activation of targets. Therefore, non-carrier-added ^{149}Pm can be obtained *via* neutron irradiation of a ^{148}Nd (σ_{th} = 2.503 barn) target and subsequent β^- decay of ^{149}Nd ($t_{1/2}$ = 1.728 h), *i.e.* $(n,\gamma) \rightarrow \beta^-$ (Fig. 1.11). Highly enriched ^{148}Nd target materials have to be used because of its moderate thermal neutron cross-section. This way, ^{147}Nd ($t_{1/2}$ = 10.98 d) formation *via* neutron irradiation (n,γ) of ^{146}Nd (σ_{th} = 1.4 barn) can be avoided.

^{149}Pm can be chemically separated from neodymium by means of extraction chromatography techniques described by Ketring *et al.* and Monroy-Guzman *et al.* [1, 74, 75]. The separation is based on the use of a commercial resin comprised of an inert polymeric absorbent impregnated with the extractant di-(2-ethylhexyl)phosphoric acid (HDEHP, *e.g.* Eichrom Ln resin). The acidity of the aqueous phase determines the extraction mechanism and extraction capability of HDEHP, as the distribution ratios of lanthanides substantially increase with HNO_3 concentration. Separation was achieved by increasing distribution ratios with increasing atomic number because of the changing stability constant. Neodymium eluted first from the column owing to its slightly lower charge density and ionic radius. In the separation method described by Ketring *et al.*, the irradiated target was dissolved in 0.15 mol L^{-1} HCl and loaded onto the column [1]. Neodymium was eluted using a 0.5 mol L^{-1} HNO_3 solution, while ^{149}Pm was stripped from the column by a 5 mol L^{-1} HNO_3 solution. The ^{149}Pm fractions could be evaporated and re-dissolved in the desired solution, typically dilute HCl.

The more recent method described by Monroy-Guzman *et al.* used a similar strategy, eluting neodymium with a 0.18 mol L^{-1} HNO_3 solution and stripping ^{149}Pm with a 1.5 mol L^{-1} HNO_3 solution. ^{149}Pm obtained at high HNO_3 concentration was transferred to its chloride salt *via* precipitation as hydroxide and re-dissolving in dilute HCl. Carrier-free ^{149}Pm was obtained with a radionuclide purity of > 99.9 %.

1.6.3 Samarium-153

^{153}Sm is most often used for the preparation of the radiopharmaceutical compound ^{153}Sm-ethylene diamine tetramethylene phosphonate (^{153}Sm-EDTMP,

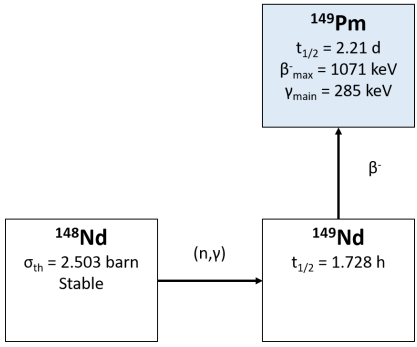

Figure 1.11: Production pathway of the medical ^{149}Pm radionuclide (highlighted) *via* neutron capture of ^{148}Nd and subsequent β^- decay of ^{149}Nd.

commercial names: Lexidronam and Quadramet) [76]. This compound is primarily used in nuclear medicine for palliative care of patients who are suffering from bone pain due to skeletal metastasis as the EDTMP chelate is responsible for the specific uptake into the newly formed bone matrix laid down by osteoblasts [77–84]. Bone metastases are often a result of different types of cancer and are very painful. Bone metastases occur in more than 50 % of the cancer patients. Breast, lung and prostate cancer patients even have a probability up to 80 % to develop these skeletal metastases. Thus, a large group of patients can benefit from this type of radiotherapy. ^{153}Sm-EDTMP can be easily administered intravenously by injection of a standard dose of 37 MBq kg^{-1} (or 1 mCi kg^{-1}) body weight to treat these bone metastases. Despite its simplicity, ^{153}Sm remains underutilized for improving cancer pain in the skeleton. Recent studies investigated the possibilities to connect ^{153}Sm with different targeting vectors to treat other types of cancer, like the use of ^{153}Sm-labeled microparticles for selective internal radiotherapy (SIRT) of liver tumors [85, 86].

The use of ^{153}Sm is very interesting in nuclear medicine because of its favorable decay characteristics. The radionuclide has a reasonable physical half-life of 46.284 h, emitting β^- particles with a mean energy of 233 keV. These β^- particles can penetrate soft tissue with an average range of 0.5 mm and an effective range of 2 – 3 mm. The emission of β^- particles is accompanied by the emission of γ photons of 103.2 keV (28 %), which can be used for imaging.

^{153}Sm is commonly carrier-added produced *via* thermal neutron activation of isotopically enriched ^{152}Sm (n,γ) (> 99.8 % enrichment, σ_{th} = 206.2 barn) (Fig. 1.12). Sometimes a natural samarium (^{144}Sm (3.1 %), ^{147}Sm (15 %), ^{148}Sm (11.2 %), ^{149}Sm (13.8 %), ^{150}Sm (7.4 %), ^{152}Sm (26.7 %) and ^{154}Sm (22.8 %))

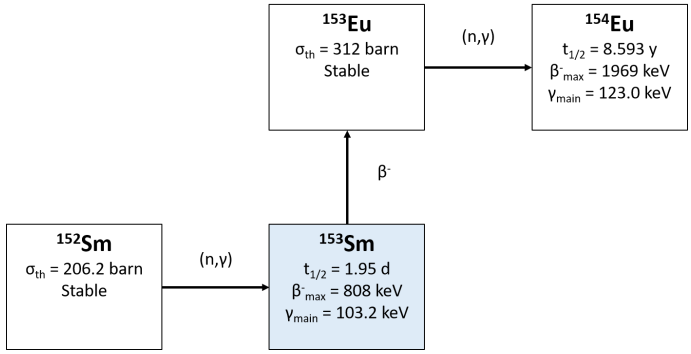

Figure 1.12: Production pathway of the medical ^{153}Sm radionuclide (highlighted) *via* neutron capture of ^{152}Sm with the co-production of the long-lived ^{154}Eu impurity.

target is being used, resulting in an isotopically very impure product containing several long-lived isotopes (*e.g.* ^{154}Sm ($t_{1/2}$ = 340 d), ^{151}Sm ($t_{1/2}$ = 88.8 y) and ^{155}Sm ($t_{1/2}$ = 4.76 y)) [87–90]. Therefore, irradiation of a natural samarium target is not preferred. The isotopically enriched ^{152}Sm target is usually irradiated for several days to achieve a sufficiently high yield of ^{153}Sm.

During irradiation, minor amounts of long-lived ^{154}Eu ($t_{1/2}$ = 8.593 y) are formed because of neutron caption of ^{153}Eu (σ_{th} = 312 barn), the daughter isotope of ^{153}Sm (see example above). The ingrowth of ^{154}Eu limits the shelf life of the product because the maximum amount of ^{154}Eu that can be administered to a patient is strictly regulated [89, 91]. A maximum of only 0.093 kBq of ^{154}Eu per MBq of ^{153}Sm is allowed. Irradiation parameters have to be well chosen to obtain a high production yield for ^{153}Sm with limited ingrowth of ^{154}Eu if additional purification steps have to be avoided. In some irradiated targets, also the long-lived ^{152}Eu ($t_{1/2}$ = 13.537 y) and ^{156}Eu ($t_{1/2}$ = 15.19 d) are found in trace amounts. So far, no commercial ^{153}Sm for medical use is being purified after irradiation. The use of ^{153}Sm in nuclear medicine is hampered by its relatively short half-life, which impedes any purification and distribution procedures. Nevertheless, higher production yields and more efficient use of the valuable target material can be reached if an efficient purification method can be implemented, also leading to extended expiration dates and increased transport and distribution flexibility. Moreover, removal of the europium contaminants leads to a facilitated waste management (residuals of the radiopharmaceutical, syringes, patient excreta *etc.*) in hospitals. Therefore, some research groups are investigating different pathways for post-irradiation purification [87, 88, 92].

Most of these purification techniques are based on the ability to reduce europium

to its divalent state ($E^0 = -0.34\,\mathrm{V}$). Europium is the only lanthanide that is relatively stable in its divalent state in aqueous solutions because of its favorable electronic configuration ([Xe]$4f^7$). However, re-oxidation by any oxidizing species, like dissolved oxygen gas, present in solution might occur fast. For this reason, the solutions are extensively purged by an inert gas prior to europium reduction and the solutions usually contain reduction stable counter ions (*e.g.* chloride) only. Selective reduction of europium is mainly acquired by chemical or electrochemical techniques. Photochemical reduction by UV radiation is usually not considered for purification of radiolanthanides because of its rather slow kinetics [93–95].

Chemical reduction of europium usually involves the use of zinc ($E^0 = -0.76\,\mathrm{V}$) or zinc amalgam (Zn(Hg), Jones reductor), whereas electrochemical reduction by electrolysis is established by applying a potential difference [96–100]. The major disadvantage of the chemical reduction method is the addition of Zn^{2+} impurities to the solution, which will have to be considered in the purification steps. The zinc content in the final radiopharmaceutical compound is also strictly regulated. Electrolysis does not introduce any additional impurities. Subsequent precipitation of Eu^{2+} by sulfate as the highly insoluble $EuSO_4$ already proved to be inefficient, as yield and purity (typically lower than 80 % and 90 %, respectively) were sacrificed by leaving behind the amount of europium required to surpass solubility and by co-precipitating contaminants with the sulfate solid [101]. Subsequent re-dissolution and precipitation steps were used in some cases to enhance purity, albeit at the price of lowering the overall yield. Therefore, other separation techniques are being developed.

Chakravarty *et al.* presented recently an electrochemical approach to remove the radionuclidic contaminants of europium from ^{153}Sm *via* electro-amalgamation (Fig. 1.13) [88, 102]. An overall yield of > 85 % ^{153}Sm was obtained after the purification process. Europium (Eu^{3+}) was reduced to its divalent state (Eu^{2+}) in an electrolysis cell making use of a mercury-pool cathode. The separation method is based on the preferential transfer of Eu^{2+} onto the mercury electrode. After dissolution of the target material in a $0.1\,\mathrm{mol\,L^{-1}}$ HCl solution, separation took place in a $0.15\,\mathrm{mol\,L^{-1}}$ lithium citrate solution to prevent hydroxide precipitation during the course of electrolysis. Brisk hydrogen evolution at the cathode might turn the electrolyte in the vicinity of the cathode alkaline, leading to hydrolysis of uncoordinated Sm^{3+} ions. Inactive europium carrier material ($EuCl_3$) was added to the electrolyte to maintain a sufficiently high concentration of Eu^{3+} ions. It was shown by Peppard *et al.* that Eu^{2+} is much more difficult to stabilize when europium is present in very low concentrations, *i.e.* trace amounts, as Eu^{2+} ions become much more vulnerable to re-oxidation [103]. Moreover, an increased europium concentration improves the kinetics of the electro-amalgamation reaction. pH of the solution

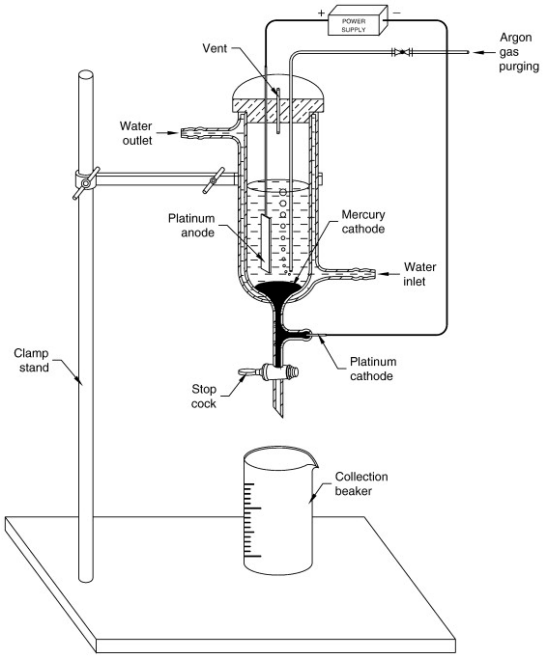

Figure 1.13: Schematic diagram of the experimental electro-amalgamation set-up for the electrochemical purification of ^{153}Sm, ^{169}Er and ^{177}Lu for radiotherapy. Reprinted with permission from Chakravarty *et al.* [104] Copyright © 2010 Elsevier Inc.

was adjusted to 6–7 by addition of 0.1 mol L^{-1} NH_4OH solution. Electrolysis took place by applying a constant of 6 V (current 800 mA), after which the mercury was drained off from the cell. Remaining mercury colloidal particles were removed from the aqueous ^{153}Sm-containing electrolyte by a filtration step. Using this electro-amalgamation separation process, a 10 – 15 % loss in ^{153}Sm was observed. However being less stable and less favorable, samarium (Sm^{3+}) can be reduced to its divalent state (Sm^{2+}, $E^0 = -1.55$ V) in the applied conditions. Sm^{2+}, having a near-half filled electronic configuration ([Xe]$4f^6$]), gets also amalgamated in the mercury cathode. Although the lost samarium fraction remained small, a significant loss in specific activity was observed.

Other separation methodologies are based on more conventional techniques, like solvent extraction and ion-exchange techniques. Some of these techniques are based on the small difference in coordination behavior between the two trivalent lanthanides. For example, Islami-Rad *et al.* developed a method based on ion-exchange chromatography [87]. After dissolution of the irradiated target material in 1 mol L^{-1} HCl, the solution was eluted over a Dowex-50W

cation-exchange resin (polymeric supported sulfonic acid, 200 – 300 mesh) at room temperature using a 0.2 mol L^{-1} α-hydroxyisobutyric acid (α-HIBA) at pH 4.8 and a flow velocity of 1 mL cm^2 min^{-1}. Samarium and europium were eluted from the column at different rates, with europium eluting from the column first because of the lanthanide contraction. The smaller ionic radius of europium leads to a slightly higher stability of the Eu-α-HIBA complex, resulting in less affinity of europium for the cation-exchange resin. The recovery yield of ^{153}Sm was found to be > 66 % with a radionuclidic purity of > 99.8 %.

More efficient separation techniques, with higher recovery yields for ^{153}Sm, include a preliminary step to reduce europium to its divalent state prior to the separation step. Advantage can be taken of the significantly different chemical properties of europium in its divalent state. Eu^{2+} shows chemical similarities to the alkali and alkaline earth metal ions. Reduction of the oxidation state, *i.e.* the addition of an electron, leads to an increased ionic radius, a decreased charge density and a decreased hydration enthalpy ($-\Delta H_{hydr}$), leading to a different extraction behavior compared to the trivalent lanthanides. For this reason, solvent extraction and ion-exchange chromatography techniques are frequently applied, some of them making use of an extraction system in which Sm^{3+} is preferentially coordinated by di-(2-ethylhexyl)phosphoric acid (HDEHP, DEHPA or D2EHPA)[62, 99–101, 103]. Eu^{2+} remains unaffected in the aqueous solution. The use of a HDEHP-based ion-exchange chromatography method results in the elution of Eu^{2+} prior to the elution of Sm^{3+}.

The use of the size selective extractant dicyclohexane-18-crown-6 (DCH18C6) in a quaternary ammonium ionic liquid phase was investigated (Reaction 1.6) in a recent feasibility study by Van de Voorde *et al.* [92, 105]. The basic idea of this separation method is in analogy with the ones that are frequently used for Sr^{2+}, as both ions share very similar chemical properties and ionic radius (1.25 Å). However, the study did not result in an efficient separation method.

$$M^{2+}{}_{(aq)} + 2\,NO_3^-{}_{(aq)} + \text{DCH18 C6}_{(org)} \rightleftharpoons [M(NO_3)_2\text{DCH18 C6}]_{(org)} \quad [1.6]$$

More promising is a second approach that was presented in the same study, in which the alkaline extraction capacities of the undiluted tertiary ammonium ionic liquid Aliquat 336 nitrate ([A336][NO_3]) were investigated. No additional extractants were used and the system fully complies with the CHON principle [106–108]. In other studies was already shown that trivalent lanthanide ions have the advantage of being able to form anionic complexes with bidentate nitrate ligands (Reaction 1.7), whereas divalent metal ions are unable to form these species [109–111]. Sm^{3+} could thus be extracted to the water-immiscible ionic liquid phase from an aqueous feed solution containing a high salt concentration

(Reaction 1.7), whereas Eu^{2+} remained in the aqueous phase. In this study, it was also shown that europium could be reduced to its divalent state in aqueous solutions containing high nitrate salt concentrations, and remains sufficiently stable to conduct the efficient separation process (see Chapter 2). The high salt concentration in the aqueous feed solution, established by the addition of an inert salt like $Ca(NO_3)_2$, NH_4NO_3 or $LiNO_3$, changed the hydration and activity of the ions significantly. This led to the predominant salting out of the tertiary samarium ions to the ionic liquid phase, with the nitrate anions coordinated bidentately to Sm^{3+} [112]. EXAFS data revealed that the bulky ionic liquid cations do not coordinate directly to the lanthanide ion as they were only found in the second coordination sphere. The ionic liquid cation only ensured charge neutrality of the non-aqueous phase. High separation factors for the samarium-europium couple were reached in a relatively short time frame. Similar extractions from chloride aqueous media proved (Reaction 1.8) to be less efficient because of the higher hydration energy of the chloride anion.

$$Sm^{3+}{}_{(aq)} + 3\,NO_3^-{}_{(aq)} + 2\,[A336]\,[NO_3]_{(org)} \rightleftharpoons [A336]_2[Sm(NO_3)_5]_{(org)} \quad [1.7]$$

$$Sm^{3+}{}_{(aq)} + 3\,Cl^-{}_{(aq)} + 5\,[A336]\,[NO_3]_{(org)} \rightleftharpoons [A336]_2[Sm(NO_3)_5]_{(org)} + 3\,[A336]\,[Cl]_{(org)} \quad [1.8]$$

Zinc impurities originating from the chemical reduction method were also not extracted in case of the nitrate containing aqueous feed solution. Simultaneous removal of Eu^{2+} and Zn^{2+} from Sm^{3+} can thus be achieved in the forward extraction step. Nevertheless, reduction of europium by electrolysis could be another viable option to avoid zinc impurities being introduced in the system. Back-extraction of samarium could be easily achieved by reducing the salt concentration of in the system, *i.e.* by the addition of water. The remaining cations from the inert salt can be removed by means of cation-exchange chromatography. After purification, the mixture can be dried to almost complete dryness, after which it can be re-dissolved in a proper solution for further radiopharmaceutical processing, frequently in dilute HCl solution. Precipitation by hydrolysis of samarium in alkaline media and subsequent re-dissolution is another possibility. More details of this method, and its further development towards an extraction chromatography process, will be treated in the following chapters.

1.6.4 Terbium-161

The interest of using ^{161}Tb ($t_{1/2}$ = 6.9 d) in nuclear medicine has grown over the last decade. ^{161}Tb is being considered as an alternative to the very popular ^{177}Lu radionuclide for targeted radionuclide therapy because of their similar radionuclidic characteristics [113–117]. ^{161}Tb emits low-energy β^- particles of 593 keV (10.0 %), 567 keV (10.0 %), 518 keV (66.0 %) and 461 keV (26.0 %), which are accompanied by γ photons in low abundance, *i.e.* 74.6 keV (9.8 %) and 49 keV (14.8 %), useful for imaging. In addition, ^{161}Tb partially decays by conversion with the emission of conversion and Auger electrons, with energies between 3 and 50 keV [1, 114, 118]. These conversion and Auger electrons represent 27 % of the β^- energy, providing much higher local radiation dose density because of their shorter range in soft tissue (0.5 – 30 mm). The therapeutic application of pure Auger electron emitters is limited by the targeting strategy needed to get close to the radiosensitive target. DNA internalization of the radiopharmaceutical compound is needed. ^{161}Tb, however, offers the unique possibility to simultaneously emit β^-, conversion and Auger electrons. The crossfire effect caused by the β^- particles is complemented by the additionally emitted low-energy electrons. Consequently, more localized radiation damage to the harmful tumor cells can be delivered due to the very high cytotoxicity levels. For these reasons, ^{161}Tb is considered to have a higher therapeutic effect than ^{177}Lu with comparable β^- energy.

Compared to ^{177}Lu, ^{161}Tb provides a higher electron-to-photon dose ratio. Studies showed that ^{161}Tb provides two to three times higher energy transfer in small volumes (10 – 100 mesh), leading to the possibility of intensifying the therapeutic effect of radiopharmaceuticals. Identical radiolabeling approaches can be used for both ^{161}Tb and ^{177}Lu because of their high chemical similarities. Several *in vivo* and *in vitro* studies made use of this advantage to test ^{161}Tb for future targeted radiotherapy [113–119]. Müller *et al.* combined ^{161}Tb with three other terbium isotopes, *i.e.* ^{149}Tb, ^{152}Tb and ^{155}Tb, to arrive at a unique matched quadruplet [119]. The identical chemical characteristics of the four terbium radioisotopes allow the preparation of radiopharmaceuticals with identical pharmacokinetics. These terbium quadruplet radiopharmaceuticals can be used in PET (^{152}Tb) and SPECT (^{155}Tb) diagnosis methods to obtain excellent tumor visualization and can be used for α (^{149}Tb) and β^- (^{161}Tb) targeted therapy.

^{161}Tb can be produced in a nuclear reactor by means of double neutron capture $(2n, \gamma)$ of ^{159}Tb (σ_{th} = 23.23 barn) in natural terbium (Fig. 1.14). The specific activity obtained from this production route is low because of the double neutron capture and carrier-added production. In addition, the longer-lived ^{160}Tb ($t_{1/2}$ = 72.3 d, σ_{th} = 525.6 barn) is present as contaminant. Therefore, ^{161}Tb is

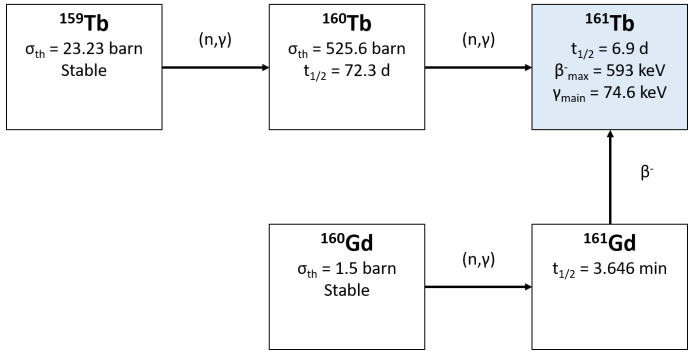

Figure 1.14: Production pathways of the medical ^{161}Tb radionuclide (highlighted). Only the non-carrier-added production pathway *via* neutron capture of ^{160}Gd and subsequent β^- decay leads to ^{161}Tb with sufficiently high radionuclidic purity for medical use.

preferentially produced *via* the alternative non-carrier-added reactor production route, *i.e.* neutron irradiation (n,γ) of an enriched ^{160}Gd (σ_{th} = 1.5 barn) target [114]. This way, short-lived ^{161}Gd ($t_{1/2}$ = 3.646 min) is produced, which decays *via* β^- emission to the ^{161}Tb medical radionuclide. Radionuclidic pure ^{161}Tb can be obtained at the end of the irradiation because of the very short half-life of ^{161}Gd if a highly enriched ^{160}Gd target material is used.

Other gadolinium isotopes that occur in natural gadolinium target material might significantly decrease the specific activity and the yield of ^{161}Tb. For example, the presence of ^{157}Gd can be a major concern. ^{157}Gd can act as a neutron poison because of its very high thermal neutron cross-section (σ_{th} = 254.000 barn), with ^{158}Gd being produced. Neutron irradiation of ^{158}Gd (σ_{th} = 2.3 barn), also present in natural gadolinium target material, leads to the production of ^{159}Gd ($t_{1/2}$ = 18.479 h), which forms the stable ^{159}Tb *via* β^- decay. Presence of stable ^{159}Tb decreases the specific activity of ^{161}Tb and might lead to accumulation of the relatively long-lived ^{160}Tb when being irradiated (n,γ). Undeniably, the use of a highly enriched target material is a key importance to obtain ^{161}Tb with high radionuclidic purity and high specific activity.

Decay of ^{161}Tb leads to the formation of stable ^{161}Dy in the system, which can interfere with ^{161}Tb during radiolabeling because of its similar chemical properties. The accumulation of ^{161}Dy leads to a significantly lower specific activity for ^{161}Tb, which decreases proportionally after irradiation (Fig. 1.15) [114]. Therefore, isolation of ^{161}Tb from ^{161}Dy should be considered, although radiochemical strategies mainly focus on isolating the micro-amounts of ^{161}Tb from macro-amounts of gadolinium target material. The gadolinium and

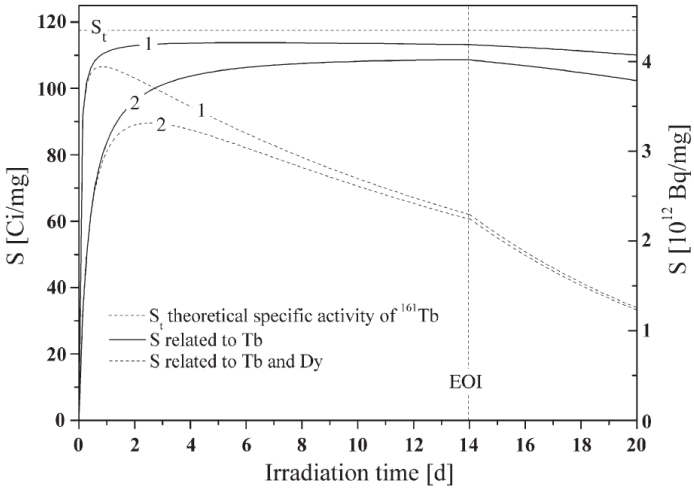

Figure 1.15: Specific activity of ^{161}Tb for irradiation of 10^{15} and $10^{14}\,\mathrm{n\,cm^{-2}\,s^{-1}}$ ((1) and (2) respectively). Enriched target material contained 98.2 % ^{160}Gd, 0.85 % ^{158}Gd, 0.27 % ^{157}Tb and 5 ppm stable terbium. High specific activity can be achieved, which is here expressed as the ratio of the mass of ^{161}Tb over the total mass of all lanthanides present in the irradiated target material. Accumulation of stable ^{161}Dy in the system reduces the quality significantly. Reprinted with permission from Lehenberger *et al.* [114] Copyright © 2011 Elsevier Inc.

dysprosium content have to be reduced by a factor of $> 10^5$ and > 10, respectively, to obtain high-quality ^{161}Tb preparations.

The well-established separation method making use of a cation-exchange resin and α-hydroxyisobutyric acid (α-HIBA) is used most frequently to isolate ^{161}Tb from redundant gadolinium material. A separation factor for Tb^{3+}/Gd^{3+} of 2.40 can be achieved this way. Lehenberger *et al.* [114] demonstrated this purification method by using an Aminex-A6 (NH_4^+ form) cation-exchange resin in a column chromatography setup and a $0.13\,\mathrm{mol\,L^{-1}}$ α-HIBA (pH 4.5, adjusted with NH_3 solution) eluent. ^{161}Tb was eluted first because of the slightly higher stability of the Tb-α-HIBA complex in the eluent. This higher stability originates from the higher charge density and lower ionic radius of Tb^{3+} compared to Gd^{3+} as a result of the lanthanide contraction. Gadolinium was stripped from the cation-exchange column by a $0.5\,\mathrm{mol\,L^{-1}}$ α-HIBA solution. The elution of terbium prior to gadolinium is advantageous to isolate the micro-amounts from the bulk material. Additionally, the use of this separation system provided a separation factor of 2.30 for the Dy^{3+}/Tb^{3+} pair, with dysprosium eluting first. The ^{161}Tb fraction was acidified with $1\,\mathrm{mol\,L^{-1}}$ HCl to reach a pH of *ca.* 1,

after which the solution was loaded onto a small secondary column filled with a cation-exchanger in H^+ form. Acidification breaks the Ln^{3+}-α-HIBA complex. After washing of the column for α-HIBA removal, the ^{161}Tb was stripped with a $4\,\mathrm{mol\,L^{-1}}$ HCl solution.

Monroy-Guzman *et al.* [74, 75] presented a different column chromatographic approach, using an extraction column loaded with Eichrom LN resin. This commercial resin exists of an inert polymeric absorbent impregnated with the extractant di-(2-ethylhexyl)phosphoric acid (HDEHP). As already mentioned before, the extraction capability of HDEHP is determined by the pH of the solution, *i.e.* the distribution ratios increase with increasing acid concentration. Stability of the Ln^{3+}-HDEHP complex increases with atomic number because of the increasing charge density originating from the lanthanide contraction. Therefore, gadolinium was eluted from the column prior to ^{161}Tb. After dissolution of the irradiated target in $0.15\,\mathrm{mol\,L^{-1}}$ HNO_3 and loading onto the column, gadolinium was desorbed by elution with a $0.8\,\mathrm{mol\,L^{-1}}$ HNO_3 solution. ^{161}Tb was recovered from the column by a $3.0\,\mathrm{mol\,L^{-1}}$ HNO_3 solution. ^{161}Tb was precipitated as hydroxide and redissolved by a dilute HCl solution for conversion into a suitable form for further radiopharmaceutical processing.

1.6.5 Dysprosium-165

The use of ^{165}Dy ($t_{1/2}$ = 2.334 h) in modern nuclear medicine is rather scarce, if not abandoned because of better available alternatives (*e.g.* ^{169}Er). Examples of ^{165}Dy being used in nuclear medicine mainly describe application in radiosynovectomy [120–125]. Joints affected by arthritis can be treated by its β^- particle emission of 1.286 MeV, which has a maximum soft tissue range of 5.7 mm and a mean soft tissue range of 1.8 mm.

The production of ^{165}Dy involves neutron irradiation (n,γ) of a highly enriched ^{164}Dy (σ_{th} = 2720 barn) target material. Obtaining a radionuclidic pure ^{165}Dy is rather complicated because of its short half-life and its large thermal and epithermal neutron cross-section (σ_{th} = 3900 barn, σ_{epi} = 22.000 barn) [24] (Fig. 1.16). This high thermal neutron cross-section ensures an easy uptake of a second neutron ^{164}Dy$(2n,\gamma)$, producing the longer-lived β^- particle emitting ^{166}Dy ($t_{1/2}$ = 81.6 h). Separation of ^{165}Dy from the ^{164}Dy target material and ^{166}Dy isotope is chemically impossible, and thus will remain carrier-added. It is clear that obtaining radionuclidic pure ^{165}Dy is very difficult. Another problem preventing widespread use is its short half-life. Besides, ^{166}Dy is the parent isotope for ^{166}Ho ($t_{1/2}$ = 26.83 h), which is another useful medical radiolanthanide, *i.e.* ^{164}Dy$(n,\gamma)^{165}$Dy$(n,\gamma)^{166}$Dy$(\beta^-)^{166}$Ho. As will be discussed in the next section, ^{166}Ho isotopes can be easily isolated from

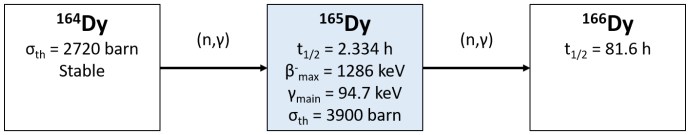

Figure 1.16: Production pathway of the medical ^{165}Dy radionuclide (highlighted) *via* neutron capture of ^{164}Dy. The high neutron cross-section of ^{165}Dy results in the longer-lived ^{166}Dy.

dysprosium *via* a radionuclide generator system after it has been accumulating in the system over time.

1.6.6 Holmium-166

^{166}Ho ($t_{1/2}$ = 26.83 h) can be used in theranostics because of its interesting physical decay properties, making it an interesting radionuclide in nuclear medicine. ^{166}Ho emits two major β^- particles, *i.e.* 1.854 MeV (50.0 %) and 1.774 MeV (48.7 %), which have a mean soft tissue penetration range of 4 mm and a maximum soft tissue penetration range of 8.7 mm [32, 126].

Despite its relatively short half-life, ^{166}Ho is an excellent radionuclide for *in vivo* therapeutic applications. ^{166}Ho-DOTMP (DOTMP = 1,4,7,10-tetraazacyclododecane-1,4,7,10-tetramethylene phosphonic acid) is the most common ^{166}Ho-based therapeutic radiopharmaceutical, targeting multiple myeloma (cancer of the plasma white blood cells) in the bone marrow of patients. Like several other radiolanthanides, the use of ^{166}Ho-EDTMP has been explored for bone pain palliation [127]. The use of ^{166}Ho loaded poly(L-lactic acid) (PLLA) microspheres, which are commercially available as QuiremSpheres, was investigated for the treatment of liver malignancies [126, 128–130]. Due to the average diameter of these microspheres of 30 mm, the microspheres lodge preferentially in the microvasculature surrounding the tumor, maximizing tumorcidal effects and minimizing the effects on healthy liver parenchyma. Many other ^{166}Ho radiopharmaceuticals were also explored [1, 131–133]. The emission of β^- particles is accompanied with an 80.6 keV (6.2 %) γ photon emission, which is perfectly suitable for effective imaging. Owing to the paramagnetic properties of holmium and dysprosium, visualization can also proceed *via* magnetic resonance imaging (MRI) [134]. Outpatient therapy with ^{166}Ho is possible because of the absence of high-energy γ rays, *i.e.* there is no significant external radiation to other individuals.

Distribution of ^{166}Ho-labeled radiopharmaceuticals is often hampered by its relatively short half-life, reaching only a limited area within short proximity of

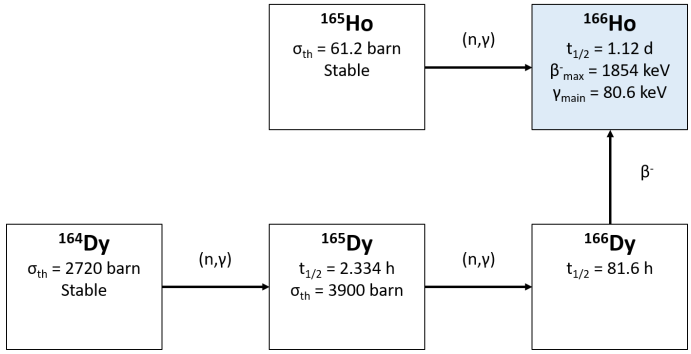

Figure 1.17: Production pathways of the medical ^{166}Ho radionuclide (highlighted). The neutron capture of ^{165}Ho leads carrier-added ^{166}Ho with modest specific activities. Double neutron capture of ^{164}Dy and subsequent β^- decay leads to non-carrier-added ^{166}Ho, which can be isolated with high specific activity by using a nuclide generator system.

the production site. Efficient production and purification methods are of key importance (Fig. 1.17). In a first method, ^{166}Ho can be produced *via* direct neutron irradiation (n,γ) of ^{165}Ho (100 % natural abundance). ^{166}Ho remains carrier-added, with the only possible radionuclidic impurity being the long-lived ^{166m}Ho ($t_{1/2}$ = 1200 y). The relatively high thermal neutron cross-section of ^{165}Ho (σ_{th} = 61.2 barn) leads to the production of high activity levels of ^{166}Ho. However, only modest specific activities are reached since only a very small portion of target atoms are converted to ^{166}Ho at saturation yields. These modest specific activities cannot be used for radiolabeling of most targeting molecules, but are suitable for applications where higher radiopharmaceutical masses can be administered.

High specific activities for ^{166}Ho can be efficiently obtained non-carrier-added *via* β^- decay of reactor produced ^{166}Dy ($t_{1/2}$ = 81.6 h), using ^{164}Dy (σ_{th} = 2720 barn) as initial target material [25, 135–139]. This production route involves a double neutron capture $(2n,\gamma)$ reaction *via* the short-lived ^{165}Dy ($t_{1/2}$ = 2.334 h, σ_{th} = 3900 barn) intermediate, *i.e.* $^{164}\text{Dy}(n,\gamma)^{165}\text{Dy}(n,\gamma)^{166}\text{Dy}(\beta^-)^{166}\text{Ho}$.

A radionuclide generator system is often used to separate the ^{166}Ho isotopes from the bulk dysprosium (containing ^{166}Dy). ^{166}Dy has a significantly longer half-life with respect to ^{166}Ho, causing ^{166}Ho to accumulate in the system over time. ^{166}Ho isotopes can be selectively eluted or 'milked' from this radionuclide generator system, leaving dysprosium behind [135, 138]. Major advantage of this system is that no direct access to a nuclear reactor is needed as the desired ^{166}Ho medical radionuclide can be obtained on demand. A more flexible distribution of

^{166}Ho can be achieved this way. However, the generator system has to be replaced frequently due to the relatively short half-life of ^{166}Dy. Most of these ^{166}Ho radionuclide generator systems are already well established. Majority of them are based on an ion-exchange chromatography method, typically making use of a metal-free HPLC system equipped with a Dowex-50W or Aminex-A5 cation-exchange column and the weekly complexing agent α-HIBA ($0.085\,\mathrm{mol\,L^{-1}}$, pH = 4.3 adjusted with NH_3 solution) as the eluent [136, 140]. The smaller ionic radius and higher charge density of holmium as a result of the lanthanide contraction leads to a slightly higher thermodynamic stability of the Ho-α-HIBA complex compared to the Dy-α-HIBA complex in the eluent. Therefore, the Ho-α-HIBA complex is being eluted first. Dadachova *et al.* presented the applicability of this method mid-1990s by achieving a high separation factor for holmium and dysprosium [140]. The Ho-α-HIBA complex was subsequently destroyed by the addition of acidic chloride solutions. A small-scale cation-exchange column separation from acidic chloride solutions ensured final removal of α-HIBA and ^{166}Ho being present in a solvent suitable for radiolabeling of pharmaceuticals. Separation was achieved within 2 h with a 95 % overall radiochemical yield for carrier-free ^{166}Ho. Breakthrough of dysprosium remained below 0.1 %. Purification of non-carrier-added ^{166}Ho from Dy_2O_3 targets with electrophoresis or ion-exchange chromatography using HDEHP or TBP (TBP = tri-*n*-butyl phosphate) as stationary phase and $3 - 12\,\mathrm{mol\,L^{-1}}$ HNO_3 as mobile phases proved to be unsatisfactory for biomedical applications of ^{166}Ho [141]. Only partial separation could be achieved.

Recently, Vosoughi *et al.* presented a method to separate ^{166}Ho from ^{166}Dy by an extraction chromatographic method based on 2-ethylhexyl 2-ethylhexylphosphonic acid (HEH[EHP], Eichrom LN2 resin)[138]. Quantitative separation was achieved in 1.5 h at 25 °C by using an eluent comprised of $1.5\,\mathrm{mol\,L^{-1}}$ HNO_3. Impurities were removed by a preliminary washing step with $0.1\,\mathrm{mol\,L^{-1}}$ HNO_3. In this method, dysprosium was eluted prior to holmium. Coordination of holmium by HEH[EHP] in the stationary phase is energetically more stable because of its slightly higher charge density originating from its smaller ionic radius. A radionuclide purity of > 99.9 %, a separation yield of 76 % and a radiochemical purity of > 99 % were reached.

Another extraction chromatographic method was presented by Monroy-Guzman *et al.* [74, 75], making use of the Eichrom LN resin (HDEHP-based). The extraction mechanism and extraction capability of HDEHP is highly dependent upon the acidity of the aqueous phase, *i.e.* the distribution ratios of lanthanides substantially increase with atomic number and concentration of the nitric acid because of the changing stability constant with atomic number. The first step involved dissolution of the irradiated nitrate salt in $0.15\,\mathrm{mol\,L^{-1}}$ HNO_3 and adsorption onto the chromatographic column loaded with Eichrom LN resin.

Elution with a 1.5 mol L^{-1} HNO_3 solution ensured desorption of the ^{166}Dy parent prior to the ^{166}Ho isotope. ^{166}Ho was eluted afterwards using a 3 mol L^{-1} HNO_3 solution. Precipitation of $Ho(OH)_3$ by addition of NaOH and re-dissolution of the hydroxide with 0.1 mol L^{-1} HCl delivered a ^{166}Ho chloride solution with high radionuclide purity (> 99.9 %) for further processing of the radiopharmaceutical. According to Monroy-Guzman *et al.* the purification method could be completed in less than 30 min [74, 75].

1.6.7 Erbium-169

^{169}Er ($t_{1/2}$ = 9.392 d) is used in targeted therapy as a soft β^- emitting (350 keV) radionuclide with an average soft tissue range of 0.3 mm. ^{169}Er is the most preferred choice for radiosynovectomy (RSV) of inflamed small joints such as the metacarpophalangeal, metatarsophalangeal and digital interphalangeal joints in treatment of rheumatoid arthritis and degenerative joint diseases (hydroxyapatite (HA) or citrate particles) [1, 142–146]. In some cases, ^{169}Er can also be used for bone pain palliation applications (DOTA-based ligand particles). Radiotherapy with ^{169}Er usually involves intra-articular injection of the β^- emitting ^{169}Er in colloidal or particulate form (1 – 10 mm). Low volumes containing 18 – 37 MBq (0.5 – 1 mCi) are typically administered to the patient.

^{169}Er has been found to be cost effective in providing long-term relief of pain and deformity of the inflamed joints in comparison to other therapeutic approaches. Radiation damage to surrounding healthy tissue is minimal as only minor damage to the cartilage and adjacent bones was observed. Additionally, the use of ^{169}Er does not involve any radiation risk. Therefore, treatment with ^{169}Er can be performed on outpatient basis, meaning that the patient does not necessarily have to be hospitalized overnight. The rather poor neutron capture cross-section of ^{168}Er (σ_{th} = 1.28 barn) leads to production of radionuclides with only low specific activity (Fig. 1.18). Therefore, the use of ^{169}Er for labeling of tumor receptors or antigen-targeting vectors is excluded, as much higher specific activities are required for these applications.

Reactor production and electrochemical purification of ^{169}Er as a potential step towards its use in *in vivo* therapeutic applications was reported by Chakravarty *et al.* [143]. For its production, high-purity enriched ^{168}Er (> 98 %) is irradiated by thermal neutrons. ^{169}Yb ($t_{1/2}$ = 32 d) was reported to be present as radionuclidic impurity after irradiation in some cases, impeding the clinical use of ^{169}Er [143]. ^{169}Yb originates from the trace level ^{168}Yb impurities (*ca.* 20 ppm) present in the target material. ^{168}Yb possesses a high thermal neutron cross-section (σ_{th} = 2300 barn), leading to significant amounts of ^{169}Yb after irradiation. Major concerns lie within the electron capture decaying route of ^{169}Yb, which is

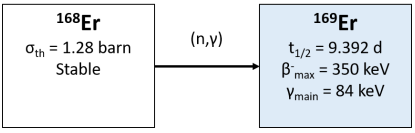

Figure 1.18: Production pathway of the medical ^{169}Er radionuclide (highlighted) *via* neutron capture of ^{168}Er.

followed by the emission of high abundance γ photons to stable ^{169}Tm. These γ photons may deliver unnecessary dose to non-targeted organs, affecting the dosimetric evaluation of the administered ^{169}Er radiopharmaceutical.

As ^{169}Er and ^{169}Yb are chemically very similar, their separation *via* chromatographic ion-exchange and solvent extraction methods is not straightforward and might take a large amount of separation steps. Therefore, Chakravarty *et al.* investigated a purification method based on the difference in electrode potential of Er and Yb [143, 147]. A two-step electro-amalgamation separation technique was established, based on the selective reduction of ytterbium to the divalent state and its preferential transfer on to a mercury-pool cathode (Fig. 1.13). The purification method was demonstrated for ^{169}Er and ^{169}Yb dissolved in a 0.15 mol L^{-1} lithium citrate solution, of which the pH was adjusted to 6–7 by drop-wise addition of 0.1 mol L NH_3 solution. Subsequent electrolysis was carried out by applying a constant potential of 8 V (current of 500 mA) for 15 min. After the electrolysis, mercury was removed from the electrolysis cell, whereas the aqueous electrolyte was transferred to a new electrolysis cell for a repetition of the procedure. After evaporation of the purified ^{169}Er phase to near dryness, 0.1 mol L^{-1} HCl was added for subsequent radiolabeling processes. The purification process showed a negligible (< 5 %) loss of ^{169}Er activity. The level of ^{169}Yb impurities (1 % before purification) in ^{169}Er after the first electrolysis step was shown to be reduced to < 0.1 %, and to trace levels after repetition of the electrolysis procedure.

1.6.8 Thulium-170

Despite its longer half-life, ^{170}Tm ($t_{1/2}$ = 128.4 d) was investigated to be used in bone pain palliation [76, 148–152]. ^{170}Tm emits β^- particles with a maximum energy of 968 keV, which are accompanied by the emission of γ photons of 84 keV (3.26 %). These photons are suitable for imaging and dosimetry purposes, and can be used safely in medicine.

^{170}Tm can be produced *via* neutron capture of ^{169}Tm (σ_{th} = 109 barn) by irradiation of a natural thulium target (n, γ) (Fig. 1.19). This target contains

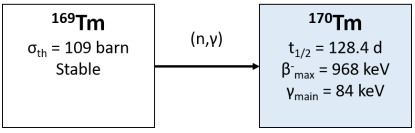

Figure 1.19: Production pathway of the medical ^{170}Tm radionuclide (highlighted) *via* neutron capture of ^{169}Tm.

100 % ^{169}Tm, *i.e.* mononuclidic, because ^{169}Tm is the only stable isotope of thulium found in nature. Sufficiently high specific activity for ^{170}Tm can be reached using a medium- or high-flux research reactor. ^{170}Tm remains carrier-added, and can therefore not be used for radiolabeling. No further radiochemical purification steps are required after the irradiation for ^{170}Tm to be used in nuclear medicine. The ability to use a natural thulium target for irradiation and the ability to omit radiochemical purification steps result in a relatively cost-efficient production process.

1.6.9 Lutetium-177

^{177}Lu ($t_{1/2}$ = 6.65 d) became one of the most important therapeutic radionuclides in nuclear medicine over the last decades because of its high theranostic potential and convenient production logistics [41, 153–159]. Principal applications of ^{177}Lu include radiosynovectomy and treatment of bone metastases for bone pain relief, neuroendocrine tumors, liver cancer, breast cancer and ovarian cancer [113, 160–168]. Studies on the development and reports on *in vivo* and *in vitro* application of modified and new ^{177}Lu-based radiopharmaceutical compounds are being published at a fast pace. The possible applications for ^{177}Lu seem to be endless, as shown in the comprehensive review of Banerjee *et al.* in 2015 [41]. Potential radiopharmaceuticals based on a wide range of targeting vectors are being investigated, including, monoclonal antibodies, peptides, bone pain palliation agents (*e.g.* EDTMP), particulates, steroids, porphyrins, nitroimidazoles, bacteria (*e.g.* E. Coli), fullerenes and nanobodies. Most of these targeting vectors are based on a bifunctional chelating agent (BFCA, *e.g.* DOTA-based), *i.e.* they consist of an organic molecule that possesses a chelating moiety located at one terminus of the agent and an active functionality located at the other end of the molecule to connect with the vector molecule.

^{177}Lu owns its high theranostic potential to its favorable radionuclidic characteristics. ^{177}Lu emits low to medium energy β^- particles (498 keV (79.3 %), 380 keV (9.1 %) and 176 keV (12.2 %)) with a soft tissue penetration range

of several millimeters. Simultaneous low-abundance emission of γ photons (321.3 keV (0.219 %), 249.7 keV (0.212 %), 208.37 keV (11.1 %), 112.95 keV (6.40 %) and 71.65 keV (0.15 %)) allows the use of imaging. The attractive β^- emission and half-life lead to convenient production logistics. Additionally, different available options exist to efficiently produce ^{177}Lu with high specific activities in a nuclear reactor, advancing its production flexibility. A comprehensive review on these different production pathways was written by Dash *et al.* in 2015 [154]. Although it would be possible to produce ^{177}Lu by charged particle acceleration in a cyclotron, neutron activation in a nuclear reactor is the most practical and cost-effective route [19, 20, 41, 139, 169].

^{177}Lu can be efficiently produced by two different routes making use of neutron irradiation, *i.e.* (1) carrier-added by neutron activation (n,γ) of a natural (97.4 % ^{175}Lu, 2.6 % ^{176}Lu) or an enriched (in ^{176}Lu) lutetium target or (2) non-carrier-added by neutron activation of an enriched (in ^{176}Yb) ytterbium target and subsequent β^- decay of ^{177}Yb ($(n,\gamma) \rightarrow \beta^-$), followed by radiochemical separation of the ^{177}Lu isotopes from the redundant ytterbium material (Fig. 1.20) [41, 154, 169]. Both production routes lead to products having different specific activities.

Despite the usually low specific activities obtained by (n,γ) activation, relatively high specific activities can be achieved for ^{177}Lu. Even direct neutron activation of a natural target results in reasonable high specific activity because of the high thermal neutron cross-section of ^{176}Lu (σ_{th} = 2090 barn). This is among the highest thermal neutron cross-sections among the presently (n,γ) produced radionuclides [169]. The high cross-section also ensures that there will be no constraints with respect to large-scale production of the ^{177}Lu radionuclide with high specific activity, suitable for developing agents for targeted radiotherapy [20]. Nevertheless, the irradiation time will have to be carefully optimized to obtain these high specific activities because of the considerably high target burn up due to the high thermal neutron cross-section of ^{176}Lu [41, 154, 169]. As well described by Pillai *et al.* for three different thermal neutron fluxes, a maximum specific activity will be reached after a certain irradiation time, after which the activity will decrease again [169]. The higher the thermal neutron flux of the reactor, the shorter the time of irradiation for attaining maximum specific activity will be.

Despite its lower cross-section, double neutron capture $(2n,\gamma)$ by ^{175}Lu (σ_{th} = 25.9 barn) in a natural lutetium target can lead to a significant contribution of the specific activity of the ^{177}Lu in case high thermal neutron fluxes are applied [41, 139, 154, 170]. However, neutron activation of ^{176}Lu (σ_{th} = 2 barn) might lead to the concomitant production of long-lived $^{177\mathrm{m}}$Lu ($t_{1/2}$ = 160.4 d). Nuclei with the same atomic number and mass number but different energy are called nuclear isomers. 78.6 % of $^{177\mathrm{m}}$Lu decays *via* β^- emission to $^{177\mathrm{m}}$Hf and

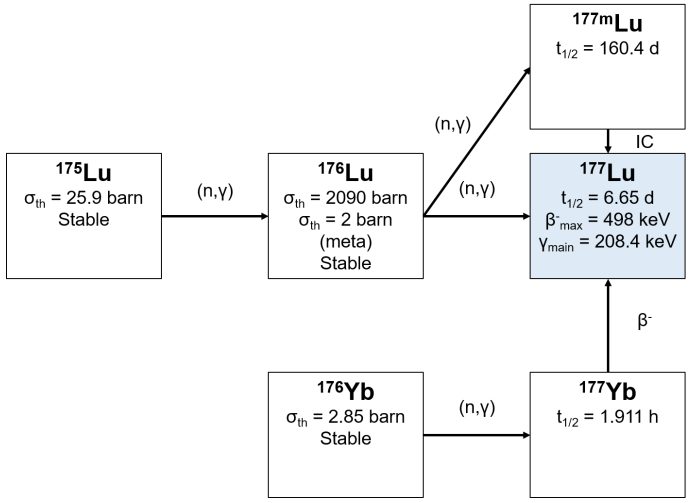

Figure 1.20: Production pathways for the medical ^{177}Lu radionuclide (highlighted). Direct neutron capture of ^{176}Lu leads to efficient production of carrier-added ^{177}Lu with high specific activities. Long-lived ^{177m}Lu is present in minor amounts in the target after irradiation. Indirect production *via* neutron capture of ^{176}Yb and subsequent β^- decay of ^{177}Yb leads to non-carrier-added ^{177}Lu, which can be obtained with high specific activity after radiochemical purification.

^{177}Hf and 21.4 % decays to the ground state, *i.e.* ^{177}Lu, *via* isomeric transition. Isomeric transition is possible *via* γ emission or internal conversion, where the excess of nucleus energy is transferred radiationless to an electron in the K-, L- or M-shell. The latter one leads to an Auger electron cascade, resulting in a highly charged state that ultimately provokes bond rupture. The presence of ^{177m}Lu isomer might restrict the use of carrier-added ^{177}Lu in some countries. The ^{177m}Lu content present in the irradiated material depends on the irradiation time, but also on the time elapsed after the end of irradiation because of its long half-life. Owing to the low neutron cross-section of ^{176}Lu, the specific activity of ^{177m}Lu will be low. The resulting radiation dose increase arising from the isomeric transition of ^{177m}Lu is insignificant at clinically significant dose levels [154]. Nevertheless, the presence of ^{177m}Lu requires separate waste collection, including excreta of the patients, and special waste treatment for disposal. According to European radiation safety regulation, the maximum permissible radioactive concentration of ^{177m}Lu in municipal sewage is 50 kBq m^{-3}.

Recently, Bhardwaj *et al.* presented a method to separate the ^{177}Lu and ^{177m}Lu nuclear isomers *via* the Szilard-Chalmers process [170]. The separation method combines the nuclear after-effects of the nuclear decay caused by the

internal conversion and the use of a very stable chemical complex with slow association-dissociation kinetics. The internal conversion process is able to break the chemical bonds of the complex due to the highly charge state created. A subsequent chromatographic separation step is able to separate a complexed lutetium ion from a free one. Based on this concept, a new type of radionuclide generator was established with the unique feature of comprising a parent and daughter radionuclide from the same element. Bhardwaj *et al.* proved this concept by applying a reversed phase chromatographic system in which a ^{177m}Lu-DOTA-(Tyr^3)-octreotate (^{177m}Lu- DOTATATE) complex (dissociation constant $k_d = 2 \times 10^{-8}\,\mathrm{s}^{-1}$ at 20 °C) was retained on a tC-18 silica column. This apolar silica column does not show any affinity towards polar metal ions. Therefore, bond ruptured ^{177}Lu ions could be easily eluted from the column using a mobile phase with the proper polarity, whereas the ^{177m}Lu-DOTATATE exhibited a very long retention time, *i.e.* the complex remained immobilized on the column. The mobile phase consisted of a solution containing 5 % methanol, 150 mmol L^{-1} NaCl and 10 mmol L^{-1} NaAc–HAc buffer (pH 4.3).

Neutron activation of an enriched ^{176}Yb (σ_{th} = 2.85 barn) target leads to non-carrier-added ^{177}Lu *via* β^- decay of ^{177}Yb ($t_{1/2}$ = 1.911 h). The rather low thermal neutron capture crosssection leads to significantly lower production yields compared to the direct irradiation of ^{176}Lu. It is required to irradiate the target with a medium to high thermal neutron flux for a relatively long irradiation time to provide an adequate production yield. No long-lived ^{177m}Lu ($< 10^{-5}$ %, below detection limit) is produced concurrently in this indirect production route, but radiochemical separation of ^{177}Lu from the redundant ytterbium target material is required to obtain a radionuclidic pure product with high specific activity [154]. The presence of ytterbium will reduce the effective specific activity in the final product and will interfere in the radiolabeling process. An efficient separation method has to be established to isolate a very low quantity of ^{177}Lu from a large quantity of the irradiated ytterbium target material. A decontamination factor of approximately 104 has to be obtained. This way, the enriched ^{176}Yb target material can also be carefully recovered. Combining the need of using highly enriched target material, a high thermal neutron flux, longer irradiation times and the requirement for radiochemical processing, this indirect production route will be more cost-intensive. Nevertheless, the ability to obtain non-carrier-added ^{177}Lu is a major advantage for radiolabeling, which is required for targeted radiotherapy. Additionally, the non-carrier-added production method provides ^{177}Lu with a longer shelf-life because of its slower decrease in specific activity and absence of ^{177m}Lu.

Numerous different methods exist to separate ^{177}Lu from the redundant ytterbium target material. ^{177}Lu/Yb can be considered as the most widely studied lanthanide couple in scope of radiolanthanide purification. Some of

them are based on the slight differences in stability constants of both adjacent lanthanide ions with a particular ligand *via* ion-exchange chromatography or solvent extraction techniques, while others are based on electrochemical methods as it is possible to reduce ytterbium to its divalent state. Yb^{2+} is relatively stable because of its fully filled $4f$ subshell, by which its properties become similar to alkaline earth cations (*e.g.* Ca^{2+} and Sr^{2+}).

Ion-exchange and extraction chromatography techniques proved to be reliable and straightforward to separate the radionuclides of interest. The order of elution of both lanthanides and the resolution of the elution bands depend on the stability constant values of the formed complexes, and in which phase these complexes are being formed [154]. The smaller Lu^{3+} ions, originating from the lanthanide contraction, tend to form slightly more stable complexes compared to the Yb^{3+} ions. If the well-characterized α-HIBA complexing agent is used as eluting agent, ^{177}Lu will be eluted prior to ytterbium. In contrast to other adjacent lanthanides, a separation factor of only *ca.* 1.55 was reached for Lu/Yb. Peak tailing might cause the lutetium fraction to still contain significant levels of ytterbium. An additional purification step is required to remove the complexing agent prior to labeling. α-HIBA can be removed from ^{177}Lu by adsorption onto a cation-exchange resin, followed by elution with a highly acidic eluent (*e.g.* concentrated HCl solution). Despite the relatively low separation factor for Lu/Yb by using α-HIBA, plenty of research was conducted to establish a useful purification method [171–174].

Balasubramanian *et al.* developed a separation method using a Dowex-50Wx8 (200 – 400 mesh) cation-exchanger in its Zn^{2+} form and using a 0.04 mol L^{-1} α-HIBA (pH 4.6) solution as eluent [172]. ^{177}Lu was separated with a yield of 70 % and a radionuclidic purity of > 99 %. 30 % of the ^{177}Lu remained contaminated with ytterbium, and was disposed after separation. An additional purification step to remove Zn^{2+} after Lu/Yb separation was required in this method.

Hashimoto *et al.* [173] described a method using a Resolve C18 column in reverse-phase ion-chromatography and an eluent containing 0.25 mol L^{-1} α-HIBA as complexing agent and 0.1 mol L^{-1} 1-octanesulfonate as ion-pairing agent. Radiochemical pure ^{177}Lu was obtained with a 84 % yield. However, this method proved to be suitable for relatively low quantities (0.01 – 1 mg) only.

Barkhausen [171] investigated different approaches by using a macroporous cation-exchange resin and changing the composition of the mobile phase. The target was dissolved in a 0.05 mol L^{-1} NH_4Cl solution to load the column. A gradient mobile phase of α-HIBA (pH 4.75) was used as eluent. The ^{177}Lu fraction eluted at a α-HIBA concentration of 0.08 mol L^{-1}, whereas ytterbium was eluted by using a 0.5 mol L^{-1} α-HIBA solution. Decontamination factors of > 10^5 were achieved. Removal of the complexant by releasing ^{177}Lu from

α-HIBA was obtained by the use of an additional cation-exchange resin. α-HIBA was eluted using a $0.5\,\mathrm{mol\,L^{-1}}$ HCl eluent, whereas ^{177}Lu was eluted using a $4\,\mathrm{mol\,L^{-1}}$ HCl eluent. Different methods, *i.e.* cation-exchange, extraction chromatography and precipitation, can be applied to recover the ytterbium target material. The purification process demonstrated by Barkhausen *et al.* proved to be applicable for bigger sample loadings (*ca.* 150 mg target material) [171].

Lebedev *et al.* investigated a separation process in which ytterbium is selectively extracted by sodium amalgam (Na(Hg)) from Cl^-/CH_3COO^- electrolytes (*i.e.* cementation) prior to the ion-exchange chromatography step [175]. Advantage was taken of the higher solubility of metallic ytterbium in mercury. After dissolution of the target material in $4\,\mathrm{mol\,L^{-1}}$ HCl, a $4.5\,\mathrm{mol\,L^{-1}}$ CH_3COONa solution was added (pH 3.4). The solution was stirred with sodium amalgam, which is a powerful reducing agent. Ytterbium was reduced to its metallic state and migrates to the mercury more easily than lutetium. The total process comprised eight cementation cycles, after which 99 % ytterbium was removed and 85 % ^{177}Lu remained in solution. Subsequently, the remaining ^{177}Lu and ytterbium impurities were precipitated as hydroxides and removed from the mercury compounds by centrifugation. The hydroxides were re-dissolved in $0.1\,\mathrm{mol\,L^{-1}}$ HCl for a subsequent ion-exchange step making use of an Aminex A6 column (NH_4^+ form) and a $0.07\,\mathrm{mol\,L^{-1}}$ α-HIBA solution (pH 4.7). An overall separation yield of 75 % with an ytterbium contamination of $< 10^{-6}$ % was obtained within 4 – 5 h for a 100 mg ^{176}Yb target. This method, however, is rather complicated and time-consuming.

Bilewicz *et al.* investigated the use of Na(Hg) for the reduction of ytterbium to its divalent state, *i.e.* Yb^{3+} to Yb^{2+} [176]. Instead of using ion-exchange chromatography immediately after the reduction step, Bilewicz *et al.* precipitated Yb^{2+} as its sulfate ($YbSO_4$). From a 50 mg irradiated target, the remaining ^{177}Lu solution contained only 1 mg of ytterbium after removal of the precipitate. An overall recovery of ^{177}Lu was estimated at 73 %. A subsequent ion-exchange chromatography process increased the radionuclidic purity of ^{177}Lu.

A slightly different use of amalgam for ^{177}Lu/Yb separation was demonstrated by Chakravarty *et al.* [104, 177]. Like for the purification of ^{153}Sm and ^{169}Er, Chakravarty *et al.* investigated the use of electro-amalgamation to isolate non-carrier-added ^{177}Lu from ytterbium in a lithium citrate medium (Fig. 1.13). A mercury pool serves well as cathode material in this setup because of its large over-potential for hydrogen. Moreover, ytterbium shows the ability to form amalgam (Yb(Hg)), whereas lutetium possesses no amalgam forming properties [147]. In a two-cycle electrolysis procedure, ytterbium was selectively reduced to its divalent state and migrated to the mercury pool cathode. The ^{177}Lu/Yb

feed solution (pH 6) was subjected to a potential of 8 V for 50 min in a first electrolysis cycle. The same process was repeated in a second electrolysis cycle after replacement of the mercury pool cathode material. ^{177}Lu with a > 99.99 % radionuclidic purity and overall separation yield of *ca.* 99.9 % was achieved within 3 – 4 h. The mercury content in the final ^{177}Lu product was reported to be < 1 ppm. This method, however, did not show the ability to recover the valuable ^{176}Yb target material from the amalgam to be used in a new irradiation cycle.

In addition to ion-exchange and electrochemical methods, the use of extraction chromatography techniques have been explored widely [1, 59, 139, 178]. Knapp *et al.* developed a one-step extraction chromatography separation process making use of the commercial available LN resin (Eichrom), which comprises di-(2-ethylhexyl) phosphoric acid (HDEHP) [1, 52, 139, 179]. Both ^{177}Lu and the redundant ytterbium were loaded onto the column, after which the column was eluted with a 2 mol L^{-1} HCl solution. Lutetium forms more stable complexes with HDEHP in the resin because of its slightly higher charge density, smaller ionic radius and lower hydration number. Therefore, ytterbium was eluted from the column first. Lutetium was eluted from the column using a 6 mol L^{-1} HCl solution. A recovery yield of 91 % for ^{177}Lu was obtained using this method.

Horwitz *et al.* further explored this extraction chromatography technique by making use of an extraction chromatographic resin containing 2-ethylhexyl 2-ethylhexylphosphonic acid (HEH[EHP]) sorbed onto a 25 – 53 mm Amberchrom CG-71 substrate (*i.e.* LN2 resin, Eichrom) [59, 177, 178]. Dilute HNO_3 solutions were used to elute the target material on the LN2 column. In their approach, Horwitz *et al.* comprised a front-end target removal system, a primary separation system and a secondary separation system [59, 180]. Each of these steps involved the separation of ytterbium and lutetium using the HEH[EHP] resin followed by concentration and acid adjustment of the ^{177}Lu-rich fraction using an extraction chromatographic material containing a diglycolamide (DGA) extractant. DGA allowed to avoid lengthy evaporations and acidity adjustments between successive HEH[EHP] column runs while removing adventitious impurities, such as metal ions (*e.g.* Zr^{4+} and Hf^{3+}), from ^{177}Lu. Dilute HCl solutions were used to strip the DGA-column. A small anion-exchange column was added in the final step of the secondary separation step to eliminate all traces of nitrate ions. An overall recovery of *ca.* 73 % was obtained for ^{177}Lu, with a decontamination factor of 106 for ytterbium. The separation system proved to serve well for a 300 mg of irradiated target. Ytterbium can be recovered from all separation steps to be recycled for a successive neutron irradiation campaign, which is considered an important feature.

Monroy-Guzman *et al.* described a purification method making use of an Eichrom LN resin (HDEHP-based) in nitrate media [74, 75]. The extraction

capability of HDEHP is highly dependent upon the acidity of the aqueous phase. The first step of this process comprised of the dissolution of the irradiated nitrate salt in a 0.15 mol L^{-1} HNO_3 and adsorption onto the chromatographic column loaded with Eichrom LN resin. Ytterbium was desorbed first from the column by using a 3.4 mol L^{-1} HNO_3 solution. Subsequently, ^{177}Lu was eluted by using a 9 mol L^{-1} HNO_3 solution. Precipitation of lutetium hydroxide by addition of NaOH and re-dissolution of the hydroxide with 0.1 mol L^{-1} HCl delivered a $^{177}LuCl_3$ solution with high radionuclide purity (> 99.9 %) for further processing of the radiopharmaceutical.

An alternative chromatographic process was presented by Le Van So *et al.* [181, 182]. A conventional multi-column solid phase extraction chromatography, with HDEHP impregnated on an OASIS-HLB sorbent (OASIS-HDEHP), was used to separate the non-carrier-added ^{177}Lu from the bulk quantity of ytterbium target. This separation technique exploits the large variation of Ln^{3+} distribution ratios in different acidity HCl solution – OASIS-HDEHP resin systems for consecutive loading-eluting cycles performed on different columns. Le Van So *et al.* described the use of this separation system in a multi-column chromatographic process and a conventional column chromatographic separation combined with HPLC [181, 182]. The final non-carrier-added $^{177}LuCl_3$ product was obtained after evaporation to dryness and reconstituting the residue in 0.05 mol L^{-1} HCl. Production batches of several GBq (*i.e.* several hundred mCi) non-carrier-added ^{177}Lu were successfully separated from 50 mg of ytterbium target material using this multi-column chromatographic technique. A ^{177}Lu production yield of > 82 % was obtained for a clinically applicable, high purity non-carrier-added ^{177}Lu radionuclide.

1.6.10 Scandium-47

^{47}Sc ($t_{1/2}$ = 3.35 d) is recently being looked at as a radioisotope for the production of therapeutic agents based on peptides and antibodies [183]. ^{47}Sc is considered as an alternative for non-carrier-added ^{177}Lu. ^{47}Sc serves well in therapy because of its moderate β^- particle emission (441 keV (68 %) and 600 keV (32 %)) and simultaneous imageable γ emission (159 keV (68 %)). Additionally, ^{47}Sc can be accompanied by ^{44}Sc, satisfying the desired physical aspects for radionuclide therapy and PET imaging, respectively.

^{47}Sc can be non-carrier-added produced in a nuclear reactor *via* two different methods (Fig. 1.21). The first method consists of the neutron irradiation of an enriched ^{46}Ca (σ = 0.7405 barn) target to produce ^{47}Ca ($t_{1/2}$ = 4.538 d), which subsequently decays *via* β^- emission to produce ^{47}Sc, *i.e.* $(n, \gamma) \rightarrow \beta^-$ [183–185]. This way, a pseudo-generator can be established, enabling multiple separations

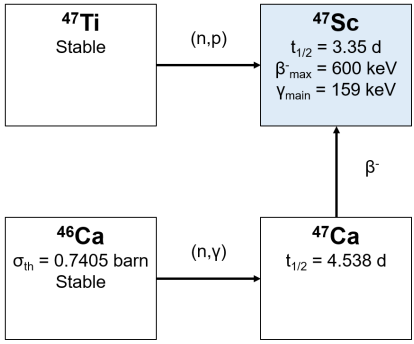

Figure 1.21: Production pathways of the medical ^{47}Sc radionuclide (highlighted). The neutron capture of ^{46}Ca leads to ^{47}Ca, which decays into the ^{47}Sc radionuclide. A ^{47}Ca/^{47}Sc pseudo-generator system can be established. A different production method for ^{47}Sc involves neutron capture of ^{47}Ti followed by proton emission.

of ^{47}Sc. A sufficient amount of reactors with a sufficiently high thermal neutron flux is available to produce ^{47}Ca/^{47}Sc pseudo-generator systems. However, the need of enriched ^{46}Ca (0.004 % natural abundance) impedes its wide-scale use because of the exorbitant price of 30 % enriched ^{46}Ca [186]. In a second method, ^{47}Ti is irradiated by neutrons in a nuclear reactor to obtain ^{47}Sc after proton emission, *i.e.* ^{47}Ti(n,p)^{47}Sc [184, 185].

The latter production method, however, yields only low activities of ^{47}Sc. Additionally, ^{46}Sc might be co-produced, making direct use of ^{47}Sc *via* this production method for radiopharmaceutical applications impossible. Therefore, a highly enriched $^{47}TiO_2$ target and radiochemical processing are required. Separation of ^{47}Sc from titanium is relatively easy because of the large difference between chemical properties of scandium and titanium. Several research groups investigated radiochemical purification of ^{47}Sc from titanium targets [186, 187]. Domnanich *et al.* described comprehensively various possibilities to isolate ^{47}Sc obtained *via* different production methods from its target material [188].

1.6.11 Yttrium-90

The use of ^{90}Y ($t_{1/2}$ = 2.67 d) is already well established in targeted therapy as a pure β^- emitter. Advantages of using ^{90}Y as therapeutic radionuclide include its suitable physical half-life and its decay to the stable ^{90}Zr daughter isotope *via* high-energy β^- particles (2.28 MeV). In nuclear medicine, ^{90}Y is frequently linked to peptides (*e.g.* ^{90}Y-DOTATOC) and antibodies (*e.g.* ibritumomab tiuxetan (commercial name: Zevalin)) [183]. ^{90}Y-containing

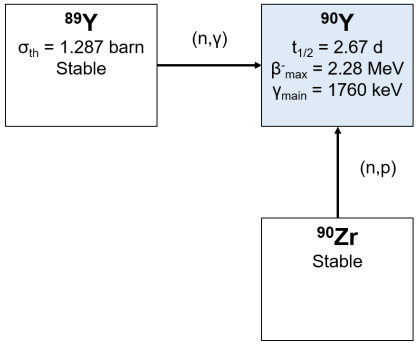

Figure 1.22: Production pathways of the medical ^{90}Y radionuclide (highlighted). The neutron capture of ^{89}Y produces the carrier-added ^{90}Y. Production of non-carrier-added ^{90}Y *via* neutron irradiation involves neutron capture of ^{90}Zr followed by proton emission.

radiopharmaceuticals can be applied for radiosynovectomy, treatment of hepatocellular carcinoma, peptide receptor radionuclide therapy and for therapy of non-Hodgkin's lymphoma [1]. The use of ^{90}Y radiopharmaceuticals for radioimmunotherapy has been approved by the FDA in 2002.

Carrier-added ^{90}Y can be directly produced by neutron activation of ^{89}Y in a nuclear reactor (Fig. 1.22). ^{89}Y (1.287 barn) is mononuclidic (100 % natural abundance), and therefore does not require any target material enrichment prior to irradiation. The radionuclidic purity of ^{90}Y is generally very high, but the specific activities remain relatively low because of the low neutron cross-section of ^{89}Y. Nevertheless, low levels of ^{89}Sr ($t_{1/2}$ = 50.57 d) might be detected. Depending on the reactor epithermal neutron flux, ^{89}Sr is generated *via* the (n, p) reaction. carrier-added ^{90}Y can be used for treatment of bone metastases.

Non-carrier-added ^{90}Y for the preparation of labeled antibodies and peptides used for targeted radiotherapy can be produced using a 100 % enriched ^{90}Zr target and a fast neutron flux (*ca.* $7.5 \times 10^{13}\,\mathrm{cm^2\,s^{-1}}$) [189] (Fig. 1.22). This method is considered as a viable approach to produce non-carrier-added ^{90}Y with moderate specific activity. However, long-term availability of enriched ^{90}Zr cannot be assured, resulting in expensive target materials. Recycling of the ^{90}Zr target material after radiochemical processing is thus of high importance. Additionally, a fast neutron flux has to be available. Therefore, large amounts of non-carrier-added ^{90}Y are usually obtained *via* radionuclide generator system using ^{90}Sr ($t_{1/2}$ = 28.79 y) as a parent radionuclide [1]. ^{90}Sr is a major ^{235}U fission product with a fission yield of 5.93 %. ^{90}Sr can be isolated from nuclear

fuel *via* processing of high-level liquid waste (HLLW). However, it is highly important to remove all ^{90}Sr impurities from the ^{90}Y radionuclides before being used in nuclear medicine, as ^{90}Sr is able to accumulate in the skeleton.

1.7 Conclusion

Radionuclides are considered to be a very useful tool in medicine as malicious tumor cells can be imaged and treated in a very eficient way. In the future, many more patients will suffer from different kinds of diseases were the use of radionuclides in endoradiotherapy and imaging can be a clear asset. Therefore, safeguarding a reliable supply to make radionuclides available for all patients who require radiotherapy or imaging is highly important. A selection of radiolanthanides offers very interesting properties that can be exploited in nuclear medicine, with some of them considered to be even more suitable for endoradiotherapy than conventional radionuclides that are being used on routine basis nowadays. Their use in nuclear medicine is being studied intensively over the last few decades. Therefore, the use of radiolanthanides is expected to increase further as new targeted therapies are still being developed at a fast pace.

A range of β^- particles with different energies and varying penetration depths originating from different radiolanthanides becomes available. This way, it might be possible to select carefully a radiolanthanide isotope for a very specific treatment. Because of their very similar chemical properties, trivalent radiolanthanides are easily interchangeable in targeting vectors and carrier molecules. Some radiolanthanides possess the ability to be used in theranostics, *i.e.* besides their use in endoradiotherapy, some of radiolanthanides can also be used for imaging and dosimetry purposes because of their favorable simultaneous γ photon emission.

A high radionuclidic and chemical purity of these radiolanthanides is required for application in nuclear medicine. Key challenges lie within the separation of two neighboring lanthanides. Carrier-added-produced radiolanthanides cannot be chemically separated from their target material because isotopes of the same element are being formed. Nevertheless, some of these carrier-added radiolanthanides might require radiochemical treatment after irradiation as no long-lived side-products are allowed to be present in the radiopharmaceutical to limit the background radiation of the patient after treatment. Purification of the radiolanthanide can be considered to extend the expiration date of the radiopharmaceutical, which would enhance a more widespread use of several radiolanthanides in medicine. Especially ^{153}Sm, which combines favorable β^-

and γ emission, would become more accessible. In the non-carrier-added production strategy, radiolanthanides can be separated from their target material. A radiolanthanide with high radionuclidic purity and high specific activity can be obtained, which is suitable for targeted radiotherapy. These radioisotopes are of key importance in future application of radiolanthanides in medicine, and will be the main focus of future research. Development and optimization of separation and purification techniques for the already heavily investigated ^{177}Lu radiolanthanide will be continued, whereas interest in ^{161}Tb isolation is growing fast.

Notwithstanding the difficult separation of two adjacent lanthanides, different separation and purification techniques are being developed to isolate the radiolanthanide of interest or to remove the unwanted impurities or redundant target material. Most of them are based on ion-exchange or extraction chromatography techniques, making use of the small difference in stability constant between both trivalent lanthanides and a complexing agent. These differences originate from the increase in charge density with decreasing ionic radius along the lanthanide series (lanthanide contraction). However, these separation strategies often result in relatively low separation factors and often require quite some time to reach the desired purity. In some cases, advantage can be taken of the ability to reduce a lanthanide to its divalent state, *i.e.* Eu^{2+} and Yb^{2+}. Reduction followed by selective extraction or ion-exchange can lead to a fast and efficient separation. Another technique making use of the relatively stable divalent state is amalgamation, where the divalent lanthanides are preferentially being migrated to the mercury pool. Some of the presented separation techniques still require optimization, while others are already well established. In the next decades, more research will be needed to find efficient radiochemical separation and purification approaches to meet the future demand for medical radionuclides at a reasonable cost. In the development of new complexing agents with increased selectivity for separating two adjacent lanthanides, compatibility with the radiopharmaceutical application and radiation resistance are of high importance.

Obtaining a high separation efficiency, with separation time and radionuclidic purity as two key factors, will be the major driving force to arrive at a higher availability of radiolanthanides and their application in nuclear medicine.

Chapter 2

Objectives

The research conducted within this PhD project focused on the development a novel and innovative purification method for the processing of medical radiolanthanides. A comprehensive overview of the current state-of-art concerning radiolathanide processing was given in Chapter 1. In the presented PhD project, the main focus was put on the separation of europium and samarium in scope of the purification of medical ^{153}Sm.

The objectives of this PhD project comprised the use of *ionic liquids* (ILs), and the resulting *supported ionic liquid phases* (SILPs) thereof, for the separation of two adjacent lanthanides, *i.e.* samarium and europium. Within the development strategy for a purification protocol for ^{153}Sm, two major steps can be distinguished. A first one being the reduction of Eu^{3+} to Eu^{2+}. In a second step, Eu^{2+} is isolated from Sm^{3+} using solvent extraction and extraction chromatographic techniques.

Following the proposed strategy, the reduction of Eu^{3+} to Eu^{2+} and, consequently, the stability of Eu^{2+} were investigated as a first step. During these studies, it was discovered for the first time that reduction of Eu^{3+} is also possible aqueous solutions containing a high nitrate salt concentration. Previous reports only focused on the reduction of Eu^{3+} in media that are insensitive to reducing conditions, most often making use of chlorides. Therefore, different measurement techniques were deployed to support our observations. After all, it was important to properly study the reduction rate of Eu^{3+} to Eu^{2+} and the stability of the latter in respect of developing an efficient separation method. These observations are presented and discussed in Chapter 3.

After establishing reduction of Eu^{3+}, the separation of Sm^{3+} and Eu^{2+} was

studied making use of *solvent extraction* (SX, Chapter 4) and *extraction chromatography* (XC, Chapter 5) methods. Both methods comprised the use of an ionic liquid phase, either in bulk or impregnated onto an inert solid support, respectively. The solvent extraction method served as a selection step in which the ionic liquid phase and the separation parameters were determined. Important parameters included the ability to selectively extract either Sm^{3+} or Eu^{2+}, a high hydrophobicity for easy phase separation and prevention of ionic liquid loss to the aqueous phase, and compliance with the CHON-principle (only Carbon, Hydrogen, Oxygen and Nitrogen). Also the use of an 18-crown-6-based size-selective extractant for Eu^{2+} was looked at, but did not lead to increased selectivity in combination with the basic extractant properties of the ionic liquid itself.

The final goal was to demonstrate the ability to separate Sm^{3+} and Eu^{2+} by making use of an extraction chromatography method based on the selected separation parameters of the solvent extraction method. For this reason, the ionic liquid was immobilized onto an inert solid support. Extraction chromatography is an important technique in radionuclide processing because of its ease of operation, its ability to separate minor amounts from major amounts, and its automation possibilities. The latter is important towards a remote-controlled separation system, which allows for proper shielding when working with the highly active target material.

Chapter 3

Stability of europium(II) in aqueous nitrate media

This chapter is based on a manuscript that was submitted for publication to *Dalton Transactions* (2019):

Michiel Van de Voorde, Bart Geboes, Tom Vander Hoogerstraete, Karen Van Hecke, Thomas Cardinaels and Koen Binnemans, Dalton Transactions, 2019

The text might contain minor adjustments to the original publication.

All experimental work and compilation of the manuscript were performed by the author of this thesis.

3.1 Abstract

In the lanthanide series, Eu^{3+} is the most easily reduced to its divalent state. Reduction of Eu^{3+} has been studied extensively in aqueous media that are insensitive to reducing conditions. Recently, it was reported that reduction of Eu^{3+} is also feasible in aqueous nitrate solutions, and that Eu^{2+} remained sufficiently stable in these media to conduct separation experiments. However, additional fundamental research on the reduction efficiency of Eu^{3+} and stability of Eu^{2+} in these media has not been reported yet. In this chapter, cyclic voltammetry, magnetic susceptibility measurements, UV-Vis absorption spectroscopy and X-ray absorption near edge structure (XANES) were used to gain more insight in the reduction of Eu^{3+} in aqueous nitrate media. Within the parameters used in this work, near-quantitative reduction of Eu^{3+} could be achieved within 120 min in highly concentrated nitrate salt solutions, using both chemical and electrochemical reduction techniques. Moreover, Eu^{2+} was remarkably stable in these solutions, showing just a few percent of back-oxidation after 5 h in a sealed measurement cell.

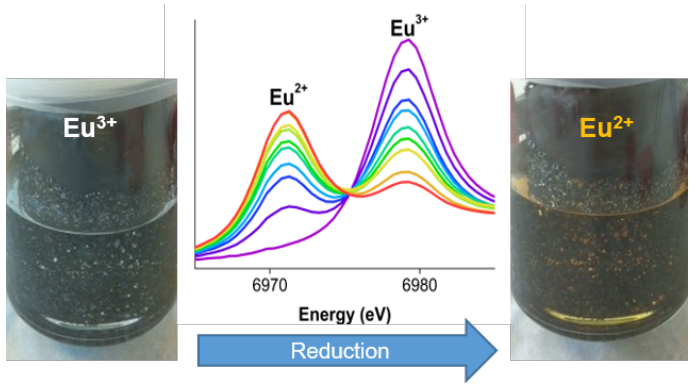

Figure 3.1: Graphical abstract describing the investigation on the reduction of Eu^{3+} and the stability of Eu^{2+} in aqueous solutions containing high nitrate salt concentrations.

3.2 Introduction

Lanthanides are crucial elements in lamp phosphors and permanent magnets, and several radiolanthanides have found their application in nuclear medicine [10, 190–192]. For some of these applications, a very high level of purity is required. In the past, europium had a high supply risk because of its use in lamp phosphors [192–194]. A lot of research was conducted to obtain europium from various resources, including both primary (by-product in ores, *e.g.* monazite) and secondary (end-of-life products, *e.g.* fluorescent lamps) ones [195]. In these resources, europium is always found together with other lanthanides. However, separation of europium from other lanthanides by ion-exchange and solvent extraction is very challenging. The lanthanide ions possess very similar electronic structures ([Xe] $4f^{0–14}$) with a predominant trivalent oxidation state (Ln^{3+}). The $4f$ subshell is filled with electrons across the lanthanide series, which are shielded by the electrons in the filled $5s$ and $5p$ subshells. As a consequence, the $4f$ electrons show a core-like behavior, *i.e.* they do not participate in bond formation or ligand interactions [196, 197]. This results in very similar chemical properties across the lanthanide series.

Changing the oxidation state induces significant changes in chemical properties, which opens perspectives for the development of efficient separation technologies. Ce^{3+} ($E^0(Ce^{4+}/Ce^{3+}) = +1.72\,V$) and Tb^{3+} ($E^0(Tb^{4+}/Tb^{3+}) = +3.10\,V$) can be oxidized to the +IV oxidation state, by which they are stabilized by an empty $4f$ subshell ([Xe] $4f^0$) and by a half-filled $4f$ subshell ([Xe] $4f^7$), respectively. Sm^{3+} ($E^0(Sm^{3+}/Sm^{2+}) = -1.55\,V$), Eu^{3+} ($E^0(Eu^{3+}/Eu^{2+}) = -0.34\,V$) and Yb^{3+} ($E^0(Yb^{3+}/Yb^{2+}) = -1.05\,V$) can be reduced to the +II oxidation state because of a stabilizing effect of a near-half filled ([Xe] $4f^6$), a half-filled ([Xe] $4f^7$) and a filled $4f$ subshell ([Xe] $4f^{14}$), respectively. However, Sm^{2+} and Yb^{2+} in aqueous solutions tend to be very short-lived because of their high oxygen-sensitivity and their high tendency to reduce water. Eu^{2+} is known to have a reasonably long lifetime in aqueous solutions, despite its reduction potential lying outside the stability region of water.

Eu^{3+} can be selectively reduced using chemical, electrochemical or photochemical techniques [93, 94, 98, 99, 198–200]. Oxidizing agents, such as dissolved oxygen ($E^0(O_2/H_2O) = +1.23\,V$), H^+ ($E^0(H^+/H_2) = 0.00\,V$) or nitrate anions ($E^0(NO_3^-/NO) = +0.95\,V$, in presence of H^+), are usually avoided because of the high possibility for back-oxidation of Eu^{2+}. Consequently, reduction of Eu^{3+} is usually performed in media that are insensitive to reducing conditions, most often containing chlorides [98–100, 198, 200–203]. Nevertheless, our research group recently observed that Eu^{3+} could also be successfully reduced in nitrate media at quasi-neutral pH [92, 204]. Reducibility of Eu^{3+} in aqueous nitrate media opens new perspectives to isolate europium from other trivalent lanthanides. The

ability of trivalent lanthanide ions to form extractable nitrate complexes, whereas divalent lanthanide ions cannot, is important with respect to development of efficient separation and purification techniques [110–112]. In the following chapters, it will be shown that Eu^{2+} is sufficiently stable in deaerated aqueous solutions with high nitrate salt concentrations to perform solvent extraction, leading to a very efficient method to separate samarium and europium [92]. The formation of europium in its divalent state was evident from a color change of the aqueous solution upon reduction, *i.e.* from a colorless solution to a yellow-orange solution. The colored solutions showed to be stable over time in an inert atmosphere, but they gradually lost their color upon contact with air (with O_2 as oxidizing agent) or upon acidification (addition of H^+ as oxidizing agent).

In this chapter, fundamental research was conducted to investigate the reducibility of Eu^{3+} and the stability of Eu^{2+} in aqueous nitrate media. Chemical and electrochemical reduction of Eu^{3+} in nitrate aqueous media were demonstrated and investigated by using various techniques. The influence of the nitrate salt concentration in solution on the reducibility of Eu^{3+} was elucidated, and the time needed to reach maximum reduction of Eu^{3+} was determined. The relative amounts of Eu^{2+} and Eu^{3+} as a function of reduction time were determined by X-ray absorption near-edge structure (XANES) measurements using the europium L_{III}-edge [205–211]. More detailed quantification of the reduction rate using electrochemical reduction techniques is subject of current investigations.

3.3 Experimental

3.3.1 Materials

$Eu(NO_3)_3{\cdot}6H_2O$ (99.9 %) was purchased from Strem Chemicals, Inc. (Newburyport, USA). $LiNO_3$ (anhydrous, 99 %) was purchased from Alfa Aesar (Karlsruhe, Germany). $EuCl_3{\cdot}6H_2O$ (99.9 %) and granular zinc (30 mesh, ≥ 99.7 %) were purchased from Acros Organics (Geel, Belgium). LiCl (99 %) was purchased from Sigma-Aldrich (Overijse, Belgium). Europium and zinc standard solutions (≥ 99.99 %, 1000 µg mL^{-1}, 2 – 5 % HNO_3, Plasma HIQU), $Ca(NO_3)_2{\cdot}4H_2O$ (> 99 %), NH_4NO_3 (> 99 %) and $CaCl_2{\cdot}2H_2O$ (> 99.5 %) were purchased from Chem Lab (Zedelgem, Belgium). All products were used as received, without any further purification. Aqueous samples were prepared with MilliQ water (18.2 MΩ cm at 25 °C).

3.3.2 Methods

Chemical reduction of europium was performed by using a large excess of granular metallic zinc, *i.e.* at least hundred stoichiometric equivalents. The solutions contained various concentrations of europium (0.66, 6.6 and 66 mmol L^{-1}) and nitrate salt (0, 1, 3, 6 or 9 mol L^{-1} NO_3^-). Analogous chloride solutions were studied for comparison. The aqueous solutions were purged with argon before and during reduction of Eu^{3+} to remove aerial and dissolved oxygen to prevent back-oxidation of Eu^{2+} by O_2. The pH of the aqueous feed solution was kept between 4.5 and 6.5. This way, the pH of the final feed solution remained sufficiently high to avoid back-oxidation of Eu^{2+} by H^+ or NO_3^- (in the presence of H^+), and sufficiently low to prevent precipitation of Eu^{3+} as europium hydroxide. The majority of Zn^{2+} formed during reduction of Eu^{3+} was found to precipitate as the white, highly insoluble zinc(II) hydroxide in these conditions. The pH was measured before and after reduction of Eu^{3+} by means of a Hamilton Slimtrode pH electrode coupled to a Mettler-Toledo SevenCompact pH meter. The solutions were filtered after chemical reduction through a Millipore syringe filter with a pore size of 0.45 µm before being analyzed.

Electrochemical reduction of europium was performed in a three-electrode electrochemical cell. The potential at the working electrode was controlled by a Metrohm Autolab PGSTAT302N potentiostat in potentiostatic mode, operated by Nova 2.1.2 software. *Cyclic voltammetry* (CV) experiments were performed in a custom-made glass electrochemical cell with a 50 mL inner volume. The solution was purged by argon gas prior to the measurements. A constant argon flow was maintained over the solution while cyclic voltammograms were recorded, providing an inert gas blanket. Dissolved oxygen (O_2) might slow down the kinetics of Eu^{3+} reduction because of possible competition with O_2 at the cathode [212]. This is especially likely if protons are available, leading to the production of H_2O. A glassy carbon electrode (∅ = 4 mm) served as the working electrode, and a coiled platinum wire (∅ = 1 mm) served as the counter electrode. Platinum working electrodes are less efficient for the reduction of Eu^{3+} because of their low overpotential for hydrogen generation. The reference electrode consisted of a Ag/Ag^+ redox couple in a 3 mol L^{-1} KCl solution (E^0 = +0.2225 V *vs.* SHE at 25 °C) [213]. A scan rate of 50 mV s^{-1} was used, unless stated differently. Solutions containing 10 mmol L^{-1} of Eu^{3+} and various concentrations of nitrate and chloride salts (0, 1, 3, 6 and 9 mol L^{-1} NO_3^- or Cl^-) were studied. Electrolytic reduction of Eu^{3+} was performed in a BASi bulk electrolysis cell at a constant potential of -0.7 V *vs.* Ag/Ag^+. A BASi MF 2077 reticulated vitreous carbon electrode (RVC, surface area: 10.5 cm^2 effective/cm^2 geometric) was used as working electrode. The BASi MF-2052 reference electrode consisted of a Ag/Ag^+ redox couple in a 3 mol L^{-1}

KCl solution. A BASi MW 1033 coiled platinum wire auxiliary electrode ($\varnothing = 0.5\,\text{mm}$, $l = 23\,\text{cm}$), separated from the electrolysis solution by a sintered glass frit (pore size: 4–5 µm), served as a counter electrode in these experiments.

UV-VIS absorption spectra were recorded to investigate the change in absorbance upon reduction of Eu^{3+}. Reduction of Eu^{3+} in aqueous nitrate media yielded a yellow-orange solution, whereas the start solutions were colorless. The reduction of Eu^{3+} in aqueous nitrate medium was compared to the reduction of Eu^{3+} in aqueous chloride medium. Chemical reduction was performed by stirring the solutions with zinc grains for 2 h in an inert atmosphere. Matching quartz cuvettes with a path length of 1 mm were used for Eu^{2+} samples, whereas matching quartz cuvettes with a path length of 10 mm were used for Eu^{3+} samples. Absorption spectra were recorded in the 200 – 800 nm range using a Agilent Cary 6000i UV-VIS-NIR spectrophotometer in double beam mode, operated by Cary WinUV software. Source changeover occurred at 350 nm. A scan rate of $150\,\text{nm}\,\text{min}^{-1}$ and a resolution of 0.5 mm were used. The blank solutions consisted of a $3\,\text{mol}\,\text{L}^{-1}$ $Ca(NO_3)_2$ and a $3\,\text{mol}\,\text{L}^{-1}$ $CaCl_2$ solution for measurement in aqueous nitrate and chloride media, respectively. These blank solutions were used to account for the broad absorption band of nitrate (ranging from 200 to 320 nm) [214]. Spectra of the solutions containing europium were recorded in duplicate before and after reduction. A europium concentration of $6.6\,\text{mmol}\,\text{L}^{-1}$ was used in solutions containing $3\,\text{mol}\,\text{L}^{-1}$ $Ca(NO_3)_2$ and a $3\,\text{mol}\,\text{L}^{-1}$ $CaCl_2$.

Magnetic susceptibility measurements were performed to monitor the chemical and electrochemical reduction of Eu^{3+} in aqueous nitrate solutions containing $3\,\text{mol}\,\text{L}^{-1}$ $Ca(NO_3)_2$ at room temperature as a function of time. The magnetic susceptibility of the solution was measured every 15 min using a Sherwood Scientific MSB AUTO magnetic susceptibility balance. Polished quartz sample tubes with an inner diameter of 4 mm were used to load the sample into the magnetic susceptibility balance. These quartz sample tubes were measured immediately after filling, and remained open during the short measurement. A sample tube sealed with Parafilm® was used to monitor the stability of Eu^{2+} in solution for 2.5 h after reduction.

X-ray absorption spectroscopy (XAS) was used to determine the Eu^{2+}/Eu^{3+} ratios in the nitrate solutions containing different europium (0.66, 6.6 and $66\,\text{mmol}\,\text{L}^{-1}$) and nitrate (0, 3 and $6\,\text{mol}\,\text{L}^{-1}$) concentrations as a function of reduction and oxidation time in steps of 15 min. The XAS spectra were collected at room temperature at the Dutch-Belgian Beamline (DUBBLE, BM26A) at the European Synchrotron Radiation Facility (ESRF) in Grenoble, France.

The energy of the X-ray beam was tuned by a double-crystal monochromator operating in fixed-exit mode using a Si(111) crystal pair. The energy was calibrated by means of a metallic iron foil. The measurements were performed in transmission mode using Ar/He-gas-filled ionization chambers at ambient pressure. A brass sample holder with Kapton® windows and a flexible polymeric spacer (VITON®) with a thickness of 2 mm was used as a sample holder. The spectra were recorded by scanning through the europium L_{III} absorption edge (*ca.* 6977 eV), from 6775 to 7000 eV, focusing on the region in the spectrum near the edge. High-energy resolution (< 0.5 eV) was used when scanning the region of 6964 to 6995 eV. Deconvolution of the spectra by fitting procedures allowed spectral analysis [215]. The ratio between the integrated peaks allows calculation of the relative amount of Eu^{2+} and Eu^{3+} in the samples ($Eu^{x+}/(Eu^{2+} + Eu^{3+})$, with x = 2 or 3). The white line transition was approximated by fitting with a pseudo-Voigt function, whereas an arctangent background function for each oxidation state was used to fit the absorption edge step. The arctangent background function for both oxidation states had to be accounted for and the relative amounts of Eu^{2+} and Eu^{3+} changed as a function of the reduction time. Therefore, construction of the arctangent functions and peak deconvolution were solved iteratively in Origin 2016 (*v*9.3). Additionally, a correction factor for Eu^{2+} had to be taken into account, as it was observed in previous studies that the technique is not equally sensitive for both oxidation states [205, 206, 216, 217]. Peak amplitudes almost twice as high for Eu^{3+} compared to Eu^{2+} were already reported. In our work, the correction factor was determined to be 1.5, based on the peak amplitudes and peak areas. As mentioned by Moreau *et al.*, a very weak peak at slightly higher energy than the white line might appear in the spectrum, which is commonly attributed to multiple-scattering effects [217]. These effects, however, were not accounted for when calculating the relative amounts Eu^{2+} and Eu^{3+} in the samples.

The viscosities of the solutions containing 10 mmol L^{-1} europium and different concentrations of $Ca(NO_3)_2$ and $CaCl_2$ were measured *via* the rolling ball principle using an Anton Paar Lovis 2000 M/ME viscometer. A capillary with inner diameter of 1.59 mm was used. The average viscosity was determined on seven measurements. For completeness, density of the saline solutions was measured simultaneously using an Anton Paar DMA 4500 M.

3.4 Results and discussion

3.4.1 Chemical reduction of europium

Reduction of Eu^{3+} to Eu^{2+} changes the chemical properties of the europium ion significantly, leading to different characteristics and ligand interactions [218]. The structural properties of Eu^{2+} are very similar to the ones of alkaline earth metals, *i.e.* the ionic radius of Eu^{2+} (1.25 Å) is similar to that of Sr^{2+} (1.26 Å) [217, 219]. The approach of altering chemical properties of Eu^{3+} by reduction has been studied frequently to improve the isolation of europium from other trivalent lanthanides [92, 99, 100, 198]. Eu^{3+} can be reduced either chemically, electrochemically or photochemically [93, 94, 98, 100, 220]. Chemical reduction of Eu^{3+} typically involves the use of metallic zinc powder or zinc amalgam (Zn(Hg), Jones reductor, $E^0(Zn^{2+}/Zn) = -0.76\,V$):

$$2\,Eu^{3+}{}_{(aq)} + Zn^0{}_{(s)} \rightleftharpoons 2\,Eu^{2+}{}_{(aq)} + Zn^{2+}{}_{(aq)} \qquad [3.1]$$

$$\Delta E^0_{cell,298\,K} = +0.42\,V$$

Despite the efficient reduction of Eu^{3+}, Eu^{2+} is relatively sensitive towards back-oxidation. Therefore, oxidizing agents, such as dissolved oxygen (O_2) protons (H^+) or nitrate anions (NO_3^-) have to be avoided:

$$4\,Eu^{2+}{}_{(aq)} + O_{2(g)} + 4\,H^+{}_{(aq)} \rightleftharpoons 4\,Eu^{3+}{}_{(aq)} + 2\,H_2O_{(aq)} \qquad [3.2]$$

$$\Delta E^0_{cell,298\,K} = +1.57\,V$$

$$2\,Eu^{2+}{}_{(aq)} + 2\,H^+{}_{(aq)} \rightleftharpoons 2\,Eu^{3+}{}_{(aq)} + 2\,H_{2(g)} \qquad [3.3]$$

$$\Delta E^0_{cell,298\,K} = +0.34\,V$$

$$2\,Eu^{2+}{}_{(aq)} + NO_3^-{}_{(aq)} + 3\,H^+{}_{(aq)} \rightleftharpoons 2\,Eu^{3+}{}_{(aq)} + HNO_{2(aq)} + H_2O_{(aq)} \qquad [3.4]$$

$$\Delta E^0_{cell,298\,K} = +1.28\,V$$

Consequently, reduction of Eu^{3+} is usually performed only in media that are insensitive to reducing conditions. For example, reduction of Eu^{3+} in an aqueous chloride media is already well established [87, 98–100, 103, 212].

Taking into account the reduction potential of nitrate, the redox behavior of europium in aqueous nitrate media has not been intensively studied in literature

yet. Only the work of Holleck in the 1940s [221, 222], and a more recent study of Zelić in 2003 report electrochemical experiments on europium in aqueous nitrate media [204]. Nevertheless, the formation and existence of Eu^{2+} in aqueous nitrate media in our experiments was clearly indicated by a change in color of the solution, *i.e.* the solution containing $6.6\,mmol\,L^{-1}$ europium changed from colorless to yellow upon formation of Eu^{2+} (*vide infra*). At higher europium concentrations ($66\,mmol\,L^{-1}$), the solution turned orange (Fig. 3.2). Reduction of Eu^{3+} in chloride media did not result in a colored solution.

The colored solutions remained stable over time when stored in a sealed vial under inert atmosphere (Ar or N_2). In the following chapters it will be shown that the colored solutions remain stable during solvent extraction and extraction chromatography processes, where Sm^{3+} can be efficiently separated from Eu^{2+} [92]. The Eu^{2+}-rich aqueous phases retained their yellow color after these separation experiments, indicating stabilization of Eu^{2+} species in these concentrated nitrate media.

Nevertheless, the Eu^{2+} nitrate solutions lost their color gradually upon exposure to oxygen in air (Reaction 3.2). Fast back-oxidation of Eu^{2+} by contact with oxygen was already observed by Jelinek *et al.* in aqueous chloride media [212]. In order to achieve efficient reduction of Eu^{3+}, it is important to remove all oxygen from the solution by purging with an inert gas prior to reduction. The solutions also lost their color instantly upon acidification (addition of H^+, Reactions 3.3 and 3.4). An excess of H^+ in the solution before reduction is not considered problematic as the excessive H^+ will be efficiently reduced by Zn^0 or Eu^{2+}, producing H_2. This automatically results in an increase of pH, leading to more neutral pH, so that Eu^{2+} is not further back-oxidized. The presence of H^+ in the initial solution will result only in slightly longer reduction times and H_2 generation. Nevertheless, an initial acidity is required to avoid precipitation by

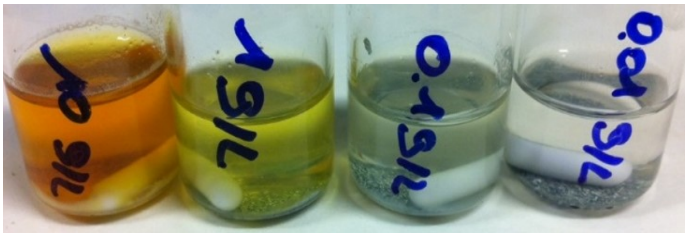

Figure 3.2: Colored solutions of Eu^{2+} in aqueous solution containing $6\,mol\,L^{-1}$ $LiNO_3$ after chemical reduction for 2 h. The color changes as a function of the Eu^{2+} concentration in the solution, *i.e.* orange ($66\,mmol\,L^{-1}$ Eu^{2+}), bright yellow ($6.6\,mmol\,L^{-1}$ Eu^{2+}), pale yellow ($0.66\,mmol\,L^{-1}$ Eu^{2+}) and colorless ($0.066\,mmol\,L^{-1}$ Eu^{2+}).

hydrolysis of Eu^{3+} (at pH > 6.5). Additionally, it is known that reactions of nitrogen-oxygen compounds are generally slow at ambient temperatures and low acidity, which is beneficial for the lifetime of Eu^{2+} in nitrate salt solutions.

Remarkably, solutions with low nitrate salt concentrations (< 3 mol L^{-1}) did not change color upon reduction, indicating that a minimum nitrate concentration is required to reduce Eu^{3+} and stabilize Eu^{2+}. Presumably, the lower nitrate salt concentrations, and consequently lower ionic strengths, were insufficient to stabilize Eu^{2+} species in solution (*vide infra*). A change in counter ion of the inert nitrate salt (*i.e.* NH_4NO_3, $Ca(NO_3)_2$ or $LiNO_3$) did not influence these observations. The behavior of a 3 mol L^{-1} $Ca(NO_3)_2$ blank solution and a 3 mol L^{-1} $Ca(NO_3)_2$ solution containing another Ln^{3+}, *i.e.* Sm^{3+}, in contact with Zn^0 were tested as well. No color change was observed after vigorous stirring for ≥ 2 h. Therefore, it can be concluded that yellow coloring of the solution only occurs in case Eu^{2+} is present.

3.4.2 Electrochemical reduction of europium

Electrochemical techniques are very helpful to investigate reactions involving electron transfer. This way, the flow of electrons can be related to chemical changes. In this respect, cyclic voltammetry was used to investigate the reduction of Eu^{3+} to Eu^{2+} in aqueous media containing different nitrate salt concentrations (1 – 9 mol L^{-1}). The redox behavior of Eu^{3+}/Eu^{2+} in analogous aqueous chloride media was studied for comparison.

The formal reduction potential of a redox compound is affected by the interaction with ligands, *i.e.* the coordination of Eu^{3+} and Eu^{2+}, and is a function of the ligand dissociation constants [223]. Changing the electrolyte concentration leads to a considerable variation in activity, ionic strength and hydration of the ions in solution, also changing their inner coordination sphere significantly. Additionally, the ionic conductivity and the viscosity of the solution change significantly with increasing salt concentrations.

Different counter ions, *i.e.* Li^+, Ca^{2+} and NH_4^+, were used to investigate the effect of the origin of the supporting electrolyte on the redox behavior of the europium ions (Fig. 3.3). The total nitrate concentration was held constant at 6 mol L^{-1}. The reduction of Eu^{3+} in a solution containing 6 mol L^{-1} LiCl was conducted for comparison. Measurements of the blank solutions are presented in Fig. 3.4, whereas a measurement of a solution containing 10 mmol L^{-1} Sm^{3+} in 3 mol L^{-1} $Ca(NO_3)_2$ can be found in Fig. 3.5. These results show that the reduction and oxidation signals solely originate from the Eu^{3+}/Eu^{2+} redox couple. Only minor differences were observed when using Ca^{2+} or Li^+ as counter ion in the nitrate salt. Both resulted in similar reduction potentials for

Eu^{3+} ($E_{P,c}$ = −0.65 V and −0.68 V *vs.* Ag/Ag^+, respectively). Calcium nitrate (1290 g L^{-1} at 20 °C for $Ca(NO_3)_2 \cdot 4H_2O$), however, has a higher solubility in water, and was therefore preferred over lithium nitrate (522 g L^{-1} at 20 °C for $LiNO_3$) for subsequent experiments. Reduction of Eu^{3+} in ammonium nitrate shows slightly different behavior, with a larger current density and slightly more negative reduction potential. Additionally, hydrogen generation is more pronounced, which can be attributed to the acidity of NH_4^+, leading to a less negative cathodic limit potential. NH_4NO_3 is therefore not the preferred nitrate salt for electrochemical reduction of Eu^{3+} ($E_{P,c}$ = −0.73 V *vs.* Ag/Ag^+). Reduction of Eu^{3+} in a LiCl solution ($E_{P,c}$ = −0.78 V *vs.* Ag/Ag^+) resulted in a more negative reduction potential compared to reduction of Eu^{3+} in $Ca(NO_3)_2$ or $LiNO_3$ solution, with a slightly smaller current density. This is a first indication that reduction of Eu^{3+} occurs more efficiently in aqueous nitrate media.

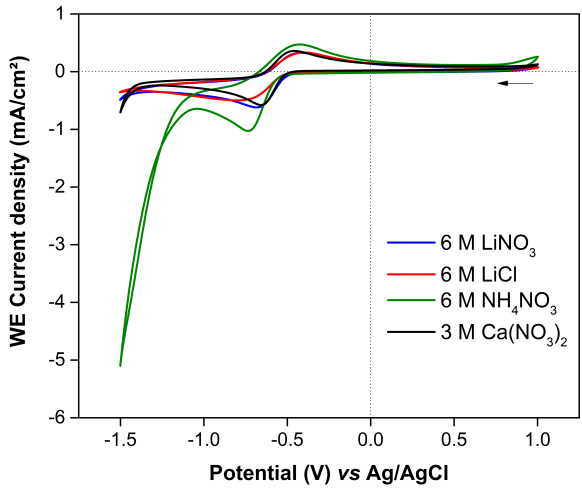

Figure 3.3: Cyclic voltammograms (second cycle) of solutions containing 10 mmol L^{-1} europium and 6 mol L^{-1} nitrate or chloride anions. Different counter ions (Li^+, Ca^{2+}, NH_4^+) for the nitrate salts were investigated for comparison. WE: glassy carbon, RE: Ag/Ag^+, CE: Pt wire, scan rate: 50 mV s^{-1}.

Cyclic voltammograms of 3 mol L^{-1} $Ca(NO_3)_2$ solutions containing different europium concentrations, *i.e.* 1, 5, 10, 50 and 100 mmol L^{-1}, were recorded (Fig. 3.6). The cathodic peak current density j_P of each reduction peak was plotted as a function of the europium concentration in Fig. 3.7. This plot clearly shows that the absolute value of the peak current density is linearly proportional with the europium concentration in solution. This results follows the Randles Sevcik equation (Eq. 3.1), where concentration is proportional to the (peak)

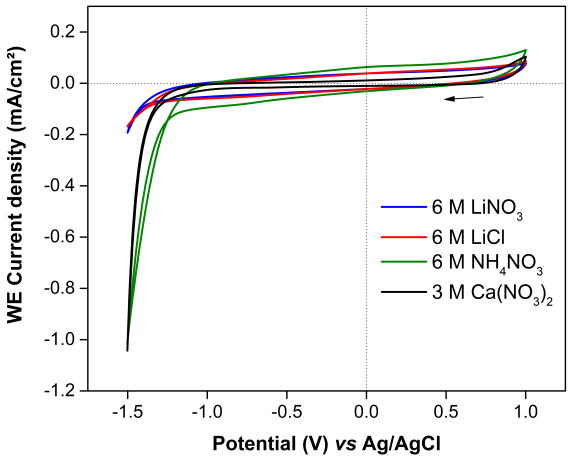

Figure 3.4: Cyclic voltammograms (second cycle) of blank solutions $6\,\mathrm{mol\,L^{-1}}$ nitrate or chloride anions. Different counter ions (Li^+, Ca^{2+}, NH_4^+) for the nitrate salts were investigated for comparison. WE: glassy carbon, RE: Ag/Ag^+, CE: Pt wire, scan rate: $50\,\mathrm{mV\,s^{-1}}$.

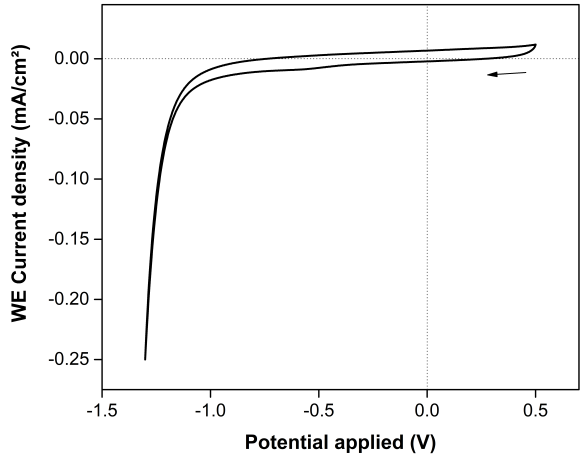

Figure 3.5: Cyclic voltammogram (second cycle) of a solution containing $10\,\mathrm{mmol\,L^{-1}}$ samarium and $6\,\mathrm{mol\,L^{-1}}$ $Ca(NO_3)_2$. WE: glassy carbon, RE: Ag/Ag^+, CE: Pt wire, scan rate: $50\,\mathrm{mV\,s^{-1}}$.

current density. After all, the Faradaic current is a direct measure of the electrochemical reactions taking place at the electrode surface. Consequently, the resulting peaks in the cyclic voltammograms can be assigned to the reduction and oxidation of europium.

$$i_P = (2.69 \cdot 10^5) n^{3/2} A D_0^{1/2} C_0^* \upsilon^{1/2} \tag{3.1}$$

where i_P is the peak current in amperes, n the number of electrons transferred in the redox event, A the surface area in cm^2 of the work electrode, D_0 the diffusion coefficient of the redox sensitive species in $\mathrm{cm}^2\,\mathrm{s}^{-1}$, C_0^* the bulk concentration of the redox sensitive species in $\mathrm{mol\,cm}^{-3}$ and υ the linear potential scan rate in $\mathrm{V\,s}^{-1}$.

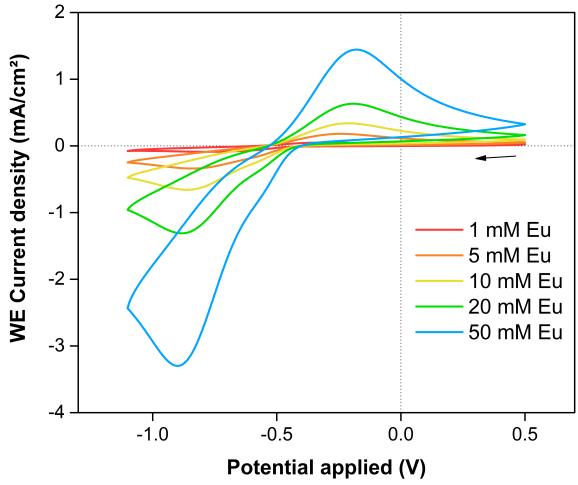

Figure 3.6: Cyclic voltammograms (second cycle) of solutions containing different europium concentrations and $3\,\mathrm{mol\,L}^{-1}$ $Ca(NO_3)_2$. WE: glassy carbon, RE: Ag/Ag^+, CE: Pt wire, scan rate: $50\,\mathrm{mV\,s}^{-1}$.

Cyclic voltammetry measurements were conducted on solutions containing $10\,\mathrm{mmol\,L}^{-1}$ europium and $3\,\mathrm{mol\,L}^{-1}$ $Ca(NO_3)_2$ using different scan rates, *i.e.* 10, 20, 50, 100, 200, 300, 500 and $1000\,\mathrm{mV\,s}^{-1}$ (Fig. 3.8). According to the Randles-Sevcik equation (Eq. 3.1), the (peak) current density is proportional to the square root of the scan rate in a reversible system. The resulting plot of the peak current density as a function of the square root of the scan rate does not result in a perfect linear correlation (Fig. 3.9). The shift in the peak potential as a function of scan rate indicates that there is no contribution of surface-

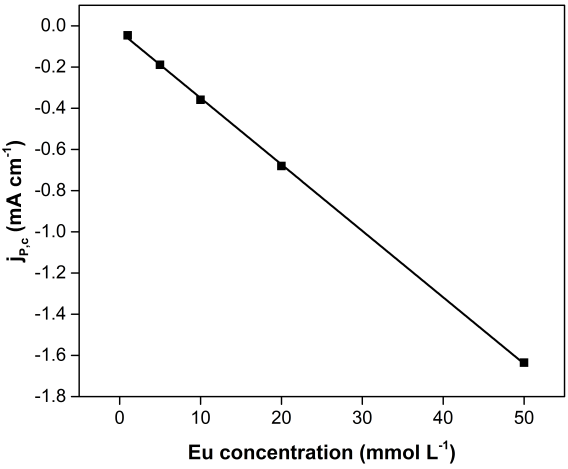

Figure 3.7: Cathodic peak current densities as a function of the europium concentration in 3 mol L^{-1} $Ca(NO_3)_2$ (R^2: 0.99979).

adsorbed species (Fig. 3.10), so that the deviation from linearity indicates a quasi-reversible system. The quasi-reversible nature of the Eu^{3+}/Eu^{2+} redox system is confirmed by the increase in peak separation potential as a function of the scan rate.

The influence of the supporting electrolyte concentration on the reduction of Eu^{3+} was investigated in both nitrate (Fig. 3.11, Table 3.1) and chloride (Fig. 3.12, Table 3.2) media. The *peak potentials* E_P are presented in Fig. 3.13 as function of the supporting electrolyte concentration for reduction of Eu^{3+} and oxidation of Eu^{2+}. In aqueous nitrate media, the cathodic ($E_{P,c}$) and anodic ($E_{P,a}$) peak potentials shifted from -0.66 V to -0.53 V (*vs.* Ag/Ag^+) and 0.08 to 0.12 V (*vs.* Ag/Ag^+), respectively, when the nitrate concentration in solution was increased from 1 to 9 mol L^{-1}. In his studies making use of a mercury drop electrode, Holleck also observed a shift in reduction potential with changing nitrate salt concentration [221, 222]. In aqueous chloride media, $E_{P,c}$ and $E_{P,a}$ were shifted from -0.67 V to -0.55 V (*vs.* Ag/Ag^+) and 0.17 to 0.32 V (*vs.* Ag/Ag^+), respectively, upon increasing the chloride concentration from 1 to 9 mol L^{-1}. Thus, it is clear that the shift in peak potential is directly proportional to the supporting electrolyte concentration, for both nitrate and chloride media, and that the reduction of Eu^{3+} is more favorable in aqueous solutions containing higher supporting electrolyte concentrations. It is also clear that the reduction of Eu^{3+} and the oxidation of Eu^{2+} were consistently more

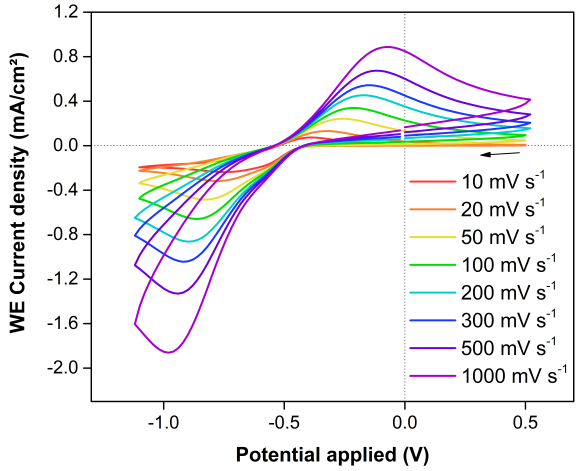

Figure 3.8: Cyclic voltammograms (second cycle) of solutions containing 10 mmol L^{-1} europium and 3 mol L^{-1} $Ca(NO_3)_2$ using different scan rates. WE: glassy carbon, RE: Ag/Ag^+, CE: Pt wire.

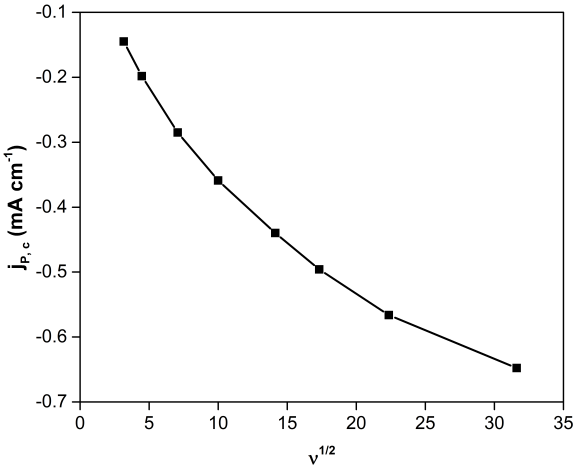

Figure 3.9: Cathodic peak current density as a function of the square root of the scan rate using a solution containing 10 mmol L^{-1} europium and 3 mol L^{-1} $Ca(NO_3)_2$.

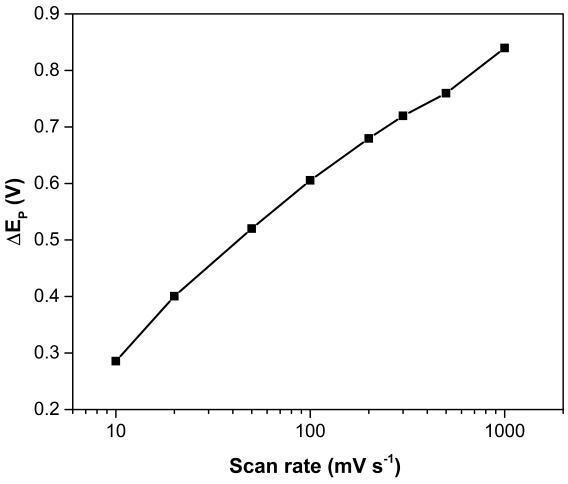

Figure 3.10: Peak separation potentials as a function of the square root of the scan rate (logarithmic scale) using a solution containing 10 mmol L^{-1} europium and 3 mol L^{-1} $Ca(NO_3)_2$.

efficient in nitrate aqueous media compared to chloride aqueous media. On average, reduction of Eu^{3+} in nitrate aqueous media occurred at a potential ±25 mV less negative than reduction of Eu^{3+} in similar aqueous chloride media. Oxidation of Eu^{2+} in aqueous nitrate media occurred at more negative potentials compared to oxidation of Eu^{2+} in aqueous chloride media (±60 mV on average). Consequently, *peak separation potentials* (ΔE_P) were consistently lower in aqueous nitrate media. The peak separation potentials also increased with increasing supporting electrolyte concentration in both media. The change in peak separation potential with changing supporting electrolyte concentration indicates the dependency of the quasi-reversible system on the viscosity of the solution. The increase in peak separation potential was found to be higher in aqueous chloride media.

A change of the supporting electrolyte concentration in a solution also leads to changes in the physical properties of the solution. In particular, *viscosity* η and *density* ρ of the solution are affected. In electrochemical experiments, viscosity of the solution has a major influence on the behavior of the electrochemical cell. The mass transfer and the *diffusion coefficient* D are inversely proportional to the viscosity of the solution *via* the Stokes-Einstein equation (Eq. 3.2).

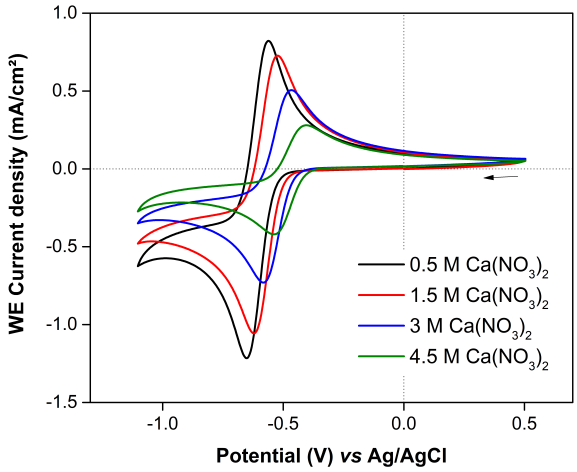

Figure 3.11: Cyclic voltammograms (second cycle) of solutions containing 10 mmol L^{-1} europium and different concentrations of $Ca(NO_3)_2$ (1 to 9 mol L^{-1} NO_3^-). WE: glassy carbon, RE: Ag/Ag^+, CE: Pt wire, scan rate: 50 mV s^{-1}.

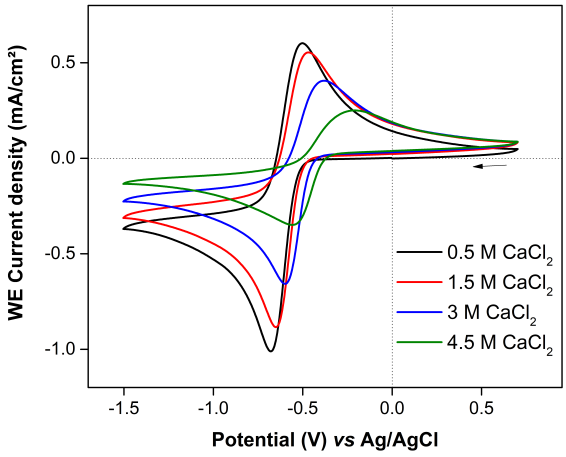

Figure 3.12: Cyclic voltammograms (second cycle) of solutions containing 10 mmol L^{-1} europium and different concentrations of $CaCl_2$ (1 to 9 mol L^{-1} Cl^-). WE: glassy carbon, RE: Ag/Ag^+, CE: Pt wire, scan rate: 50 mV s^{-1}.

Table 3.1: Peak potentials and peak separation potentials of cathodic and anodic sweep for 10 mmol L^{-1} europium in various aqueous nitrate media (second cycle). Scan rate: 0.05 V s^{-1}.

$[Ca(NO_3)_2]$ (mol L^{-1})	$E_{P,c}$ (V)	$E_{P,a}$ (V)	ΔE_P (V)
0.5	-0.647	-0.563	0.084
1.5	-0.619	-0.524	0.095
3	-0.579	-0.468	0.111
4.5	-0.531	-0.409	0.122

Table 3.2: Peak potentials and peak separation potentials of cathodic and anodic sweep for 10 mmol L^{-1} europium in various aqueous chloride media (second cycle). Scan rate: 0.05 V s^{-1}.

$[CaCl_2]$ (mol L^{-1})	$E_{P,c}$ (V)	$E_{P,a}$ (V)	ΔE_P (V)
0.5	-0.674	-0.504	0.170
1.5	-0.647	-0.472	0.175
3	-0.595	-0.389	0.206
4.5	-0.551	-0.230	0.321

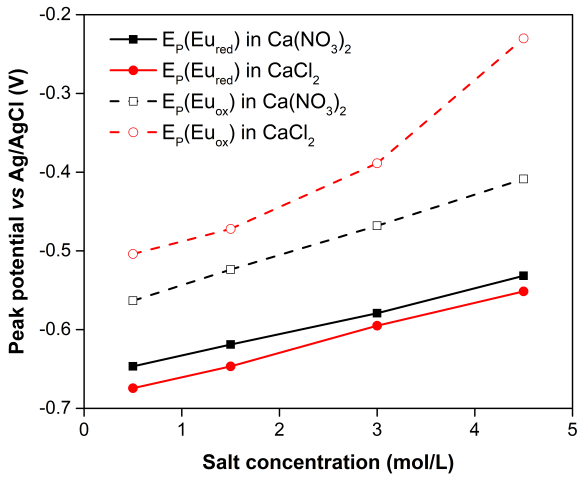

Figure 3.13: Change of the peak potential (*vs.* Ag/Ag^+, second cycle) for reduction (solid line) and oxidation (dashed line) of europium in nitrate (■) and chloride (●) aqueous solution as function of the salt concentration. Scan rate: 50 mV s^{-1}.

$$D = \frac{k_B \cdot T}{6\pi\eta r} \tag{3.2}$$

where k_B is the Boltzmann's constant, T the absolute temperature, η the dynamic viscosity and r the radius of particle. The peak current i_P and peak current density j_P are proportional to the square root of the diffusion coefficient according to the Randles-Sevcik equation (Eq. 3.1, at 25 °C).

It is clear that the change in current density upon changing supporting electrolyte concentration, as observed in Figs. 3.11 and 3.12, can be related to the change in viscosity. For this reason, it was important to measure the viscosity of the solutions used in electrochemical experiments (Table 3.3).

The change of peak current density as a function of viscosity is presented in Fig. 3.14. The trends of the curves was analyzed by Origin 2016 (v9.3) software by fitting the curves using a $f(x) = a \cdot x^b$ function model (allometric). Outcome of the function parameters a and b and the accompanying coefficient of determination (R^2, adjusted) after curve analysis can be found in Table 3.4. This curve analysis proves that the peak current density is indeed inversely proportional to the square root of the viscosity. Thus, the current density decreases with increasing supporting electrolyte concentrations, as increasing supporting electrolyte concentration results in an increasing viscosity and a change in capacitive contribution of the electrochemical double layer. In a (quasi-)reversible electrochemical system, the *peak current density* j_P is inversely

Table 3.3: Dynamic and kinematic viscosity (with variation coefficient) and density of the different saline solutions used in electrochemical experiments. All solutions contained 10 mmol L^{-1} europium and were measured at 25 °C.

Salt concentration	Dynamic viscosity (mPa s)	Kinematic viscosity ($mm^2\,s^{-1}$)	Density ($g\,cm^{-3}$)
0 mol L^{-1} $Ca(NO_3)_2$	0.846 ± 0.001	0.842 ± 0.001	1.00
0.5 mol L^{-1} $Ca(NO_3)_2$	0.941 ± 0.003	0.889 ± 0.003	1.06
1.5 mol L^{-1} $Ca(NO_3)_2$	1.272 ± 0.002	1.086 ± 0.001	1.17
3 mol L^{-1} $Ca(NO_3)_2$	2.482 ± 0.002	1.886 ± 0.001	1.33
4.5 mol L^{-1} $Ca(NO_3)_2$	5.866 ± 0.005	3.985 ± 0.004	1.47
0 mol L^{-1} $CaCl_2$	0.844 ± 0.001	0.844 ± 0.001	1.00
0.5 mol L^{-1} $CaCl_2$	0.935 ± 0.001	0.896 ± 0.001	1.04
1.5 mol L^{-1} $CaCl_2$	1.258 ± 0.001	1.111 ± 0.001	1.13
3 mol L^{-1} $CaCl_2$	2.383 ± 0.001	1.890 ± 0.001	1.26
4.5 mol L^{-1} $CaCl_2$	5.988 ± 0.002	4.342 ± 0.002	1.38

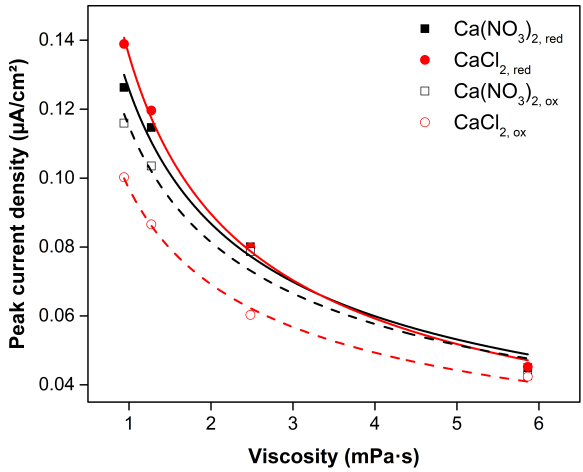

Figure 3.14: Change of peak current density (absolute values, second cycle) for reduction (solid line) and oxidation (dashed line) of europium as a function of the viscosity of the nitrate (■) and chloride (●) solutions. Scan rate: 50 mV s^{-1}.

Table 3.4: Outcome of the curve parameters a and b for the function model $f(x) = a \cdot x^b$ after curve analysis of the peak current density as a function of the viscosity

Medium	a	b	R^2
$Ca(NO_3)_{2,red}$	1.26E-4 ± 3.89E-6	-0.54 ± 0.0052	0.98057
$CaCl_{2,red}$	1.36E-4 ± 1.93E-6	-0.60 ± 0.0025	0.99633
$Ca(NO_3)_{2,ox}$	1.15E-4 ± 4.30E-6	-0.50 ± 0.0060	0.96924
$CaCl_{2,ox}$	9.70E-5 ± 1.34E-6	-0.49 ± 0.0022	0.99539

proportional to the square root of the viscosity [224]. This relation also holds for the systems studied here.

From the presented cyclic voltammograms it can be concluded that an increase in supporting electrolyte concentration results in a shift of reduction and oxidation potential to less negative values. A similar trend was observed for reduction/oxidation in both nitrate and chloride media, by which these shifts in reduction and oxidation potentials can be attributed to the strong change in ionic strengths and entropy. This indicates that formation and stability of Eu^{2+} at higher nitrate salt concentrations are based on thermodynamic principles. After all, the redox potential is dependent on the Gibbs free energy change and the equilibrium constants of the reduction-oxidation reactions. Consequently,

the redox potential is highly dependent on the thermodynamic activity of the redox active species (Nernst equation, Eq. 3.3)

$$E = E^0 + \frac{RT}{nF}\ln\frac{a_{Eu^{3+}}}{a_{Eu^{2+}}} = E^0 + \frac{RT}{nF}\ln\frac{\gamma_{Eu^{3+}}[Eu^{3+}]}{\gamma_{Eu^{2+}}[Eu^{2+}]} \tag{3.3}$$

Here, E^0 is the standard reduction potential, R the universal gas constant, T the temperature, n the number of electrons exchanged, F the Faraday constant, a the activity and γ the activity coefficient of the europium species.

An increasing ionic strength with increasing supporting electrolyte concentration causes the mixture of chemical species to deviate more from thermodynamic ideal behavior, by which the activity coefficients of the chemical species become increasingly important. The increase of the ionic strength of the medium alters the ionic atmosphere and changes the charge densities around the ions. As a consequence, the rate constants increase for higher ionic strengths.

Europium ions are strongly hydrated in aqueous media because of their high charge densities, with the highest charge density for Eu^{3+}. Consequently, Eu^{3+} and Eu^{2+} possess very negative hydration enthalpies, *i.e.* 3501 kJ mol^{-1} and 1458 kJ mol^{-1}, respectively. Eu^{3+} is known to be coordinated by 8 to 9 water molecules, whereas Eu^{2+} is coordinated by 7 to 8 water molecules [217, 219, 225]. Chloride and nitrate ions (with $Cl^- < NO_3^-$) show only modest levels of association with lanthanide ions in aqueous solutions, mostly in the form of double-solvent-separated ion pairs [226]. Therefore, they are found to predominantly form outer-sphere complexes, even at high salt concentrations [227–229]. Thus, Eu^{3+} and Eu^{2+} ions in aqueous media can be considered fully hydrated ions. However, the increasing supporting electrolyte concentration in solution leads to significant decrease of the solvent activity and significant increase in entropy, resulting in lower hydration of the europium ions in solutions and affecting the thermodynamics and stability constants of the complexes. After all, the oxidation of Eu^{2+} is dependent on the hydration enthalpies of both europium species to overcome the *third hydration energy* I_3 (2404 kJ mol^{-1} and the *activation energy* E_a. The shift towards less negative reduction potentials with increasing salt concentration in solution indicates higher stability of the Eu^{2+} species. In general, reduction is favored in case a more stable species is formed when the metal ion is present in the lower oxidation state of the redox couple, resulting in a more positive reduction potential [230].

Holleck stated in his work that the ion fields of the nitrate ions deform with increasing nitrate concentration when Eu^{3+} is reduced, leading to a change in polarization and, consequently, a change in charge distribution [222, 231]. As a result, the nitrate ions show transitions from a planar to a pyramidal structure,

enhancing a polar binding character that increases the stability of the Eu^{2+} aqua ion. Whether or not (catalytic) amounts of reduction products of nitrates are formed to increase Eu^{2+} stability remains unclear to date. Detection of such species is not straightforward because of the high nitrate concentration in solution. Nevertheless, investigation of the inner- and outer-coordination spheres of Eu^{3+} and Eu^{2+} in more detail would provide more information about the change in hydration as a function of the supporting electrolyte concentration and the nature of the coordinating ligands.

3.4.3 UV-VIS absorption measurements

Reduction of Eu^{3+} in concentrated aqueous nitrate media yielded a yellow-orange solution (Fig. 3.2), whereas aqueous chloride media remained colorless after reduction of Eu^{3+}. Therefore, UV-VIS absorption measurements were performed to compare the absorbance of Eu^{2+} in aqueous media containing high nitrate and chloride salt concentrations. Solutions containing lower nitrate salt concentrations remained colorless upon reduction of Eu^{3+}, and were therefore not measured by UV-VIS absorption spectroscopy. XANES measurements on these samples showed that almost no Eu^{2+} is formed in solutions containing lower nitrate salt concentrations (*vide infra*).

Most solutions containing trivalent lanthanide ions are only weakly colored as their transitions in the visible region of the spectrum are symmetry-forbidden f–f transitions. Moreover, the $4f$ subshells are positioned relatively deep inside the electron shell, shielded by the fully occupied $5s$ and $5p$ orbitals, so that the f–f transitions are only very weakly influenced by the surrounding ligands. Sharp emission bands can originate from these transitions [232]. The fine structure of Eu^{3+} with very low molar absorptivity was clearly observed in UV-VIS absorption measurements of solutions containing 6.6 mmol L^{-1} Eu^{3+} in 3 mol L^{-1} $Ca(NO_3)_2$ and 3 mol L^{-1} $CaCl_2$ when using a longer path length (10 mm). The spectra showed to be very similar in both nitrate and chloride media (Fig. 3.15). The spectra were limited to 320 nm because of the strong absorption by nitrate ions at shorter wavelengths, and consequently low reliability of the detector signal. The most intense absorption band is located at 390 – 400 nm, and originates from the $^5L_6 \leftarrow ^7F_0$ transition. A smaller peak at 400 – 410 nm, originating from the $^5L_6 \leftarrow ^7F_1$ transition, is present as a shoulder of this intense absorption peak. The smaller absorption bands at 355 – 370 nm originate from the weak f–f transitions from the ground state $^7F_0$ and the first excited multiplet $^7F_1$ to the multiplet manifolds $^5D_0$, $^5D_1$ and $^5D_2$ and higher lying excited states [233]. More detailed information on the interpretation of Eu^{3+} spectra can be found in the comprehensive review by Binnemans [191].

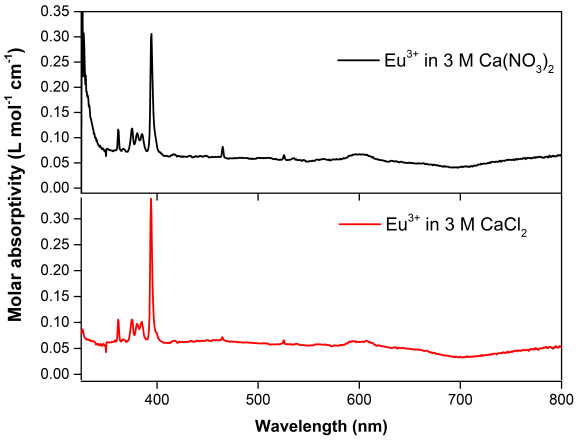

Figure 3.15: UV-VIS absorption spectra of Eu^{3+} (6.6 mmol L^{-1}) in aqueous nitrate and chloride media (3 mol L^{-1} CaX_2, with X NO_3^- or Cl^-). Blank solutions of these aqueous nitrate and chloride media were used for background correction. The lamp changeover occurred at 350 nm. Path length: 10 mm, resolution: 0.5 nm, scan rate: 150 nm min^{-1}.

Eu^{2+} possesses different photophysical properties, stemming from the lowest-energy ($4f^7$) and first excited-state ($4f^6 5d^1$) configurations [218]. $4f \rightarrow 5d$ transitions become more likely for Eu^{2+} because crystal and ligand field effects reduce the energy of the $5d$ states [234]. Inclusion of $5d$ levels implies broadband transitions, as the ground and excited states differ as a function of the distance of the electrons from the core. The $4f$ orbitals of Eu^{2+} remain largely unaffected by the presence of ligands, whereas the $5d$ orbitals are readily affected by ligand interactions. Characteristic spectra arise from the splitting by the crystal field of the five-fold degenerate $5d$ orbital into double degenerate $5d(e_g)$ and triple degenerate $5d(t_{2g})$ orbitals [235, 236]. Consequently, the luminescence properties of Eu^{2+} can be changed with different coordinating compounds, and its use has been investigated intensively [36, 218, 232].

Solutions of Eu^{2+} in aqueous chloride media are known to be colorless and non-luminescent, as was also observed in our experiments and confirmed by UV-VIS absorption measurements in a 3 mol L^{-1} $CaCl_2$ solution (Fig. 3.16). The affinity of chloride ions for Eu^{2+} is low, forming very unstable complexes [212]. Therefore, Eu^{2+} is predominantly coordinated by solvent molecules only, *i.e.* H_2O, which have a quenching effect on the luminescence. Absorption occurred only in the UV region of the spectrum, with two absorption maxima at 252 nm (39 682 cm^{-1}) and 322 nm (31 056 cm^{-1}). This is similar to what was reported

previously on the electro-reduction of Eu^{3+} in 0.1 mol L^{-1} HCl by Jelinek *et al.* [212]. After deconvolution, the four Gaussian-shaped absorption bands at 240, 270, 317 and 350 nm were attributed to the Laporte-allowed $4f^7 \rightarrow 4f^6 5d^1$ transition, where the $5d$ orbitals are split by the ligand field. Analogous with Eu^{3+}, Jelinek *et al.* reported that Eu^{2+} is probably coordinated by eight to nine water molecules, depending on the pH of the aqueous solution. Moreau *et al.*, however, determined *via* EXAFS (*vide infra*) that Eu^{2+} is predominantly coordinated by seven water molecules [217, 219].

A comparable absorption spectrum was recorded for Eu^{2+} in a 3 mol L^{-1} $Ca(NO_3)_2$ solution (Fig. 3.16), indicating a similar behavior of Eu^{2+} in both media [234]. The part of the UV region at shorter wavelengths could, however, not be investigated because of the high UV absorption by the nitrate ions, causing an unreliable detector signal. Compared to the Eu^{2+} absorption spectrum in chloride media, the broad absorption bands originating from the $4f^7 \rightarrow 4f^6 5d^1$ transition are slightly shifted to longer wavelengths. Additionally, the molar absorptivity of the Eu^{2+} species is higher in nitrate media. As a consequence, absorption occurs partially in the blue region of the visible spectrum, and explains the yellow to orange color of Eu^{2+} in aqueous nitrate media. In addition, it was observed that the absorption bands are also shifted to longer wavelengths with increasing europium concentration (Fig. 3.17). Solutions containing different Eu^{2+} concentrations, *i.e.* 3.29, 6.58, 32.9 and 65.8 mmol L^{-1}. This red shift (or bathochromic effect) is the origin of the color change of the solution as a function of the europium concentration. It remains unclear if any ligand interactions occur to increase stability of Eu^{2+} in aqueous nitrate media. In-depth structural analysis is required to further investigate the nature of the inner coordination sphere of Eu^{2+} in concentrated nitrate media.

3.4.4 Magnetic susceptibility measurements

Only a few techniques are available to study different oxidation states of an element. One of those techniques distinguishes a difference in magnetic properties upon changing valence state.

The magnetic susceptibility of a compound represents the degree of magnetization of this compound according to an *induced magnetic field* (H) to which it is subjected, and indicates whether a compound is attracted into the induced magnetic field or repelled from the induced magnetic field. Thus, the magnetic susceptibility can be regarded as a measure of the ease with which a material is magnetized by a given field. A positive value for the magnetic susceptibility indicates paramagnetism, whereas a negative value indicates diamagnetism. A change in electron configuration (*e.g.* a different oxidation state or a different

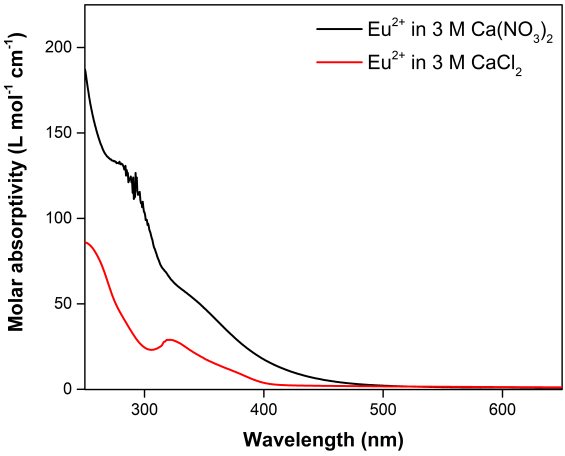

Figure 3.16: UV-VIS absorption spectra of 6.6 mmol L^{-1} Eu^{2+} in 3 mol L^{-1} $Ca(NO_3)_2$ and 3 mol L^{-1} $CaCl_2$. Blank solutions of these aqueous nitrate and chloride media were used for background correction. Lamp changeover occurred at 350 nm. Path length: 1 mm, resolution: 0.5 nm, scan rate: 150 nm min^{-1}.

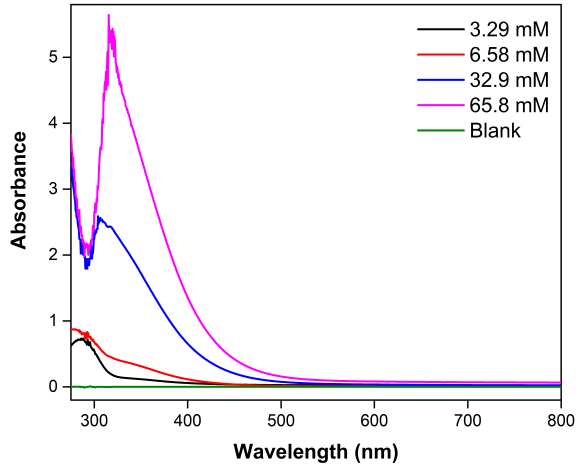

Figure 3.17: UV-VIS absorption spectra of solutions containing different Eu^{2+} concentrations in 3 mol L^{-1} $Ca(NO_3)_2$. Lamp changeover occurred at 350 nm. Path length: 1 mm, resolution: 0.5 nm, scan rate: 150 nm min^{-1}.

element) induces a change in magnetic susceptibility. This change disturbs the applied magnetic field significantly. The current needed to compensate for the change in magnetic field, and to re-establish the equilibrium, can be directly correlated to the level of magnetic susceptibility in the sample.

With the exception of La^{3+} and Lu^{3+}, all Ln^{3+} ions contain unpaired electrons, and are therefore paramagnetic. In general, the magnetic properties of lanthanide ions are determined entirely by the ground state, as the excited states are well separated from the ground state owing to the spin-orbital coupling, making them thermally inaccessible. Therefore, the magnetic properties of Ln^{3+} ions are independent of the environment as they are only determined by the electron configuration of the free ion. However, for Eu^{3+} ($[Xe]4f^6$), the ground state ($^7F_0$) does not contribute to the magnetic moment despite its six unpaired electrons. The orbital angular momentum of Eu^{3+} cancels out the electron angular momentum, whereby Eu^{3+} is considered diamagnetic at 0 K. Nevertheless, the first excited state of Eu^{3+} ($^7F_1$) is thermally accessible at room temperature and contributes to the magnetic moment, resulting in overall paramagnetic properties of Eu^{3+} at room temperature [237]. Because the magnetic properties of Eu^{3+} are predominantly determined by the occupation of the $^7F_1$ energy level, differences in Eu^{3+} coordination can affect the resulting effective magnetic moment since the energy difference between the ground state ($^7F_0$) and the first excited state ($^7F_1$) depends on the environment of Eu^{3+} at a given temperature. By contrast, Eu^{2+} ($[Xe]4f^7$) is strongly paramagnetic (μ_B = 7.63–8.43) in its ground state ($^8S_{7/2}$, *i.e.* similar to Gd^{3+}) because of its seven unpaired electrons [238]. Therefore, a change in oxidation state, *i.e.* a change in electron configuration, induces a strong change in magnetic properties.

The change in *effective magnetic moment* (μ) as a consequence of the change in oxidation state can be followed by means of *magnetic susceptibility* (χ) measurements, making use of a *magnetic susceptibility balance* (MSB) [239, 240]. The applicability of this technique for Eu^{3+} and Eu^{2+} was already demonstrated in various crystallographic and geological studies [240, 241]. In this study, the volume magnetic susceptibility (χ_V, dimensionless) was measured, which is defined as:

$$\chi_V = \frac{I}{H} \tag{3.4}$$

With I the intensity of magnetism induced in the substance in $A\,m^{-1}$, and H the intensity of the applied external magnetic field in $A\,m^{-1}$. Magnetic susceptibility measurements at room temperature were conducted to monitor the reduction of Eu^{3+} to Eu^{2+} as a function of the reduction time in aqueous nitrate media (3 mol L^{-1} $Ca(NO_3)_2$) for both chemical (Zn^0 grains) and electrochemical (-0.7 V

vs. Ag/Ag^{+}) reduction. The results of these measurements are presented in Fig. 3.18, and clearly show a change in volume magnetic susceptibility as a function of the reduction time. The result clearly shows the ability to (electro-)chemically reduce Eu^{3+} in aqueous nitrate media. Reduction of Eu^{3+} reached an equilibrium after *ca.* 120 min of reduction for both reduction methods. A comparison with the chemical reduction of Eu^{3+} in chloride media (6 mol L^{-1} LiCl) can be found in Fig. 3.18 (parameters of exponential fit are listed in Table 3.5). Chemical reduction of Eu^{3+} in chloride media proceeded slightly faster, reaching an equilibrium situation after *ca.* 90 min using the similar experimental parameters. The plateau value for the volume magnetic susceptibility with respect to the reduction of Eu^{3+} in both media is somewhat different, and can be attributed to the high sensitivity of the magnetic susceptibility balance to the composition of the samples. First, the total europium concentration in both media was not exactly the same. Second, different species with various effective magnetic moments were present in both samples, originating from the nature of Eu^{3+} and the salts used in this study.

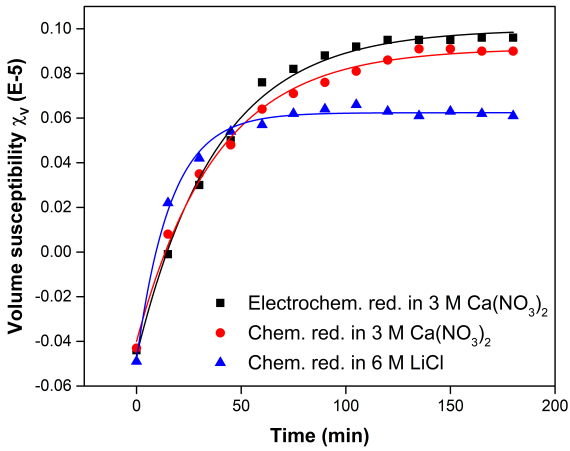

Figure 3.18: Comparison of the reducibility of europium (66 mmol L^{-1}) in 3 mol L^{-1} $Ca(NO_3)_2$ (electrochemical (■) and chemical (●)) and 6 mol L^{-1} LiCl (▲) *via* magnetic susceptibility measurements. The results are fitted with an exponential function.

Nevertheless, different parameters can influence the reduction rate of Eu^{3+} to Eu^{2+} for both reduction methods. Therefore, conclusions on reduction efficiency for Eu^{3+} should be treated with caution. The reduction rate in the electrochemical reduction method is highly dependent on the current, which is determined by the applied potential, the surface area and type of the working electrode and the conductivity of the solution. The particle size of the zinc

Table 3.5: Outcome of the curve parameters A, y_0 and R_0 for the function model $f(x) = y_0 + A \cdot e^{R_0 \cdot x}$ after curve analysis of the volume magnetic susceptibility as a function of the reduction time

Medium	A	y_0	R_0
$Ca(NO_3)_{2,\ elect.\ red.}$	-0.146 ± 0.003	0.0998 ± 0.0018	-0.0261 ± 0.0014
$Ca(NO_3)_{2,\ chem.\ red.}$	-0.131 ± 0.003	0.0912 ± 0.0016	-0.0264 ± 0.0014
$LiCl_{\ chem.\ red.}$	-0.111 ± 0.002	0.0624 ± 0.0008	-0.0617 ± 0.0031

grains, *i.e.* the specific surface area, and the zinc oxide surface layer covering the zinc grains are of high importance in the chemical reduction method. The influence of the zinc grains on the reduction of Eu^{3+} was reporded by Sayed *et al.* [98].

After reduction, a sealed sample tube was measured every 30 min for a period of 2.5 h (Fig. 3.19). These measurements did not result in large variations in volume magnetic susceptibility, again indicating the relatively high stability of Eu^{2+} in these solutions when an inert atmosphere is maintained.

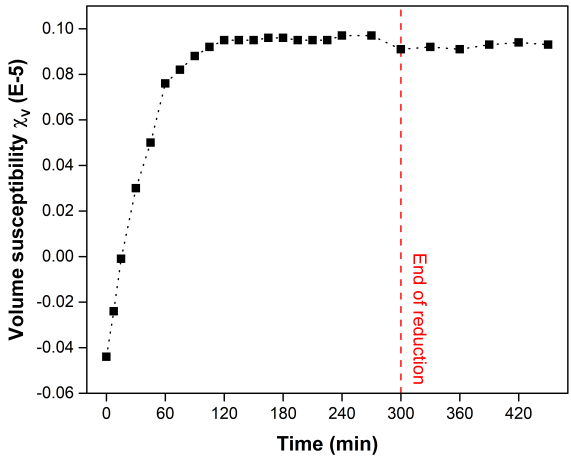

Figure 3.19: Magnetic susceptibility measurements of the electrochemical reduction of 66 mmol L^{-1} europium in 3 mol L^{-1} $Ca(NO_3)_2$. The reduction was stopped after 300 min, after which the sample resided in a sealed tube.

3.4.5 XAFS measurements

X-ray absorption near-edge structure (XANES) measurements have already been proven successful in determining valence states of europium in several mineralogical and crystallographic studies, making use of its high sensitivity and selective detection of target elements [205–209, 242, 243]. The strong absorption resonances, *i.e.* white lines, at the europium L_{III} edge in the X-ray absorption spectra yield information on the electronic structure of the absorbing species. The divalent and trivalent oxidation state can be easily distinguished because the XANES spectra for Eu^{2+} and Eu^{3+} have distinct resonance peaks separated by *ca.* 8 eV, at 6971.3 and 6979.3 eV, respectively. These resonance peaks originate from the electron transitions between $2p_{3/2}$ and $5d$ electronic states. Increased shielding of the nucleus by the additional $4f$ electron results in a slightly lower binding energy of the core electrons in Eu^{2+}. This is the main reason for the resonance peak for Eu^{2+} being observed at a slightly lower X-ray energy. Deconvolution of the resonance peaks in the XANES spectrum yields information on the relative ratio of Eu^{2+} and Eu^{3+} present in the sample. In addition to the resonance peaks, the spectrum contains continuum steps at which the core electron is excited to a continuum of final states such as free electron states [215]. These transitions to the continuum occur at slightly higher energies than the $2p_{3/2} \rightarrow 5d$ transitions. The L adsorption edge or continuum step, at which a $2p$ electron is excited to different energy levels, has to be accounted for when deconvoluting the XANES spectra. However, the adsorption edge step is difficult to examine experimentally as it is usually obscured by other spectral features [215]. The line shape of the continuum step, *i.e.* the transition to unoccupied cluster orbitals in the metal, is represented by a single Lorentzian function, with a width determined principally by the $2p$ core hole lifetime [244]. Integration of this function yields an arctangent function, which can be used for simulation of the continuum step. Such arctangent function was constructed for both Eu^{2+} and Eu^{3+}, and was accounted for using Eq. 3.5 as a function of the energy (in eV):

$$\begin{aligned} f(E) = \frac{(\mathrm{Eu}^{2+})_{RF}}{\pi}\left(atan\left(\frac{\pi}{R}(E - E_{\mathrm{Eu}^{2+},RP})\right) + \frac{\pi}{2}\right) \\ + \frac{(\mathrm{Eu}^{3+})_{RF}}{\pi}\left(atan\left(\frac{\pi}{R}(E - E_{\mathrm{Eu}^{3+},RP})\right) + \frac{\pi}{2}\right) \end{aligned} \tag{3.5}$$

With $(\mathrm{Eu}^{2+})_{RF}$ and $(\mathrm{Eu}^{3+})_{RF}$ the relative amounts of Eu^{2+} and Eu^{3+} in the sample, respectively; R the resolution of the arctangent function (*i.e.* determines the width of the step; a resolution of 5 was used); $E_{\mathrm{Eu}^{2+},RP}$ and $E_{\mathrm{Eu}^{3+},RP}$ the

position of the resonance peaks for Eu^{2+} (6971.5 eV) and Eu^{3+} (6979.5 eV), respectively. Sum of the relative amounts of Eu^{2+} and Eu^{2+} (total height of the arctangent jump) is equal to 1 as the absorbance in the XANES spectra were normalized to 1. Examples of the arctangent background for a sample containing 100 % Eu^{3+} (0 min of chemical reduction) and a sample containing *ca.* 82 % Eu^{2+} and *ca.* 18 % Eu^{2+} (90 min of chemical reduction) are presented in Fig. 3.20 and Fig. 3.21, respectively. An example of the resulting peak deconvolution using multiple peak analysis (*via* Origin 2016, *v*9.3 software) by means of Pseudo-Voigt functions is shown in Fig. 3.22.

The XANES spectra of the chemical reduction of Eu^{3+} in steps of 15 min are presented in Fig. 3.23. A solution containing 66 mmol L^{-1} europium and 6 mol L^{-1} $LiNO_3$ was used to record these spectra. Li^+ was used as the counter ion for nitrate because of the low absorbance of this light element, limiting the interference in the XANES spectra. An indication of the relative amounts of Eu^{2+} and Eu^{3+} after deconvolution of the XANES spectra is presented in Fig. 3.24 (parameters of the exponential fit are listed in Table 3.6). A trend similar to the one observed for the magnetic susceptibility measurements can be distinguished, *i.e.* a plateau value is reached after *ca.* 120 min. Small deviations from the trend can be attributed to the partial back-oxidation of Eu^{2+} as a

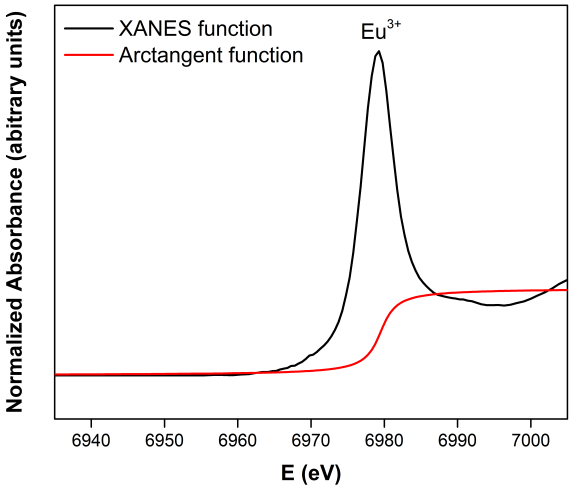

Figure 3.20: Arctangent background simulation (red) for a XANES spectrum after pre-edge background subtraction (black) of a solution containing 100 % Eu^{3+} (66 mmol L^{-1}, 0 min of chemical reduction) in 6 mol L^{-1} $LiNO_3$.

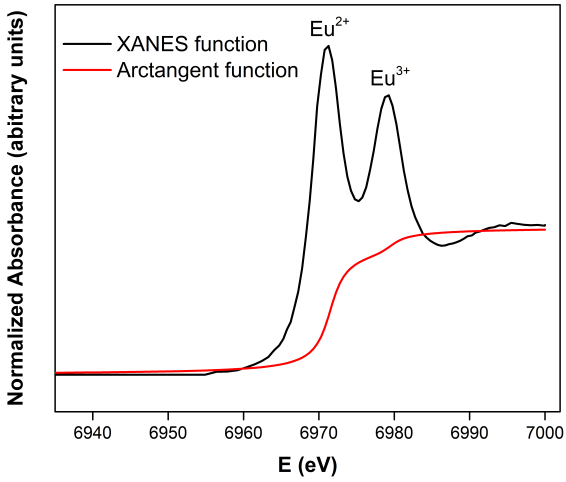

Figure 3.21: Arctangent background simulation (red) for a XANES spectrum after pre-edge background subtraction (black) of a solution containing Eu^{2+} and Eu^{3+} (66 mmol L^{-1}, 90 min of chemical reduction) in 6 mol L^{-1} $LiNO_3$.

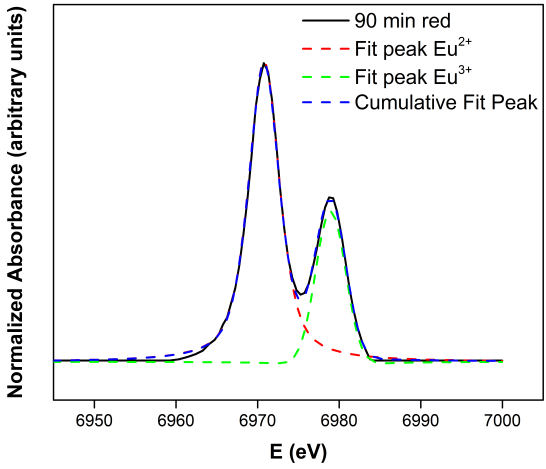

Figure 3.22: Peak deconvolution of a XANES spectrum after pre-edge and arctangent background subtraction of a 6 mol L^{-1} $LiNO_3$ solution containing both Eu^{2+} and Eu^{3+} (66 mmol L^{-1}, 90 min of chemical reduction) *via* Pseudo-Voigt peak analysis.

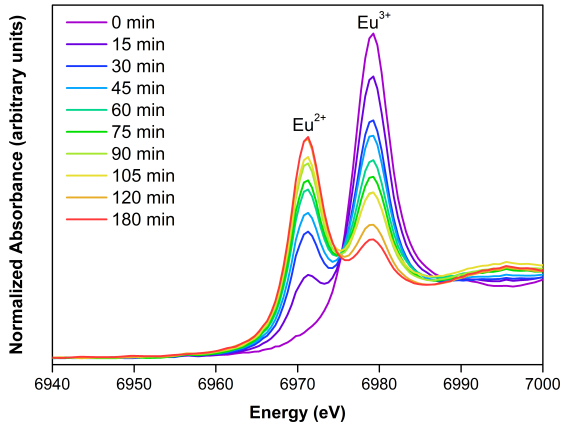

Figure 3.23: Normalized XANES spectra of the reduction of europium (66 mmol L^{-1}) in a 6 mol L^{-1} $LiNO_3$ aqueous solution as a function of time. Spectra were recorded every 15 min. The solution contained 100 % Eu^{3+} at 0 min.

result of the filling of the measurement cell. Short contact with air (oxidation by O_2, Reaction 3.2) could not be avoided during this operation. Additionally, a high conversion rate of Eu^{3+} to Eu^{2+} by chemical reduction can be observed, *i.e.* > 95 % after 120 min.

XANES measurements on the chemical reduction of europium as a function of time were conducted on solutions containing different lithium nitrate salt concentrations (0, 3 and 6 mol L^{-1}). The results of these measurements can be found in Figs. 3.25 to 3.27, respectively. The concentration of europium in these samples was 10 times lower, *i.e.* 6.6 mmol L^{-1}, for which the XANES technique is less sensitive. The resulting data have poorer quality with high background noise levels. Relatively concentrated samples are needed for good quality XANES spectra. The requirement of relatively concentrated samples is a disadvantage of the XAFS measurement techniques. Notwithstanding the

Table 3.6: Outcome of the curve parameters A, y_0 and R_0 for the function model $f(x) = y_0 + A \cdot e^{R_0 \cdot x}$ for the curve analysis of the relative amount of Eu^{x+} as a function of the reduction time

Eu^{x+}	A	y_0	R_0
Eu^{2+}	-0.950 ± 0.045	0.984 ± 0.039	-0.0209 ± 0.00
Eu^{3+}	0.950 ± 0.045	0.016 ± 0.039	-0.0209 ± 0.00

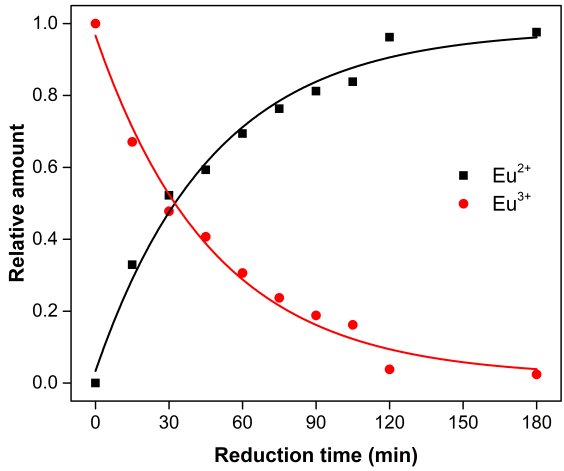

Figure 3.24: Relative amounts of Eu^{2+} (■) and Eu^{3+} (●) in a 6 mol L^{-1} $LiNO_3$ aqueous solution upon chemical reduction with zinc grains as a function of the reduction time. The data were fitted with an exponential function.

lower quality of the spectra, general trends that support previous statements in this research can be distinguished. First of all, it is clear that reduction of Eu^{3+} in aqueous media containing lower nitrate salt concentration was less efficient. This might be attributed to the higher hydration of europium at these nitrate salt concentrations. Another reason might be an insufficient stabilization of the Eu^{2+} species in solutions containing lower nitrate salt concentrations. Secondly, 6.6 mmol L^{-1} europium remained equally well reducible in a 6 mol L^{-1} $LiNO_3$ solution compared to the samples containing 66 mmol L^{-1} europium. Thus, the reducibility of europium strongly depends on the nitrate salt concentration, with consequent change in ionic strength and activity, and seems to be independent of the europium concentration. This latter statement, however, is only valid for macro concentrations of europium in solution, as trace concentrations (10^{-10} mol L^{-1}) were impossible to test by XAFS. Peppard *et al.* already proved that stabilization of Eu^{2+} in solution at trace concentration is different compared to macro concentrations [103, 245].

After chemical reduction of europium (66 mmol L^{-1}) in aqueous nitrate media (6 mol L^{-1} $LiNO_3$) for 180 min, the stability of Eu^{2+} in these media was investigated by recording a XANES spectrum every 60 min for a period of 5 h (Fig. 3.28). The sample remained in the measurement cell, which was closed with Kapton® tape to avoid contact with oxygen in the air. The resulting

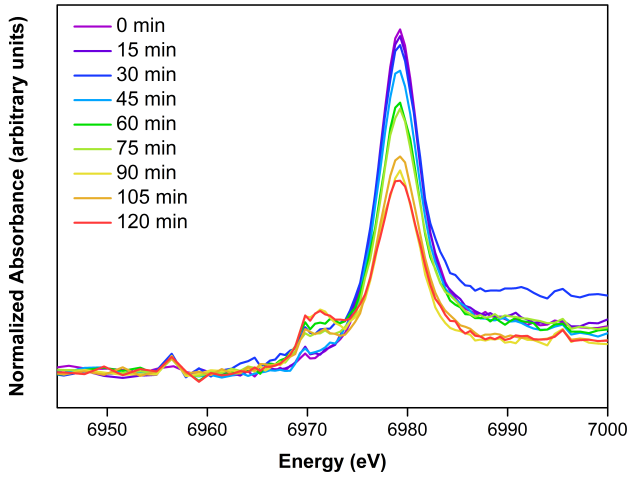

Figure 3.25: Normalized XANES spectra of the reduction of europium (6.6 mmol L^{-1}) in a 0 mol L^{-1} $LiNO_3$ aqueous solution as a function of time. Spectra were recorded every 15 min. The solution contained 100 % Eu^{3+} at 0 min.

spectra were subjected to a peak analysis similar to the one described before to determine the relative amounts of Eu^{2+} and Eu^{3+} in the sample. The change in relative amounts of Eu^{2+} and Eu^{3+} as a function of time after reduction is presented in Fig. 3.29 (parameters of the exponential fit are listed in Table 3.7).

From these data, it is clear that Eu^{2+} remains remarkably stable over time, and is not readily oxidized after removal of the reducing agent. Over the course of 240 min, only a few percent of Eu^{2+} was re-oxidized to Eu^{3+}. Therefore, it can be concluded that Eu^{2+} remains fairly stable in concentrated aqueous nitrate media if contact with air (O_2) or any other oxidizing agent is excluded. Because of their relatively high stability, Eu^{2+} solutions containing high nitrate salt concentrations are suitable for manipulations. Its use can be tested in different

Table 3.7: Outcome of the curve parameters A, y_0 and R_0 for the function model $f(x) = y_0 + A \cdot e^{R_0 \cdot x}$ for the curve analysis of the relative amount of Eu^{x+} as a function of the oxidation time after 3 h of reduction

Eu^{x+}	A	y_0	R_0
Eu^{2+}	-0.0451 ± 0.040	1.022 ± 0.043	0.0031 ± 0.001
Eu^{3+}	0.0451 ± 0.040	-0.022 ± 0.040	-0.0031 ± 0.001

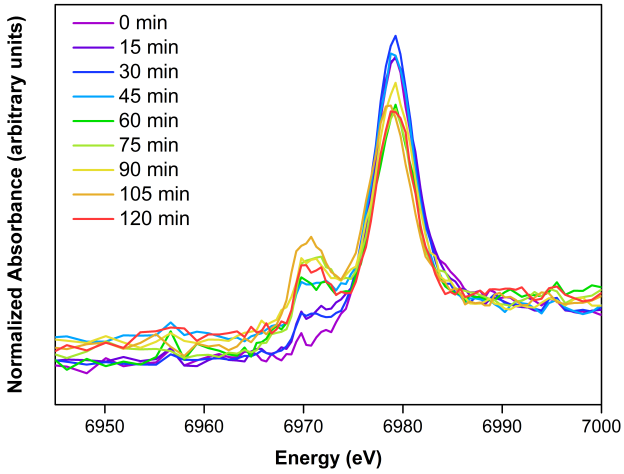

Figure 3.26: Normalized XANES spectra of the reduction of europium (6.6 mmol L^{-1}) in a 3 mol L^{-1} $LiNO_3$ aqueous solution as a function of time. Spectra were recorded every 15 min. The solution contained 100 % Eu^{3+} at 0 min.

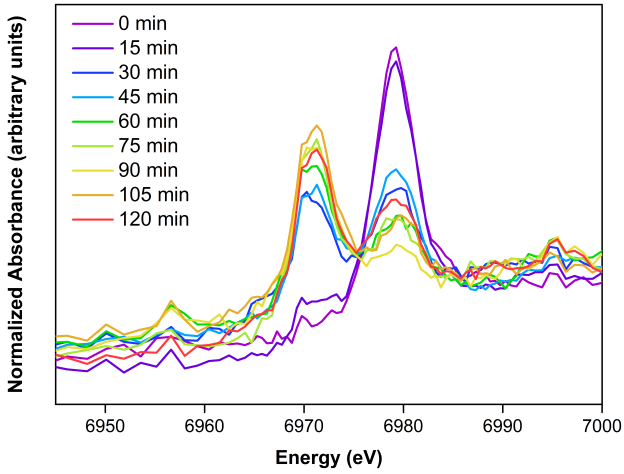

Figure 3.27: Normalized XANES spectra of the reduction of europium (6.6 mmol L^{-1}) in a 6 mol L^{-1} $LiNO_3$ aqueous solution as a function of time. Spectra were recorded every 15 min. The solution contained 100 % Eu^{3+} at 0 min.

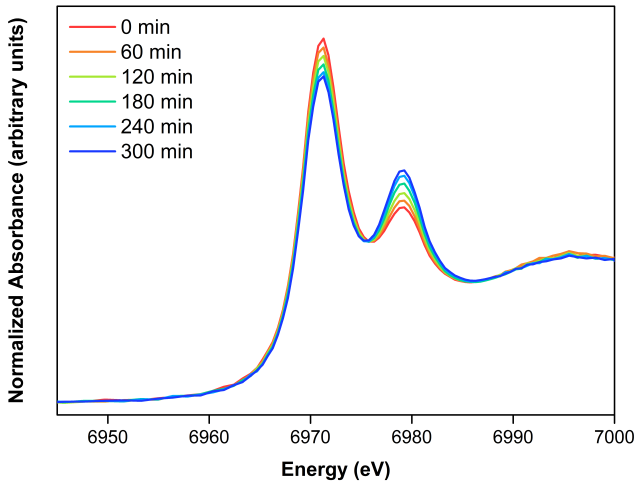

Figure 3.28: Normalized XANES spectra of the oxidation of europium (66 mmol L^{-1}) in a 6 mol L^{-1} $LiNO_3$ aqueous solution as a function of time after 480 min of reduction. Spectra were recorded every 60 min.

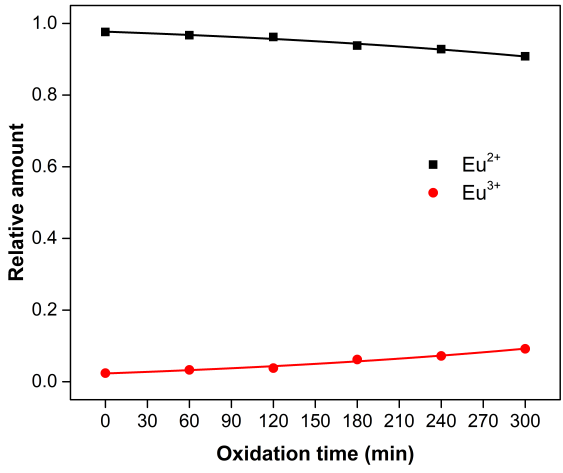

Figure 3.29: Indication of the relative amounts of Eu^{2+} (■) and Eu^{3+} (●) in a 6 mol L^{-1} $LiNO_3$ aqueous solution a function of time after europium was chemically reduced for 180 min. The XANES spectra were analyzed *via* Pseudo-Voigt peak deconvolution.

types of applications.

The XAS studies were limited to the near-edge region of the spectrum to be able to follow the reduction as a function of time. A spectrum of a new aliquot was recorded every 15 min, cutting off the measurements at 7000 eV. Consequently, the EXAFS region was not recorded. Therefore, no structural information on the coordination of Eu^{2+} in aqueous nitrate media could be derived, and is topic of future investigations.

3.5 Conclusions

The chemical and electrochemical reduction of Eu^{3+} in aqueous media containing high nitrate salt concentrations was monitored by magnetic susceptibility and XANES measurements. Maximum reduction, reaching high relative amounts of Eu^{2+} (> 95 %), was achieved after 120 min of reduction. Moreover, it was proven by these techniques that Eu^{2+} in these media is relatively stable for several hours when kept in an inert atmosphere. Cyclic voltammetry studies showed that the reduction potential for Eu^{3+} becomes less negative with increasing supporting electrolyte concentrations. The increase in ionic strength causes a change in solution thermodynamics ensuring a higher stability of Eu^{2+} species by which the reduction reaction is favored. Cyclic voltammetry studies also showed that the reduction of Eu^{3+} and oxidation of Eu^{2+} in aqueous nitrate solutions occurs at slightly less negative potentials compared to similar chloride media. Aqueous solutions containing high nitrate salt concentrations colored yellow-orange upon reduction of Eu^{3+} to Eu^{2+}, whereas similar reduction in aqueous chloride media remained colorless. UV-VIS absorption studies revealed a small shift towards longer wavelengths and broadening of the Eu^{2+} absorption band in nitrate media. This causes Eu^{2+} to absorb in the blue region of the visible light spectrum in nitrate media, whereas absorption of Eu^{2+} in chloride media is restricted to the UV region. From the experiments conducted in this chapter, it is evident that high ionic strengths are required for an efficient reduction of Eu^{3+} and high stabilization of Eu^{2+} in nitrate media.

Chapter 4

Separation of samarium and europium by solvent extraction with an undiluted quaternary ammonium ionic liquid

This chapter is based on the published research article:

Michiel Van de Voorde, Karen Van Hecke, Koen Binnemans and Thomas Cardinaels, RSC Advances, 2018, 8, 20077–20086

The text might contain slight adjustments to the original publication.

All experimental work and compilation of the manuscript were performed by the author of this thesis.

4.1 Abstract

Long-lived europium-154 impurities are formed during the production of medical samarium-153 in a high-flux nuclear reactor. A method to separate these europium impurities from samarium was investigated using the hydrophobic quaternary ammonium ionic liquid Aliquat 336 nitrate. The separation method consists of the selective reduction of Eu^{3+} by zinc metal in an aqueous feed solution containing a high nitrate salt concentration. Subsequent extraction using undiluted Aliquat 336 nitrate leads to an efficient separation of both lanthanides in a relatively short time frame. Sm^{3+} was extracted to the neat ionic liquid phase much more efficiently than Eu^{2+}. An initial approach using the addition of dicyclohexano-18-crown-6 to capture Eu^{2+} in the ionic liquid phase proved to be less efficient.

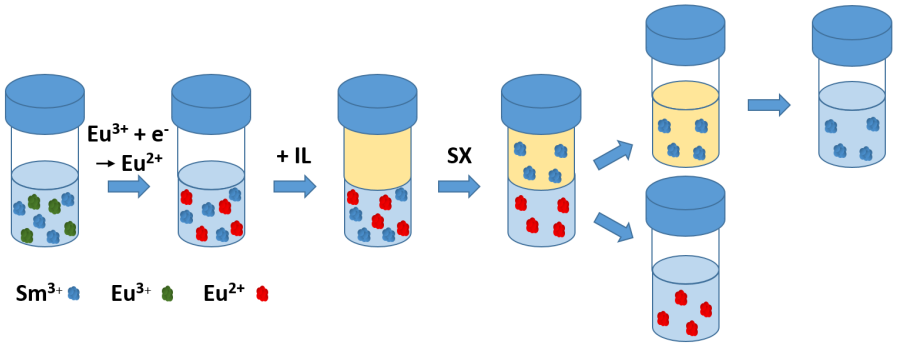

Figure 4.1: Graphical abstract describing the separation method for samarium and europium using solvent extraction. Eu^{3+} is selectively reduced to Eu^{2+} in a first step, after which Sm^{3+} can be selectively extracted to the organic phase

4.2 Introduction

The radiolanthanide samarium-153 (^{153}Sm) is applied in nuclear medicine, where it is known under its commercial names Quadramet and Lexidronam [4, 77]. In these radiopharmaceuticals, the ^{153}Sm radioisotope is coordinated to an ethylenediamine tetra(methylene phosphonate) chelating ligand (^{153}Sm-EDTMP, Fig. 4.2) [10]. ^{153}Sm serves well in nuclear medicine because of its favorable half-life of 46.284 h and because it decays to the stable ^{153}Eu nuclide. This causes no severe additional side effects in the human body after treatment. ^{153}Sm-EDTMP is very selective towards the skeleton [12, 246–248]. The ^{153}Sm radionuclide is commonly produced *via* neutron-irradiation of an enriched $^{152}Sm_2O_3$ target in a nuclear research reactor with a high thermal neutron flux [20]. A product with high yield, high purity and high specific activity is formed. However, since the target is usually irradiated for several days, part of the ^{153}Sm is already decaying during irradiation and the daughter isotope ^{153}Sm will be neutron-irradiated as well, leading to the simultaneous production of trace amounts of ^{154}Eu [249, 250]. This radiochemical impurity has a much longer half-life (8.593 y) compared to that of ^{153}Sm. Relatively large quantities of ^{154}Eu lead to an unacceptable radiation dose delivered to the patient. The maximum level of impurities is strictly regulated by international and national organizations (*e.g.* WHO, IAEA, FDA). Consequently, Quadramet has a limited shelf life of only a few days after being produced, since expiration is reached at the threshold ratio of 0.093 µCi (= 3400 Bq) of ^{154}Eu per mCi (37 MBq) of ^{153}Sm [89, 249, 250]. Additionally, long-lived ^{154}Eu impurities end up in the waste generated in the hospitals. Removal of these ^{154}Eu impurities would imply a longer product shelf-life for medical use, leading to an increased availability of ^{153}Sm and a lower background radioactivity of the treated patient. Waste treatment procedures in hospitals can become easier because waste containing short-lived isotopes only can be treated *via* decay storage. Moreover, distribution and transportation deadlines can become more flexible, opening perspectives of feeding a world-wide market. This way, an unexpected outage of a research reactor can be backed-up more easily by another research reactor, ensuring the supply of ^{153}Sm. Valuable and expensive enriched target material can also be used more efficiently by increasing the irradiation time because the long-lived side-products are removed afterwards. Undeniably, purification of the irradiated target material by separation of ^{154}Eu from ^{153}Sm would be beneficial in medical and economical perspective.

Separation of two neighboring lanthanides is very challenging because of their very similar chemical properties. A separation method based on a very small difference in complexation behavior would be too time-consuming to be feasible for the separation of these relatively short-lived radionuclides. Approaches

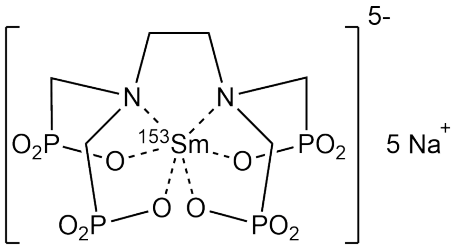

Figure 4.2: Chemical structure of ^{153}Sm-EDTMP (commercial names: Quadramet and Lexidronam).

based on the selective reduction of europium from the trivalent to the divalent state, either chemically or electrochemically, changing the chemical properties of europium significantly, have proven to be efficient for the recovery of highly valuable europium from rare-earth ores on an industrial scale [96, 198, 201, 218, 251, 252]. In these processes, a phosphorus-containing acidic extractant with high affinity for lanthanides (Ln^{3+}) is used most frequently, leaving the Eu^{2+} unaffected in the aqueous phase. The use of ion exchange resins is another popular purification method. Taking into account the relatively short half-lives of the medical radionuclides, gravimetrical separation methods are too time-consuming to be used. High performance ion chromatography (HPIC) methods to separate radiolanthanides are more suitable, but require more advanced equipment [253].

In this chapter, we conducted a feasibility study to separate samarium and europium *via* two different solvent extraction processes. Prior to the separation process, Eu^{3+} was selectively reduced to Eu^{2+} by Zn^0. The water-immiscible phase of the extraction system consisted of the highly hydrophobic *ionic liquid* (IL) Aliquat 336 nitrate ([A336][NO_3], Fig. 4.3a). Ionic liquids are solvents that consist entirely of ions. Moreover, previous studies have shown that the use of undiluted ionic liquids in solvent extraction is a very promising approach for separation of *rare-earth elements* (REEs) [109, 254–257].

The separation process was performed with and without the addition of a size-selective extractant. The size-selective extractant dicyclohexano-18-crown-6 (DCH18C6, Fig. 4.3b) was selected because of its capability to efficiently extract Sr^{2+}, which has a comparable ionic radius and charge density as Eu^{2+} [217, 219, 258, 259]. The process including DCH18C6 was aimed at the size-selective extraction of Eu^{2+} to the water-immiscible phase, while leaving Sm^{3+} in the aqueous phase. The process without addition of DCH18C6 uses the alkaline extraction capacities of the ionic liquid itself to separate samarium and europium.

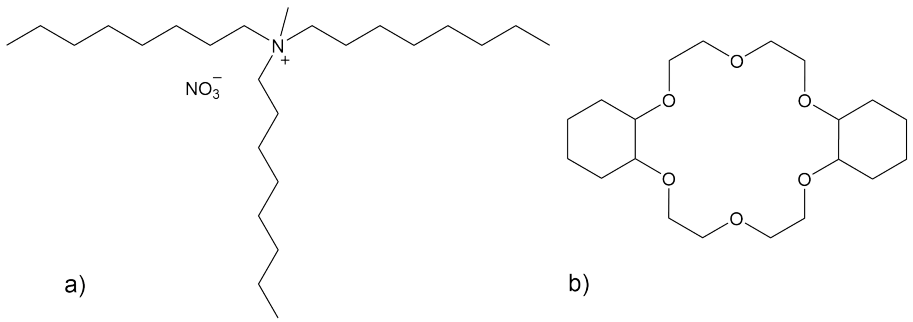

Figure 4.3: Chemical structures of a) the main component of Aliquat 336 nitrate ([A336][NO_3]) and (b) dicyclohexano-18-crown-6 (DCH18C6).

4.3 Experimental

4.3.1 Materials

Tricaprylmethylammonium chloride (Aliquat® 336, [A336][Cl], 88.2 – 90.6 %), dicyclohexano-18-crown-6 (DCH18C6, ≥ 98 %), LiCl (99 %) and HNO_3 (≥ 65 %) were purchased from Sigma-Aldrich (Diegem, Belgium). $SmCl_3{\cdot}6H_2O$ (99.9 %) and $Eu(NO_3)_3{\cdot}6H_2O$ (99.9 %) were purchased from Strem Chemicals, Inc. (Newburyport, USA). $Sm(NO_3)_3{\cdot}6H_2O$ (99.9 %) and $LiNO_3$ (anhydrous, 99 %) were purchased from Alfa Aesar (Karlsruhe, Germany). $EuCl_3{\cdot}6H_2O$ (99.9 %), $Sr(NO_3)_2$ (99.9 %) and granular zinc (30 mesh, ≥ 99.7 %) were purchased from Acros Organics (Geel, Belgium). $SrCl_2{\cdot}6H_2O$ (≥ 99 %), NH_4Cl (≥ 99.8 %), Na_2SO_4 (≥ 99 %) and acetonitrile (≥ 99.5 %) were purchased from Chem-Lab (Zedelgem, Belgium), as well as the Sm, Eu, Zn and Cu standard solutions (≥ 99.99 %, 1000 µg mL^{-1}, 2 – 5 % HNO_3, Plasma HIQU). NH_4NO_3 (≥ 99 %) was purchased from Merck Millipore (Darmstadt, Germany). All products were used as received, without any further purification steps. Aqueous samples were prepared with MilliQ water (18.2 MΩ cm at 25 °C).

4.3.2 Reduction of Eu^{3+}

In all experiments, Eu^{3+} (E^0 = -0.34 V) was reduced chemically using zinc granules (E^0 = -0.76 V) taking into account the minimal requirements to obtain maximal reduction established by Sayed *et al.* [98]. This study proved that a minimal contact time of 1 hour and a minimal zinc-to-europium molar ratio of 2.5 are needed to reach maximum reduction of Eu^{3+}. Therefore, the aqueous

feed solutions, both chloride and nitrate ones, were mixed with a large excess of granular zinc (30 mesh) for 2 h at room temperature. The remarkably high stability of Eu^{2+} in aqueous solutions containing high nitrate salt concentrations was already discussed in the previous chapter. The aqueous solutions were purged with nitrogen gas during reduction of Eu^{3+} to remove atmospheric and dissolved oxygen. This is necessary to prevent re-oxidation of Eu^{2+} by O_2 ($E^0 = +1.23\,V$). The pH of the aqueous feed solution was kept between 4 and 6.5. This way, the pH of the final feed solution remained sufficiently high to avoid re-oxidation of Eu^{2+} by H^+ ($E^0 = 0.00\,V$) and sufficiently low to prevent hydrolysis of Sm^{3+} or Eu^{3+}. Too low pH levels lead to preferential H_2 generation in contact with Zn^0, *i.e.* Eu^{3+} will only be reduced as soon as the H^+ concentration is sufficiently low. Therefore, pH of the aqueous feed solution after reduction will only be slightly acidic. The pH was measured after Eu^{3+} reduction and after extraction by means of a Hamilton Slimtrode pH electrode coupled to a Mettler-Toledo SevenCompact pH meter.

4.3.3 Preparation of the water-immiscible phase

The water-immiscible phase consisted of neat [A336][NO_3] or [A336][NO_3] containing $0.05\,mol\,L^{-1}$ DCH18C6. Neat [A336][NO_3] was prepared from commercially available [A336][Cl] *via* a metathesis reaction. [A336][Cl] was dissolved in acetonitrile to decrease the viscosity of the IL and to enhance phase separation. An aqueous solution containing $6\,mol\,L^{-1}$ NH_4NO_3 was mixed intensively with the [A336][Cl]–acetonitrile solution. This way, chloride anions were replaced by nitrate anions, a process that is favorable according to the Hofmeister series since nitrate ions are less strongly solvated than chloride ions [193]. After mixing and phase separation, the aqueous phase was removed and tested for remaining chloride by addition of a $AgNO_3$ solution. This process was repeated until no chloride traces could be found in the aqueous phase. After achieving full conversion of [A336][Cl] to [A336][NO_3], acetonitrile was removed by means of a rotary evaporator, followed by treatment at high vacuum using a Schlenk line.

The final chloride content after conversion of the commercially available [A336][Cl] to [A336][NO_3] was determined by *total reflection X-ray fluorescence* (TXRF) spectroscopy, using a Bruker Picofox S2 TXRF spectrometer [260]. A sample of [A336][NO_3] was prepared by the addition of 100 µL of a Cu^{2+} standard solution, 100 µL of a NH_3 solution (25 wt%) and 750 µL of ethanol to 40 mg of the ionic liquid. A droplet (2.5 µL) of this mixture was placed on a quartz glass carrier after vigorous homogenization. Subsequently, the quartz glass carrier was dried in a hot air oven at 60 °C for 30 min and measured the TXRF spectrometer for 200 s. The results were processed using the Bruker

Spectra Picofox software (version 7.5.3.0). Analysis of the final, dry [A336][NO_3] by TXRF showed a remaining chloride concentration of *ca.* 4 ppm. Afterwards, the ionic liquid was equilibrated with water (MilliQ) prior to its use in solvent extraction experiments to avoid any significant volume changes during the extraction experiments.

4.3.4 Extraction experiments

The aqueous feed solutions contained both Sm and Eu. The concentration of each lanthanide was 1 g L^{-1} (6.6 mmol L^{-1}). Only stable isotopes of samarium and europium were used. The chloride or nitrate concentrations in the aqueous feed solutions were adjusted by the addition of the respective ammonium or lithium salts. Exact concentrations of samarium and europium in the solution after reduction by zinc were determined by ICP-OES. A 1 mL aliquot of the aqueous feed solution was mixed with 1 mL of organic phase, after the reduction of Eu^{3+} to Eu^{2+}. This organic phase consisted of neat [A336][NO3] or [A336][NO_3] containing 0.05 mol L^{-1} DCH18C6. Both phases were purged intensively with nitrogen gas before extraction to prevent oxidation of Eu^{2+} by dissolved oxygen. Both phases were mixed in a 4 mL glass reaction vial at 1700 rpm making use of an Allsheng TMS-200 thermoshaker. Various mixing times (5, 15, 30 and 60 min) and temperatures (25, 40 and 60 °C) were tested in triplicate to find the most suitable separation conditions. After mixing, the reaction vials were centrifuged for 1 min at 5300 rpm using a Thermo Scientific Heraeus 200 Centrifuge to accelerate phase disengagement. Next, the aqueous phase was separated from the ionic liquid phase prior to analysis by ICP-OES. The efficiency of the separation method was evaluated by means of the distribution ratio, the fraction extracted and the separation factor. The *distribution ratio* (D) of a compound is defined as the ratio of the total concentration of this compound in the extract phase to its total concentration in the initial phase:

$$D = \frac{[M]_{\mathrm{IL,final}}}{[M]_{\mathrm{Aq,final}}} = \frac{[M]_{\mathrm{Aq,initial}} - [M]_{\mathrm{Aq,final}}}{[M]_{\mathrm{Aq,final}}} \tag{4.1}$$

In this equation, the volumes of both phases are equal. $[M]_{\mathrm{Aq,initial}}$ represents the initial concentration of the compound in the aqueous feed solution, $[M]_{\mathrm{Aq,final}}$ and $[M]_{\mathrm{IL,final}}$ represent the concentration of the compound in the aqueous and ionic liquid phase, respectively, after extraction.

The *fraction extracted* (%E, also percentage extraction) is defined as the ratio of the amount of compound extracted to its total amount in the system. In

case both phases are present in equal volume, the fraction extracted can be expressed as:

$$\%E = \frac{[M]_{\mathrm{IL,final}}}{[M]_{\mathrm{total}}} \times 100 = \frac{[M]_{\mathrm{Aq,initial}} - [M]_{\mathrm{Aq,final}}}{[M]_{\mathrm{Aq,initial}}} \times 100 \tag{4.2}$$

In case more elements are present, one can describe the *separation factor* (α), which is the ratio of the distribution ratios of two compounds A and B:

$$\alpha = \frac{D_{\mathrm{A}}}{D_{\mathrm{B}}} \qquad \text{with } D_{\mathrm{A}} \geq D_{\mathrm{B}} \tag{4.3}$$

Aqueous solutions, *i.e.* the feed solution after reduction by Zn^0 and the aqueous phase after extraction, were analyzed by using a Perkin Elmer Optima 8300 inductively coupled plasma optical emission spectrometer (ICP-OES) in axial view, with a GemTip CrossFlow II nebulizer, a Scott spray chamber assembly, a sapphire injector and a Hybrid XLT quartz-ceramic torch. Calibration curves were constructed by fitting the results of standard solutions containing 0.01, 0.1, 1 and 10 ppm Sm, Eu, Sr and/or Zn through the origin. Samples of the aqueous solutions to be measured by ICP-OES were diluted 100 times by a 2 wt% HNO_3 solution.

4.3.5 EXAFS measurement and data treatment

Extended X-ray Absorption Fine Structure (EXAFS) spectra of Sm L_{III}-edge (6716 eV) were collected at the Dutch–Belgian Beamline (DUBBLE, BM26A) at the European Synchrotron Radiation Facility (ESRF) in Grenoble (France). The energy of the X-ray beam was tuned by a double-crystal monochromator operating in fixed-exit mode using a Si(111) crystal pair. The measurements were done in transmission mode using Ar/He gas filled ionization chambers at ambient pressure. A brass sample holder with Kapton® windows and a flexible polymeric spacer (VITON®) with a thickness of 2 mm was used as a sample holder.

Standard procedures were used for pre-edge subtraction and data normalization in order to isolate the EXAFS function (χ). The EXAFS oscillations, isolated by a smoothing spline using the program VIPER (v11.00), were k^4-weighed and Fourier transformed between $k = 3.68$ and 11.13 Å^{-1} using a Gaussian rounded ends window function [261]. The data were fitted in $R + \Delta$ (Å) space, between 0 and 2.78 Å, using the *ab initio* code FEFF 7.0 , which was used to calculate the theoretical phase and amplitude functions that were subsequently used in the

non-linear least-squares refinement of the experimental data [262]. Estimated standard deviations are shown between parentheses and calculated by VIPER. The amplitude reduction factor S_0 was fixed at 1.1.

4.4 Results and Discussion

4.4.1 Defining two separation approaches

In this study, the separation of samarium and europium was investigated with and without the use of a size selective extractant. Many studies report on the efficient extraction of Sr^{2+} by a 18-crown-6 (18C6) derivative as extractant [263–266]. These 18C6-based crown ethers are able to capture a metal ion with a specific ion size in their cavity (2.6 – 3.2 Å). The six oxygen atoms of the crown ether serve as donor atoms to coordinate the metal ion [267]. Therefore, they are considered to be highly size-selective [268]. Ions that are either too large or too small do not interact properly with the crown ether. This also accounts for the trivalent lanthanides (Ln^{3+}), which have an ionic radius varying from 0.977 Å for Lu^{3+} to 1.16 Å for La^{3+} (values given for coordination number 8). Moreover, the considerable hydration energy of trivalent lanthanide ions prevents efficient coordination by the crown ether.

Lowering of the oxidation state, *i.e.* the addition of an electron, leads to an increased ionic radius, a decreased charge density and a decreased hydration enthalpy ($-\delta H_{hydr}$). Thus, Ln^{2+} ions are more favorable to properly interact with 18C6-based extractants [269]. In the lanthanide series, only europium has a relatively stable divalent state in aqueous solutions because of its half-filled $4f$ subshell. Therefore, the use of a size-selective extractant to selectively trap the Eu^{2+} impurities in the 18C6-cavity in the organic phase, leaving Sm^{3+} behind in the aqueous phase, was studied as a first approach to separate the Sm/Eu couple. In this study, dicyclohexano-18-crown-6 (DCH18C6) was used because of its high hydrophobicity and because DCH18C6 already served well in extracting Sr^{2+} in numerous studies. The ionic radius of Eu^{2+} (1.25 Å) is similar to the one of Sr^{2+} (1.26 Å). Moreover, DCH18C6 already proved to be significantly radiation-resistant [270–274].

The alkaline extraction capacities of the ionic liquid itself were used in a second approach, without the addition of any extractants. Trivalent lanthanide ions have the advantage of being able to form anionic complexes with bidentate nitrate ligands, whereas divalent metal ions are unable to form these species [109, 111]. Sm^{3+} will thus be extracted to the water-immiscible ionic liquid phase, while Eu^{2+} remains in the aqueous phase. Vander Hoogerstraete *et*

al. showed the efficiency of this strategy to recycle rare-earth elements from permanent magnets and nickel metal hydride batteries [109]. Both approaches were studied in parallel throughout the experiments.

In both approaches, the water-immiscible phase consisted of the highly hydrophobic ionic liquid Aliquat 336 nitrate ([A336][NO_3]). Indeed, the use of this type undiluted ionic liquids proved to be selective for separation of rare earth elements (REEs) in previous solvent extraction studies [109, 111, 254–257]. The rationale behind the use of [A336][NO_3] is fourfold. (1) The use of [A336][NO_3] ensures a system complying completely with the CHON principle, making use of compounds containing only carbon (C), hydrogen (H), oxygen (O) and nitrogen (N) [275, 276]. This is highly important for the final disposal and waste treatment of the ionic liquid, which becomes radioactively contaminated when applied for separation of radiolanthanides, an aspect that is frequently overlooked in nuclear applications on ionic liquids. (2) Ionic liquids have promising properties compared to conventional molecular solvents, leading to processes with increased safety, chemical stability and radiation-resistivity [277–279]. (3) [A336][NO_3] possesses a highly hydrophobic cation whereas the inorganic anion is well soluble in both the aqueous and ionic liquid phase. This ensures a minimal amount of organic compounds ending up in the aqueous phase after extraction. This is opposite to the [$C_n$mim][Tf_2N] ionic liquids that are frequently used in combination with 18C6-based crown ethers [263, 266, 280]. These ionic liquids operate *via* a cation extraction mechanism in case a short alkyl chain (C_n) is used, losing ionic liquid cations to the aqueous phase. This, however, is unfavorable because these contaminations are not compatible with any pharmaceutical application. Additionally, radiolysis of the fluorinated anion can generate harmful and hazardous compounds. (4) [A336][NO_3] is a source of nitrate ions for improved extraction efficiency in a split-anion extraction mechanism in case the feed solution contains chloride ions [110]. Nitrate ions are more efficient in coordinating the metal ions in crown ether complexes compared to chloride ions. The small bite angle of nitrate ions allows them to coordinate the metal ions bidentately, *i.e.* taking up little space in the coordination sphere, whereas chloride can only coordinate monodentately. The formation of two M−O bonds is energetically more favorable than the formation of one M−Cl bond, outweighing the considerable M−OH_2 bond energy. This way, the neutral [$Sr(NO_3)_2$–DCH18C6] and [$Eu(NO_3)_2$–DCH18C6] complexes are formed preferentially. Extraction to the ionic liquid phase will most likely occur *via* neutral complex partitioning (see Section 4.4.2). This is similar to the extraction of alkaline earth metals by crown ethers in molecular diluents, like 1-octanol [280]. In the proposed extraction mechanism, anions have to be co-extracted to maintain charge-neutrality. When extracting from chloride aqueous media, chloride anions replace the nitrate anions of the ionic liquid (Reaction 4.1), similar to the so-called split-anion extraction by Larsson and

Binnemans [110].

$$M^{2+}{}_{(aq)} + 2\,Cl^{-}{}_{(aq)} + 2\,[A336][NO_3]_{(org)} + DCH18C6{}_{(org)} \rightleftharpoons [M(NO_3)_2DCH18C6]_{(org)} + 2\,[A336][Cl]_{(org)} \quad [4.1]$$

This reaction, however, might be hampered because of the considerable hydration energy of the chloride ions [110, 265, 266]. Dehydration, extraction and solvation by the ionic liquid might thus be unfavorable. The use of high salt concentrations in the aqueous feed increases the ionic strength significantly, resulting in less hydrated ions. This way, the ions are more prone to form extractable species. Extraction from nitrate aqueous solutions can proceed more efficiently because of their lower hydration energy (Reaction 4.2). Moreover, the ionic liquid phase is composed of nitrate ions, resulting in a more favorable transfer according to the Hofmeister series [193].

$$M^{2+}{}_{(aq)} + 2\,NO_3^{-}{}_{(aq)} + DCH18C6{}_{(org)} \rightleftharpoons [M(NO_3)_2DCH18C6]_{(org)} \quad [4.2]$$

4.4.2 Selection of anion source and concentration

In a first series of screening experiments, the extraction behavior of Sr^{2+} by the crown-ether-containing ionic liquid solution was studied as a simulant for Eu^{2+}. Different anion concentrations were used in the aqueous feed solution, *i.e.* 0, 1, 3, 6 and 8 mol L^{-1}. Three different sources were used to vary the anion concentration, *i.e.* HX, NH_4X and LiX (with X = Cl^- or NO_3^-). Extractions were performed using both [A336][NO_3] (IL) and [A336][NO_3] + 0.05 mol L^{-1} DCH18C6 (IL + CE) (Fig. 4.4).

Most efficient extraction of Sr^{2+} by [A336][NO_3] + 0.05 mol L^{-1} DCH18C6 was obtained using an aqueous phase with high lithium salt concentration, *i.e.* $\geq$ 6 mol L^{-1}, whereas the extraction of Sr^{2+} was negligible at lower salt concentration. In conditions of high salt concentration, fractions of > 70 % were extracted. The use of HX and NH_4X resulted in much lower extraction efficiencies, resulting in much lower distribution ratios. The lower extraction efficiency by using HX and NH_4X can most probably be attributed to the occupation of the crown ether cavity by H_3O^+ and NH_4^+. Previous studies already proved that these ions can properly fit in the DCH18C6 cavity because of their ion size [281, 282]. Li^+ has a smaller ionic radius and therefore interacts less efficiently with the crown ether, resulting in better extraction results. Thus, the

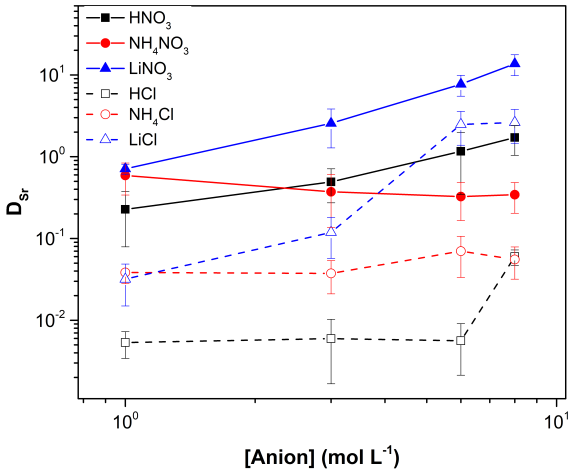

Figure 4.4: Distribution ratio of Sr^{2+} as a function of the anion concentration using HX (■), NH_4X (●) and LiX (▲) in the aqueous feed solution, with X being nitrate (solid line, solid symbol) or chloride (dashed line, open symbol). The organic phase consisted of [A336][NO_3] + 0.05 mol L^{-1} DCH18C6 (IL+CE). Extraction parameters: O:A 1:1, 60 min, 60 °C and 1700 rpm.

selection of a non-interfering source of additional anions is of high importance in these crown-ether-based extraction systems. Based on these results, the extraction experiments with Eu^{2+} were restricted to the use of lithium salts to increase the anion concentration in the aqueous feed solution.

After irradiation, the target material, *i.e.* Sm_2O_3, has to be dissolved. Most frequently, this is done by means of concentrated mineral acids, like HCl or HNO_3. However, high acid concentrations are disadvantageous for two reasons. First of all, Eu^{2+} is extracted less efficiently by the crown ether from highly acidic media because the H_3O^+ ions occupy the cavity of the crown ether. Secondly, Eu^{2+} is unable to be stabilized in a high H^+ concentration. Additionally, significant volumes of hydrogen gas would be generated during the reduction step, leading to unsafe situations. Therefore, the mixture should be adjusted to the most ideal extraction conditions after dissolution, meaning an increase in pH and anion concentration by the addition of non-interfering compounds. Evaporation to almost dryness followed by dissolution in other aqueous media is another possibility.

It is also clear that extraction from nitrate media occurs much more efficiently than extraction from chloride media. This is most probably due to the higher

hydration energy of the chloride, which hampers the co-extraction to ensure charge neutrality. Distribution ratios were negligible when no DCH18C6 was present in the ionic liquid phase, regardless the origin and concentration of the anions.

Because of their similar charge density and ionic radius, comparable extraction trends for Eu^{2+} and Sr^{2+} were to be expected. Fig. 4.5 compares the distribution ratio of Sr^{2+} and Eu^{2+} for extraction by [A336][NO_3] + 0.05 mol L^{-1} DCH18C6 as a function of the lithium salt concentration (0, 1, 3, 6 and 8 mol L^{-1}). It can be seen that Eu^{2+} follows a very similar trend as Sr^{2+}, only showing reasonable distribution ratios at high salt concentrations, *i.e.* ≥ 6 mol L^{-1} LiX. Eu^{2+} proved to be extracted even more efficiently by DCH18C6 than Sr^{2+}. Eu^{2+} fractions of > 95 % were extracted in these conditions, reaching distribution ratios well above 1. Again, the use of nitrate aqueous media yielded in much higher extraction efficiency compared to the use of chloride aqueous media. The increasing extraction efficiency with increasing anion concentration (reflected in the rising distribution ratio), denotes that extraction to the ionic liquid phase occurs *via* neutral complex partitioning (Fig. 4.5) [266]. This is similar to the extraction of alkaline earth metals by crown ethers in molecular diluents, like 1-octanol [280].

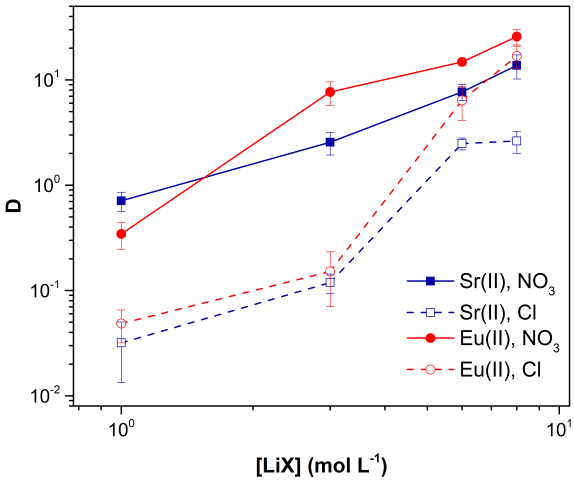

Figure 4.5: Distribution ratios of Sr^{2+} (■) and Eu^{2+} (●) as a function of the LiX concentration in the aqueous feed solution, with X being nitrate (solid line, solid symbol) or chloride (dashed line, open symbol). The organic phase consisted [A336][NO_3] + 0.05 mol L^{-1} DCH18C6 (IL+CE). Extraction parameters: O:A 1:1, 60 min, 60 °C and 1700 rpm.

Ion exchange mechanisms, like observed by Garvey *et al.* for $[C_n mim][Tf_2N]$, are unlikely to happen. Based on these results, following extraction experiments were conducted with 6 mol L^{-1} lithium salt aqueous feed solutions.

It also has to noted that a significant amount of Eu^{2+}, was also extracted towards the DCH18C6-free ionic liquid phase when using high salt concentrations. Significant extraction of Eu^{2+} in a DCH18C6-free system was not expected since it deviates from the behavior of Sr^{2+}, where no extraction was observed at all. Therefore, it is believed that a partial re-oxidation of Eu^{2+} to Eu^{3+} have occurred during these experiments, whereby Eu^{3+} is extracted towards the organic phase without the interaction of a crown ether. Therefore, it is important to keep the extraction time as low as possible.

4.4.3 Extraction kinetics of Sr^{2+} and Eu^{2+}

The extraction behavior of Sr^{2+} and Eu^{2+} in the $[A336][NO_3]$ and $[A336][NO_3]$ + 0.05 mol L^{-1} DCH18C6 systems was studied as a function of time using various mixing times (5, 15, 30 and 60 min). This way, the minimum time required for an efficient extraction can be determined. These experiments were performed using an aqueous feed solution containing 6 mol L^{-1} LiX (with X = Cl^- or NO_3^-). In Figs. 4.6 and 4.7, the distribution ratios of Sr^{2+} and Eu^{2+} from an aqueous feed solution containing 6 mol L^{-1} lithium salt are shown as a function of time. In Fig. 4.6, it is shown that the extraction of Eu^{2+} from a 6 mol L^{-1} LiCl aqueous feed solution proceeds more efficiently than the extraction of Sr^{2+} in the presence of DCH18C6. Extraction equilibrium for Sr^{2+} and Eu^{2+} was established at 15 min contact time. At this point, a fraction of about 83 % Eu^{2+} was extracted. Switching to a 6 mol L^{-1} $LiNO_3$ aqueous feed solution resulted in high distribution ratios for Eu^{2+} (Fig. 4.7). About 90 % of the initial Eu^{2+} was already extracted to the organic phase ($[A336][NO_3]$ + DCH18C6]) after an extraction time of 5 min, whereas a fraction of > 93 % Eu^{2+} was extracted after longer contact times.

4.4.4 Slope analysis of Sr^{2+} and Eu^{2+}

Extraction experiments with varying crown ether concentration in the ionic liquid phase were performed to support the proposed neutral complex partitioning. Aqueous phases containing 1 g L^{-1} Sr^{2+} and 1 g L^{-1} Eu^{2+} were contacted for 15 min at 60 °C with the ionic liquid phases containing different concentrations of DCH18C6 (0–0.1 mol L^{-1} in $[A336][NO_3]$). Log$D$–log[CE] plots were constructed to investigate the extraction mechanism *via* slope analysis. The resulting slope gives an indication about the relation between extraction efficiency and the

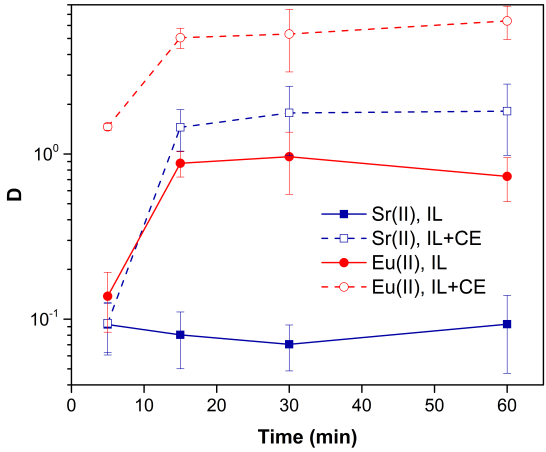

Figure 4.6: Distribution ratios of Sr^{2+} (■) and Eu^{2+} (●) as a function of time using 6 mol L^{-1} LiCl in the aqueous feed solution. The organic phase consisted of neat [A336][NO_3] (IL) or [A336][NO_3] containing 0.05 mol L^{-1} DCH18C6 (IL+CE). Extraction parameters: O:A 1:1, 60 min, 60 °C and 1700 rpm.

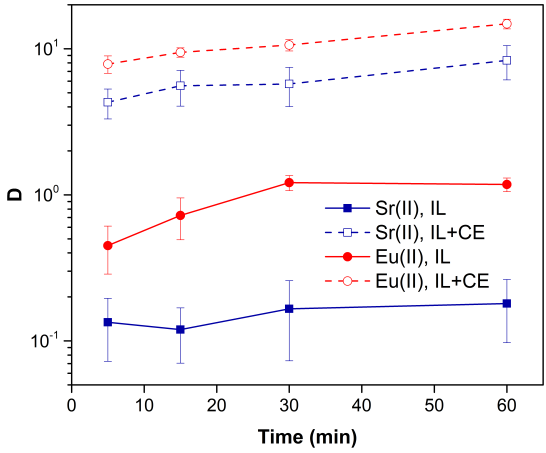

Figure 4.7: Distribution ratios of Sr^{2+} (■) and Eu^{2+} (●) as a function of time using 6 mol L^{-1} $LiNO_3$ in the aqueous feed solution. The organic phase consisted of neat [A336][NO_3] (IL) or [A336][NO_3] containing 0.05 mol L^{-1} DCH18C6 (IL+CE). Extraction parameters: O:A 1:1, 60 min, 60 °C and 1700 rpm.

amount of extractant present. The increasing slope of Fig. 4.8 denotes an increasing extraction efficiency with increasing crown ether concentration. A slope close to unity was obtained for Sr^{2+} (nitrate: 1.02, chloride: 0.82) and Eu^{2+} (nitrate: 0.72, chloride: 0.67), *i.e.* one crown ether molecule (DCH18C6) interacts with one metal ion (Sr^{2+} or Eu^{2+}).

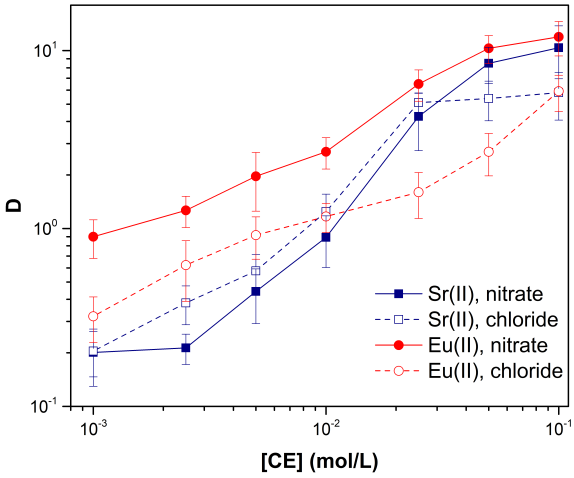

Figure 4.8: Distribution ratios of Sr^{2+} (■) and Eu^{2+} (●) as a function of the DCH18C6 concentration in [A336][NO_3]. The aqueous feed solution consisted of 6 mol L^{-1} LiX, with X being nitrate (solid line, solid symbol) or chloride (dashed line, open symbol). Extraction parameters: O:A 1:1, 60 min, 60 °C and 1700 rpm.

4.4.5 Time dependence of Sm^{3+}/Eu^{2+} separation

The significant extractability of Eu^{2+} by [A336][NO_3] + 0.05 mol L^{-1} DCH18C6 and the low extractability of Eu^{2+} by [A336][NO_3] seem to support both separation approaches so far. To arrive at a separation system, it is important to study the extraction behavior of Sm^{3+} as well. A fast separation is advantageous taking into account the decay of ^{153}Sm and possible re-oxidation of Eu^{2+}. Therefore, the distribution ratios of samarium and europium were studied as a function of time. For comparison and completeness, the distribution ratio of Eu^{3+} in the same conditions was studied in parallel.

Extraction experiments with 6 mol L^{-1} LiX (with X = Cl^- or NO_3^-) aqueous feed solutions were performed to study the extraction rates of Sm^{3+} and Eu^{2+}. The feed solutions were mixed with both [A336][NO_3] (IL) and [A336][NO_3] +

0.05 mol L^{-1} DCH18C6 (IL + CE). The distribution ratios of both lanthanides after extraction from a 6 mol L^{-1} LiCl and a 6 mol L^{-1} $LiNO_3$ aqueous feed solution are plotted as a function of time in Figs. 4.9 and 4.10. It is immediately clear that high distribution ratios were obtained for the trivalent lanthanides in both systems, especially when using a nitrate aqueous feed solution. As expected, the presence of the crown ether did not influence the extraction behavior of Sm^{3+}. Eu^{2+} was only reasonably well extracted in presence of the crown ether. Therefore, highest separation factors were reached without the use of a crown ether (Figs. 4.11 and 4.12). It is also clear that separation of the Sm^{3+}–Eu^{2+} couple from a nitrate aqueous feed solution is much more efficient compared to a chloride aqueous feed solution.

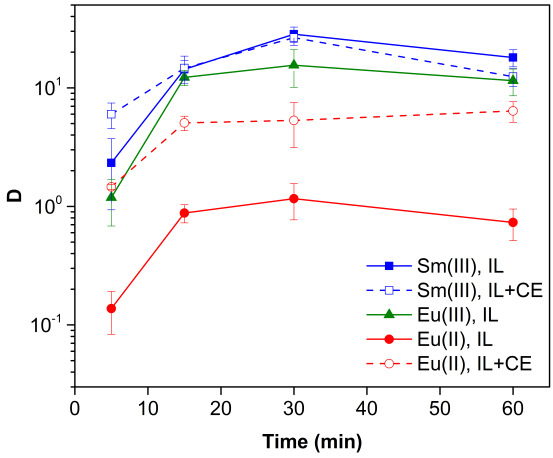

Figure 4.9: Distribution ratios (log scale) of Sm^{3+} (■), Eu^{3+} (▲) and Eu^{2+} (●) as a function of time using a 6 mol L^{-1} LiCl aqueous feed solution. The organic phase consisted of neat [A336][NO_3] (IL) or [A336][NO_3] + 0.05 mol L^{-1} DCH18C6 (IL + CE). Extraction parameters: O:A 1:1, 60 min, 60 °C and 1700 rpm.

From these extraction results, it was immediately clear that much higher distribution ratios were obtained for Sm^{3+} compared to Eu^{2+}, with and without the use of DCH18C6. As expected, the presence of DCH18C6 in the ionic liquid did not influence the extraction behavior of Sm^{3+} because of its smaller ionic radius and higher hydration energy. The high difference in distribution ratio allows an efficient Sm/Eu separation. The DCH18C6-free system is favored because of the much lower Eu^{2+} extraction. Separation factors of 24 were reached using chloride media, whereas separation factors well above 600 were reached using nitrate media.

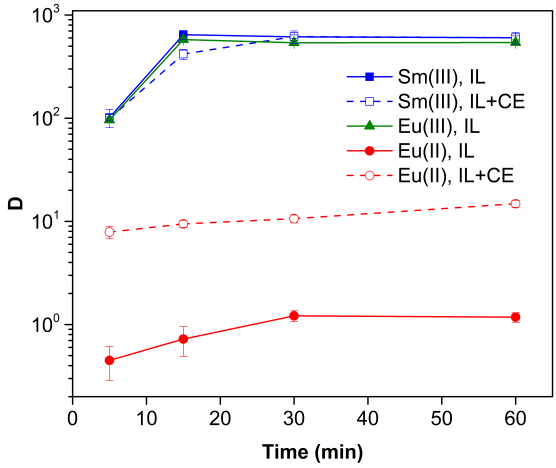

Figure 4.10: Distribution ratios (log scale) of Sm^{3+} (■), Eu^{3+} (▲) and Eu^{2+} (●) as a function of time using a 6 mol L^{-1} $LiNO_3$ aqueous feed solution. The organic phase consisted of neat [A336][NO_3] (IL) or [A336][NO_3] + 0.05 mol L^{-1} DCH18C6 (IL + CE). Extraction parameters: O:A 1:1, 60 min, 60 °C and 1700 rpm.

Sm^{3+} was extracted from the aqueous chloride phase to the ionic liquid phase *via* the split-anion extraction mechanism, as was described by Larsson and Binnemans (Reaction 4.3) [110]. This extraction mechanism makes use of the strong affinity of nitrate ions for the IL phase, while the chloride ions have a higher affinity for the aqueous phase.

$$Sm^{3+}_{(aq)} + 3\,Cl^{-}_{(aq)} + 5\,[A336][NO_3]_{(org)} \rightleftharpoons [A336]_2[Sm(NO_3)_5]_{(org)} + 3\,[A336][Cl]_{(org)} \quad [4.3]$$

According to this extraction mechanism, the ionic liquid phase serves as a source of coordinating anions. This way, no additional extractants are needed. However, chloride ions have to be transferred to the ionic liquid phase as well to ensure charge neutrality. The extraction of chloride ions is hampered because of their considerable hydration energy, as was also the case for the extraction of M^{2+} by DCH18C6 from chloride media. The much higher extraction efficiency for Sm^{3+} from nitrate aqueous media can be attributed to the lower hydration energy and higher hydrophobicity of nitrate ions [193, 266]. The high nitrate concentrations are needed to form extractable species. Trivalent lanthanide ions

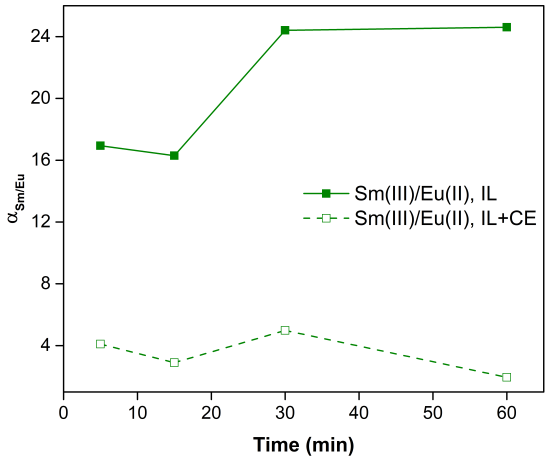

Figure 4.11: Separation factors for the separation of Sm^{3+} and Eu^{2+} as a function of time using a 6 mol L^{-1} LiCl aqueous feed solution. The organic phase consisted of neat [A336][NO_3] (IL) or [A336][NO_3] + 0.05 mol L^{-1} DCH18C6 (IL + CE). Extraction parameters: O:A 1:1, 60 min, 60 °C and 1700 rpm.

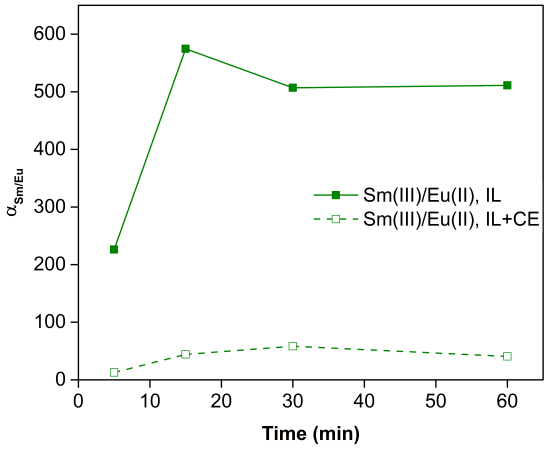

Figure 4.12: Corresponding separation factors for the separation of Sm^{3+} and Eu^{2+} as a function of time using a 6 mol L^{-1} $LiNO_3$ aqueous feed solution. The organic phase consisted of neat [A336][NO_3] (IL) or [A336][NO_3] + 0.05 mol L^{-1} DCH18C6 (IL + CE). Extraction parameters: O:A 1:1, 60 min, 60 °C and 1700 rpm.

show the advantage of being able to form anionic complexes with bidentate nitrate ligands, whereas other elements cannot [109]. Vander Hoogerstraete *et al.* already showed that the trivalent lanthanides (Ln^{3+}) are extracted as pentanitrato complexes $[Ln(NO_3)_5]^{2-}$ (Reaction 4.4). Speciation studies using *extended X-ray absorption fine structure* (EXAFS) support this extraction behavior (see Section 4.4.6).

$$Sm^{3+}{}_{(aq)} + 3\,NO_3^-{}_{(aq)} + 2\,[A336\,][NO_3]_{(org)} \rightleftharpoons [A336\,]_2[Sm(NO_3)_5]_{(org)} \quad [4.4]$$

Larsson and Binnemans already pointed out that all trivalent lanthanides (Ln^{3+}) show a similar extraction behavior with quaternary ammonium ionic liquids, with a decreasing trend in extraction efficiency across the lanthanide series [110]. Thus, the slightly lower extraction efficiency of Eu^{3+} compared to Sm^{3+} is in full agreement with these findings, and can be attributed to the slightly higher hydration energy of Eu^{3+} because of its smaller ionic radius [180, 225]. Nevertheless, it is obvious that no efficient separation can be achieved without reduction of Eu^{3+} to Eu^{2+}.

The high distribution ratios of Sm^{3+} are favorable for the second separation approach, *i.e.* the extraction of Sm^{3+} to the ionic liquid phase, while Eu^{2+} remains in the aqueous phase. Therefore, it can be concluded that the first separation approach, making use of a size-selective extractant to extract Eu^{2+}, becomes superfluous. This also implies that different chloride or nitrate salts can be used to increase the salt concentration in the aqueous feed solution, *i.e.* the origin of the salt is less of importance regarding the separation method. Therefore, a salt causing less problems regarding the intended medical application can be chosen. Of course, the salt has to be highly soluble in the aqueous feed to reach the required concentration for optimal separation.

Efficient stripping of Sm^{3+} from the loaded IL phase can be achieved by decreasing the salt concentration in the aqueous phase, *i.e.* Sm^{3+} can be stripped by water [111]. Reduction of the salt concentration in the system leads to a lower ionic strength, enhancing the hydration of Sm^{3+}. Consequently, Sm^{3+} gains higher affinity for the aqueous phase. Therefore, no harsh conditions, like highly acidic media, are needed. Sm^{3+} was quantitatively (> 98 %) back-extracted to the aqueous phase by water in a single back-extraction step. The strip solution can be slightly acidified to prevent any hydrolysis of Sm^{3+}.

4.4.6 Samarium speciation in [A336][NO_3] by EXAFS

Absorption spectra were recorded of the ionic liquid phase obtained after extraction of samarium from a 6 mol L^{-1} nitrate solution to [A336][NO_3] (Fig. 4.13). A bidentate nitrate coordinated to the Sm center was used a model and the scattering paths Sm−O, between the Sm center and the coordinating oxygen atoms, and Sm−N were used as input for the fit (Fig. 4.14). Only the first coordination shell in the Fourier transform was fitted since this provided the most accurate results on the Sm−O and Sm−N distances. The results of the Sm−O and Sm−N distances in the ionic liquid are shown in Table 4.1.

The coordination number that was obtained from the fit was quite unreliable for two reasons. Firstly, the coordination number is highly dependent on the amplitude reduction factor S_0, which cannot be estimated from the fit and

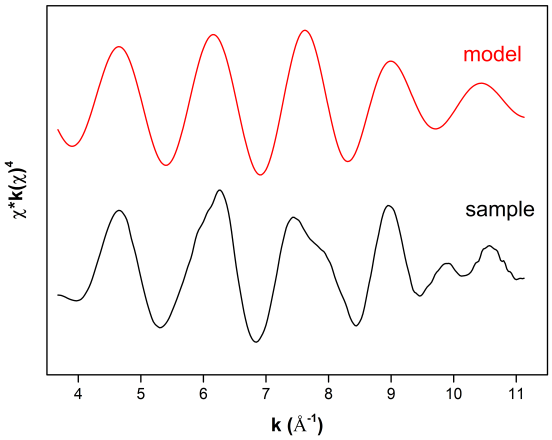

Figure 4.13: EXAFS function of the $Sm(NO_3)_5$ complex extracted to [A336][NO_3] and compared to the model.

Table 4.1: EXAFS fitting results of $[Sm(NO_3)_5]^{2-}$ in [A336][NO_3]. The data were Fourier transformed between $k = 3.68$ and 11.13 $Å^{-1}$ with a Gaussian rounded ends window function and fitted to the model between $R = 0$ and 2.78 Å.

Scattering path	N	r (Å)	σ^2 (Å)
Sm−O	12.0(5)	2.515(9)	0.013(1)
Sm−N	6.0(5)	2.971(15)	0.015(3)

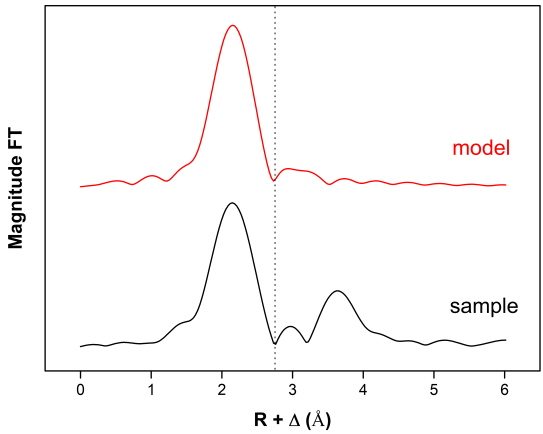

Figure 4.14: Fourier transform of the EXAFS function of the $Sm(NO_3)_5$ complex extracted to $[A336][NO_3]$ and compared to the model.

should be chosen arbitrarily. Secondly, small changes in the extraction of the EXAFS function χ had a significant influence on the coordination number of the scattering paths. On the other hand, the coordination number can also be deduced from the Sm−O and Sm−N distances, which is much more reliable. A comparison was made with the interatomic distances found in crystal structures of $Sm(NO_3)_5$ and $Sm(NO_3)_6$ described in the literature (Table 4.2) [283, 284]. The average Sm−O and Sm−N distances of $Sm(NO_3)_5$ corresponded best to the experimental data. Moreover, the Debye-Waller factors are expected to be higher in case a mixture of $[Sm(NO_3)_5]^{2-}$ and $[Sm(NO_3)_6]^{3-}$ would exists, as the Debye-Waller factor can be used as a measure for the movement of the atoms in the complex. Therefore, it can be concluded that Sm is extracted to $[A336][NO_3]$ as the pentanitrato complex, $[Sm(NO_3)_5]^{2-}$, with bidentate nitrate ions.

4.4.7 Temperature dependence of Sm^{3+}/Eu^{2+} separation

Undiluted ionic liquids are highly viscous at room temperature. This is also the case for quaternary ammonium ionic liquids containing long carbon chains, like $[A336][NO_3]$. This high viscosity implies a more difficult mass transfer, leading to reduced extraction speed. However, the viscosity drastically decreases with increasing temperature. Therefore, the above mentioned results were all obtained at 60 °C, a temperature at which $[A336][NO_3]$ has a significant lower

Table 4.2: Sm−O and Sm−N interatomic distances as determined by EXAFS analysis of the $[Sm(NO_3)_5]^{2-}$ complex extracted to $[A336][NO_3]$, compared to literature values.

	r_{Sm-O} (Å)	r_{Sm-N} (Å)
$[A336][NO_3]$	2.515(9)	2.971(15)
$[Sm(NO_3)_5]^{2-}$ (CN 10)	2.457–2.573	2.893–2.953
	2.500[(1)]	*2.930*[(1)]
$[Sm(NO_3)_5]^{2-}$ (CN 12)	2.547–2.599	2.980–3.021
	2.574[(1)]	*3.002*[(1)]

[(1)] Average interatomic distance in unit cell.

viscosity but at which experiments are still easy to handle. The viscosity of water-saturated $[A336][NO_3]$ decreases from 204 mPa s at 25 °C to 95 mPa s at 40 °C and 42 mPa s at 60 °C. Extractions of Sm^{3+} and Eu^{2+} from aqueous chloride and nitrate feed solution (6 mol L^{-1} of the respective lithium salt) were executed at these temperatures to evaluate the influence of a changing viscosity of the ionic liquid phase. The results in Figs. 4.15 and 4.16 for an aqueous chloride and nitrate feed solution, respectively, show that a change in temperature, and thus a change in viscosity, does not lead to significant changes in the extraction behavior of both Sm^{3+} and Eu^{2+}. Therefore, mass transfer might not be the rate-determining step.

4.4.8 Extraction behavior of Zn^{2+} impurities

Eu^{3+} can be efficiently and selectively reduced using chemical or electrochemical reduction methods. The chemical method makes use of Zn^0 grains, which are oxidized to Zn^{2+} (Reaction 3.1). Hence, the introduction of extra impurities in the feed solution must be taken into account when using this chemical reduction method. Therefore, the extraction behavior of Zn^{2+} from both chloride and nitrate aqueous feed solution was studied and compared to the extraction behavior of Sm^{3+}. The results in Fig. 4.17 clearly show that the extraction of Zn^{2+} is highly dependent on the anions present in the extraction system, *i.e.* Zn^{2+} is hardly extracted in case only nitrate anions are present in the extraction system, whereas the extraction of Zn^{2+} is very efficient in case of high chloride concentrations. The latter was expected because it is well known that the extraction of transition metals to quaternary ammonium and phosphonium chloride ionic liquids proceeds efficiently from chloride aqueous media [254, 285]. Therefore, the extraction of Zn^{2+} from chloride media results in very high

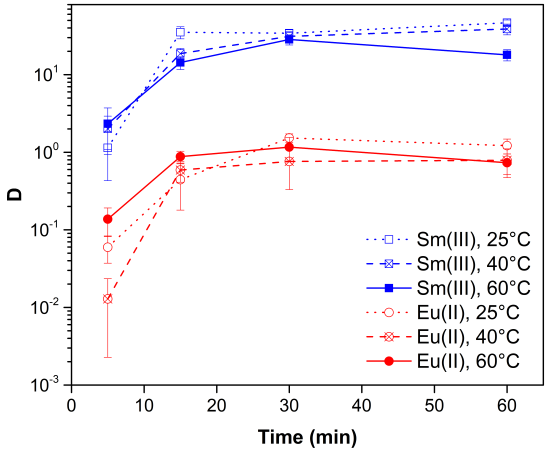

Figure 4.15: Distribution ratios (log scale) of Sm^{3+} (■) and Eu^{2+} (●) as a function of time using 6 mol L^{-1} LiCl in the aqueous feed solution at different temperatures (25, 40 and 60 °C). The organic phase consisted of neat [A336][NO_3]. Extraction parameters: O:A 1:1, 60 min, 60 °C and 1700 rpm.

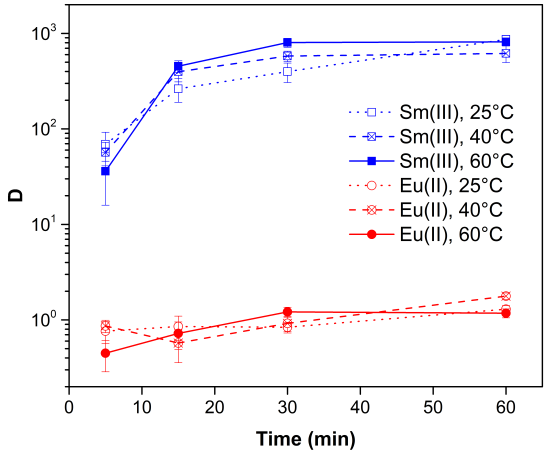

Figure 4.16: Distribution ratios (log scale) of Sm^{3+} (■) and Eu^{2+} (●) as a function of time using 6 mol L^{-1} $LiNO_3$ in the aqueous feed solution at different temperatures (25, 40 and 60 °C). The organic phase consisted of neat [A336][NO_3]. Extraction parameters: O:A 1:1, 60 min, 60 °C and 1700 rpm.

distribution ratios. Hence, Sm^{3+} can be efficiently separated from Zn^{2+} *via* selective stripping of the loaded [A336][NO_3] phase. Sm^{3+} is transferred back to the aqueous phase upon reduction of the salt concentration in the system, while Zn^{2+} remains in the organic phase because of its high affinity for the ionic liquid. However, another approach is needed in case of an extraction from nitrate media, considering the low extractability of Zn^{2+} from nitrate media. In fact, the extraction behavior of Zn^{2+} is comparable to that of Eu^{2+}. Therefore, reasonably good separation from samarium can already be achieved in the forward extraction step. Considering these results, Zn^{2+} impurities originating from the chemical reduction method can be efficiently removed.

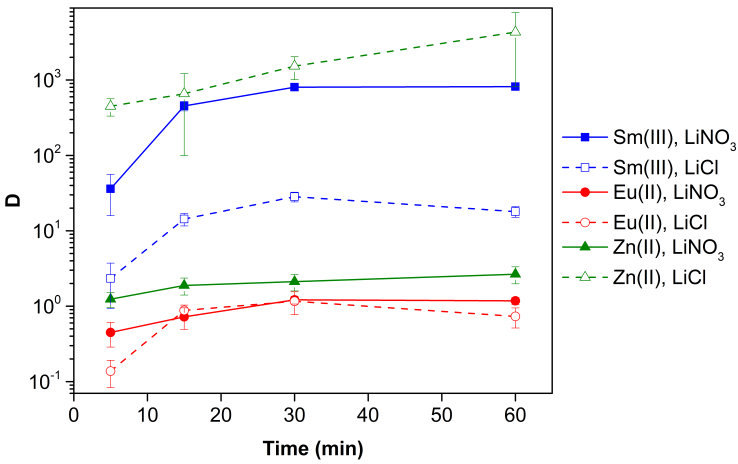

Figure 4.17: Distribution ratios (log scale) of Sm^{3+} (■), Eu^{3+} (●) and Zn^{2+} (▲) as a function of time using 6 mol L^{-1} $LiNO_3$ (solid line, solid symbol) and LiCl (dashed line, open symbol) in the aqueous feed solution. The organic phase consisted of neat [A336][NO_3]. Extraction parameters: O:A 1:1, 60 min, 60 °C and 1700 rpm.

4.4.9 Outlook

Based on this feasibility study, following full separation process concept to produce high purity samarium-153 can be proposed (Fig. 4.18): (1) dissolution of the target material by HNO_3 and adjustment of the pH (4–6.5) and anion concentration (6 mol L^{-1} NO_3^-) by the addition of a non-interfering nitrate salt (*e.g.* NH_4NO_3 or $LiNO_3$). The total europium concentration must be adjusted by the addition of stable isotopes to facilitate the separation procedure. (2) The selective reduction of europium to its divalent state by zinc metal. (3) The

forward extraction of Sm^{3+} to the ionic liquid phase, consisting of undiluted [A336][NO_3]. Eu^{2+} and Zn^{2+} remain in the aqueous phase. (4) Separation of both phases. (5) Stripping (= back-extraction) of Sm^{3+} from the loaded ionic liquid phase can be easily performed by the addition of water, lowering the total salt concentration.

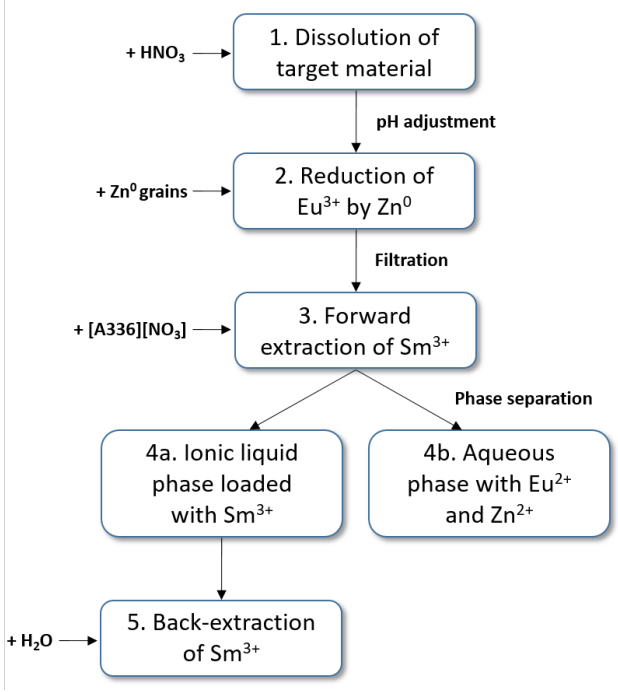

Figure 4.18: Separation concept scheme for the purification of ^{153}Sm. (1) Dissolution of the target material in HNO_3 and adjustment of the pH and salt concentration, (2) chemical reduction of Eu^{3+} by Zn^0 or electrochemical reduction, (3) forward extraction of Sm^{3+} to [A336][NO_3], leaving Eu^{2+} and Zn^{2+} (in case of chemical reduction) in the aqueous phase, (4) separation of both phases, (5) back-extraction of Sm^{3+} by addition of water.

4.5 Conclusion

A feasibility study to develop an efficient method to separate samarium and europium was conducted in scope of the purification process to produce high-purity ^{153}Sm for medical applications. The separation method consists of the selective reduction of Eu^{3+} by zinc metal in an aqueous feed solution containing

a high chloride or nitrate salt concentration ($6\,\mathrm{mol\,L^{-1}}$). Subsequent extraction using the quaternary ammonium ionic liquid [A336][NO_3] leads to a good separation of both lanthanides in a relatively short time frame. Sm^{3+} proved to be extracted to the neat [A336][NO_3] phase much more efficiently compared to Eu^{2+}. A first approach using the addition of DCH18C6 to capture Eu^{2+} in the ionic liquid phase proved to be less efficient. Therefore, the separation process using neat [A336][NO_3] is the preferred approach, extracting Sm^{3+} to the ionic liquid phase while Eu^{2+} remains in the aqueous phase. Moreover, it was shown that the use of a nitrate aqueous feed solution leads to a more efficient separation method compared to the use of a chloride aqueous feed solution. Zn^{2+} ions originating from the chemical reduction method showed a very low extractability in nitrate media. This way, simultaneous removal of Eu^{2+} and Zn^{2+} from Sm^{3+} can be achieved in the forward extraction step. Therefore, this separation method can be used to arrive at a purified product with extended shelf-life. This leads to an increased availability of ^{153}Sm radioisotopes and a decreased background radiation of ^{154}Eu in the patient after treatment. The separation method can also be applied for efficient removal of Eu^{2+} from any other Ln^{3+} because all trivalent lanthanide ions tend to have a similar extraction behavior as Sm^{3+}.

Chapter 5

Supported ionic liquid phases for the separation of samarium and europium in nitrate media

This chapter is based on a manuscript that is submitted for publication to *Separation and Purification Technology* (2019):

Michiel Van de Voorde, Karen Van Hecke, Koen Binnemans and Thomas Cardinaels, Separation and Purification Technology, 2019

The text might contain slight adjustments to the original publication.

All experimental work and compilation of the manuscript were performed by the author of this thesis.

5.1 Abstract

Samarium-153 is a medical radionuclide that serves in nuclear medicine for bone pain palliation or imaging of the skeleton, and is produced in a nuclear research reactor by irradiation of an enriched samarium-152 target with a high flux of thermal neutrons. However, long-lived europium-154 impurities are formed concurrently, which restricts the use of the samarium-153 radiopharmaceutical. In the previous chapter, the possibility was shown to separate samarium and europium efficiently by solvent extraction with the undiluted ionic liquid [A336][NO_3]. Current research efforts investigated the feasibility to convert the separation method to an extraction chromatography application, taking advantage of solid phase extraction techniques. TEVA particles, where the ionic liquid is immobilized onto a solid support, served as the stationary phase in the column. Eu^{3+} was reduced to Eu^{2+} in a concentrated nitrate salt solution prior to the separation step. After loading onto the extraction chromatography column, Eu^{2+} was not retained by the TEVA particles upon elution with a concentrated nitrate salt solution, whereas Sm^{3+} was extracted to the ionic liquid layer. Sm^{3+} could be efficiently removed from the column by elution with water, hence yielding a simple, yet efficient separation method.

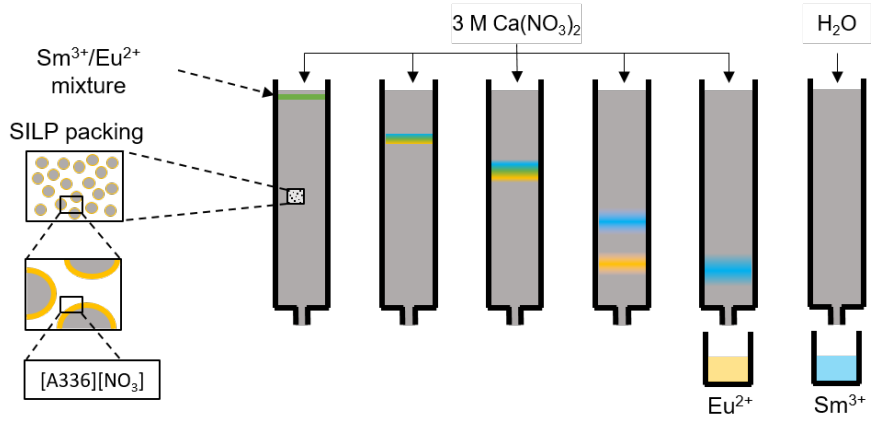

Figure 5.1: Graphical abstract describing the separation method by means of extraction chromatography for samarium and europium using supported ionic liquid phases (SILPs). Eu^{2+} can be selectively eluted from the column using a $3\,mol\,L^{-1}$ $Ca(NO_3)_2$ solution, whereas Sm^{3+} can be eluted from the column using water.

5.2 Introduction

The radiolanthanide samarium-153 (^{153}Sm) is used for the preparation of the radiopharmaceutical compound samarium-153 ethylenediamine tetramethylene phosphonate (^{153}Sm-EDTMP, Lexidronam or Quadramet) [76]. ^{153}Sm is an interesting radionuclide for nuclear medicine because of its favorable decay characteristics, *i.e.* a very manageable physical half-life of 46.284 h and the emission of β^- particles with a mean energy of 233 keV, which is suitable for radiotherapy [77, 78, 80, 83]. γ photons of 103.2 keV are emitted simultaneously with an emission probability of 28 %, and can be used for imaging.

^{153}Sm is commonly carrier-added produced *via* thermal neutron activation (n, γ) of isotopically enriched ^{152}Sm (> 98 % enrichment, $\sigma_{th} = 206.2$ barn) [20, 190]. Irradiation occurs over the course of several days to achieve an adequate yield of ^{153}Sm, resulting in a product with sufficiently high specific activity for medical use.

Because of its relatively short half-life, ^{153}Sm starts decaying while being irradiated, leading to the production of its daughter isotope ^{153}Eu. Neutron caption of ^{153}Eu ($\sigma_{th} = 312$ barn) results in the formation of minor amounts of the long-lived ^{154}Eu ($t_{1/2} = 8.593$ y). Ingrowth of ^{154}Eu limits the shelf-life of the product because the maximum amount of ^{154}Eu that can be administered to a patient is strictly regulated [89, 91].

Separation of two neighboring lanthanides is challenging due to their very similar chemical properties. Lanthanide ions exist predominantly in the trivalent state because of their characteristic electron configuration. Radiochemical separation methods for the isolation of medical radiolanthanides have been sought for by different research groups using various approaches [54, 56, 87, 190]. Frequently, the small differences in coordination behavior, mainly originating from the lanthanide contraction throughout the lanthanide series, are being exploited to achieve separation. To date, the highest selectivity for different lanthanide radii can be achieved using the aqueous complexing agent α-hydroxy isobutyric acid (α-HIBA) [75, 172, 190]. The efficiency of these methods is limited since only low throughput can be achieved, the process requires long separation times or the process involves multiple separation steps. Another approach consists of changing the oxidation state of one of the lanthanide ions, which changes its chemical properties drastically and opens perspectives for more efficient separation methods [88, 98, 99, 101].

In the previous chapter, we demonstrated that samarium and europium can be separated efficiently in concentrated aqueous nitrate media [92]. In a first step, europium was reduced to its divalent state in an aqueous solution containing a

high nitrate salt concentration at quasi-neutral pH. In a subsequent liquid-liquid extraction step, Sm^{3+} was selectively extracted to the highly hydrophobic ionic liquid (IL) Aliquat 336 nitrate ([A336][NO_3]), by making use of high nitrate salt concentration (the *salting out effect*, Reaction 5.1). The high salt concentration ensures sufficient dehydration of Sm^{3+} to migrate to the ionic liquid phase. Eu^{2+} remained almost unaffected in the aqueous phase. Back-extraction of Sm^{3+} to an aqueous solution for further processing was easily done by addition of water, thus decreasing the total salt concentration in solution.

$$Sm^{3+}_{(aq)} + 3\,NO_3^-{}_{(aq)} + 2\,[A336\,][NO_3]_{(org)} \rightleftharpoons [A336\,]_2[Sm(NO_3)_5]_{(org)} \quad [5.1]$$

In this chapter, the feasibility to convert the aforementioned solvent extraction-based separation system to an extraction chromatography system was investigated [92, 286]. Process difficulties occurring in liquid-liquid extraction, like the relatively high viscosity of the ionic liquid or an impeded phase separation, do not have to be accounted for in solid phase extractions. Setups for solid phase extraction are in general easier to handle. For this purpose, the ionic liquid was immobilized onto an inert solid support. The resulting product is often referred to as the *supported ionic liquid phase* (SILP) [287, 288]. A336-based SILPs already proved to be efficient in various purification technologies, used either in batch extractions or in extraction chromatography [289–294]. From the study by Horwitz *et al.*, it is also clear that A336-based SILPs are suitable for radionuclide separations, notwithstanding the relatively high activities that might be present in the aqueous feed solutions [295–297].

Performances of a home-made SILP, *i.e.* [A336][NO_3] impregnated on the Amberlite XAD-16N polymeric support, and the commercially available TEVA, *i.e.* [A336][NO_3] impregnated on the Amberchrom CG-71ms polymeric support, were investigated for the separation of samarium and europium in highly concentrated nitrate salt solutions (3 mol L^{-1} $Ca(NO_3)_2$). Both batch extraction and extraction chromatography methods were investigated. In this separation strategy, Sm^{3+} is extracted efficiently to the SILP, whereas Eu^{2+} remains in the aqueous phase. Thus, in extraction chromatography experiments, Eu^{2+} is not retained and will elute first, whereas Sm^{3+} elutes only after decreasing the ionic strength of the mobile phase.

5.3 Experimental

5.3.1 Materials

Tricaprylmethylammonium chloride (Aliquat® 336, [A336][Cl], 88.2 – 90.6 %), Amberlite XAD-16N (20 – 60 mesh, 200 Å mean pore size) and acetone (> 99.5 %) were purchased from Sigma-Aldrich (Overijse, Belgium). $Sm(NO_3)_3{\cdot}6H_2O$ (99.9 %) and $Eu(NO_3)_3{\cdot}6H_2O$ (99.9 %) were purchased from Strem Chemicals, Inc. (Newburyport, USA). Granular zinc (30 mesh) was purchased from Acros Organics (Geel, Belgium). NH_4NO_3 (≥ 99 %), $Ca(NO_3)_2{\cdot}4H_2O$ (≥ 99 %) and acetonitrile (≥ 99.5 %) were purchased from Chem-Lab (Zedelgem, Belgium), as well as the samarium, europium, zinc and copper standard solutions (≥ 99.99 %, 1000 µg mL^{-1}, 2 – 5 % HNO_3, Plasma HIQU). The nitrate form of TEVA resin (bulk 50 – 100 µm and bulk 100 – 150 µm and 2 mL cartridges 50 – 100 µm) was purchased from TrisKem International (Bruz, France). Except for Amberlite XAD-16N (*vide infra*), all products were used as received, *i.e.* without any further purification steps. Aqueous solutions were prepared with MilliQ water (18.2 MΩ cm at 25 °C).

5.3.2 Reduction of europium

The first step of the separation method consisted of the reduction of europium in an aqueous solution containing a high nitrate salt concentration (3 mol L^{-1} $Ca(NO_3)_2$). Europium was reduced chemically in the majority of the separation experiments because of its higher flexibility of use. The chemical reduction of europium was performed in a vial sealed with a septum by vigorously stirring the feed solution with a large excess of zinc grains (30 mesh, E^0 = -0.76 V) for at least 2 h. The aqueous solutions were purged with an inert gas (*i.e.* nitrogen or argon) before and during reduction of Eu^{3+} to remove aerial and dissolved oxygen to prevent back-oxidation of Eu^{2+} by O_2 (E^0 = +1.23 V). An indication of the pH of the feed solution before and after reduction of Eu^{3+} was obtained by means of a Hamilton Slimtrode pH electrode coupled to a Mettler-Toledo SevenCompact pH meter. It is important to note that only an indication of the pH could be obtained because of the high ionic strength in solution as a consequence of the high $Ca(NO_3)_2$ concentration. In these measurements, the pH of the aqueous feed solution before reduction was between 4.5 and 6.5, depending on the lanthanide concentration used. After reduction, pH of the aqueous feed solution was ≈ 6.5 as the excess of H^+ was reduced to H_2 prior to the Eu^{3+} reduction. The pH of the final feed solution remained sufficiently high to avoid back-oxidation of Eu^{2+} by H^+ (E^0 = 0.00 V) or NO_3^- (E^0 = +0.95 V, in the presence of H^+) and sufficiently low to prevent hydrolysis of Eu^{3+}.

The majority of Zn^{2+}, formed during the counter-reaction in the reduction of Eu^{3+}, was precipitated at these pH levels as the white, highly insoluble zinc(II) hydroxide. Before use, the feed solutions were filtered making use of a syringe filter (pore size: 0.45 µm).

In some experiments, europium was reduced electrochemically in a three-electrode BASi bulk electrolysis cell. The potential at the working electrode was controlled by a Metrohm Autolab PGSTAT302N potentiostat, used in chrono amperometric mode and operated by the Nova 2.1.2 software. A constant potential of -0.7 V *vs.* Ag/AgCl was applied for at least 2 h. The solution was purged by argon gas before and during the electrolysis. A BASi MF 2077 reticulated vitreous carbon electrode (RVC, surface area 10.5 cm^2 effective/cm^2 geometric) was used as working electrode. The BASi MF 2052 reference electrode consisted of an Ag/AgCl redox couple in a 3 mol L^{-1} NaCl solution. A BASi MW 1033 coiled platinum wire auxiliary electrode ($\varnothing$ = 0.5 mm, l = 23 cm), separated from the electrolysis solution by a sintered glass membrane (pore size: 4 – 5 µm), served as a counter electrode in these experiments. A chrono amperogram was recorded to follow the reduction process.

The feed solutions were analyzed before and after reduction by inductively coupled plasma - optical emission spectroscopy (ICP-OES, see Section 5.3.6)

5.3.3 Preparation and characterization of the supported ionic liquid phase

At first, the commercially available *ionic liquid* (IL) [A336][Cl] was converted into the nitrate form, *i.e.* [A336][NO_3], *via* a metathesis reaction [92]. Without any purification steps prior to the metathesis step, [A336][Cl] was dissolved in acetonitrile to decrease the viscosity of the ionic liquid and to enhance phase separation after the metathesis reaction. [A336][Cl] was vigorously mixed with a 6 mol L^{-1} NH_4NO_3 aqueous solution in a separatory funnel for 2 h, exchanging the chloride ions for the more hydrophobic nitrate ions according to the Hofmeister series [193]. After mixing and phase separation, the aqueous phase was removed and tested for the presence of chloride using $AgNO_3$. The metathesis reaction was repeated three times, until the $AgNO_3$ test was negative. After achieving full conversion to [A336][NO_3], acetonitrile was removed using a rotary evaporator and subsequently on a vacuum line. The dry [A336][NO_3] was analyzed qualitatively using a benchtop Bruker S2 Picofox *Total Reflection X-Ray Fluorescence spectrometer* (TXRF), operated with a molybdenum X-ray source at a potential of 50 kV and a current of 600 µA. The absence of a chloride absorbance peak in the resulting TXRF spectrum confirmed the quantitative conversion of the chloride form of the ionic liquid to the nitrate form.

Amberlite XAD-16N, a porous polystyrene divinylbenzene co-polymer serving as *solid support* (SS) in the self-made SILP, was purified prior to impregnation with the ionic liquid. The sodium chloride, present to retard bacterial growth in the polymer, was washed out by successive rinsing with ethanol and water *via* vacuum filtration. After purification and drying, [A336][NO_3] was physically impregnated onto the Amberlite XAD-16N *via* a wet impregnation technique in a 1:1 IL:SS weight ratio. Because of its high viscosity, [A336][NO_3] was dissolved in acetone. The mixture was shaken for 24 h, after which acetone was slowly removed using a rotary evaporator to ensure uniform impregnation. Stirring of the mixture during impregnation is not recommended as the polymer beads of the solid support might be damaged. In a final step, the SILP was dried in on a Schlenk line to remove residual traces of acetone.

The resulting SILP, [A336][NO_3]-Amberlite XAD-16N (A336-XAD), was characterized using various techniques. Scanning electron microscopy was carried out using a JEOL Scanning Electron Microscope JSM-6610. *Fourier-transform infrared* (FTIR) spectra were recorded between 4000 and 400 cm^{-1} with a resolution of 4 cm^{-1} using a Bruker Vertex 70 spectrometer equipped with a platinum ATR module. CHN elemental analysis was performed using a Thermo Scientific Interscience Flash 2000 CHN(SO) elemental analyzer. Density and nitrogen adsorption–desorption isotherms were recorded with a Quantachrome Instruments NOVA 2000e volumetric adsorption analyzer to determine the specific surface area, the pore volume (Brunauer-Emmet-Teller method, BET) and the pore size distribution (Barret-Joyner-Halenda method, BJH). The SILP was degassed under vacuum for *ca.* 30 h at 100 °C prior to the measurement. The density of the SILP was determined using an AccuPyc II 1340 pycnometer with helium gas displacement system.

5.3.4 Batch extraction experiments

Small-scale batch extraction experiments were performed to determine the extraction performance of the SILPs (self-made XAD-A336 and commercial TEVA particles). Single element samarium solutions were used, *i.e.* the SILPs were mixed with 250 µL of an aqueous feed solution with a concentration of *ca.* 6.65 mmol L^{-1} samarium and 3 mol L^{-1} $Ca(NO_3)_2$. Batch extraction experiments were performed both as a function of time and as a function of the mass of SILP. The batch experiments as a function of time were performed with 25 mg of SILP, whereas the ones as a function of mass were performed with 1.5, 3, 5, 10, 15, 25 and 30 mg of SILP. These experiments were executed in 4 mL glass reaction vials at room temperature ((23 ± 1) °C). The vials were shaken at 300 rpm using a Thermo Scientific MaxQ 2000 orbital shaker. After mixing, the reaction vials containing fine TEVA particles were centrifuged for 1 min in at 5000 rpm using

a Thermo Scientific Heraeus 200 centrifuge to enhance sample collection for analysis. The self-made bigger A336-XAD particles allowed for proper sample collection without centrifuging. The aqueous phases were analyzed by ICP-OES (*vide infra*).

Batch extraction experiments, performed in tripliclate, were evaluated *via* the determination of the *amount of metal ion M extracted to the SILP per gram of dry SILP* (q, in mg g^{-1} SILP, Eq. 5.1):

$$q = \frac{[M]_{\text{SILP,final}} \times V_{\text{Aq}}}{m_{\text{SILP}}} = \frac{([M]_{\text{Aq,initial}} - [M]_{\text{Aq,final}}) \times V_{\text{Aq}}}{m_{\text{SILP}}} \tag{5.1}$$

where $[M]_{\text{Aq,initial}}$ is the metal ion concentration in the aqueous feed solution (in mg L^{-1}), $[M]_{\text{Aq,final}}$ the metal concentration in the aqueous solution after contact with the SILP (in mg L^{-1}), V_{Aq} the volume of the aqueous feed solution (in L) and m_{SILP} the mass of the dry SILP (in g). Subsequently, the *weight distribution ratio* (D_w, in mL g^{-1} SILP) was calculated as the ratio of the amount of metal ion M extracted to the SILP (q) over its remaining concentration in the aqueous phase after extraction ($[M]_{\text{Aq,final}}$) (Eq. 5.2):

$$D_w = \frac{q}{[M]_{\text{Aq,final}}} \times 10^3 \tag{5.2}$$

The *fraction of metal ion M extracted to the SILP* (%E) was determined by the ratio of the amount of metal ion M extracted to the SILP over the total amount of that metal ion present in the entire system (Eq. 5.3):

$$\%E = \frac{[M]_{\text{SILP,final}}}{[M]_{\text{total}}} \times 100 = \frac{[M]_{\text{Aq,initial}} - [M]_{\text{Aq,final}}}{[M]_{\text{total}}} \times 100 \tag{5.3}$$

5.3.5 Extraction chromatography experiments

Resulting from the batch extraction experiments (*vide infra*), the TEVA particles were selected for extraction chromatography. Extraction chromatography experiments were conducted in a column separation setup using BIO-RAD Econo glass columns with 0.5 cm inner diameter and a total length of 10 cm (Fig. 5.2). The flow rate of the mobile phase was regulated with an ISMATEC IPC 8-channel peristaltic pump. Fractions were collected using a Spectrum Laboratories CF-2 fraction collector, equipped with a drop sensor. The glass columns were packed with the TEVA particles *via* the wet method. The packed column was preconditioned with a purged 3 mol L^{-1} $Ca(NO_3)_2$ solution. The

bed material was fixed in the glass column using glass wool. A septum was used to seal the column, allowing to maintain an inert atmosphere and avoid underpressure in the column by the use of a balloon filled with argon. The feed solution and the different mobile phases were also fed to the column *via* the septum. The aqueous feed solution contained 6.6 mmol L^{-1} samarium, 6.6 mmol L^{-1} europium and 3 mol L^{-1} $Ca(NO_3)_2$ (after reduction, *vide supra*). A 3 mol L^{-1} $Ca(NO_3)_2$ solution served as the initial mobile phase for the forward extraction step of Sm^{3+} to the SILP column material. Water was used as a second mobile phase for the back-extraction of Sm^{3+}. The mobile phases were purged extensively with nitrogen gas prior to use. All extraction chromatography experiments were performed at room temperature ((23 ± 1) °C).

Subsequently, the use of commercially available prepacked TEVA cartridges (bed volume 2 mL, particle size 50 – 100 µm) was investigated. Similar aqueous feed solutions and mobile phases were used as in the previous extraction chromatography experiments. A syringe was connected to the cartridge *via* the Luer-lock system to feed the aqueous solutions. The syringe was sealed with a septum, in which an inert atmosphere was maintained using a balloon filled with argon. The flow rate was regulated using a peristaltic pump and fractions were collected using a fraction collector. All fractions originating from extraction chromatography experiments were analyzed by ICP-OES (*vide infra*).

5.3.6 Analysis of the aqueous phases and fractions

The aqueous phases of the batch extraction experiments and the fractions of the extraction chromatography experiments were analyzed using a Perkin Elmer Optima 8300 inductively coupled plasma optical emission spectrometer (ICP-OES), equipped with axial/radial dual plasma view, a GemTip CrossFlow II nebulizer, a Scott Spray Chamber Assembly, a sapphire injector and a Hybrid XLT ceramic torch. Calibration curves were constructed by fitting the measured intensities of standard solutions containing 0.01, 0.1, 1 and 10 ppm samarium, europium and zinc through the origin. As a standard procedure, the samples originating from the batch extraction and extraction chromatography experiments were diluted 100 times by a 2 wt% HNO_3 solution before being measured by ICP-OES. All spectra were recorded in triplicate.

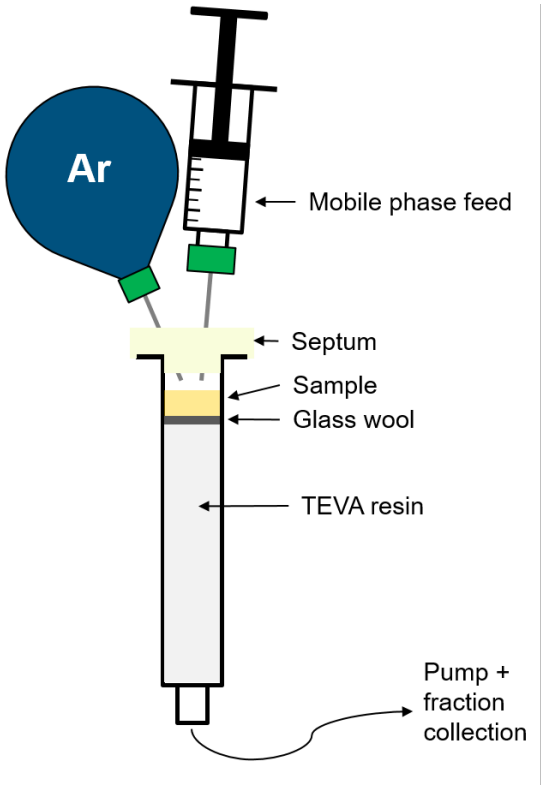

Figure 5.2: Schematic representation of the extraction chromatography experiments making use of a glass column packed with TEVA resin.

5.4 Results and Discussion

5.4.1 Preparation and characterization of the supported ionic liquid phase

A large variety of solid supports can be combined with a solvent for the preparation of so-called *solvent impregnated resins* (SIRs). In case the solvent is an ionic liquid, the term *supported ionic liquid phases* (SILPs) generally applies. The use of SILPs has been tested for solid phase extractions in a wide variety of metal separation applications [288, 294, 298–308]. The extraction mechanism involved depends on the nature of the sorbent and the analyte. Both inorganic and polymeric materials can be used as a solid support. As a polymeric support, the commercially available Amberlite resins have been found

very promising for the development of SILPs because of their beneficial physical and chemical properties [309]. In this study, Amberlite XAD-16N, a non-ionic macroretical compound consisting of a styrene-divinylbenzene copolymer, was selected because of its large specific surface area ($800\,m^2\,g^{-1}$), medium pore size (200 Å on average), high chemical resistance, and its ability to efficiently adsorb hydrophobic compounds with medium to high molar mass (up to 40 000 u). Amberlite XAD-16N particles have a size of 20 – 60 mesh (0.25 – 0.85 mm), and already proved to be inert towards metal adsorption, *i.e.* separation of metal ions are solely due to interactions with the supported ionic liquid.

The morphology and impregnation of the A336-XAD particles was investigated using various characterization techniques. First of all, the presence of the quaternary ammonium ionic liquid on the styrene-divinylbenzene copolymer was confirmed using FTIR spectroscopy (Fig. 5.3). A broad characteristic absorption band with a minimum at $3400\,cm^{-1}$ can be attributed to the O−H stretches of trace amounts of water. The absorption bands in the region of $3000 - 2800\,cm^{-1}$ can be assigned to the C−H stretches of methylene and methyl groups of Aliquat 336. The weak to medium absorption bands in the region of $1670 - 1600\,cm^{-1}$ can be attributed to C=C stretches of the aromatic rings, originating from the Amberlite XAD-16N solid support, *i.e.* styrene and divinylbenzene. The absorption bands in the region of $1600 - 1300\,cm^{-1}$ correspond to the C−H bending of the methylene and methyl groups of Aliquat 336. The absorption bands in the region of $1000 - 700\,cm^{-1}$ originate from C=C bending, whereas several absorption bands in the region of $900 - 700\,cm^{-1}$ can also be ascribed to the C−H out-of-plane bends. The C−H stretching and bending vibrations arising from methylene and methyl groups in the spectrum of the A336-XAD supported ionic liquid are very similar to those in the spectrum of bulk [A336][NO_3] ionic liquid. Additional CHN analyses of the solid support, [A336][NO_3] (C: 71.1 ± 1.3; H: 12.8 ± 0.1; N: 5.7 ± 0.1) and A336-XAD clearly indicate the presence of the ionic liquid in the SILP. Thus, both analysis techniques give convincing proof of the ionic liquid being successfully impregnated on the polymeric solid support.

Analysis of the nitrogen adsorption–desorption isotherms was performed for determination of the specific surface area, pore volume and pore size distribution, and for examining the textural properties of the SILP materials. The obtained adsorption–desorption isotherms showed a hysteresis loop type IV for the neat Amberlite XAD-16N solid support and both TEVA particle sizes (50 – 100 µm and 100 – 150 µm), and showed a subtle change towards hysteresis loop type V for A336-XAD. The results of the nitrogen adsorption–desorption analyses are summarized in Table 5.1. From these results, it is clear that the macroporous structure of the Amberlite XAD-16N solid support disappears largely upon impregnation with the ionic liquid [A336][NO_3]. Weak adsorbate–adsorbent

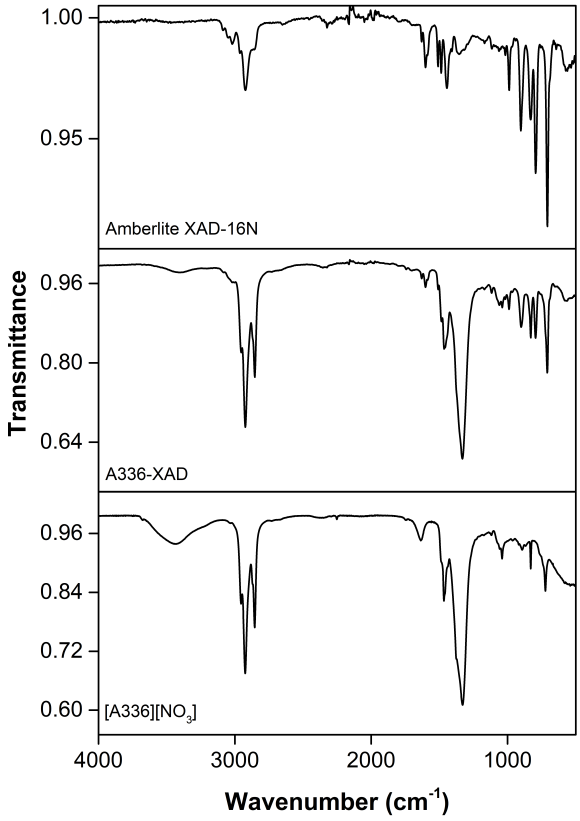

Figure 5.3: FTIR spectra of the Amberlite XAD-16N solid support (top), A336-XAD supported ionic liquid (middle) and [A336][NO_3] ionic liquid (bottom).

interactions remain as a result of the much lower specific surface area of A336-XAD. Another indication for the ionic liquid covering the pores of the porous solid support is the very low average pore volume of A336-XAD. The resulting average values for pore volume and pore radius most probably originate from surface defects caused by drying of the SILP particles after impregnation. Similar observations were obtained by Van Roosendael *et al.* in comparable research with Amberlite XAD-16N impregnated with [A336][I] or [A336][Cl] [294]. The TEVA particles have a much higher specific surface area compared to A336-XAD because of their much smaller particle sizes.

SEM images of A336-XAD confirmed the fairly homogeneous layer of ionic liquid covering the outer surface of the solid polymer support spheres Fig. 5.4. Except for the typical surface defects (*e.g.* scales, shallow cavities or cracks) originating from the swelling stress of the matrix, no signs for a porous structure could be detected. These observations are similar to the ones described previously by Saha *et al.* [290]. The absence of a porous structure indicates that the pores of the reticulated copolymer were clogged and covered with ionic liquid.

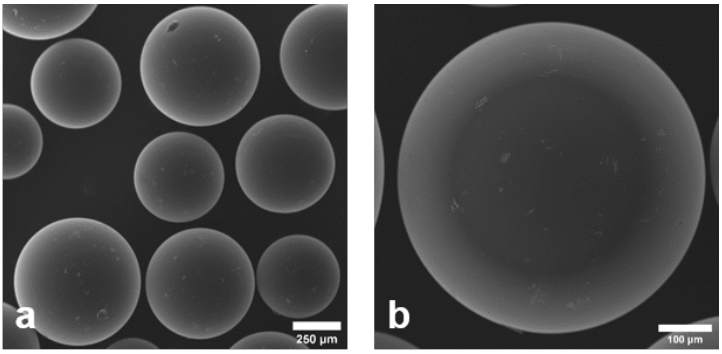

Figure 5.4: SEM images of the A336-XAD, demonstrating integrity of the surface of the SILP. The ionic liquid layer [A336][NO_3] is impregnated fairly homogeneous onto the polystyrene-divinylbenzene solid support particles. Acceleration voltage: 7 keV, working distance: 10 mm, 37× (a) and 120× (b) magnification.

5.4.2 Batch extraction experiments

The prepared A336-XAD and a commercial variety (TEVA resin, TrisKem International) available in two different particle sizes (50 – 100 µm and 100 – 150 µm) were subjected to batch extraction experiments to evaluate their extraction performance. The weight distribution ratios as a function of contact time are presented in Fig. 5.5. It is immediately clear that higher weight distribution ratios were reached in case TEVA ($D_w \approx 20\,\mathrm{mL\,g^{-1}}_{\mathrm{SILP}}$, $\%E_{\mathrm{Sm}} \approx 67\,\%$) was used compared to A336-XAD ($D_w \leq 5\,\mathrm{mL\,g^{-1}}_{\mathrm{SILP}}, \%E_{\mathrm{Sm}} \leq 35\,\%$). Both TEVA particle sizes performed very similarly in these conditions. The extraction equilibrium was reached very quickly when using TEVA, *i.e.* steady distribution ratios were reached already with short contact times. In contrast, it took much longer to reach an extraction equilibrium when using A336-XAD. The extraction equilibrium was not reached after 30 min in the experimental conditions applied. The weight distribution ratios as a function of the total SILP mass are shown in Fig. 5.6. For A336-XAD, a maximum D_w value of *ca.* $6\,\mathrm{mL\,g^{-1}}_{\mathrm{SILP}}$ was reached for 30 mg SILP, with only a minor

Table 5.1: Summary of the physical properties of the supported ionic liquid phases as derived from the nitrogen adsorption–desorption isotherms and CHN analysis.

	Amberlite XAD-16N	A336-XAD	TEVA 100–150	TEVA 50–100
Solid support	-	Amberlite XAD-16N	Amberchrom CG-71ms	Amberchrom CG-71ms
Particle size (µm)	250–850[(1)]	250–850[(1)]	100–150[(1)]	50–100[(1)]
Specific surface area ($m^2\,g^{-1}$)	676.9 ± 23.6	3.8 ± 1.1	156.5 ± 15.1	113.1 ± 12.9
Pore radius (Å)	50[(1)]	23.64 ± 7.15	30.52 ± 3.51	43.23 ± 9.02
Pore volume ($mL\,g^{-1}$)	2.03 ± 0.32	0.015 ± 0.001	0.779 ± 0.013	0.667 ± 0.018
Impregnation ratio (g IL per g SS)	0	1	0.4[(2)]	0.4[(2)]
Density ($g\,cm^{-3}$, dry)	1.020[(1)]	0.997	1.1304	1.1109
C (wt%)	35.4 ± 1.0	78.6 ± 0.3	66.3 ± 0.4	66.9 ± 0.7
H (wt%)	3.8 ± 1.2	10.8 ± 0.1	9.7 ± 0.1	9.6 ± 0.2
N (wt%)	0.1 ± 0.1	3.8 ± 0.5	1.0 ± 0.1	1.0 ± 0.1

[(1)] Value as published by the manufacturer
[(2)] Value as published by Horwitz *et al.* [297]

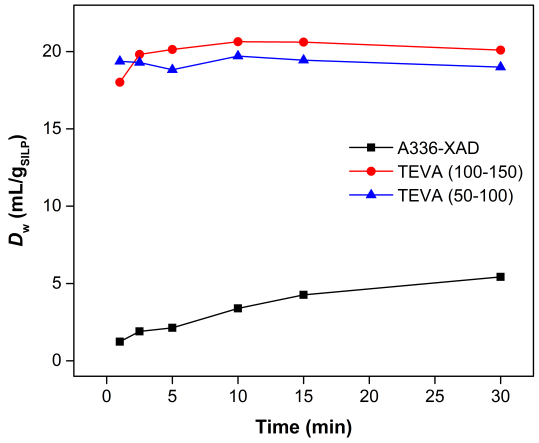

Figure 5.5: Weight distribution ratio (D_w) for Sm^{3+} as a function of time in batch extraction experiments making use of A336-XAD (■), TEVA 100 – 150 µm (●) and TEVA 50 – 100 µm (▲). 25 mg SILP was contacted with 250 µL of feed solution (6.65 mmol L^{-1} Sm in 3 mol L^{-1} $Ca(NO_3)_2$) (pH ≈ 6.5). Shaking speed: 300 rpm, temperature: (23 ± 1) °C.

increasing trend with increasing SILP mass. For both TEVA varieties, a more pronounced increase of D_w, from 15 to 20 mL $g^{-1}{}_{SILP}$, was observed. 72 % Sm^{3+} was extracted to the TEVA resin when using 30 mg of SILP.

From these bulk extraction experiments, the TEVA particles show to be the preferred SILP for extraction of Sm^{3+}. The differences in extraction performances might originate from the different ionic liquid loadings onto the solid support for both SILPs. 0.4 g IL (28.6 wt%) per gram of solid support was used for the production of TEVA (by manufacturer), whereas 1 g IL (50 wt%) per gram of solid support was used in the preparation of A336-XAD [297]. Most probably, the A336-XAD suffered from overloading of the solid support by the ionic liquid, resulting in lower extraction performances. Analysis of the nitrogen adsorption–desorption isotherms already pointed out that most of the pores of the Amberlite XAD-16N solid support were filled and covered with the viscous ionic liquid. This significantly reduced the total specific surface area available for contact between the feed solution and A336-XAD. The TEVA resins preserved a very large surface area because of the much smaller solid support particles (50 – 150 µm), resulting in a much higher probability for interaction with the aqueous feed solution and better extraction performance for Sm^{3+}. The finer TEVA particles will also assure a more dense packing of the column, leaving less

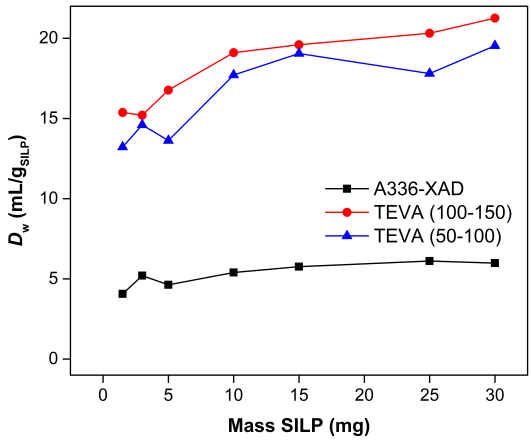

Figure 5.6: Weight distribution ratio (D_w) for Sm^{3+} as a function of the SILP mass in batch extraction experiments making use of A336-XAD (■), TEVA 100 – 150 µm (●) and TEVA 50 – 100 µm (▲). Different amounts of SILP (1.5, 3, 5, 10, 15, 20 and 30 mg) were contacted with 250 µL of feed solution (6.65 mmol L^{-1} Sm in 3 mol L^{-1} $Ca(NO_3)_2$) (pH ≈ 6.5). Shaking speed: 300 rpm, temperature: (23 ± 1) °C, contact time: 30 min.

open spaces in between the separate particles and resulting in a better contact between the stationary and mobile phase. For these reasons, TEVA particles were selected for further investigation on their use in extraction chromatography.

Stripping experiments to recover Sm^{3+} from the SILPs were performed by the addition of water. This way, the total salt concentration in the system was reduced, counteracting the salting out effect of Sm^{3+}. All experiments resulted in quantitative back-extraction (≥ 99.7 %) of Sm^{3+} to the aqueous phase, which is similar to what was previously observed for the solvent extraction method using bulk ionic liquid phases [92].

5.4.3 Extraction chromatography experiments

The batch extraction experiments resulted in the selection of TEVA particles to serve as packing material in extraction chromatography experiments for the separation of samarium and europium. The TEVA particles were conditioned in a blank 3 mol L^{-1} $Ca(NO_3)_2$ solution prior to packing of the column to avoid swelling of the particles in the column. During conditioning, the mixture was

purged with inert gas to remove as much oxygen as possible as Eu^{2+} is sensitive to oxidation in presence of aerial or dissolved oxygen. The TEVA particles were packed into a glass column as a slurry to ensure uniform packing, and to avoid cracks or holes in the SILP bed. Cracks and holes might lead to channel formation, *i.e.* preferred pathways, and affect the column performances and separation capabilities. Additionally, the use of commercially available TEVA cartridges (bed volume (BV): 2 mL), which are prepacked with dry TEVA 50 – 100 µm particles, was investigated. These cartridges were conditioned and extensively rinsed using a purged 3 mol L^{-1} $Ca(NO_3)_2$ solution as well before use to remove as much oxygen as possible.

The breakthrough curves of the TEVA-filled glass column (BV: 1.53 mL, 1.7 g TEVA, Fig. 5.7) and cartridge (BV: 2 mL, 2.2 g TEVA, Fig. 5.8) for a solution containing 6.6 mmol L^{-1} Sm^{3+} and 3 mol L^{-1} $Ca(NO_3)_2$ were recorded using a flow rate of 0.70 mL min^{-1}. Breakthrough capacity ($C/C_0 \leq 0.1$) for the glass column was determined to be 4.2 BVs (≈ 6.4 mL), whereas the breakthrough capacity for the cartridge was determined to be 3.6 BVs (≈ 7.2 mL). In total, 8.2 mg Sm^{3+} (≈ 8.2 mg Sm^{3+}/g of SILP) and 11.2 mg Sm^{3+} (≈ 5 mg Sm^{3+}/g of SILP) could be loaded on the TEVA-filled glass column and cartridge, respectively. Both columns have a different bed volume originating from their different column dimensions, with the glass column being longer (h: 7.8 cm) and thinner (∅: 0.5 cm) and the cartridge being shorter (h: 2.5 cm) and wider (∅: 1 cm). Because of the different column dimensions, less bed volumes were needed for the cartridge to achieve breakthrough. However, a higher total volume of the eluate was collected before achieving breakthrough, denoting a higher breakthrough capacity for the cartridge. Additionally, the particle sizes in both columns were slightly different, *i.e.* 100 – 150 µm particles were used to pack the glass columns, whereas the commercially available cartridges consisted of the 50 – 100 µm TEVA particles. The latter will only have a minor impact for similar bed densities and free column volume, as the batch extraction experiments already pointed out that both TEVA particle sizes showed a comparable extraction behavior. Only different back-pressures might be observed in the column because of the different particle sizes, but this was of minor importance in this study.

Differences in the physical properties of chromatography columns lead to differences in the column performance. The length of the column is proportional to the separation efficiency, affecting the number of theoretical plates in the column and its resolution, *i.e.* longer columns result in higher separation efficiencies. However, longer columns increase the time Eu^{2+} spends in the column bed, increasing the risk of partial oxidation to Eu^{3+}. Any formation of Eu^{3+} species in the column will lead to the extraction of europium to the ionic liquid layer of the TEVA particles, resulting in a worse separation of

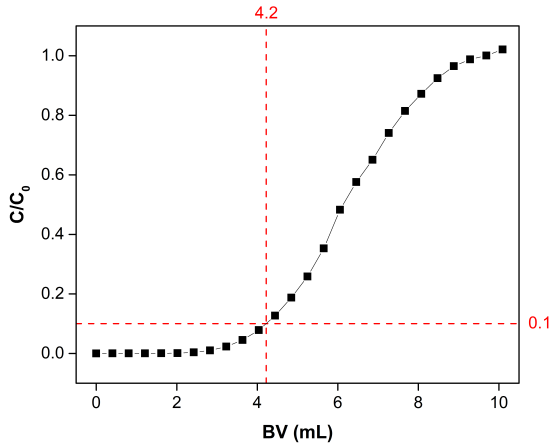

Figure 5.7: Breakthrough curve for Sm^{3+} on a TEVA (50–100 µm) packed glass column (BV: 1.53 mL) using a feed solution containing 6.6 mmol L^{-1} Sm^{3+} and 3 mol L^{-1} $Ca(NO_3)_2$ (pH ≈ 6.5). Flow rate: 0.7 mL min^{-1}.

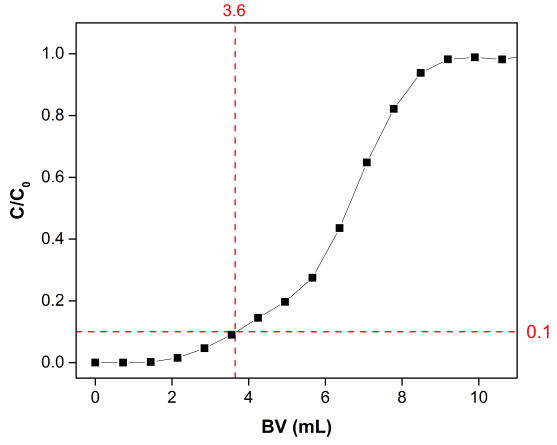

Figure 5.8: Breakthrough curve for Sm^{3+} on a commercial TEVA (50 – 100 µm) cartridge (BV: 2 mL) using a feed solution containing 6.6 mmol L^{-1} Sm^{3+} and 3 mol L^{-1} $Ca(NO_3)_2$ (pH ≈ 6.5). Flow rate: 0.7 mL min^{-1}.

samarium and europium. Therefore, the length of the column should be well-considered. The diameter of the column affects the capacity of the column, *i.e.*

more analytes can be loaded in a single run. This was already clear from the breakthrough experiments, *i.e.* the shorter, but wider cartridge showed a higher breakthrough capacity. Therefore, the capability of the TEVA glass column and TEVA cartridge to separate Sm^{3+} and Eu^{2+} was investigated. All other parameters that can largely affect the separation capability (*e.g.* flow rate and temperature) were kept constant.

In the proposed separation method, Sm^{3+} is extracted to the ionic liquid layer of the TEVA particles using a concentrated nitrate salt solution, whereas Eu^{2+} species are not retained by the TEVA particles. Zn^{2+} species, originating from the chemical reduction step (if used), also do not interact with the TEVA particles. Therefore, Eu^{2+} and Zn^{2+} will elute together from the extraction column first, ending up in the first fractions. Sm^{3+} is eluted from the column by reducing the salt concentration in the mobile phase, *i.e.* changing the mobile phase to water. Sm^{3+} being present in the fractions containing a low nitrate salt concentration is advantageous in scope of further production steps of the ^{153}Sm radiopharmaceutical.

In a first extraction chromatography experiment, a glass column (∅: 0.7 cm, h: 20 cm) was packed with TEVA particles, reaching a bed height of 11.5 cm (BV: 4.43 mL), and conditioned with the 3 mol L^{-1} $Ca(NO_3)_2$ mobile phase. After being in contact with Zn^0 grains for 2 h to reduce Eu^{3+} to Eu^{2+}, 1.5 mL of a solution containing 6.6 mmol L^{-1} Sm, 6.6 mmol L^{-1} Eu and 3 mol L^{-1} $Ca(NO_3)_2$ was loaded onto the column. The total Zn^{2+} concentration in the feed solution remained relatively low, because majority of Zn^{2+} hydrolyzed to the insoluble $Zn(OH)_2$ at the pH levels close to neutral. $Zn(OH)_2$ was removed from the feed solution by filtration. Afterwards, the column was eluted with a blank 3 mol L^{-1} $Ca(NO_3)_2$ mobile phase with a flow rate of 0.7 mL min^{-1} for the forward extraction of Sm^{3+}. The mobile phase was switched to water after collecting 16 fractions of 1.5 mL. The resulting chromatogram is presented in Fig. 5.9, and showed already a high separation potential for Sm^{3+} and Eu^{2+}. As expected, Eu^{2+} and Zn^{2+} did almost not interact with the TEVA particles, and consequently were not retained on the column. Both ions ended up in the first fractions, collecting 61 % of the initial europium and > 99 % of zinc. Also a small amount of Sm^{3+} (7 %) ended up in the first fractions. The remaining europium fraction (39 %) eluted together with Sm^{3+} (93 %) while stripping with water. This indicates that not all Eu^{3+} was reduced, or that Eu^{2+} was partially oxidized during extraction chromatography.

Smaller column dimensions were used in subsequent extraction chromatography experiments, reducing the time that Eu^{2+} spends in the extraction column, *i.e.* minimizing the possibility to oxidize to Eu^{3+}. Glass columns (∅: 0.5 cm, h: 10 cm) were packed with TEVA particles, reaching a bed height of *ca.* 8 cm (BV: 1.57 mL). The mobile phases were switched earlier as less volume was

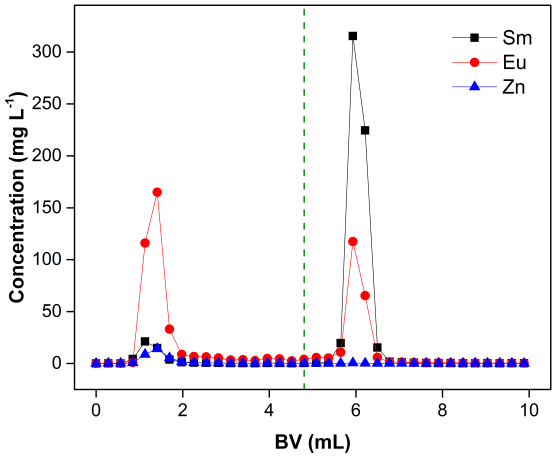

Figure 5.9: Elution curves of samarium (■), europium (●) and zinc (▲) using a TEVA packed glass column (BV: 4.43 mL). Feed: 1.5 mL (6.6 mmol L^{-1} Sm^{3+} and 6.6 mmol L^{-1} Eu^{2+} (after chemical reduction) in 3 mol L^{-1} $Ca(NO_3)_2$) (pH ≈ 6.5). The dashed line denotes the change of mobile phase. Flow rate: 0.7 mL min^{-1}.

needed to pass through the column. Less fractions had to be collected in total, arriving at a faster and more efficient separation method. The other parameters remained the same. The separation of samarium and europium after chemical and electrochemical reduction are presented in Figs. 5.10 and 5.11, respectively.

It is immediately clear that a much bigger fraction of europium ended up in the first fractions in both experiments. In case of the chemical reduction, 75 % europium, 9 % samarium and > 99 % zinc present in the feed solution was found in the first fractions. However, separation after electrochemical reduction proved to be even more efficient, *i.e.* more than 85 % of the initial amount of europium in the feed was found in the first fractions, whereas < 0.2 % of the initial samarium was found in these fractions. In both experiments, samarium and the remaining amount of europium were quantitatively eluted with water. The reason why a bigger amount of Sm^{3+} eluted in the first fractions after chemical reduction, whereas this was not the case after electrochemical reduction, remains unclear. It is notable that the amount of Sm^{3+} in these fractions is consistently comparable to the amount of Zn^{2+} in these fractions. Whether any interaction between Zn^{2+} and Sm^{3+} species gives rise to the early partial elution of Sm^{3+} will have to be investigated in more detail. Nevertheless, both experiments show the high potential of the proposed strategy for the separation of Sm and Eu, *i.e.* a high potential for the removal of long-lived

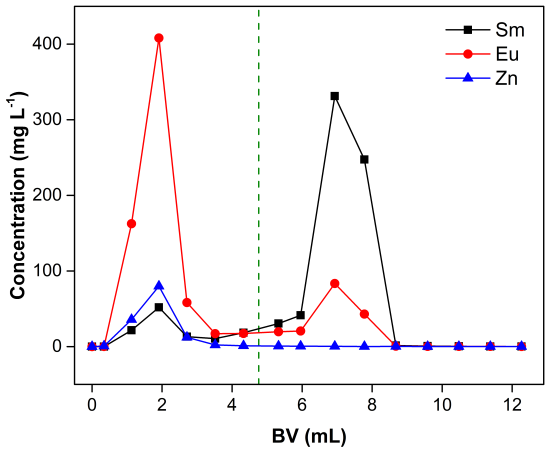

Figure 5.10: Elution curves of samarium (■), europium (●) and zinc (▲) using a TEVA packed glass column (BV: 1.57 mL). Feed: 1.5 mL (6.6 mmol L^{-1} Sm^{3+} and 6.6 mmol L^{-1} Eu^{2+} (after chemical reduction) in 3 mol L^{-1} $Ca(NO_3)_2$) (pH ≈ 6.5). The vertical line denotes the change of mobile phase. Flow rate: 0.7 mL min^{-1}.

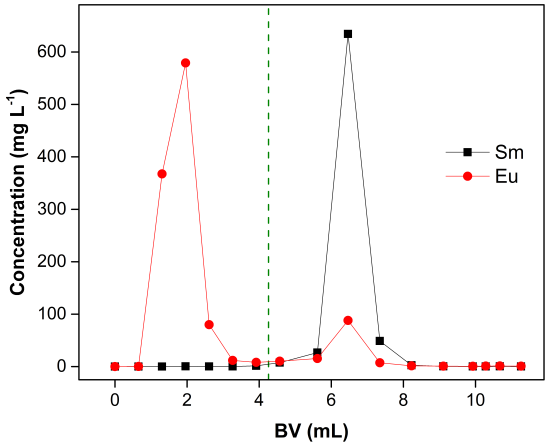

Figure 5.11: Elution curves of samarium (■) and europium (●) using a TEVA packed glass column (BV: 1.53 mL). Feed: 1.5 mL (6.6 mmol L^{-1} Sm^{3+} and 6.6 mmol L^{-1} Eu^{2+} (after electrochemical reduction) in 3 mol L^{-1} $Ca(NO_3)_2$) (pH ≈ 6.5). The vertical line denotes the change of mobile phase. Flow rate: 0.7 mL min^{-1}.

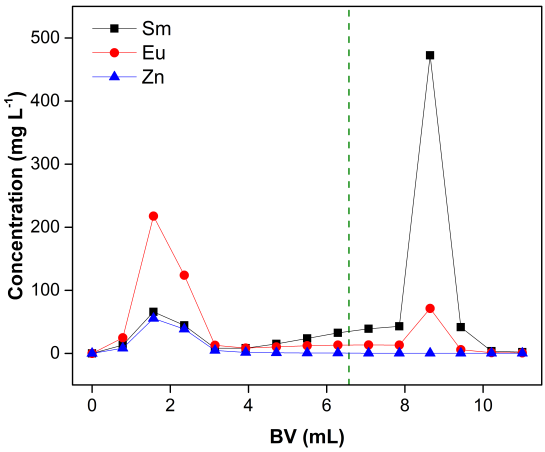

Figure 5.12: Elution curves of samarium (■), europium (●) and zinc (▲) using a TEVA packed glass column (BV: 1.57 mL). Feed: 1.5 mL (6.6 mmol L^{-1} Sm^{3+} and 3.3 mmol L^{-1} Eu^{2+} (after chemical reduction) in 3 mol L^{-1} $Ca(NO_3)_2$) (pH ≈ 6.5). The vertical line denotes the change of mobile phase. Flow rate: 0.7 mL min^{-1}.

^{154}Eu from the medical ^{153}Sm. Removal of more than 85 % of the initial ^{154}Eu present after irradiation would increase the shelf-life, *i.e.* the time during which the ^{153}Sm radiopharmaceutical can be safely used, significantly. The exact profit depends on the irradiation parameters applied (*i.e.* thermal neutron flux, irradiation time *etc.*) and, consequently, the composition after irradiation [190]. The amount of ^{154}Eu produced highly depends on these irradiation parameters.

The separation method using a TEVA packed glass column was also tested for samples containing lower europium concentrations, *i.e.* 3.3, 1.65 and 0.66 mmol L^{-1}. The samarium concentration in the feed solutions remained the same as before (6.6 mmol L^{-1}). The resulting chromatograms are presented in Figs. 5.12 to 5.14, respectively. In these experiments, Eu^{3+} was chemically reduced to Eu^{2+} prior to the extraction chromatography step. From these chromatograms it is clear that the majority of europium and all zinc were collected in the first fractions while eluting with a concentrated nitrate salt solution, whereas a vast majority of samarium was collected after changing the mobile phase to water. Only small amounts of europium ended up in these fractions. However, a significant amount of samarium (*ca.* 15 %) already eluted before the mobile phase was changed. Overloading of the column was not expected, but interaction of Sm^{3+} with Zn^{2+} species present after chemical reduction of Eu^{3+} might be a possible explanation (*vide supra*).

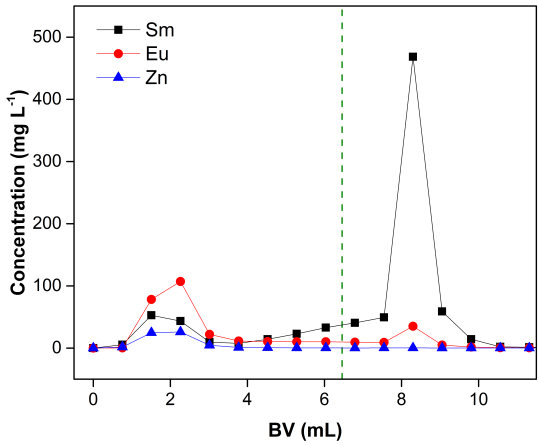

Figure 5.13: Elution curves of samarium (■), europium (●) and zinc (▲) using a TEVA packed glass column (BV: 1.57 mL). Feed: 1.5 mL (6.6 mmol L^{-1} Sm^{3+} and 1.65 mmol L^{-1} Eu^{2+} (after chemical reduction) in 3 mol L^{-1} $Ca(NO_3)_2$) (pH ≈ 6.5). The vertical line denotes the change of mobile phase. Flow rate: 0.7 mL min^{-1}.

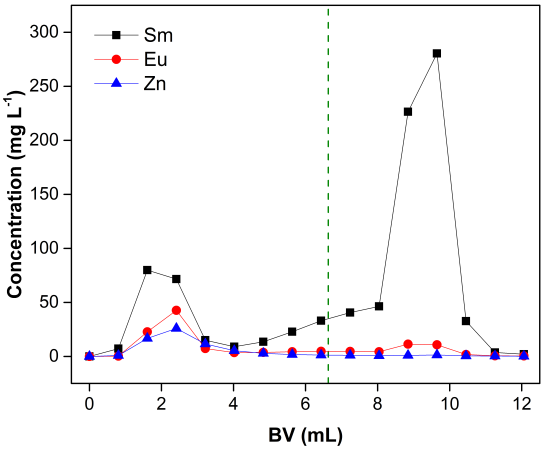

Figure 5.14: Elution curves of samarium (■), europium (●) and zinc (▲) using a TEVA packed glass column (BV: 1.57 mL). Feed: 1.5 mL (6.6 mmol L^{-1} Sm^{3+} and 0.66 mmol L^{-1} Eu^{2+} (after chemical reduction) in 3 mol L^{-1} $Ca(NO_3)_2$) (pH ≈ 6.5). The vertical line denotes the change of mobile phase. Flow rate: 0.7 mL min^{-1}.

The use of commercially available TEVA cartridges (BV: 2 mL) for the separation of samarium and europium was also investigated. The cartridges were conditioned with a purged 3 mol L^{-1} $Ca(NO_3)_2$ solution, similar to the packed glass columns. Also a feed solution similar to the previous experiments was used, *i.e.* 6.6 mmol L^{-1} Sm, 6.6 mmol L^{-1} Eu and 3 mol L^{-1} $Ca(NO_3)_2$. The feed solution was contacted with zinc grains for the chemical reduction of Eu^{3+}. Only 1 mL of the feed solution was loaded onto the column because of the lower bed height of the column. The feed solution and mobile phase were carefully added to the cartridge, making sure there was no gas bubble trapped in the empty space above the upper frit of the Luer-lock system, which might impede feeding of the column. The resulting chromatogram is presented in Fig. 5.15, and looks similar to the ones obtained with the TEVA packed glass columns.

About 85 % of europium and > 99.9 % zinc were collected in the first fractions, whereas the majority of samarium (*ca.* 65 %) was found in the fractions after changing the mobile phase to water. These fractions contained a small amount of europium (only 10 % of the initial europium concentration). A higher amount of Sm^{3+} was not retained by the TEVA particles when making use of the cartridge, and eluted together with Eu^{2+} and Zn^{2+} in the first fractions. Imperfections in the TEVA bed (*e.g.* cracks and holes) due to the dry packing of the cartridge,

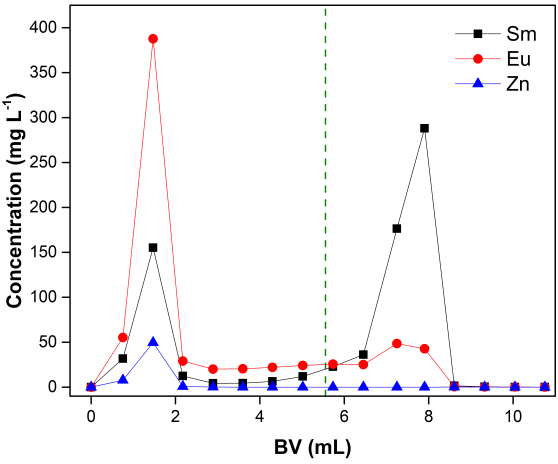

Figure 5.15: Elution curves of samarium (■), europium (●) and zinc (▲) using a commercial TEVA cartridge (BV: 2 mL). Feed: 1 mL of a solution containing 6.6 mmol L^{-1} Sm^{3+}, 6.6 mmol L^{-1} Eu^{2+} (after chemical reduction) and 3 mol L^{-1} $Ca(NO_3)_2$ (pH ≈ 6.5). The vertical line denotes the change of mobile phase. Flow rate: 0.7 mL min^{-1}.

or the different column dimensions may have caused a lower interaction between Sm^{3+} and the TEVA particles leading to a higher amount of Sm^{3+} that was not retained on the column.

5.5 Conclusion

The impregnation of the ionic liquid [A336][NO_3] onto the Amberlite XAD-16N was found to be successful. The resulting A336-XAD supported ionic liquid was fully characterized, and its extraction performance for Sm^{3+} was compared to the commercially available TEVA particles. Different characterization methods pointed out that a layer of the viscous ionic liquid covered and clogged the pores of the porous solid support structure, making only the outer surface of the SILP accessible for extraction. The smaller particle size, and hence much larger specific surface area of the TEVA particles, as well as the lower ionic liquid loading proved to be more efficient for the extraction of Sm^{3+}. Therefore, TEVA particles were selected to serve as packing in the columns for subsequent extraction chromatography experiments. In the separation strategy, Eu^{2+} was not retained by the TEVA particles, whereas Sm^{3+} was extracted to the TEVA particles using a concentrated nitrate salt solution. On average, more than 80 % of the initial europium was found in the first fractions. The amount of europium eluting in the first fractions is highly dependent on the reduction efficiency of the reduction step and any possible factors that might cause oxidation of Eu^{2+} during the separation process. The vast majority of Sm^{3+} could only be eluted after significant reduction of the nitrate salt concentration in the mobile phase, *i.e.* by pure water. It was notable that a small fraction of Sm^{3+}, consistently comparable to the total amount of Zn^{2+} present, eluted early in case Eu^{3+} was chemically reduced by Zn^0. No Sm^{3+} was eluted early after electrochemical reduction of Eu^{3+}. The reason for this behavior remains unclear and was not further studied here. The samarium-rich fractions contain lower nitrate salt concentrations, which is advantageous for further radiopharmaceutical processing steps. If required, the Ca^{2+} concentration in the final product can be further reduced by introducing a secondary separation step, for example by making use of a cation exchanger. The extraction chromatography experiments demonstrated the feasibility of using TEVA particles in extraction chromatography for the separation of Eu^{2+} and Sm^{3+}. Therefore, the separation method looks promising towards a purification system for the medical radionuclide ^{153}Sm, increasing the shelf-life significantly. Nevertheless, further optimization of the extraction chromatography step and automation of the full process to increase the separation efficiency are still required.

Chapter 6

Conclusions

A variety of radiolanthanides produced in a nuclear research reactor are eligble to be used in nuclear medicine. Their application is highly dependent on their physical decay properties, achievable specific activity and availability. The half-life of the radiolanthanide and the accompanying particle emission and particle emission energy are characteristic for every radiolanthanide, and cannot be changed. Therefore, the decay characeristics serve as a first selection tool to consider the use of a radiolanthanide in nuclear medicine. The production route followed, carrier-added or non-carrier-added, has a major impact on the achievable specific activities and possible ingrowth of any long-lived radionuclidic impurities. The possibility to efficiently isolate the desired radiolanthanide from the redundant target material in the non-carrier-added method, and to efficiently remove radionuclidic impurities form the carrier-added produced radiolanthanide are of key importance to achieve high availability. Besides, recovery of unused and valuable target material to be irradiated in a new production cycle is important in support of a circular economy. Moreover, these target materials are usually highly enriched, and might therefore be very expensive. For these reasons, radiochemists have been studying different isolation and purification approaches intensively over the last decades. A comprehensive overview of the current-state methods for separation of the most relevant medical radiolanthanides was listed in Chapter 1 of this dissertation.

The research performed within the framework of this PhD dissertation comprises an innovative approach towards development of a new and efficient method for the removal of long-lived ^{154}Eu impurities from medical ^{153}Sm. The investigated separation method involves two major steps. In a first step, Eu^{3+} is selectively reduced to Eu^{2+}, whereas in a second step Sm^{3+} and Eu^{2+} are separated. Both

steps were investigated here in more detail.

It was demonstrated in Chapter 3 that Eu^{3+} can be selectively reduced to Eu^{2+} in aqueous nitrate solutions. Moreover, it was proven that Eu^{2+} remains relatively stable for several hours in these media, provided that no oxidizing agents are present. For this reason, it is important that the reduction of Eu^{3+} takes place in inert atmosphere and at quasi neutral pH. Both chemical and electrochemical reduction methods were deployed, as well as different analysis techniques in an attempt to study the reduction of Eu^{3+} and the stability of Eu^{2+} in nitrate media. Based on XANES measurements, the reduction was found to be more efficient in solutions containing high nitrate salt concentrations, *i.e.* a nitrate concentration of $\geq 6\,\mathrm{mol\,L^{-1}}$ was needed to achieve high reduction ratios. The high nitrate salt concentration causes a severe change in ionic strength and hydration of the europium ions in solution. Cyclic voltammetry experiments proved that the reduction potential of Eu^{3+} becomes less negative with increasing nitrate salt concentration. This indicates that reduction is facilitated and that more stable Eu^{2+}–nitrate complexes are formed with increasing nitrate salt concentration. Additionally, the cyclic voltammetry experiments showed that reduction of Eu^{3+} takes place at a less negative potential in aqueous nitrate solutions compared to similar aqueous chloride solutions, indicating a more efficient reduction in nitrate media. Reduction of Eu^{3+} in aqueous chloride media remained colorless, but reduction of Eu^{3+} in aqueous nitrate media yielded a yellow-orange solution. UV-VIS absorption spectra of Eu^{2+} in both media showed significant differences. It was suggested that the change in color might be linked to the formation of Eu^{2+}–nitrate charge transfer complexes, as the color disappeared readily upon acidification and faded gradually upon exposure to the air. XANES and magnetic susceptibility measurements pointed out that a reduction time of *ca.* 2 h is required to attain a high reduction ratio for the parameters investigated. The ability to stabilize divalent europium in aqueous nitrate media is appealing to new developments within coordination and lanthanide chemistry.

In this dissertation, the ability to stabilize Eu^{2+} in aqueous nitrate media was used as a basis for the separation of europium and samarium. Reduction of Eu^{3+} to Eu^{2+} severely changed the chemical properties of europium, by which separation from samarium becomes less challenging. Because of the high sensitivity of Eu^{2+} towards acidity, the use of acidic extractants was excluded. Therefore, the extraction approaches were limited to the use of neutral and basic extractants, and were studied in detail in Chapter 4. The separation possibilities for Sm^{3+} and Eu^{2+} were studied in parallel for both nitrate and chloride feed solutions. The size-selective DCH18C6 crown ether dissolved in [A336][NO_3] was investigated as neutral extractant to selectively extract Eu^{2+}. Significant amounts of Eu^{2+} could be extracted by the crown ether using high

nitrate salt concentrations. This approach, however, did not result in high separation efficiencies as Sm^{3+} was extracted concurrently by the ionic liquid. Consequently, the basic extractant properties of neat [A336][NO_3] were deployed to selectively extract Sm^{3+}, leaving behind Eu^{2+} in the aqueous feed solution. Thus, the high nitrate salt concentration ensured a high stability of Eu^{2+} in the aqueous feed solution, and functioned as the driving force for the salting out of Sm^{3+} to the ionic liquid. Similar extraction experiments making use of aqueous chloride solutions turned out to be consistently less efficient. Additionally, any Zn^{2+} ions originating from the chemical reduction method could not be extracted from nitrate media, whereas they would be extracted very efficiently from chloride media. Therefore, the separation approach making use of aqueous nitrate media showed to have high potential for efficient separation of Eu^{2+} and Zn^{2+} from Sm^{3+}. By extension, this separation method can be considered to isolate Eu^{2+} from any Ln^{3+} as all trivalent lanthanide ions have similar chemical properties. The separation strategy might also be applied in applications other than medical radiolanthanide purification, like the recovery of europium in industrial processes.

The possibilities to convert the promising solvent extraction method into an extraction chromatography method were explored in Chapter 5. The [A336][NO_3] ionic liquid was immobilized onto an inert porous polymeric support in formation of a *supported ionic liquid phase* (SILP). The impregnation of [A336][NO_3] was investigated, and the SILP was fully characterized using different analysis methods, and proved to be successful. However, these characterization methods also pointed out that the viscous ionic liquid covered and clogged the pores of the solid support. Consequently, only the outer surface of the SILP sphere was accessible for extraction. The smaller particle size and larger specific surface area of commercially available TEVA particles proved to be more efficient in extraction of Sm^{3+} in comparison with the self-made SILP particles. Subsequent extraction chromatography experiments using TEVA particles as column packing material proved their ability to separate Sm^{3+} and Eu^{2+}. Like in the solvent extraction method, Sm^{3+} could be selectively extracted to the ionic liquid layer using a concentrated nitrate salt solution, whereas Eu^{2+} remained in the aqueous mobile phase. Eu^{2+} was not retained by the TEVA particles and eluted in the first fractions. Sm^{3+} could be easily and quantitatively recovered from the loaded column by using water as the mobile phase, *i.e.* decreasing the salt concentration in the extraction system. The low nitrate salt concentration in the samarium rich fractions can be considered advantageous for further radiopharmaceutical processing. Using the parameters investigated, about 85 % of the initial europium was removed from samarium in a single run and a short period of time. This result clearly showed the feasibility to separate Sm^{3+} and Eu^{2+} using SILPs in an extraction chromatography method, and looks promising for being applied in the purification of medical

^{153}Sm.

Chapter 7

Outlook

Based on the separation approach presented in this dissertation, the extraction chromatography method can be further developed and optimized towards actual application in ^{153}Sm purification. Increase of the column capacity by varying the column dimensions is required for being able to extract all Sm^{3+} present in target material. After all, it would be beneficial to be able to handle the entire target at once in a single run, limiting the amount of process steps and possible contamination risks. Additionally, the limited half-life of ^{153}Sm does not allow for long purification times, and requires a fast and efficient method.

The ability to remotely operate the separation system is of high importance in radiochemistry when handling materials with high activities. A remote-controlled separation system allows proper shielding of the setup (*e.g.* in a hotcell), and limits the dose rate to which the operator is exposed. Therefore, automation of the full process for the development of a remote-controlled separation system is another topic of investigation. Besides, automation might also increase the separation efficiency and yield of the separation method. The reduction of Eu^{3+} and transfer of the feed solution to the column require special attention. Automation of the electrolytic reduction of Eu^{3+} can be a first step in this direction, where the use of a flow cell can be studied. The use of a flow cell for electrolytic reduction also allows for online follow-up of the reduction ratio and an automated feed of the extraction column. Chemical reduction methods are harder to automate and control. Moreover, chemical reduction methods introduce additional impurities that have to be removed and monitored for radiopharmaceutical purposes. Although the separation method investigated in this dissertation showed to be able to take care of the Zn^{2+} impurities, it is always more beneficial to avoid introduction of these impurities in first place.

The effect of applying an irradiated target to the TEVA particles can also be studied in more detail. At first, a target with trace amounts of active material can be used to check the viability of the method. Radioactive tracers can be easily monitored using various radiochemical analysis techniques (*e.g.* γ spectrometry). After positive evaluation, the activities can be gradually increased to arrive at activities representative for an actual irradiated target for medical applications. This way, the effect of radiation on extraction and separation efficiency can be studied.

Radiation resistivity of the TEVA particles can also be assessed by means of γ irradiation experiments, after which the performance of the TEVA particles can be fully investigated. Also formation of any radiolysis products originating from the ionic liquid layer or the polymeric support of the TEVA particles can be evaluated. Harmful radiolysis products are not allowed in the final radiopharmaceutical product, and thus have to be accounted for in the purification protocol. Such γ irradiation experiments can be conducted in dedicated irradiation facilities making use of a ^{60}Co γ radiation source, like the Brigitte or Rita irradiation facilities at BR2 (SCK•CEN). After dose calibration of the irradiation facility for specific sample positions, the total absorbed dose that the TEVA particles have received can be determined.

The above mentioned development and optimization possibilities are currently being explored, with the highest focus on increase of column capacity and automation of the electrolytic reduction of Eu^{3+} by the use of a flow cell.

The approach of changing the oxidation state of one of the lanthanides prior to a separation step proved to be an efficient strategy in separation of the samarium-europium lanthanide couple. The same approach can also be explored for other lanthanide couples, and can also find its application in medical radiolanthanide purification. In the lanthanide series, Yb^{3+} can be reduced to its divalent state, whereas Ce^{3+} and Tb^{3+} can be oxidized to their tetravalent state. The ability to reduce Yb^{3+} to its divalent state opens perspectives for the isolation of Lu^{3+} from Yb^{2+} in scope of the production of non-carrier-added produced ^{177}Lu *via* (n,γ) irradiation. Over the last decades, the latter became one of the most important radionuclides in current nuclear medicine. With mixed success, many researchers have tried to find efficient separation methods for the ytterbium-lutetium couple. The reduction of Yb^{3+} is, however, challenging as Yb^{2+} is readily oxidized by H_2O. Therefore, aqueous solutions cannot be used, and solvometallurgical techniques will have to be deployed. Development of such a non-aqueous separation process will become topic of a future research project. Oxidation of Ce^{3+} for lanthanide separation was already widely explored. In Chapter 1, its application was mentioned as an example for isolation of the medical ^{143}Pr. The oxidation of Tb^{3+} is much less studied to current date as Tb^{4+} also faces some challenges towards stability. Nevertheless, preliminary

results within an ongoing research project look promising, and might form the basis for further developments towards an efficient separation method for the isolation of the medical ^{161}Tb from its ^{160}Gd target material.

This dissertation focused primarily on radiochemical separation techniques for medical radiolanthanides produces *via* (n,γ) irradiation in a nuclear research reactor. Currently, this production method is still the most efficient technique, and supplies the vast majority of radionuclides being used in nuclear medicine. However, the number of medium to high flux nuclear research reactors in the world is very limited, which might restrict the accessibility of radionuclides in some parts of the world. Therefore, the use of other production techniques are being investigated, opening the possibility to also generate different radionuclides with different decay characteristics. In particular, particle accelerators (*e.g.* MEDICIS-ISOLDE at CERN and MINERVA-MYRRHA at SCK•CEN) are being looked at to produce various medical radionuclides, including several radiolanthanides. Additionally, radionuclides with different properties complementary to the ones produced in a nuclear research reactor could become available. This way, multiple radionuclides can be used in tandem in a radiopharmaceutical to serve multiple purposes at once. The ^{149}Tb-^{152}Tb-^{155}Tb-^{161}Tb quadruplet already showed high potential for combining PET and SPECT imaging with α and β^- therapy. Separation techniques developed for the isolation and purification of nuclear-reactor-produced radiolanthanides might also find their application in isolation and purification of radiolanthanides produced *via* these alternative production routes. Accordingly, it is clear that further development and optimization towards efficient separation processes for (radio-)lanthanides is still of high importance and far from being complete.

The approaches to isolate europium from samarium presented within the framework of this dissertation can find their use in fields other than medical radiolanthanide processing. Europium is still being used in some high-technological applications. Therefore, development of more efficient processes to recover europium from primary and secondary resources is still of high relevance. The separation methods developed in this dissertation are not solely applicable on the separation of the samarium-europium couple, but can be extended to the isolation of europium from any other rare earth element. Additionally, existing separation processes making use of molecular solvents (*e.g. n*-dodecane, *n*-octanol, kerosene) and different types of extractants (*e.g.* HDEHP, TODGA) can make use of the ability to reduce Eu^{3+} and to stabilize Eu^{2+} in aqueous nitrate media. It was already shown that the extraction of trivalent rare earth elements is more efficient when making use of nitrate media. Also, the separation approach making use of a crown ether as size selective extractant for the extraction of Eu^{2+} to the organic phase can be tested using a conventional molecular solvent. This way, the basic extractant properties of the ionic liquid

are excluded, *i.e.* trivalent rare earth ions, like Sm^{3+}, will not be extracted to the organic phase. This latter approach can also be converted to an extraction chromatography method as crown ether-based resins for the isolation of Sr^{2+} are already commercially available, (*e.g.* SR-resins).

Chapter 8

Health, safety and environment

The experimental work performed within the framework of this PhD dissertation was conducted partially in the laboratories of the Chem&Tech core facilities at KU Leuven and partially in the laboratories of SCK•CEN. Working in a chemical environment requires awareness of very specific risks connected to the work conducted. Both KU Leuven and SCK•CEN require people that work in these environments to follow some strict guidelines, as safety, health and environment prevail in both institutes. These guidelines include the normal aspects of industrial safety and common lab practice, but also include additional regulations depending on the specific tasks to be performed by the researcher. Several introduction sessions and training courses were followed to raise awareness of the possible risks.

At KU Leuven, the training session *Safety in the Lab* organized by the Health, Safety and Environment (HSE) department was followed at the start of the research project. Additional guidelines applying to the laboratories of Chem&Tech were introduced by the local HSE officer. Personal protection equipment, including lab coat, safety goggles and gloves, was used whenever lab work was performed. Working with hazardous chemicals was preceded by evaluation of the potential risks making use of dedicated risk analysis assessments. Risks related to the experimental setup, the used chemicals and final waste disposal were considered. These risk analysis assessments were approved by the supervisor and the HSE department prior to performance of the experiments. Within the framework of this dissertation, no special clearance by the HSE department for the use of any compound was needed. All experiments conducted

at KU Leuven comprised the use of stable isotopes, *i.e.* no radioactive material was treated in KU Leuven laboratories. General and specific instructions to handle potentially hazardous situations could be found *via* the personal HSE file. Whenever required, experiments were performed in a fume hood. Different waste fractions originating from the experiments were collected in dedicated, color coded containers.

Working in the laboratories of SCK•CEN, *i.e.* the Belgian Nuclear Research Institute, required several additional training courses. Large parts of the chemistry building are designated as controlled or supervised areas dedicated to the handling of radioactive materials. For this reason, special regulations and alarms apply for which a dedicated training had to be followed and a time-limited license to enter these areas was granted. Entering the controlled and supervised areas also implies the use of a personal dosimeter (thermo-luminescence type, TLD), and is regulated by law. The personal TLD is read out on a monthly basis by an internal, licensed service. Additionally, the PhD candidate was subjected to a whole-body-count to determine the background radiation on a yearly basis and a blood value assessment every six months. Dedicated training sessions were followed, including an extensive five-day course on radiation protection and a course on working in fume hoods and glove boxes. Different precautions were listed and summarized in full risk analysis assessment prior to the start of an experiment, identifying all possible risks and properties of any hazardous compounds.

Work related to the manipulation of radioactive compounds is subjected to the *as low as reasonably achievable* (ALARA) principle, which implies that exposure of the researcher to ionizing radiation is minimized as much as reasonably achievable. Measures to limit the dose to the researcher and to meet the ALARA principle include deployment of radiation shielding, minimization of the time spent in the vicinity of radioactive sources, enlargement of the distance to possible radioactive sources, and selection of radioactive sources with the lowest possible activity. The experiments conducted in this research could largely be performed by making use of lanthanide salts containing stable isotopes only. This allowed the researcher to conduct optimization experiments in a normal chemical laboratory without taking additional precautions. Only the experiments were the performance of TEVA resin is tested with radioactive tracers require special attention.

The lipophilicity of the hydrophobic ionic liquids considered in this research topic required special attention because of the possible toxicological effect on living organisms, including the human body. However these effects are not fully assessed yet, it is already known that hydrophobic ionic liquids are able to enter, and possibly damage or destroy, the phospholipid bilayer of the cell membranes. Care must be taken to properly wear the personal protection

equipment whenever handling these ionic liquids. Because of the high viscosity of the quaternary ammonium ionic liquids, positive displacement pipettes were used for safe transfer.

Bibliography

[1] F. F. Knapp, A. Dash, Radiopharmaceuticals for therapy, Springer, 2016.

[2] World Nuclear Association, Radioisotopes in Medicine, `http://www.world-nuclear.org/information-library/non-power-nuclear-applications/radioisotopes-research/radioisotopes-in-medicine`, (Accessed: 2018-05-14).

[3] Ad hoc Interservice Group on Sufficiency in Supply of Radioisotopes for Medical Use, Preliminary report on supply of radioisotopes for medical use and current developments in nuclear medicine, Technical Report, European Commission, 2009.

[4] P. J. Blower, A nuclear chocolate box: the periodic table of nuclear medicine, *Dalton Transactions* 44 (2015) 4819–4844.

[5] S. M. Qaim, Nuclear data for production and medical application of radionuclides: Present status and future needs, *Nuclear Medicine and Biology* 44 (2017) 31–49.

[6] C. S. Cutler, C. J. Smith, G. J. Ehrhardt, T. T. Tyler, S. S. Jurisson, E. Deutsch, Current and potential therapeutic uses of lanthanide radioisotopes, *Cancer Biotherapy and Radiopharmaceuticals* 15 (2000) 531–545.

[7] D. Nayak, S. Lahiri, Application of radioisotopes in the field of nuclear medicine, *Journal of Radioanalytical and Nuclear Chemistry* 242 (1999) 423–432.

[8] T. Das, M. R. A. Pillai, Options to meet the future global demand of radionuclides for radionuclide therapy, *Nuclear Medicine and Biology* 40 (2013) 23–32.

[9] F. Rösch, Radiolanthanides in endoradiotherapy: An overview, *Radiochimica Acta* 95 (2007) 303–311.

[10] A. J. Amoroso, I. A. Fallis, S. J. A. Pope, Chelating agents for radiolanthanides: Applications to imaging and therapy, *Coordination Chemistry Reviews* 340 (2017) 198–219.

[11] R. D. Teo, J. Termini, H. B. Gray, Lanthanides: Applications in cancer diagnosis and therapy, *Journal of Medicinal Chemistry* 59 (2016) 6012–6024.

[12] S. Bhattacharyya, M. Dixit, Metallic radionuclides in the development of diagnostic and therapeutic radiopharmaceuticals, *Dalton Transactions* 40 (2011) 6112–6128.

[13] A. Chylewska, M. Biedulska, P. Sumczynski, M. Makowski, Metallopharmaceuticals in therapy - a new horizon for scientific research, *Current Medicinal Chemistry* 25 (2018) 1729–1791.

[14] I. G. Finlay, M. D. Mason, M. Shelley, Radioisotopes for the palliation of metastatic bone cancer: a systematic review, *The Lancet Oncology* 6 (2005) 392–400.

[15] S. Ferreira, I. Dormehl, M. F. Botelho, Radiopharmaceuticals for bone metastasis therapy and beyond: A voyage from the past to the present and a look to the future, *Cancer Biotherapy and Radiopharmaceuticals* 27 (2012) 535–551.

[16] W. A. Volkert, T. J. Hoffman, Therapeutic Radiopharmaceuticals, *Chemical Reviews* 99 (1999) 2269–2292.

[17] S. M. Qaim, The present and future of medical radionuclide production, *Radiochimica Acta* 100 (2012) 635–651.

[18] International Atomic Energy Agency, Research Reactor Database, `https://nucleus.iaea.org/RRDB`, (Accessed: 2018-06-21).

[19] G. C. Krijger, B. Ponsard, M. Harfensteller, H. T. Wolterbeek, J. W. F. Nijsen, The necessity of nuclear reactors for targeted radionuclide therapies, *Trends in Biotechnology* 31 (2013) 390–396.

[20] B. Ponsard, Production of radioisotopes in the BR2 high-flux reactor for applications in nuclear medicine and industry, *Journal of Labelled Compounds and Radiopharmaceuticals* 50 (2007) 333–337.

[21] H. Uusijärvi, P. Bernhardt, F. Rösch, H. R. Maecke, E. Forssell-Aronsson, Electron- and positron-emitting radiolanthanides for therapy: Aspects of dosimetry and production, *The Journal of Nuclear Medicine* 47 (2006) 807–814.

[22] M. Neves, A. Kling, R. M. Lambrecht, A. J. Blocky, Utilization of low power research reactors for production of therapeutic radiopharmaceuticals, in: Proceedings of International Symposium on Research Reactor Utilization, Safety and Management, IAEA-SM-360/10, IAEA.

[23] B. L. Zhuikov, Production of medical radionuclides in Russia: Status and future — A review, *Applied Radiation and Isotopes* 84 (2014) 48–56.

[24] D. Ma, A. R. Ketring, G. J. Ehrhardt, W. Jia, Production of radiolanthanides and radiotherapy research at MURR, *Journal of Radioanalytical and Nuclear Chemistry-Articles* 206 (1996) 119–126.

[25] L. Safavi-Tehrani, G. E. Miller, M. Nilsson, Production of high specific activity radiolanthanides for medical purposes using the UC Irvine TRIGA reactor, *Journal of Radioanalytical and Nuclear Chemistry* 303 (2015) 1099–1103.

[26] C. S. Cutler, H. Engelbrecht, M. Embree, S. Wilder, M. Cantorias, A. Ketring, Comparison of methods to produce high specific activity radiolanthanides, *Transactions of the American Nuclear Society* 98 (2008) 907–907.

[27] G. T. Ehrhardt, A. R. Ketring, C. S. Cutler, Radioisotope radiotherapy research and achievements at the University of Missouri Research Reactor, *Czechoslovak Journal of Physics* 53 (2003) A707–A712.

[28] Industrial Applications and Chemistry Section, Manual for reactor produced radioisotopes, Technical Report IAEA-TECDOC-1340, International Atomic Energy Agency, 2003.

[29] M. Neves, A. Kling, R. M. Lambrecht, Radionuclide production for therapeutic radiopharmaceuticals, *Applied Radiation and Isotopes* 57 (2002) 657–664.

[30] J. G. Tracy, W. S. Aaron, Stable isotope enrichment - current and future potential, *Nuclear Instruments and Methods in Physics Research Section A: Accelerators, Spectrometers, Detectors and Associated Equipment* 334 (1993) 45–50.

[31] SCK•CEN, Belgian Reactor 2 - BR2, `http://science.sckcen.be/en/Facilities/BR2`, (Accessed: 2018-06-26).

[32] F. Marques, A. Paulo, M. P. Campello, S. Lacerda, R. F. Vitor, L. Gano, R. Delgado, I. Santos, Radiopharmaceuticals for targeted radiotherapy, *Radiation Protection Dosimetry* 116 (2005) 601–604.

[33] F. Zoller, M. Eisenhut, U. Haberkorn, W. Mier, Endoradiotherapy in cancer treatment — Basic concepts and future trends, *European Journal of Pharmacology* 625 (2009) 55–62.

[34] S. Maschauer, O. Prante, Radiopharmaceuticals for imaging and endoradiotherapy of neurotensin receptor-positive tumors, *Journal of Labelled Compounds and Radiopharmaceuticals* 61 (2018) 309–325.

[35] A. J. Amoroso, S. J. A. Pope, Using lanthanide ions in molecular bioimaging, *Chemical Society Reviews* 44 (2015) 4723–4742.

[36] K. Binnemans, Lanthanide-based luminescent hybrid materials, *Chemical Reviews* 109 (2009) 4283–4374.

[37] S. Faulkner, S. J. A. Pope, B. P. Burton-Pye, Lanthanide complexes for luminescence imaging applications, *Applied Spectroscopy Reviews* 40 (2005) 1–31.

[38] S. A. Cotton, Establishing coordination numbers for the lanthanides in simple complexes, *Comptes Rendus Chimie* 8 (2005) 129–145.

[39] W. A. Volkert, W. F. Goeckeler, G. J. Ehrhardt, A. R. Ketring, Therapeutic radionuclides: Production and decay property consideration, *Journal of Nuclear Medicine* 32 (1991) 174–185.

[40] S. C. Srivastava, Bone-seeking therapeutic radiopharmaceuticals, *Brazilian Archives of Biology and Technology* 45 (2002) 45–55.

[41] S. Banerjee, M. R. A. Pillai, F. F. Knapp, Lutetium-177 therapeutic radiopharmaceuticals: Linking chemistry, radiochemistry, and practical applications, *Chemical Reviews* 115 (2015) 2934–2974.

[42] R. Chakravarty, S. Goel, H. F. Valdovinos, R. Hernandez, H. Hong, R. J. Nickles, W. Cai, Matching the decay half-Life with the biological half-life: Immuno-PET imaging with ^{44}Sc-labeled cetuximab fab fragment, *Bioconjugate Chemistry* 25 (2014) 2197–2204.

[43] N. Schieda, J. I. Blaichman, A. F. Costa, R. Glikstein, C. Hurrell, M. James, P. Jabehdar Maralani, W. Shabana, A. Tang, A. Tsampalieros, C. B. van der Pol, S. Hiremath, Gadolinium-based contrast agents in kidney disease: A comprehensive review and clinical practice guideline issued by the Canadian Association of Radiologists, *Canadian Journal of Kidney Health and Disease* 5 (2018) 1–17.

[44] J. I. Silberzweig, M. Chung, Removal of gadolinium by dialysis: Review of different strategies and techniques, *Journal of Magnetic Resonance Imaging* 30 (2009) 1347–1349.

[45] G. R. Choppin, J.-O. Liljenzin, J. Rydberg, C. Ekberg, Radiochemistry & Nuclear Chemistry, Elsevier, 2013.

[46] S. A. Enger, T. Hartman, J. Carlsson, H. Lundqvist, Cross-fire doses from β^- emitting radionuclides in targeted radiotherapy. A theoretical study based on experimentally measured tumor characteristics, *Physics in Medicine & Biology* 53 (2008) 1909–1920.

[47] E. D. Read, P. Eu, P. J. Little, T. J. Piva, The status of radioimmunotherapy in CD20+ non-Hodgkin's lymphoma, *Targeted Oncology* 10 (2015) 15–26.

[48] D. Brady, J. O'Sullivan, K. Prise, What is the role of the bystander response in radionuclide therapies?, *Frontiers in Oncology* 3 (2013) 1–5.

[49] G. T. Seaborg, Overview of the actinide and lanthanide (the f) elements, *Radiochimica Acta* 61 (1993) 115–122.

[50] J. K. Marsh, The separation of the lanthanons (rare-earth elements), *Quarterly Reviews, Chemical Society* 1 (1947) 126–143.

[51] S. L. Bertha, G. R. Choppin, Hydration thermodynamics of the lanthanide ions, *Inorganic Chemistry* 8 (1969) 613–617.

[52] S. Lahiri, D. Nayak, M. Nandy, N. R. Das, Separation of carrrier free lutetium produced in proton activated ytterbium with HDEHP, *Applied Radiation and Isotopes* 49 (1998) 911–913.

[53] M. Bottrill, L. Kwok, N. J. Long, Lanthanides in magnetic resonance imaging, *Chemical Society Reviews* 35 (2006) 557–571.

[54] K. L. Nash, A review of the basic chemistry and recent developments in trivalent f-elements separations, *Solvent Extraction and Ion Exchange* 11 (1993) 729–768.

[55] K. L. Nash, M. P. Jensen, Analytical-scale separations of the latnhanides: A review of techniques and fundamentals, *Separation Science and Technology* 36 (2001) 1257–1282.

[56] G. R. Choppin, J. A. Chopoorian, Complexes of the lanthanide elements with α-hydroxy carboxylate ligands, *Journal of Inorganic and Nuclear Chemistry* 22 (1961) 97–113.

[57] H. L. Smith, D. C. Hoffman, Ion-exchange separations of the lanthanides and actinides by elution with ammonium alpha-hydroxy-isobutyrate, *Journal of Inorganic and Nuclear Chemistry* 3 (1956) 243–247.

[58] K. L. Nash, R. E. Barrans, R. Chiarizia, M. L. Dietz, M. P. Jensen, P. G. Rickert, B. A. Moyer, P. V. Bonnesen, J. C. Bryan, R. A. Sachleben, Fundamental investigations of separations science for radioactive materials, *Solvent Extraction and Ion Exchange* 18 (2000) 605–631.

[59] E. P. Horwitz, D. R. McAlister, A. H. Bond, R. E. Barrans, J. M. Williamson, A process for the separation of ^{177}Lu from neutron irradiated ^{176}Yb targets, *Applied Radiation and Isotopes* 63 (2005) 23–36.

[60] S. Siekierski, I. Fidelis, Extraction chromatography of lanthanides, volume 2, Elsevier, pp. 226–253.

[61] D. Qi, Ion-Exchange and Extraction Chromatography Separation of Rare Earth Elements, Hydrometallurgy of REEs, Elsevier, pp. 631–669.

[62] D. Qi, Chemical Separation Method, Hydrometallurgy of REEs, Elsevier, pp. 671–741.

[63] C. Marie, B. Hiscox, K. L. Nash, Characterization of HDEHP-lanthanide complexes formed in a non-polar organic phase using ^{31}P NMR and ESI-MS, *Dalton Transactions* 41 (2012) 1054–1064.

[64] K. V. Vimalnath, M. K. Das, M. Venkatesh, N. Ramamoorthy, Prospects and problems in the production of ^{143}Pr for radionuclide therapy applications, *Radiochimica Acta* 93 (2005) 419–426.

[65] M. Kubota, Preparation of high purity praseodymium-143 from neutron irradiated cerium oxide by cation-exchange separation, *Journal of Nuclear Science and Technology* 13 (1976) 492–496.

[66] D. F. Peppard, G. W. Mason, S. W. Moline, The use of dioctyl phosphoric acid extraction in the isolation of carrier-free ^{90}Y, ^{140}La, ^{144}Ce, ^{143}Pr, and ^{144}Pr, *Journal of Inorganic and Nuclear Chemistry* 5 (1957) 141–146.

[67] M. Gras, N. Papaiconomou, E. Chainet, F. Tedjar, I. Billard, Separation of cerium(III) from lanthanum(III), neodymium(III) and praseodymium(III) by oxidation and liquid-liquid extraction using ionic liquids, *Separation and Purification Technology* 178 (2017) 169–177.

[68] M. R. Lewis, J. Zhang, F. Jia, N. K. Owen, C. S. Cutler, M. F. Embree, J. Schultz, L. J. Theodore, A. R. Ketring, S. S. Jurisson, D. B. Axworthy, Lu-DOTA-biotin pretargeted by CC49 scFv-streptavidin fusion protein in xenograft-bearing nude mice, *Nuclear Medicine and Biology* 31 (2004) 213–223.

[69] H. Mohsin, F. Jia, G. Sivaguru, M. J. Hudson, T. D. Shelton, T. J. Hoffman, C. S. Cutler, A. R. Ketring, P. S. Athey, J. Simón, R. K. Frank, S. S. Jurisson, M. R. Lewis, Radiolanthanide-labeled monoclonal antibody CC49 for radioimmunotherapy of cancer: Biological comparison of DOTA conjugates and ^{149}Pm, ^{166}Ho, and ^{177}Lu, *Bioconjugate Chemistry* 17 (2006) 485–492.

[70] M. F. Embree, B. Ochoa, K. Bailey, A. Ketring, T. Hoffman, N. Owen, H. R. Maecke, C. S. Cutler, Production and evaluation of Pm-149-DOTATOC as a radiotherapy agent, *Journal of Nuclear Medicine* 43 (2002) 374P–374P.

[71] F. Hu, C. S. Cutler, T. Hoffman, G. Sieckman, W. A. Volkert, S. S. Jurisson, Pm-149 DOTA bombesin analogs for potential radiotherapy: *in vivo* comparison with Sm-153 and Lu-177 labeled DO3A-amide-β-ala-BBN(7–14)NH_2, *Nuclear Medicine and Biology* 29 (2002) 423–430.

[72] W. P. Li, C. J. Smith, C. S. Cutler, A. R. Ketring, S. S. Jurisson, Development of receptor-based radiopharmaceuticals using carrier-free promethium-149: Syntheses, *in vitro* stability studies, and *in vivo* biodistribution studies of DTPA, DOTA, and DTPA-octreotide complexes, *Journal of Nuclear Medicine* 41 (2000) 246P–246P.

[73] E. B. Nieschmidt, V. R. Potnis, L. D. Ellsworth, C. E. Mandeville, Nuclear states of ^{149}Pm, *Nuclear Physics* 72 (1965) 236–240.

[74] F. Monroy-Guzman, F. J. Barreiro, E. J. Salinas, A. L. V. Treviño, Radiolanthanides device production, *World Journal of Nuclear Science and Technology* 05 (2015) 111–119.

[75] F. Monroy-Guzman, E. Jaime Salinas, Separation of micro-macrocomponent systems: ^{149}Pm–Nd, ^{161}Tb–Gd, ^{166}Ho–Dy and ^{177}Lu–Yb by extraction chromatography, *Journal of the Mexican Chemical Society* 59 (2015) 143–150.

[76] T. Das, S. Banerjee, Radiopharmaceuticals for metastatic bone pain palliation: available options in the clinical domain and their comparisons, *Clinical & Experimental Metastasis* 34 (2017) 1–10.

[77] P. Anderson, R. Nunez, Samarium lexidronam (Sm-153-EDTMP): skeletal radiation for osteoblastic bone metastases and osteosarcoma, *Expert Review of Anticancer Therapy* 7 (2007) 1517–1527.

[78] J. M. van Dodewaard-de Jong, D. E. Oprea-Lager, L. Hooft, J. M. H. de Klerk, H. J. Bloemendal, H. M. W. Verheul, O. S. Hoekstra, A. J. M. van den Eertwegh, Radiopharmaceuticals for palliation of bone pain in

patients with castration-resistant prostate cancer metastatic to bone: A systematic review, *European Urology* 70 (2016) 416–426.

[79] S. P. Fricker, The therapeutic application of lanthanides, *Chemical Society Reviews* 35 (2006) 524–533.

[80] W. F. Goeckeler, B. Edwards, W. A. Volkert, R. A. Holmes, J. Simon, D. Wilson, Skeletal localization of samarium-153 chelates: Potential therapeutic bone agents, *Journal of Nuclear Medicine* 28 (1987) 495–504.

[81] W. F. Goeckeler, D. E. Troutner, W. A. Volkert, B. Edwards, J. Simon, D. Wilson, Sm-153 radiotherapeutic bone agents, *Nuclear Medicine and Biology* 13 (1986) 479–482.

[82] J. C. Lattimer, J. Louis A. Corwin, J. Stapleton, W. A. Volkert, G. J. Ehrhardt, A. R. Ketring, S. K. Anderson, J. Simon, W. F. Goeckeler, Clinical and clinicopathologic response of canine bone tumor patients to treatment with samarium-153-EDTMP, *The Journal of Nuclear Medicine* 31 (1990) 1316–1325.

[83] H. L. Atkins, Overview of nuclides for bone pain palliation, *Applied Radiation and Isotopes* 49 (1998) 277–283.

[84] J. Simon, K. R. Frank, D. A. Wilson, High purity therapeutic bone agents, US Patent 2016/0250359, 2016.

[85] N. A. A. Hashikin, C. H. Yeong, B. J. J. Abdullah, K. H. Ng, L. Y. Chung, R. Dahalan, A. C. Perkins, Samarium-153 Labelled Microparticles For Targeted Radionuclide Therapy Of Liver Tumor, *World Congress on Medical Physics and Biomedical Engineering* (2015) 471–474.

[86] M. Nikzad, A. R. Jalilian, S. Shirvani-Arani, M. Arabieh, S. Shanesaz-zadeh, H. Golchoobian, Sm-zoledronate complex as a possible bone pain palliative agent, *Iranian Journal of Nuclear Medicine* 25 (2017) 81–91. 1681-2824.

[87] S. Z. Islami-Rad, M. Shamsaei, R. Gholipour-Peyvandi, M. Ghannadi-Maragheh, Sm target irradiation, *Radiochemistry* 53 (2011) 642–645.

[88] R. Chakravarty, S. Chakraborty, M. S. Khan, R. Ram, H. D. Sarma, A. Dash, An electrochemical approach for removal of radionuclidic contaminants of Eu from ^{153}Sm for effective use in metastatic bone pain palliation, *Nuclear Medicine and Biology* 58 (2018) 8–19.

[89] J. A. Kalef-Ezra, S. T. Valakis, S. Pallada, Samarium-153 EDTMP for metastatic bone pain palliation: The impact of europium impurities, *Physica Medica* 31 (2015) 104–107.

[90] N. Ramamoorthy, P. Saraswathy, M. K. Das, K. S. Mehra, M. Ananthakrishnan, Sm for radionuclide therapy, *Nuclear Medicine Communications* 23 (2002) 83–89.

[91] M. Bourgeois, H. Isnard, A. Gourgiotis, G. Stadelmann, C. Gautier, S. Mialle, A. Nonell, F. Chartier, Sm isotope composition and Sm/Eu ratio determination in an irradiated Eu-153 sample by ion exchange chromatography-quadrupole inductively coupled plasma mass spectrometry combined with double spike isotope dilution technique, *Journal of Analytical Atomic Spectrometry* 26 (2011) 1660–1666.

[92] M. Van de Voorde, K. Van Hecke, K. Binnemans, T. Cardinaels, Separation of samarium and europium by solvent extraction with an undiluted quaternary ammonium ionic liquid: Towards high-purity medical samarium-153, *RSC Advances* 8 (2018) 20077–20086.

[93] B. Van den Bogaert, D. Havaux, K. Binnemans, T. Van Gerven, Photochemical recycling of europium from Eu/Y mixtures in red lamp phosphor waste streams, *Green Chemistry* 17 (2015) 2180–2187.

[94] B. Van den Bogaert, L. Van Meerbeeck, K. Binnemans, T. Van Gerven, Influence of irradiance on the photochemical reduction of europium(III), *Green Chemistry* 18 (2016) 4198–4204.

[95] S.-C. Li, S.-C. Kim, C.-S. Kang, C.-J. Kim, C.-J. Kang, Separation of samarium, europium and gadolinium in high purity using photochemical reduction-extraction chromatography, *Hydrometallurgy* 178 (2018) 181–187.

[96] J. S. Preston, A. C. du Preez, The separation of europium from a middle rare earth concentrate by combined chemical reduction, precipitation and solvent-extraction methods, *Journal of Chemical Technology and Biotechnology* 65 (1996) 93–101.

[97] E. I. Onstott, The separation of europium from samarium by electrolysis, *Journal of the American Chemical Society* 77 (1955) 2129–2132.

[98] S. A. Sayed, K. A. Rabie, I. E. Salama, Studies on europium separation from a middle rare earth concentrate by *in situ* zinc reduction technique, *Separation and Purification Technology* 46 (2005) 145–154.

[99] L. Jelinek, Y. Z. Wei, T. Arai, M. Kumagai, Study on separation of Eu(II) from trivalent rare earths *via* electro-reduction and ion exchange, *Journal of Alloys and Compounds* 451 (2008) 341–343.

[100] L. Jelinek, Y. Z. Wei, T. Arai, M. Kumagai, Selective Eu(III) electroreduction and subsequent separation of Eu(II) from rare earths(III) *via* HDEHP impregnated resin, *Solvent Extraction and Ion Exchange* 25 (2007) 503–513.

[101] J. M. Schwantes, R. Sudowe, H. Nitsche, D. C. Hoffman, Applications of solvent extraction in the high-yield multi-process reduction/separation of Eu from excess Sm, *Journal of Radioanalytical and Nuclear Chemistry* 276 (2008) 543–548.

[102] J. K. Marsh, Rare-earth metal amalgams. Part IV. The isolation of europium, *Journal of the Chemical Society* (1943) 531–535.

[103] D. F. Peppard, E. P. Horwitz, G. W. Mason, Comparative liquid-liquid extraction behaviour of europium(II) and europium(III), *Journal of Inorganic & Nuclear Chemistry* 24 (1962) 429–439.

[104] R. Chakravarty, T. Das, A. Dash, M. Venkatesh, An electro-amalgamation approach to isolate no-carrier-added ^{177}Lu from neutron irradiated Yb for biomedical applications, *Nuclear Medicine and Biology* 37 (2010) 811–820.

[105] K. Binnemans, Lanthanides and actinides in ionic liquids, *Chemical Reviews* 107 (2007) 2592–2614.

[106] B. A. Moyer, Ion Exchange and Solvent Extraction, volume 19, CRC Press, 2010.

[107] B. J. Mincher, G. Modolo, S. P. Mezyk, Review article: The effects of radiation chemistry on solvent extraction 3: A review of actinide and lanthanide extraction, *Solvent Extraction and Ion Exchange* 27 (2009) 579–606.

[108] G. Modolo, A. Geist, M. Miguirditchian, Minor actinide separations in the reprocessing of spent nuclear fuels: Recent advances in Europe, Reprocessing and Recycling of Spent Nuclear Fuel, Woodhead Publishing, pp. 245–287.

[109] T. Vander Hoogerstraete, K. Binnemans, Highly efficient separation of rare earths from nickel and cobalt by solvent extraction with the ionic liquid trihexyl(tetradecyl) phosphonium nitrate: a process relevant to the recycling of rare earths from permanent magnets and nickel metal hydride batteries, *Green Chemistry* 16 (2014) 1594–1606.

[110] K. Larsson, K. Binnemans, Separation of rare earths by split-anion extraction, *Hydrometallurgy* 156 (2015) 206–214.

[111] K. Larsson, K. Binnemans, Separation of rare earths by solvent extraction with an undiluted nitrate ionic liquid, *Journal of Sustainable Metallurgy* 3 (2017) 73–78.

[112] B. Onghena, E. Papagni, E. R. Souza, D. Banerjee, K. Binnemans, T. Vander Hoogerstraete, Speciation of lanthanide ions in the organic phase after extraction from nitrate media by basic extractants, *RSC Advances* 8 (2018) 32044–32054.

[113] J. Grünberg, D. Lindenblatt, H. Dorrer, S. Cohrs, K. Zhernosekov, U. Köster, A. Türler, E. Fischer, R. Schibli, Anti-L1CAM radioimmunotherapy is more effective with the radiolanthanide terbium-161 compared to lutetium-177 in an ovarian cancer model, *European Journal of Nuclear Medicine and Molecular Imaging* 41 (2014) 1907–1915.

[114] S. Lehenberger, C. Barkhausen, S. Cohrs, E. Fischer, J. Grünberg, A. Hohn, U. Köster, R. Schibli, A. Türler, K. Zhernosekov, ^{177}Lu for targeted radionuclide therapy, *Nuclear Medicine and Biology* 38 (2011) 917–924.

[115] C. Müller, J. Reber, S. Haller, H. Dorrer, P. Bernhardt, K. Zhernosekov, A. Türler, R. Schibli, Direct *in vitro* and *in vivo* comparison of ^{161}Tb and ^{177}Lu using a tumour-targeting folate conjugate, *European Journal of Nuclear Medicine and Molecular Imaging* 41 (2014) 476–485.

[116] C. Champion, M. A. Quinto, C. Morgat, P. Zanotti-Fregonara, E. Hindié, Comparison between three promising β^--emitting radionuclides, ^{67}Cu, ^{47}Sc and ^{161}Tb with emphasis on doses delivered to minimal residual disease, *Theranostics* 6 (2016) 1611–1618.

[117] M. de Jong, W. A. P. Breeman, B. F. Bernard, E. J. Rolleman, L. J. Hoflande, T. J. Visser, B. Setyono-Han, W. H. Bakker, M. E. van der Pluijm, E. P. Krenning, Tb-DTPA-octreotide, a somatostatin analogue with potential for intraoperative scanning and radiotherapy, *European Journal of Nuclear Medicine* 22 (1995) 608–616.

[118] S. Haller, G. Pellegrini, C. Vermeulen, N. P. van der Meulen, U. Köster, P. Bernhardt, R. Schibli, C. Müller, Contribution of Auger/conversion electrons to renal side effects after radionuclide therapy: preclinical comparison of ^{161}Tb-folate and ^{177}Lu-folate, *EJNMMI Research* 6 (2016) 1–11.

[119] C. Müller, K. Zhernosekov, U. Köster, K. Johnston, H. Dorrer, A. Hohn, N. T. van der Walt, A. Türler, R. Schibli, Radionuclide therapy: An *in vivo* proof-of-concept study with a new receptor-targeted folate derivative, *Journal of Nuclear Medicine* 53 (2012) 1951–1959.

[120] C. B. Sledge, J. Noble, D. J. Hnatowich, R. Kramer, S. Shortkroff, Experimental Radiation Synovectomy by ^{165}Dy Ferric Hydroxide Macroaggregate, *Arthritis & Rheumatism* 20 (1977) 1334–1342.

[121] C. Pinch, A. Pilger, E. Schwameis, D. Germadnik, U. Prufert, E. Havilk, S. Lang, H. Kvaternik, J. A. Flores, P. Angelberger, A. Wanivenhaus, H. W. Rüdiger, H. Sinzinger, Radiation synovectomy by using ^{165}Dy ferric-hydroxide and oxidative DNA damage in patients with different types of arthritis, *The Journal of Nuclear Medicine* 41 (2000) 250–256.

[122] M. E. Siegel, H. J. Siegel, J. V. Luck, Radiosynovectomy's clinical applications and cost effectiveness: A review, *Seminars in Nuclear Medicine* 27 (1997) 364–371.

[123] H. C. Manjunatha, Bremsstrahlung dose of ^{165}Dy in radiosynovectomy, *Journal of Applied Clinical Medical Physics* 15 (2014) 345–355.

[124] E. Havlik, C. Pirich, J. Preitfellner, G. Karanikas, P. Schaffarich, A. Hefner, H. Sinzinger, Radiation exposure from patients treated with Dy-165-ferric hydroxide, *Nuclear Medicine Communications* 22 (2001) 79–82.

[125] C. B. Sledge, J. D. Zuckerman, M. R. Zalutsky, R. W. Atcher, S. Shortkroff, D. R. Lionberger, H. A. Rose, B. J. Hurson, P. A. Lankenner, R. J. Anderson, W. A. Bloomer, Treatment of rheumatoid synovitis of the knee with intraarticular injection of dysprosium 165-ferric hydroxide macroaggregates, *Arthritis & Rheumatism* 29 (1986) 153–159.

[126] J. F. W. Nijsen, B. A. Zonnenberg, J. R. W. Woittiez, D. W. Rook, I. A. Swildens-van Woudenberg, P. P. van Rijk, A. D. van het Schip, Holmium-166 poly lactic acid microspheres applicable for intra-arterial radionuclide therapy of hepatic malignancies: effects of preparation and neutron activation techniques, *European Journal of Nuclear Medicine* 26 (1999) 699–704.

[127] A. Bahrami-Samani, R. Bagheri, A. Jalilian, S. Shirvani-Arani, M. Ghannadi-Maragheh, M. Shamsaee, Production, quality control and pharmacokinetic studies of ^{166}Ho-EDTMP for therapeutic applications, *Scientia Pharmaceutica* 78 (2010) 423–433.

[128] K. Yavari, E. Yeganeh, H. Abolghasemi, Production and characterization of ^{166}Ho polylactic acid microspheres, *Journal of Labelled Compounds and Radiopharmaceuticals* 59 (2016) 24–29.

[129] S. W. Zielhuis, J. F. W. Nijsen, R. de Roos, G. C. Krijger, P. P. van Rijk, W. E. Hennink, A. D. van het Schip, Production of GMP-grade radioactive holmium loaded poly(l-lactic acid) microspheres for clinical application, *International Journal of Pharmaceutics* 311 (2006) 69–74.

[130] R. J. Mumper, U. Yun Ryo, M. Jay, Neutron-activated holmium-166-poly (L-lactic acid) microspheres: A potential agent for the internal radiation therapy of hepatic tumors, *Journal of Nuclear Medicine* 32 (1991) 2139–2143.

[131] S. Thompson, B. Ballard, Z. Jiang, E. Revskaya, N. Sisay, W. H. Miller, C. S. Cutler, E. Dadachova, L. C. Francesconi, ^{166}Ho and ^{90}Y labeled 6D2 monoclonal antibody for targeted radiotherapy of melanoma: Comparison with ^{188}Re radiolabel, *Nuclear Medicine and Biology* 41 (2014) 276–281.

[132] P. R. Unni, P. R. Chaudhari, M. Venkatesh, N. Ramamoorthy, M. R. A. Pillai, Preparation and bioevaluation of ^{166}Ho labelled hydroxyapatite (HA) particles for radiosynovectomy, *Nuclear Medicine and Biology* 29 (2002) 199–209.

[133] C. H. Park, Holmium-166 therapy of malignant and benign diseases, *Materials Science Forum* 315-317 (1999) 257–261.

[134] M. Norek, J. A. Peters, MRI contrast agents based on dysprosium or holmium, *Progress in Nuclear Magnetic Resonance Spectroscopy* 59 (2011) 64–82.

[135] S. Vosoughi, A. R. Jalilian, S. Shirvani-Arani, A. Bahrami-Samani, N. Salek, Preparation of Dy-166/Ho-166-chitosan as an *in vivo* generator for radiosynovectomy, *Journal of Radioanalytical and Nuclear Chemistry* 311 (2017) 1657–1664.

[136] S. Lahiri, K. J. Volkers, B. Wierczinski, Production of ^{166}Ho through $^{164}\mathrm{Dy}(n,\gamma)^{165}\mathrm{Dy}(n,\gamma)^{166}\mathrm{Dy}(\beta^-)^{166}$Ho and separation of ^{166}Ho, *Applied Radiation and Isotopes* 61 (2004) 1157–1161.

[137] G. Ferro-Flores, O. Hernández-Oviedo, C. Arteaga de Murphy, J. I. Tendilla, F. Monroy-Guzmán, M. Pedraza-López, K. Aldama-Alvarado, [^{166}Dy]Dy/^{166}Ho hydroxide macroaggregates: an *in vivo* generator system for radiation synovectomy, *Applied Radiation and Isotopes* 61 (2004) 1227–1233.

[138] S. Vosoughi, S. Shirvani-Arani, A. Bahrami-Samani, N. Salek, A. R. Jalilian, Production of no-carrier-added Ho-166 for targeted therapy purposes, *Iranian Journal of Nuclear Medicine* 25 (2017) 15–20.

[139] F. F. Knapp, S. Mirzadeh, A. L. Beets, M. Du, Production of therapeutic radioisotopes in the ORNL High Flux Isotope Reactor (HFIR) for applications in nuclear medicine, oncologyand interventional cardiology, *Journal of Radioanalytical and Nuclear Chemistry* 263 (2005) 503–509.

[140] E. Dadachova, S. Mirzadeh, R. M. Lambrecht, E. L. Hetherington, F. F. Knapp, Separation of carrier-free holmium-166 from neutron-irradiated dysprosium targets, *Analytical Chemistry* 66 (1994) 4272–4277.

[141] E. Dadachova, S. Mirzadeh, R. M. Lambrecht, E. L. Hetherington, F. F. Knapp, Separation of carrier-free ^{166}Ho from Dy_2O_3 targets by partition chromatography and electrophoresis, *Journal of Radioanalytical and Nuclear Chemistry* 199 (1995) 115–123.

[142] L. Knut, Radiosynovectomy in the therapeutic management of arthritis, *World Journal of Nuclear Medicine* 14 (2015) 10–15.

[143] R. Chakravarty, S. Chakraborty, V. Chirayil, A. Dash, Reactor production and electrochemical purification of ^{169}Er: A potential step forward for its utilization in *in vivo* therapeutic applications, *Nuclear Medicine and Biology* 41 (2014) 163–170.

[144] S. Chakraborty, T. Das, V. Chirayil, P. Lohar Sharad, D. Sarma Haladhar, Erbium-169 labeled hydroxyapatite particulates for use in radiation synovectomy of digital joints – a preliminary investigation, *Radiochimica Acta* 102 (2014) 443–450.

[145] N. Karavida, A. Notopoulos, Radiation synovectomy: An effective alternative treatment for inflamed small joints, *Hippokratia* 14 (2010) 22–27.

[146] M. Torres, E. Ayra, O. Albuerne, M. A. Montano Delgado, Absorbed dose profiles for ^{32}P, ^{90}Y, ^{188}Re, ^{177}Lu, ^{153}Sm and ^{169}Er: radionuclides used in radiosynoviortheses treatment, *Revista Española de Medicina Nuclear* 28 (2009) 188–192.

[147] J. K. Marsh, Rare-earth metal amalgams. Part III. The separation of ytterbium from its neighbours, *Journal of the Chemical Society* (1943) 8–10.

[148] T. Das, S. Chakraborty, H. D. Sarma, P. Tandon, S. Banerjee, M. Venkatesh, M. R. A. Pillai, ^{170}Tm-EDTMP: a potential cost-effective alternative to $^{89}SrCl_2$ for bone pain palliation, *Nuclear Medicine and Biology* 36 (2009) 561–568.

[149] K. Vats, T. Das, H. D. Sarma, S. Banerjee, M. R. A. Pillai, Radiolabeling, stability studies, and pharmacokinetic evaluation of thulium-170-labeled acyclic and cyclic polyaminopolyphosphonic acids, *Cancer Biotherapy and Radiopharmaceuticals* 28 (2013) 737–745.

[150] S. Shirvani-Arani, A. Bahrami-Samani, M. Meftahi, R. Jalilian Amir, M. Ghannadi-Maragheh, Production, quality control and biodistribution studies of thulium-170-labeled ethylenediamine (tetramethylene phosphonic acid), *Radiochimica Acta* 101 (2013) 37–43.

[151] A. Polyak, T. Das, S. Chakraborty, R. Kiraly, G. Dabasi, R. P. Joba, C. Jakab, J. Thuroczy, Z. Postenyi, V. Haasz, G. Janoki, G. A. Janoki, M. R. A. Pillai, L. Balogh, Thulium-170-labeled microparticles for local radiotherapy: Preliminary studies, *Cancer Biotherapy and Radiopharmaceuticals* 29 (2014) 330–338.

[152] S. Shirvani-Arani, A. Bahrami-Samani, R. Jalilian Amir, A. Shirvani-Arani, M. Ghannadi-Maragheh, Development of ^{170}Tm-DOTA-cetuximab for radioimmunotherapy, *Journal of Labelled Compounds and Radiopharmaceuticals* 55 (2012) 103–107.

[153] M. R. P. Ambikalmajan, F. K. Furn, Evolving important role of lutetium-177 for therapeutic nuclear medicine, *Current Radiopharmaceuticals* 8 (2015) 78–85.

[154] A. Dash, M. R. A. Pillai, F. F. Knapp, Production of ^{177}Lu for targeted radionuclide therapy: Available options, *Nuclear Medicine and Molecular Imaging* 49 (2015) 85–107.

[155] U. J. Park, J.-S. Lee, K. H. Choi, S. S. Nam, K. H. Yu, Lu-177 preparation for radiotherapy application, *Applied Radiation and Isotopes* 115 (2016) 8–12.

[156] S. Chakraborty, T. Das, H. D. Sarma, M. Venkatesh, S. Banerjee, Lu–DOTMP as potential agents for palliative radiotherapy of bone metastasis, *Applied Radiation and Isotopes* 66 (2008) 1196–1205.

[157] L. Sepini, D. Jansen, N. Jarvis, J. R. Zeevaart, Complexation studies of ^{177}Lu with ethylenediaminetetramethylene phosphonic acid (EDTMP) as a bone pain palliative therapeutic radiopharmaceutical, *Polyhedron* 106 (2016) 101–105.

[158] D. Máthé, L. Balogh, A. Polyák, R. Király, T. Márián, D. Pawlak, J. J. Zaknun, M. R. A. Pillai, G. A. Jánoki, Multispecies animal investigation on biodistribution, pharmacokinetics and toxicity of ^{177}Lu-EDTMP, a potential bone pain palliation agent, *Nuclear Medicine and Biology* 37 (2010) 215–226.

[159] S. Watanabe, K. Hashimoto, N. S. Ishioka, Lutetium-177 complexation of DOTA and DTPA in the presence of competing metals, *Journal of Radioanalytical and Nuclear Chemistry* 303 (2014) 1519–1521.

[160] B. L. R. Kam, J. J. M. Teunissen, E. P. Krenning, W. W. de Herder, S. Khan, E. I. van Vliet, D. J. Kwekkeboom, Lutetium-labelled peptides for therapy of neuroendocrine tumours, *European Journal of Nuclear Medicine and Molecular Imaging* 39 (2012) 103–112.

[161] J. P. Esser, E. P. Krenning, J. J. M. Teunissen, P. P. M. Kooij, A. L. H. van Gameren, W. H. Bakker, D. J. Kwekkeboom, Comparison of [^{177}Lu-DOTA^0,Tyr^3]octreotate and [^{177}Lu-DOTA^0,Tyr^3]octreotide: which peptide is preferable for PRRT?, *European Journal of Nuclear Medicine and Molecular Imaging* 33 (2006) 1346–1351.

[162] S. Chakraborty, T. Das, S. Banerjee, L. Balogh, P. R. Chaudhari, H. D. Sarma, A. Polyák, D. Máthé, M. Venkatesh, G. Janoki, M. R. A. Pillai, ^{177}Lu-EDTMP: A viable bone pain palliative in skeletal metastasis, *Cancer Biotherapy and Radiopharmaceuticals* 23 (2008) 202–213.

[163] S. Chakraborty, T. Das, S. Banerjee, H. D. Sarma, M. Venkatesh, Preparation and preliminary biological evaluation of ^{177}Lu-labelled hydroxyapatite as a promising agent for radiation synovectomy of small joints, *Nuclear Medicine Communications* 27 (2006) 661–668.

[164] L. Bodei, M. Cremonesi, C. M. Grana, N. Fazio, S. Iodice, S. M. Baio, M. Bartolomei, D. Lombardo, M. E. Ferrari, M. Sansovini, M. Chinol, G. Paganelli, Peptide receptor radionuclide therapy with ^{177}Lu-DOTATATE: the IEO phase I-II study, *European Journal of Nuclear Medicine and Molecular Imaging* 38 (2011) 2125–2135.

[165] T. Das, S. Chakraborty, P. R. Unni, S. Banerjee, G. Samuel, H. D. Sarma, M. Venkatesh, M. R. A. Pillai, ^{177}Lu-labeled cyclic polyaminophosphonates as potential agents for bone pain palliation, *Applied Radiation and Isotopes* 57 (2002) 177–184.

[166] R. D. Alvarez, E. E. Partridge, M. B. Khazaeli, G. Plott, M. Austin, L. Kilgore, C. D. Russell, T. Liu, W. E. Grizzle, J. Schlom, A. F. LoBuglio, R. F. Meredith, Intraperitoneal radioimmunotherapy of ovarian cancer with ^{177}Lu-CC49: A phase I/II study, *Gynecologic Oncology* 65 (1997) 94–101.

[167] M. van Essen, E. P. Krenning, B. L. R. Kam, W. W. de Herder, R. A. Feelders, D. J. Kwekkeboom, Salvage therapy with ^{177}Lu-octreotate in patients with bronchial and gastroenteropancreatic neuroendocrine tumors, *Journal of Nuclear Medicine* 51 (2010) 383–390.

[168] M. D'Huyvetter, A. Aerts, C. Xavier, I. Vaneycken, N. Devoogdt, M. Gijs, N. Impens, S. Baatout, B. Ponsard, S. Muyldermans, V. Caveliers,

T. Lahoutte, Development of ^{177}Lu-nanobodies for radioimmunotherapy of HER2-positive breast cancer: evaluation of different bifunctional chelators, *Contrast Media & Molecular Imaging* 7 (2012) 254–264.

[169] M. R. A. Pillai, S. Chakraborty, T. Das, M. Venkatesh, N. Ramamoorthy, Production logistics of Lu-177 for radionuclide therapy, *Applied Radiation and Isotopes* 59 (2003) 109–118.

[170] R. Bhardwaj, A. van der Meer, S. K. Das, M. de Bruin, J. Gascon, H. T. Wolterbeek, A. G. Denkova, P. Serra-Crespo, Separation of nuclear isomers for cancer therapeutic radionuclides based on nuclear decay after-effects, *Scientific Reports* 7 (2017) 1–8.

[171] C. Barkhausen, ^{177}Lu for radiopharmaceutical applications, Ph.D. thesis, Technische Universität München, 2011.

[172] P. S. Balasubramanian, Separation of carrier-free lutetium-177 from neutron irradiated natural ytterbium target, *Journal of Radioanalytical and Nuclear Chemistry* 185 (1994) 305–310.

[173] K. Hashimoto, H. Matsuoka, S. Uchida, Production of no-carrier-added ^{177}Lu *via* the ^{176}Yb$(n,\gamma)^{177}$Yb$\rightarrow^{177}$Lu process, *Journal of Radioanalytical and Nuclear Chemistry* 255 (2003) 575–579.

[174] V. D. Kosynkin, T. V. Molchanova, E. V. Zharova, Lutetium and ytterbium separation by ion-exchange chromatography, *Atomic Energy* 121 (2017) 443–447.

[175] N. A. Lebedev, A. F. Novgorodov, R. Misiak, J. Brockmann, F. Rosch, Radiochemical separation of no-carrier-added ^{177}Lu as produced *via* the ^{176}Yb$(n,\gamma)^{177}$Yb$\rightarrow^{177}$Lu process, *Applied Radiation and Isotopes* 53 (2000) 421–425.

[176] A. Bilewicz, K. Żuchowska, B. Bartoś, Separation of Yb as $YbSO_4$ from the ^{176}Yb target for production of ^{177}Lu *via* the ^{176}Yb$(n,\gamma)^{177}$Yb$\rightarrow^{177}$Lu process, *Journal of Radioanalytical and Nuclear Chemistry* 280 (2009) 167–169.

[177] N. Salek, M. Shamsaei, M. Ghannadi Maragheh, S. Shirvani Arani, A. Bahrami Samani, Comparative studies of extraction chromatography and electro-amalgamation separation to produce no-carrier added ^{177}Lu by Tehran research reactor, *Iranian Journal of Nuclear Medicine* 25 (2017) 23–33.

[178] N. Salek, M. Shamsaei, G. Maragheh Mohammad, S. Arani Simindokht, B. Samani Ali, Production and quality control ^{177}Lu (NCA)–DOTMP

as a potential agent for bone pain palliation, *Journal of Applied Clinical Medical Physics* 17 (2016) 128–139.

[179] S. Mirzadeh, M. Du, A. L. Beets, F. F. J. Knapp, Method for preparing high specific activity ^{177}Lu, US Patent 6,716,353, 2004.

[180] M. R. Antonio, D. R. McAlister, E. P. Horwitz, An europium(III) diglycolamide complex: insights into the coordination chemistry of lanthanides in solvent extraction, *Dalton Transactions* 44 (2015) 515–521.

[181] V. S. Le, N. Morcos, M. Zaw, P. Pellegrini, I. Greguric, Alternative chromatographic processes for no-carrier added ^{177}Lu radioisotope separation - Part I - Multi-column chromatographic process for clinically applicable, *Journal of Radioanalytical and Nuclear Chemistry* 277 (2008) 663–673.

[182] V. S. Le, N. Morcos, M. Zaw, P. Pellegrini, I. Greguric, A. Nevissi, Alternative chromatographic processes for no-carrier added ^{177}Lu radioisotope separation - Part II - The conventional column chromatographic separation combined with HPLC for high purity, *Journal of Radioanalytical and Nuclear Chemistry* 277 (2008) 675–683.

[183] C. Müller, N. P. van der Meulen, M. Benešová, R. Schibli, Therapeutic radiometals beyond ^{177}Lu and ^{90}Y: Production and application of promising α-particle, β^--particle, and Auger electron emitters, *Journal of Nuclear Medicine* 58 (2017) 91S–96S.

[184] K. A. Domnanich, R. Eichler, C. Müller, S. Jordi, V. Yakusheva, S. Braccini, M. Behe, R. Schibli, A. Türler, N. P. van der Meulen, Production and separation of ^{43}Sc for radiopharmaceutical purposes, *EJNMMI Radiopharmacy and Chemistry* 2 (2017) 1–17.

[185] C. Müller, K. A. Domnanich, C. A. Umbricht, N. P. van der Meulen, Scandium and terbium radionuclides for radiotheranostics: Current state of development towards clinical application, *The British Journal of Radiology* 91 (2018) 20180074.

[186] B. Bartoś, A. Majkowska, S. Krajewski, A. Bilewicz, New separation method of no-carrier-added ^{47}Sc from titanium targets, *Radiochimica Acta* 100 (2012) 457–462.

[187] K. L. Kolsky, V. Joshi, L. F. Mausner, S. C. Srivastava, Radiochemical purification of no-carrier-added scandium-47 for radioimmunotherapy, *Applied Radiation and Isotopes* 49 (1998) 1541–1549.

[188] K. A. Domnanich, C. Müller, M. Benešová, R. Dressler, S. Haller, U. Köster, B. Ponsard, R. Schibli, A. Türler, N. P. van der Meulen, ^{47}Sc as useful β^--emitter for the radiotheragnostic paradigm: A comparative study of feasible production routes, *EJNMMI Radiopharmacy and Chemistry* 2 (2017).

[189] I. A. Abbasi, J. H. Zaidi, M. Arif, S. Waheed, M. S. Subhani, Measurement of fission neutron spectrum averaged cross sections of some threshold reactions on zirconium: Production possibility of no-carrier-added ^{90}Y in a nuclear reactor, *Radiochimica Acta* 94 (2006) 381–384.

[190] M. Van de Voorde, K. Van Hecke, T. Cardinaels, K. Binnemans, Radiochemical processing of nuclear-reactor-produced radiolanthanides for medical applications, *Coordination Chemistry Reviews* 382 (2019) 103–125.

[191] K. Binnemans, Interpretation of europium(III) spectra, *Coordination Chemistry Reviews* 295 (2015) 1–45.

[192] K. Binnemans, P. T. Jones, T. Müller, L. Yurramendi, Rare Earths and the Balance Problem: How to Deal with Changing Markets?, *Journal of Sustainable Metallurgy* 4 (2018) 126–146.

[193] D. Dupont, D. Depuydt, K. Binnemans, Overview of the effect of salts on biphasic ionic liquid/water solvent extraction systems: Anion exchange, mutual solubility, and thermomorphic properties, *Journal of Physical Chemistry B* 119 (2015) 6747–6757.

[194] Ad hoc Working Group on defining critical raw materials, Report on Critical Raw Materials for the EU, Technical Report, European Commission, 2014.

[195] A. Kumari, M. K. Jha, D. D. Pathak, S. Chakravarty, J. chun Lee, Processes developed for the separation of europium (Eu) from various resources, *Separation & Purification Reviews* 48 (2018) 91–121.

[196] J.-C. G. Bünzli, Review: Lanthanide coordination chemistry: From old concepts to coordination polymers, *Journal of Coordination Chemistry* 67 (2014) 3706–3733.

[197] W. W. Lukens, M. Speldrich, P. Yang, T. J. Duignan, J. Autschbach, P. Kögerler, The roles of *4f*- and *5f*-orbitals in bonding: A magnetochemical, crystal field, density functional theory, and multi-reference wavefunction study, *Dalton Transactions* 45 (2016) 11508–11521.

[198] T. Hirai, I. Komasawa, Separation of europium from samarium and gadolinium by combination of electrochemical reduction and solvent extraction, *Journal of Chemical Engineering of Japan* 25 (1992) 644–648.

[199] T. Hirai, N. Onoe, I. Komasawa, Separation of europium from samarium and gadolinium by combination of photochemical reduction and solvent extraction, *Journal of Chemical Engineering of Japan* 26 (1993) 64–67.

[200] C. A. Morais, V. S. T. Ciminelli, Europium recovery by photochemical reduction from Eu and Eu-Gd chloride solutions, *Separation Science and Technology* 37 (2002) 3305–3321.

[201] T. Hirai, I. Komasawa, Separation of rare metals by solvent extraction employing reductive stripping technique, *Mineral Processing and Extractive Metallurgy Review* 17 (1997) 81–107.

[202] C. A. Morais, V. S. T. Ciminelli, Recovery of europium from a rare earth chloride solution, *Hydrometallurgy* 49 (1998) 167–177.

[203] C. A. Morais, V. S. T. Ciminelli, Recovery of europium by chemical reduction of a commercial solution of europium and gadolinium chlorides, *Hydrometallurgy* 60 (2001) 247–253.

[204] M. Zelić, Electrochemical reduction of europium(3+) at increasing concentrations of different salts. Part I. Voltammetric measurements, *Croatica Chemica Acta* 76 (2003) 241–248.

[205] M. R. Cicconi, G. Giuli, E. Paris, W. Ertel-Ingrisch, P. Ulmer, D. B. Dingwell, Europium oxidation state and local structure in silicate glasses, *American Mineralogist* 97 (2012) 918–929.

[206] Y. Takahashi, G. R. Kolonin, G. P. Shironosova, I. I. Kupriyanova, T. Uruga, H. Shimizu, Determination of the Eu(II)/Eu(III) ratios in minerals by X-ray absorption near-edge structure (XANES) and its application to hydrothermal deposits, *Mineralogical Magazine* 69 (2005) 179–190.

[207] J. M. Karner, J. J. Papike, S. R. Sutton, P. V. Burger, C. K. Shearer, L. Le, M. Newville, Y. Choi, Partitioning of Eu between augite and a highly spiked martian basalt composition as a function of oxygen fugacity (IW-1 to QFM): Determination of Eu^{2+}/Eu^{3+} ratios by XANES, *American Mineralogist* 95 (2010) 410–413.

[208] N. Avci, K. Korthout, M. A. Newton, P. F. Smet, D. Poelman, Valence states of europium in $CaAl_2O_4$:Eu phosphors, *Optical Materials Express* 2 (2012) 321–330.

[209] K. Korthout, K. Van den Eeckhout, J. Botterman, S. Nikitenko, D. Poelman, P. F. Smet, Luminescence and x-ray absorption measurements of persistent $SrAl_2O_4$:Eu,Dy powders: Evidence for valence state changes, *Physical Review B* 84 (2011) 1–7 (085140).

[210] J. Rakovan, M. Newville, S. Sutton, Evidence of heterovalent europium in zoned Llallagua apatite using wavelength dispersive XANES, *American Mineralogist* 86 (2001) 697–700.

[211] C. K. Shearer, J. J. Papike, P. V. Burger, S. R. Sutton, F. M. McCubbin, M. Newville, Direct determination of europium valence state by XANES in extraterrestrial merrillite: Implications for REE crystal chemistry and martian magmatism, *American Mineralogist* 96 (2011) 1418–1421.

[212] L. Jelinek, T. Arai, W. Yuezhou, M. Kumagai, Direct spectroscopic determination of europium(II) concentration during europium(III) electroreduction in hydrochloric acid medium, *Journal of Rare Earths* 25 (2007) 1–5.

[213] R. G. Bates, J. B. Macaskill, Standard potential of the silver-silver chloride electrode, *Pure and Applied Chemistry* 50 (1978) 1701–1706.

[214] L. Lépine, R. Gilbert, G. Belanger, Ultraviolet spectrophotometric determination of gadolinium in concentrated solutions of nitrate salts, *Analytical Chemistry* 58 (1986) 1152–1156.

[215] D. A. Outka, J. Stöhr, Curve fitting analysis of near-edge core excitation spectra of free, adsorbed, and polymeric molecules, *The Journal of Chemical Physics* 88 (1988) 3539–3554.

[216] M. R. Antonio, L. Soderholm, I. Song, X-ray absorption fine structure measurements of bulk solution species, *Journal of Applied Electrochemistry* 27 (1997) 784–792.

[217] G. Moreau, R. Scopelliti, L. Helm, J. Purans, A. E. Merbach, Solution X-ray absorption fine structure study of the Eu^{2+} and Sr^{2+} ions: Unexpected solvent and metal ion dependencies of the solvation numbers, *Journal of Physical Chemistry A* 106 (2002) 9612–9622.

[218] J. Garcia, M. J. Allen, Developments in the coordination chemistry of europium(II), *European Journal of Inorganic Chemistry* 2012 (2012) 4550–4563.

[219] G. Moreau, L. Helm, J. Purans, A. E. Merbach, Structural investigation of the aqueous Eu^{2+} ion: Comparison with Sr^{2+} using the XAFS technique, *Journal of Physical Chemistry A* 106 (2002) 3034–3043.

[220] A. G. Atanasyants, A. N. Seryogin, The reaction of the electrochemical reduction Eu(III) + e^-→ Eu(II) in hydrochloric solution, *Hydrometallurgy* 37 (1995) 367–374.

[221] L. Holleck, Über die Stromspannungskurven von Europiumnitratlösungen und die Symmetrie der Felder um die Europiumionen, *Zeitschrift für Elektrochemie und angewandte physikalische Chemie* 49 (1943) 496–496.

[222] L. Holleck, Besonderheiten in den Strom-Spannungskurven von Europiumsalzlösungen und Struktur der Lösungen, *Zeitschrift für Elektrochemie und angewandte physikalische Chemie* 46 (1940) 69–71.

[223] G. Tabbì, A. Giuffrida, R. P. Bonomo, Determination of formal redox potentials in aqueous solution of copper(II) complexes with ligands having nitrogen and oxygen donor atoms and comparison with their EPR and UV–Vis spectral features, *Journal of Inorganic Biochemistry* 128 (2013) 137–145.

[224] A. J. Bard, L. R. Faulkner, Electrochemical Methods: Fundamentals and Applications, John Wiley & Sons, Inc., second edition, 2001.

[225] S. Andersson, K. Eberhardt, C. Ekberg, J.-O. Liljenzin, M. Nilsson, G. Skarnemark, Determination of stability constants of lanthanide nitrate complex formation using a solvent extraction technique, *Radiochimica Acta* 94 (2006) 469–474.

[226] S. Friesen, S. Krickl, M. Luger, A. Nazet, G. Hefter, R. Buchner, Hydration and ion association of La^{3+} and Eu^{3+} salts in aqueous solution, *Physical Chemistry Chemical Physics* 20 (2018) 8812–8821.

[227] P. J. Breen, W. D. Horrocks, Europium(III) luminescence excitation spectroscopy: Inner-sphere complexation of europium(III) by chloride, thiocyanate, and nitrate ions, *Inorganic Chemistry* 22 (1983) 536–540.

[228] H. Kanno, H. Yokoyama, On the anomalous concentration dependence of the inner-sphere hydration number change of aqua lanthanide ions, *Polyhedron* 15 (1996) 1437–1441.

[229] G. R. Choppin, Structure and thermodynamics of lanthanide and actinide complexes in solution, *Pure and Applied Chemistry* 27 (1971) 23–41.

[230] P. Atkins, T. Overton, J. Rourke, M. Weller, F. Armstrong, Shriver & Atkins' Inorganic Chemistry, Oxford University Press, 2010.

[231] L. Holleck, Über die kathodische Reduktion von Nitrationen an der Quecksilbertropfelektrode und die analytische Auswertbarkeit der

polarographischen Nitratstufen, *Zeitschrift für Elektrochemie und angewandte physikalische Chemie* 49 (1943) 400–406.

[232] J. Jiang, N. Higashiyama, K. ichi Machida, G. ya Adachi, The luminescent properties of divalent europium complexes of crown ethers and cryptands, *Coordination Chemistry Reviews* 170 (1998) 1–29.

[233] J. B. Gruber, U. V. Valiev, G. W. Burdick, S. A. Rakhimov, M. Pokhrel, D. K. Sardar, Spectra, energy levels, and symmetry assignments for stark components of $Eu^{3+}(4f^6)$ in gadolinium gallium garnet ($Gd_3Ga_5O_{12}$), *Journal of Luminescence* 131 (2011) 1945–1952.

[234] J.-C. Rybak, M. Hailmann, P. R. Matthes, A. Zurawski, J. Nitsch, A. Steffen, J. G. Heck, C. Feldmann, S. Götzendörfer, J. Meinhardt, G. Sextl, H. Kohlmann, S. J. Sedlmaier, W. Schnick, K. Müller-Buschbaum, Metal–organic framework luminescence in the yellow gap by codoping of the homoleptic imidazolate $^3_\infty[Ba(Im)_2]$ with divalent europium, *Journal of the American Chemical Society* 135 (2013) 6896–6902.

[235] C. Dujardin, B. Moine, C. Pedrini, One- and two-photon spectroscopy of f → d and f → f transitions of Eu^{2+} ions in $M_{1-x}N_xF_2$ mixed fluoride crystals (M, N = Ba, Sr, Ca; $0 \leqslant x \leqslant 1$), *Journal of Luminescence* 54 (1993) 259–270.

[236] E. Loh, $4f^n \rightarrow 4f^{n-1}5d$ spectra of rare-earth ions in crystals, *Physical Review* 175 (1968) 533–536.

[237] S. P. Sinha (Ed.), Proceedings of the NATO Advanced Study Institute on Systematics and the Properties of the Lanthanides, number 109 in Series C, Mathematical and physical sciences, NATO, D. Reidel Publishing Company, Braunlage, Germany, 1982.

[238] V. Kachkanov, M. J. Wallace, G. van der Laan, S. S. Dhesi, S. A. Cavill, Y. Fujiwara, K. P. O'Donnell, Induced magnetic moment of Eu^{3+} ions in GaN, *Scientific Reports* 2: 969 (2012) 1–5.

[239] I. R. Rodrigues, L. Lukina, S. Dehaeck, P. Colinet, K. Binnemans, J. Fransaer, Magnetomigration of rare-earth ions triggered by concentration gradients, *The Journal of Physical Chemistry Letters* 8 (2017) 5301–5305.

[240] S. Kern, R. Kostelecky, C. M. O'Donnell, Magnetic suceptibility of monoclinic Eu_2O_3, *Physics Letters* 33A (1970) 27.

[241] Y. Misawa, Y. Doi, Y. Hinatsu, Magnetic ordering of divalent europium in double perovskites Eu_2LnTaO_6 - Magnetic interactions of Eu^{2+} ions determined by magnetic susceptibility, specific heat, and ^{151}Eu Mössbauer spectrum measurements (Ln=rare earths), *Journal of Solid State Chemistry* 184 (2011) 1478–1483.

[242] J. J. Joos, K. Korthout, S. Nikitenko, D. Poelman, P. F. Smet, Origin of saturated green emission from europium in zinc thiogallate, *Optical Materials Express* 3 (2013) 1338–1350.

[243] K. Korthout, A. B. Parmentier, P. F. Smet, D. Poelman, A XAS study of the luminescent Eu centers in thiosilicate phosphors, *Physical Chemistry Chemical Physics* 15 (2013) 8678–8683.

[244] J. A. Horsley, Relationship between the area of $l_{2,3}$ xray absorption edge resonances and the d orbital occupancy in compounds of platinum and iridium, *The Journal of Chemical Physics* 76 (1982) 1451–1458.

[245] D. F. Peppard, E. P. Horwitz, G. W. Mason, Separation of europium from other lanthanide rare earths by solvent extraction, US Patent 3,077,378, 1963.

[246] M. Castro, A. Portilla, Sm-153 EDTMP - a new palliative therapy agent against pain in cases of bone metastases, *International symposium on modern trends in radiopharmaceuticals for diagnosis and therapy, Lisbon (Portugal)* (1998) 619–626.

[247] C. L. Maini, S. Bergomi, L. Romano, R. Sciuto, ^{153}Sm-EDTMP for bone pain palliation in skeletal metastases, *European Journal of Nuclear Medicine and Molecular Imaging* 31 (2004) S171–S178.

[248] T. F. Sandeman, R. S. Budd, J. J. Martin, Samarium-153-labelled EDTMP for bone metastases from cancer of the prostate, *Clinical Oncology* 4 (1992) 160–164.

[249] T. Loebe, B. Hettwig, H. W. Fischer, Detection of long-lived europium-152 in samarium-153-lexidronam, *Applied Radiation and Isotopes* 94 (2014) 40–43.

[250] L. Moro, D. Fantinato, F. Frigerio, G. Shamhan, G. Angelovski, Europium-154 contamination levels in samarium-153-EDTMP for radionuclide therapy, *Journal of Physics: Conference Series* 41 (2006) 535–537.

[251] J. S. Preston, A. C. du Preez, The recovery of a mixed rare-earth oxide and the preparation of cerium, europium and neodymium oxides from a south african phosphoric acid sludge by solvent extraction, *Mineral Processing and Extractive Metallurgy Review* 18 (1998) 175–200.

[252] S. Nishihama, T. Hirai, I. Komasawa, Advanced liquid–liquid extraction systems for the separation of rare earth ions by combination of conversion of the metal species with chemical reaction, *Journal of Solid State Chemistry* 171 (2003) 101–108.

[253] K. Van Hoecke, J. Bussé, M. Gysemans, L. Adriaensen, A. Dobney, T. Cardinaels, Isolation of lanthanides from spent nuclear fuel by means of high performance ion chromatography (HPIC) prior to mass spectrometric analysis, *Journal of Radioanalytical and Nuclear Chemistry* 314 (2017) 1727–1739.

[254] C. Deferm, M. Van de Voorde, J. Luyten, H. Oosterhof, J. Fransaer, K. Binnemans, Purification of indium by solvent extraction with undiluted ionic liquids, *Green Chemistry* 18 (2016) 4116–4127.

[255] D. Dupont, K. Binnemans, Rare-earth recycling using a functionalized ionic liquid for the selective dissolution and revalorization of Y_2O_3:Eu^{3+} from lamp phosphor waste, *Green Chemistry* 17 (2015) 856–868.

[256] B. Onghena, K. Binnemans, Recovery of scandium(III) from aqueous solutions by solvent extraction with the functionalized ionic liquid betainium bis(trifluoromethylsulfonyl)imide, *Industrial & Engineering Chemistry Research* 54 (2015) 1887–1898.

[257] A. Rout, K. Binnemans, Liquid-liquid extraction of europium(III) and other trivalent rare-earth ions using a non-fluorinated functionalized ionic liquid, *Dalton Transactions* 43 (2014) 1862–1872.

[258] G. Ye, F. Bai, J. Wei, J. Wang, J. Chen, Co-condensation synthesis of a novel DCH18C6-functionalized organosilica for strontium adsorption, *Procedia Chemistry* 7 (2012) 616–621.

[259] H. Y. Zhou, T. L. Yu, Y. Y. Ao, J. Peng, M. L. Zhai, Crystal structure and radiation stability of $Sr(NO_3)_2$·DCH18C6 complex, *Acta Physico-Chimica Sinica* 30 (2014) 1581–1586.

[260] T. Vander Hoogerstraete, S. Jamar, S. Wellens, K. Binnemans, Determination of halide impurities in ionic liquids by total reflection X-ray fluorescence spectrometry, *Analytical Chemistry* 86 (2014) 3931–3938.

[261] K. V. Klementev, Deconvolution problems in X-ray absorption fine structure spectroscopy, *Journal of Physics D: Applied Physics* 34 (2001) 2241–2247.

[262] M. Newville, EXAFS analysis using FEFF and FEFFIT, *Journal of Synchrotron Radiation* 8 (2001) 96–100.

[263] S. Dai, Y. H. Ju, C. E. Barnes, Solvent extraction of strontium nitrate by a crown ether using room-temperature ionic liquids, *Dalton Transactions* (1999) 1201–1202.

[264] D. I. Djigailo, S. V. Smirnova, I. I. Torocheshnikova, A. G. Vendilo, K. I. Popov, I. V. Pletnev, Extraction of nitrates of alkali and alkaline earth metals with crown ether into hydrophilic ionic liquid in the presence of salting out agent, *Moscow University Chemistry Bulletin* 64 (2009) 130–133.

[265] E. P. Horwitz, M. L. Dietz, D. E. Fisher, Correlation of the extraction of strontium nitrate by a crown ether with the water-content of the organic phase, *Solvent Extraction and Ion Exchange* 8 (1990) 199–208.

[266] S. L. Garvey, C. A. Hawkins, M. L. Dietz, Effect of aqueous phase anion on the mode of facilitated ion transfer into room-temperature ionic liquids, *Talanta* 95 (2012) 25–30.

[267] C. J. Pedersen, The discovery of crown ethers, *Science* 241 (1988) 536–540.

[268] A. H. Bond, M. L. Dietz, R. Chiarizia, Incorporating size selectivity into synergistic solvent extraction - A review of crown ether-containing systems, *Industrial & Engineering Chemistry Research* 39 (2000) 3442–3464.

[269] J. Christoffers, P. Starynowicz, A europium(II) complex with bis-pyridino-18-crown-6, *Polyhedron* 27 (2008) 2688–2692.

[270] V. M. Abashkin, D. W. Wester, J. A. Campbell, K. E. Grant, Radiation stability of cis-isomers of dicyclohexano-18-crown-6, *Radiation Physics and Chemistry* 48 (1996) 463–472.

[271] Y. Ao, W. Yuan, T. Yu, J. Peng, J. Li, M. Zhai, L. Zhao, Radiolysis of crown ether–ionic liquid systems: identification of radiolytic products and their effect on the removal of Sr^{2+} from nitric acid, *Physical Chemistry Chemical Physics* 17 (2015) 3457–3462.

[272] M. Draye, A. Favre-Réguillon, R. Faure, M. Lemaire, Radiation chemistry of cis-syn-cis dicyclohexano-18-crown-6 (DCH18C6): Acidity and uranyl nitrate dependence, *Radiation Physics and Chemistry* 77 (2008) 581–584.

[273] E. I. Grigorev, O. V. Mikhalitsyna, S. V. Nesterov, L. I. Trakhtenberg, The effect of structure of crown ether complexes with alkaline-earth metal chlorides on their radiation resistance, *High Energy Chemistry* 31 (1997) 16–19.

[274] S. V. Nesterov, Crown ethers in radiochemistry: Achievements and prospects, *Russian Chemical Reviews* 69 (2000) 769–782.

[275] H. H. Dam, D. N. Reinhoudt, W. Verboom, Multicoordinate ligands for actinide/lanthanide separations, *Chemical Society Reviews* 36 (2007) 367–377.

[276] J. Rydberg, M. Cox, C. Musikas, G. R. Choppin, Solvent Extraction Principles and Practice, Marcel Dekker, Inc., New York, second edition, 2004.

[277] J. N. Chubb, P. Lagos, J. Lienlaf, Electrostatic safety during the solvent extraction of copper, *Journal of Electrostatics* 63 (2005) 119–127.

[278] G. L. Hearn, Electrostatic ignition hazards arising from fuel flow in plastic pipelines, *Journal of Loss Prevention in the Process Industries* 15 (2002) 105–109.

[279] D. Allen, G. Baston, A. E. Bradley, T. Gorman, A. Haile, I. Hamblett, J. E. Hatter, M. J. F. Healey, B. Hodgson, R. Lewin, K. V. Lovell, B. Newton, W. R. Pitner, D. W. Rooney, D. Sanders, K. R. Seddon, H. E. Sims, R. C. Thied, An investigation of the radiochemical stability of ionic liquids, *Green Chemistry* 4 (2002) 152–158.

[280] M. L. Dietz, J. A. Dzielawa, Ion-exchange as a mode of cation transfer into room-temperature ionic liquids containing crown ethers: Implications for the 'greenness' of ionic liquids as diluents in liquid-liquid extraction, *Chemical Communications* (2001) 2124–2125.

[281] E. Makrlík, P. Toman, P. Vaňura, Complexation of the ammonium cation with dibenzo-18-crown-6: Extraction and DFT study, *Acta Chimica Slovenica* 60 (2013) 193–197.

[282] P. Vaňura, E. Makrlík, Stability of complexes of NH_4^+ with 18-crown-6, dicyclohexyl-18-crown-6, dibenzo-18-crown-6 and dibenzo-24-crown-8 in water saturated nitrobenzene, *Journal of Radioanalytical and Nuclear Chemistry* 250 (2001) 369–371.

[283] H. Cui, T. Otsuka, A. Kobayashi, N. Takeda, M. Ishikawa, Y. Misaki, H. Kobayashi, Structural, electrical, and magnetic properties of a series of molecular conductors based on BDT-TTP and lanthanoid nitrate complex anions (BDT-TTP = 2,5-bis(1,3-dithiol-2-ylidene)-1,3,4,6-tetrathiapentalene), *Inorganic Chemistry* 42 (2003) 6114–6122.

[284] N. Tang, Y. Zhao, L. He, W.-L. Yuan, G.-H. Tao, Long-lived luminescent soft materials of hexanitratosamarate(III) complexes with orange visible emission, *Dalton Transactions* 44 (2015) 8816–8823.

[285] K. Larsson, K. Binnemans, Selective extraction of metals using ionic liquids for nickel metal hydride battery recycling, *Green Chemistry* 16 (2014) 4595–4603.

[286] E. P. Horwitz, D. R. McAlister, M. L. Dietz, Extraction chromatography versus solvent extraction: How similar are they?, *Separation Science and Technology* 41 (2006) 2163–2182.

[287] T. Selvam, A. Machoke, W. Schwieger, Supported ionic liquids on non-porous and porous inorganic materials — A topical review, *Applied Catalysis A: General* 445–446 (2012) 92–101.

[288] D. Avdibegović, M. Regadío, K. Binnemans, Efficient separation of rare earths recovered by a supported ionic liquid from bauxite residue leachate, *RSC Advances* 8 (2018) 11886–11893.

[289] N. Kabay, M. Arda, B. Saha, M. Streat, Removal of Cr(VI) by solvent impregnated resins (SIR) containing Aliquat 336, *Reactive and Functional Polymers* 54 (2003) 103–115.

[290] B. Saha, R. J. Gill, D. G. Bailey, N. Kabay, M. Arda, Sorption of Cr(VI) from aqueous solution by Amberlite XAD-7 resin impregnated with Aliquat 336, *Reactive and Functional Polymers* 60 (2004) 223–244.

[291] E. A. El-Sofany, Removal of lanthanum and gadolinium from nitrate medium using Aliquat-336 impregnated onto Amberlite XAD-4, *Journal of Hazardous Materials* 153 (2008) 948–954.

[292] W. W. Yang, G. S. Luo, X. C. Gong, Extraction and separation of metal ions by a column packed with polystyrene microcapsules containing Aliquat 336, *Separation and Purification Technology* 43 (2005) 175–182.

[293] W. W. Yang, G. S. Luo, X. C. Gong, Polystyrene microcapsules containing Aliquat 336 as a novel packing material for separation of metal ions, *Hydrometallurgy* 80 (2005) 179–185.

[294] S. Van Roosendael, M. Regadío, J. Roosen, K. Binnemans, Selective recovery of indium from iron-rich solutions using an Aliquat 336 iodide supported ionic liquid phase (SILP), *Separation and Purification Technology* 212 (2019) 843–853.

[295] C. Jagadeeswara Rao, K. A. Venkatesan, B. V. R. Tata, K. Nagarajan, T. G. Srinivasan, P. R. Vasudeva Rao, Radiation stability of some room temperature ionic liquids, *Radiation Physics and Chemistry* 80 (2011) 643–649.

[296] B. J. Mincher, J. F. Wishart, The radiation chemistry of ionic liquids: A review, *Solvent Extraction and Ion Exchange* 32 (2014) 563–583.

[297] E. P. Horwitz, M. L. Dietz, R. Chiarizia, H. Diamond, S. L. Maxwell, M. R. Nelson, Separation and preconcentration of actinides by extraction chromatography using a supported liquid anion exchanger: Application to the characterization of high-level nuclear waste solutions, *Analytica Chimica Acta* 310 (1995) 63–78.

[298] D. Avdibegovic, M. Regadio, K. Binnemans, Recovery of scandium(III) from diluted aqueous solutions by a supported ionic liquid phase (SILP), *RSC Advances* 7 (2017) 49664–49674.

[299] J. H. Olivier, F. Camerel, R. Ziessel, Lanthanide ion extraction by trifluoromethyl-1,3-diketonate-functionalised ionic liquids adsorbed on silica, *Chemistry - a European Journal* 17 (2011) 9113–9122.

[300] Y. Liu, L. Zhu, X. Sun, J. Chen, F. Luo, Silica materials doped with bifunctional ionic liquid extractant for yttrium extraction, *Industrial & Engineering Chemistry Research* 48 (2009) 7308–7313.

[301] L. L. Zhu, L. Guo, Z. J. Zhang, J. Chen, S. M. Zhang, The preparation of supported ionic liquids (SILs) and their application in rare metals separation, *Science China Chemistry* 55 (2012) 1479–1487.

[302] R. Navarro, E. Garcia, I. Saucedo, E. Guibal, Platinum(IV) recovery from HCl solution using Amberlite XAD-7 impregnated with a tetraalkyl phosphonium ionic liquid, *Separation Science and Technology* 47 (2012) 2199–2210.

[303] R. Navarro, P. Ruiz, I. Saucedo, E. Guibal, Bismuth(III) recovery from hydrochloric acid solutions using Amberlite XAD-7 impregnated with a tetraalkylphosphonium ionic liquid, *Separation and Purification Technology* 135 (2014) 268–277.

[304] R. Navarro, I. Saucedo, C. Gonzalez, E. Guibal, Amberlite XAD-7 impregnated with Cyphos IL-101 (tetraalkylphosphonium ionic liquid) for Pd(II) recovery from HCl solutions, *Chemical Engineering Journal* 185 (2012) 226–235.

[305] R. Navarro, I. Saucedo, M. A. Lira, E. Guibal, Gold(III) recovery from HCl solutions using Amberlite XAD-7 impregnated with an ionic liquid (Cyphos IL-101), *Separation Science and Technology* 45 (2010) 1950–1962.

[306] A. W. Trochimczuk, N. Kabay, M. Arda, M. Streat, Stabilization of solvent impregnated resins (SIRs) by coating with water soluble polymers

and chemical crosslinking, *Reactive and Functional Polymers* 59 (2004) 1–7.

[307] C. A. Hawkins, M. A. Momen, M. L. Dietz, Application of ionic liquids in the preparation of extraction chromatographic materials for metal ion separations: Progress and prospects, *Separation Science and Technology* 53 (2018) 1820–1833.

[308] C. A. Hawkins, M. A. Momen, S. L. Garvey, J. Kestell, M. D. Kaminski, M. L. Dietz, Evaluation of solid-supported room-temperature ionic liquids containing crown ethers as media for metal ion separation and preconcentration, *Talanta* 135 (2015) 115–123.

[309] A. Ahmad, J. A. Siddique, M. A. Laskar, R. Kumar, S. H. Mohd-Setapar, A. Khatoon, R. A. Shiekh, New generation Amberlite XAD resin for the removal of metal ions: A review, *Journal of Environmental Sciences (China)* 31 (2015) 104–123.

List of publications

C. Deferm, **M. Van de Voorde**, J. Luyten, H. Oosterhof, J. Fransaer, K. Binnemans, Purification of indium by solvent extraction with undiluted ionic liquids, *Green Chemistry* 18 (2016) 4116–4127

M. Van de Voorde, K. Van Hecke, K. Binnemans, T. Cardinaels, Separation of samarium and europium with an undiluted quaternary ammonium ionic liquid: Towards high-purity medical samarium-153, *RSC Advances* 8 (2018) 20077–20086

M. Van de Voorde, K. Van Hecke, T. Cardinaels, K. Binnemans, Radiochemical processing of nuclear-reactor-produced radiolanthanides for medical application, *Coordination Chemistry Reviews* 382 (2019) 103–125

M. Van de Voorde, B. Geboes, T. Vander Hoogerstraete, K. Van Hecke, T. Cardinaels, K. Binnemans, Stability of europium(II) in aqueous nitrate media, *Dalton Transactions*, submitted

M. Van de Voorde, K. Van Hecke, K. Binnemans, T. Cardinaels, Supported ionic liquid phases for the separation of samarium and europium in aqueous nitrate media: towards purification of medical samarium-153, *Separation and Purification Technology*, submitted

Patent application:

M. Van de Voorde, K. Binnemans, T. Cardinaels, K. Van Hecke, Purification of medical Sm-153 from nitrate media, Patent application, PCT/EP2018/078528 (2018)

List of conferences and symposia

9th Nuclear and Radiochemistry Conference (Helsinki (Finland), 29 August–2 September 2016): 'Purification of medical ^{153}Sm using radiation-resistant ionic liquids' — Poster presentation

6th Symposium on Medical Radioisotopes (Mechelen (Belgium), 11 May 2017): 'Purification of medical ^{153}Sm using radiation-resistant ionic liquids' — Poster presentation

5th International Nuclear Chemistry Congress (Gothenburg (Sweden), 28 August–1 September 2017): 'Conditioning of ionic liquid waste streams in nuclear research applications' — Poster Presentation

10th International Conference on *f*-elements (Lausanne (Switzerland), 3–6 September 2018): 'Separation of samarium and europium by solvent extraction with an undiluted quaternary ammonium ionic liquid: towards high purity medical samarium-153' — Invited lecture

7th Symposium on Medical Radioisotopes (Liège (Belgium), 9 May 2019): 'Supported ionic liquid phases for the purification of medical samarium-153' — Poster presentation

SCK•CEN Academy's internal seminars:

Day of the PhDs, SCK•CEN Academy (Mol (Belgium), 27 October 2016): 'Purification of medical ^{153}Sm using radiation-resistant ionic liquids' — Poster

presentation

Day of the PhDs, SCK•CEN Academy (Mol (Belgium), 19 April 2017): 'Purification of medical ^{153}Sm using radiation-resistant ionic liquids' — Oral presentation

Day of the PhDs, SCK•CEN Academy (Mol (Belgium), 19 September 2018): 'Removal of long-lived europium-154 impurities from medical samarium-153 in nitrate media' – Oral Presentation

FACULTY OF SCIENCE
DEPARTMENT OF CHEMISTRY
SOLVOMET GROUP
Celestijnenlaan 200F box 2404
B-3001 Leuven
michiel.vandevoorde@kuleuven.be
http://chem.kuleuven.be/SOLVOMET